NASA CONTRACTOR REPORT

NASA CR-61198

February 1968

NASA CR-61198

# WIND FIELD ANALYSIS FOR CANTILEVER LOADS

Prepared under Contract No. NAS 8-21138 by

NORTH AMERICAN ROCKWELL CORPORATION



For

NASA-GEORGE C. MARSHALL SPACE FLIGHT CENTER
Huntsville, Alabama

February 1968

NASA CR-61198

# WIND FIELD ANALYSIS FOR CANTILEVER LOADS

Prepared under Contract No. NAS 8-21138 by

NORTH AMERICAN ROCKWELL CORPORATION

For

Aero-Astrodynamics Laboratory



NASA-GEORGE C. MARSHALL SPACE FLIGHT CENTER

# TECHNICAL REPORT INDEX/ABSTRACT

| ACCESSION NUMBER | DOCUMENT SECURITY CLASSIFICATION |
|---|---|
| | UNCLASSIFIED |

| TITLE OF DOCUMENT | LIBRARY USE ONLY |
|---|---|
| WIND FIELD ANALYSIS FOR CANTILEVER LOADS | |

AUTHOR(S)

DAVIS, J.E. *McLAUGHLIN, H.D. *UJIHARA, B.H.

| CODE | ORIGINATING AGENCY AND OTHER SOURCES | DOCUMENT NUMBER |
|---|---|---|
| | SPACE DIVISION, NORTH AMERICAN ROCKWELL CORP. | SD68-16 |

| PUBLICATION DATE | CONTRACT NUMBER |
|---|---|
| 29FEB68 | NAS8-21138 |

DESCRIPTIVE TERMS

*WIND DIRECTION, *WIND MEASUREMENT, *VORTICES, *SEPARATED FLOW

ABSTRACT

TEST DATA CONSISTING OF ANEMOMETER STRIP CHART RECORDINGS TAKEN DURING THE 1966 SATURN V WIND LOADS TEST PROGRAM ARE ANALYZED TO DETERMINE INTERFERENCE EFFECTS FROM THE UMBILICAL TOWER AND VEHICLE.

CONSIDERABLE FLOW INTERFERENCE IS SHOWN FOR THE MID-HEIGHT LEVELS, WHILE THE FLOW FIELD IS RELATIVELY UNIMPEDED AT THE ANEMOMETER POSITIONS USED AT GROUND AND EXTREME TOP LEVELS. NUMERICAL ANALYSES ARE PERFORMED IN ADDITION TO THE EXPERIMENTAL ANALYSIS TO GAIN FURTHER INSIGHT TO THE RELATIVELY LITTLE UNDERSTOOD INTERFERENCE EFFECTS IN THE LOCAL WIND FLOW ABOUT THE SATURN V - LAUNCHER UMBILICAL TOWER.

FORM M 131-V REV. 6-66

# FOREWORD

Interference effects in the local wind field about the Saturn V Vehicle and Launcher Umbilical Tower at Launch Complex 39A are analyzed herein. This study was conducted by the Space Division of North American Rockwell Corporation for the George C. Marshall Space Flight Center of National Aeronautics and Space Administration. R.F. Stevenson, supervisor of Methods and Criteria unit, was Project Manager. B.H. Ujihara was Principal Investigator. J.E. Davis developed the computer programs. H.D. McLaughlin analyzed anemometer data from the Saturn V 500 F Wind Loads Test Program and assisted in computer program development. C.D. Martin provided valuable technical advice during this study. At MSFC, the Project Manager was Mr. John Kaufman; alternate Project Monitor was Mr. C. Kelly Hill. Special appreciation is expressed for the many helpful comments and criticisms provided by the Project Monitors, by Mr. Jack Moore, R-P&VE, and by Messrs. Tom Reed and Bill Vaughn, R-AERO, in reviewing the final report rough draft.

## SUMMARY

The test data gathered during the 1966 Wind Loads Test Program at Launch Complex 39 included simultaneous wind recordings at various heights on the Umbilical Tower and near ground level. Analysis of these data (in paper strip chart form) was performed during this study, and pertinent conclusions were established regarding the nature of the interference flow field about the Saturn V/LUT on Launch Pad 39A. In addition, theoretical investigations were performed to augment these conclusions and gain further understanding of the interference flow field. The computer programs developed in this study employ a unique concept of separated flow analysis, which permits the efficient calculation of nonsteady separated flow fields.

# CONTENTS

## ILLUSTRATIONS



PRECEDING PAGE BLANK NOT FILMED.

# I. INTRODUCTION

The importance of ground winds in the structural design of vertically launched space vehicles has been recognized. Accordingly, considerable research has been expended in recent years toward a clearer definition of imposed ground wind environment and toward an accurate prediction of vehicle response to ground winds. Such research under NASA's direction reached a culmination in the design and operation of the Saturn vehicles. Wind tunnel tests of their dynamically scaled models indicated that large structural dynamic response would occur for certain wind direction and speed conditions.

Since these tests could not duplicate all the known significant environmental parameters, a Ground Wind Loads Test Program utilizing the full-scale Saturn V facilities vehicle (500 F) was conducted during the summer of 1966. Objectives of this test program were to provide full-scale data for evaluating and improving existing ground wind design criteria and methods of predicting ground wind vehicle response. Test instrumentation included wind measuring devices installed on the Launcher Umbilical Tower (LUT), and load measuring devices on the Saturn V vehicle.

The study reported herein has in part been directed towards evaluation of the wind data gathered during this Ground Wind Loads Test Program. This evaluation has revealed pertinent characteristics of the interference flow field derived from suitable reduction and correlation of simultaneously measured wind direction and speed data during the test program at Launch Complex 39.

Theoretical analyses of the flow fields have been made, in conjunction with these experimental results, to understand further the nature of mutual wind interference effects in the immediate region surrounding the Saturn V/ LUT positioned on Launch Pad 39A.

# II. ANALYSIS OF EXPERIMENTAL DATA

## GENERAL

Knowledge of the local wind field characteristics surrounding the Saturn V/LUT is important for several reasons:

- Their assessment will be helpful in correlating vehicle cantilever loads measured during the wind loads test program with those empirically predicted on the basis of wind tunnel data and analytical methods. This type of comparison is necessary to generate confidence in the validity of ground wind loads prediction methods.

- The existence of significant wind interference effects between the tower and vehicle has been amply demonstrated by wind tunnel test (Farmer and Jones, 1966). However, this mutual interference wind field has not been isolated to any significant degree. Hopefully, analysis of this wind field data will provide insight to the particular flow mechanics leading to interference-augmented vehicle cantilever loads.

- Study of the interference flow field should permit reasonable estimation of the degree of interference for analyzing wind data measured by anemometers mounted on the launcher umbilical tower, thus leading to recommendations regarding their placement to obtain more representative measurements of the local ambient free-stream flow.

Wind field analyses of interference, or wind shadow effects, have been made by several investigators to determine requirements for minimizing errors induced (i.e., measured distorted flow) because of nearby and/or supporting structures. Moses and Daubek, 1961, are generally given credit for first quantifying the type and magnitude of errors in wind speed measurement caused by structures or other obstacles. Subsequent investigations, both in the wind tunnel and in full scale, have consistently confirmed their results (Meyer, et al., 1965; Hsi, et al., 1965; Gill, et al., 1967). Induced variations in the wind velocity as measured in the lee of typical anemometer support structures have shown that the shape of the structural cross section and the solidity ratios are parameters of major importance (Gill, et al., 1967). Studies have been made of the three dimensional flow in the lee of truss type structures. The results have shown that the structure seems to lose its influence rapidly on the mean transverse velocity with downwind distance. These results have been determined by comparing the transverse velocity

PRECEDING PAGE BLANK NOT FILMED.

profiles across the wake at the same downwind distances but at different vertical points. Downstream distances as close as 1.5 tower widths have shown this similarity of profiles in wind tunnel tests by Meyers (1965). The results of studies have also shown that Reynolds number effects are not of primary importance, especially within practical wind velocity ranges. The relative unimportance of Reynolds number is understandable from the viewpoint that a truss type of tower cross section generally consists of structural members having sharply defined corners and lips. For such cross sections the flow separation points are well defined and stationary. This is the case for a flat plate normal to the free stream and, as is well known, the drag coefficient for such a plate is nearly independent of Reynolds number.

Two additional aspects of the flow field not considered in this study are the possible coupling effects that may occur between the vehicle oscillatory response and the nonsteady interference flow field; and possible coupling between normal atmospheric turbulence, and the turbulence induced by flow interference.

## TEST CONDITIONS

Full-scale test data describing the local wind field about the Saturn V launcher umbilical tower were obtained during the 1966 Saturn V Ground Wind Loads Test Program at Launch Complex 39 at KSC, Florida. Although the Ground Wind Loads Test covered a period from late May, 1966, until about mid-October, 1966, only ground wind data obtained from 25 May through 25 June were used in this study. While four weeks of meteorological observation is not sufficient to permit general predictions of ground wind behavior, it has provided a significant basis for establishing the major characteristics of mutual interference effects between the Saturn V and the LUT upon the local flow field. A chart showing this data availability is given in Figure 1.

The LUT is an integral structure designed to help support the Saturn V space vehicle in its vertical launch attitude, and to provide access to the vehicle in this position. The LUT tower does not support the vehicle, as loads imposed by the umbilical arms are considered to be negligible. In the on-pad position the LUT vehicle plane of symmetry is in the north-south direction, with umbilical tower to the north. The launcher presents a rectangular solid configuration to the wind environment measuring 7.6 by 41 by 91 meters (25 by 135 by 160 ft), with the deck-zero level 14 meters above the launch pad. The umbilical tower is a truss-type structure having rectangular base dimensions 37 by 18 meters (113 by 60 ft). The rectangular cross section decreases linearly with height to minimum rectangular cross section of 12 by 12 meters (40 by 40 ft) at a height of 24 meters (80 ft) above deck zero. This cross section is maintained to the top of the truss structure 116 meters (380 ft) above deck zero. A 25-ton crane is mounted atop the

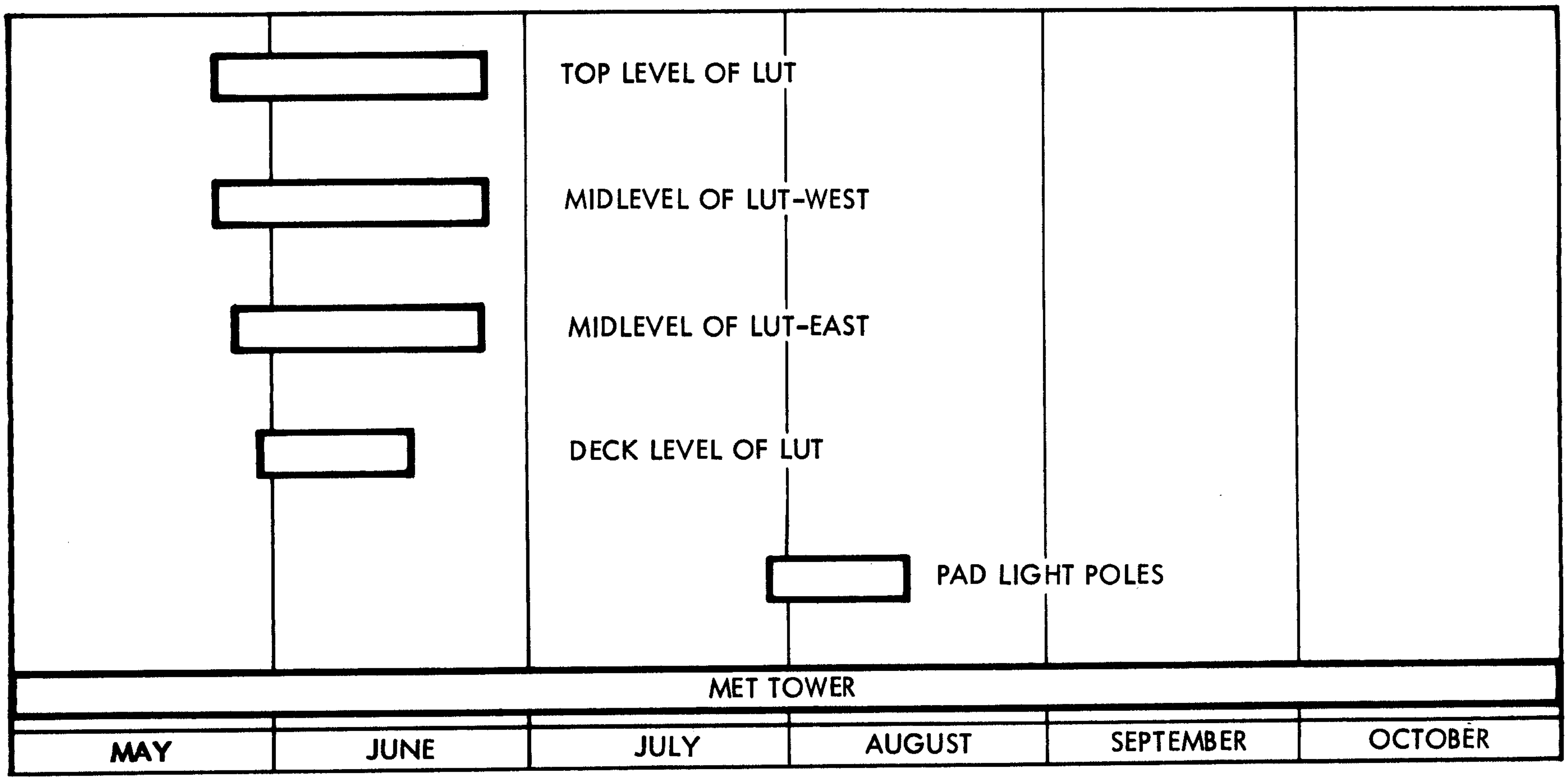


Figure 1. Available Ground Wind Data Observed at Launch Complex 39A and at NASA's Isometer Meteorological Tower

tower, measuring approximately 39 meters in length (120 ft), 6 meters in maximum height (20 ft), and 6 meters in maximum width (20 ft). A side view is shown in Figure 2. In addition to the structural framework, personnel railings extend around the tower at each deck level. An elevator housing measuring 2.7 by 5.5 meters in cross section (9 x 18 ft) and a personnel staircase run the length of the tower in the north central portion of the tower (positioned on the launch pad). In addition, several conduits extend the length of the tower along the north side effectively blocking the air flow over approximately 50 percent of its breadth. The structural framework and railings alone account for about 10 percent solidity, and together with conduit, housing, and other paraphernalia, the net solidity is estimated to be 60 to 70 percent.

The east-west launch pad elevation is essentially a trapezoid of bases 152 and 91 meters (500 and 300 ft) and a height of 15 meters (50 ft). The north-south elevation is not so conveniently defined, being characterized by the gradually inclined crawler way from the south, and the service access ramp extending approximately 300 meters (1000 ft) to the northwest. Discounting these principal features, this elevation would also be trapezoidal with bases of about 122 and 214 meters (400 and 700 ft). A top view and east-west planform are indicated in Figure 3.

Although some wind data were gathered while the Saturn V LUT was in transit between the vertical assembly building (VAB) and Pad 39A, the preponderance of wind data were obtained with the Saturn V - LUT in the launch configuration atop Launch Pad 39A. The Mobile Service Structure (MSS) was placed in service in October; it did not influence the test data from the LUT-mounted anemometers. All the pads in Launch Complex 39 are oriented in the same direction, with the plane of vertical symmetry running north and south. Launch Pad 39A is the southernmost of the two existing pads in the launch complex. It is approximately one-half mile from the Atlantic coastline which runs generally northwest-southeast at this point. Banana Creek lies generally to the south and west of Launch Pad 39A. Surrounding terrain is generally flat and sandy with low lying (about one meter in height) scrub palmetto being fairly abundant. What appears to be a sand bar approximating a 3- or 4-meter levee closely parallels the coastline in both directions as far as can be seen by naked eye from Launch Pad 39A.

The nearest sizeable structure is the VAB situated about three and one-half miles west-southwest of Pad 39A. Somewhat smaller structures (vehicle integration buildings) exist farther south within the Titan III C Launch Complex.

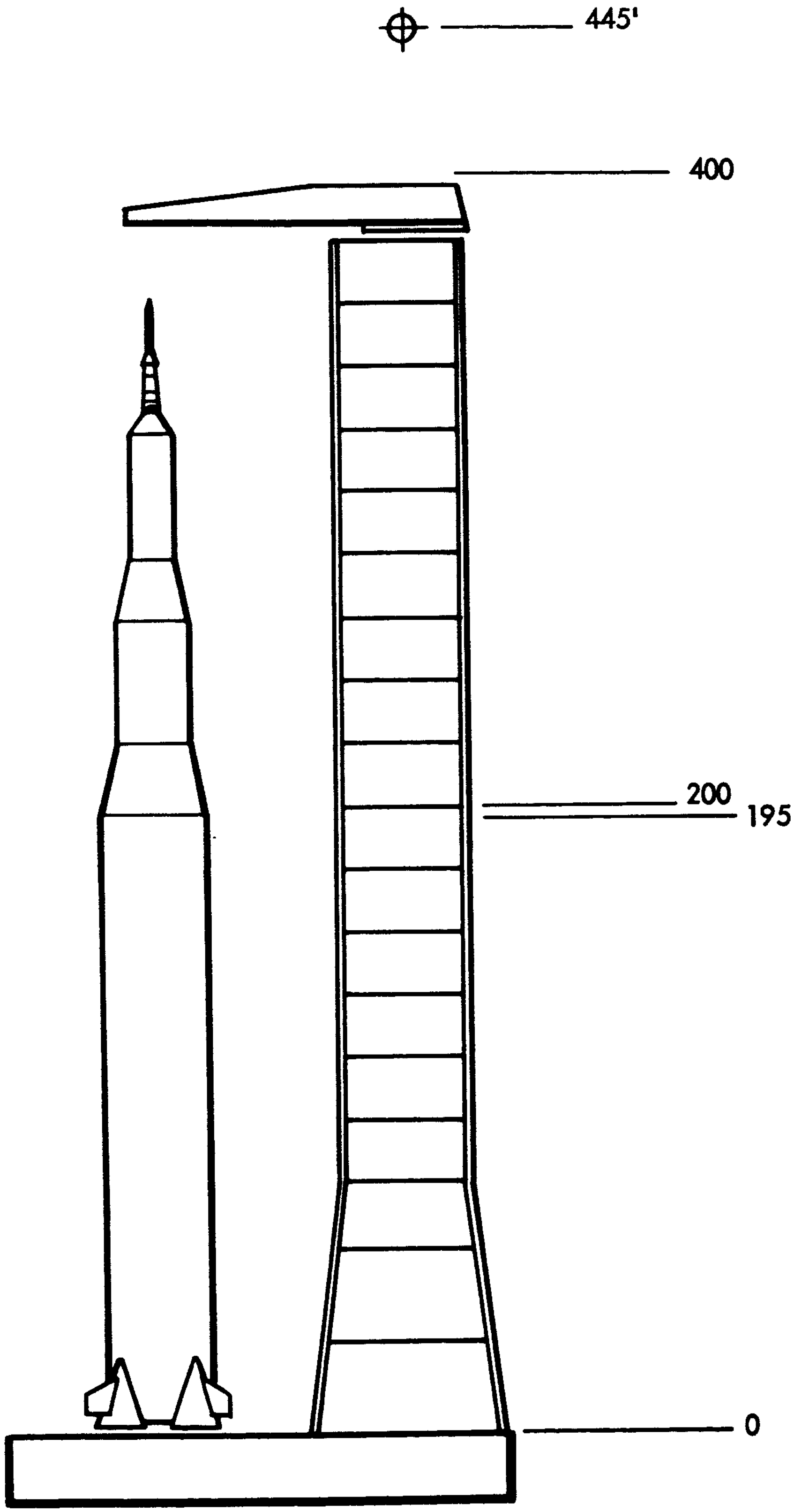


Figure 2. Saturn V Launcher Umbilical Tower

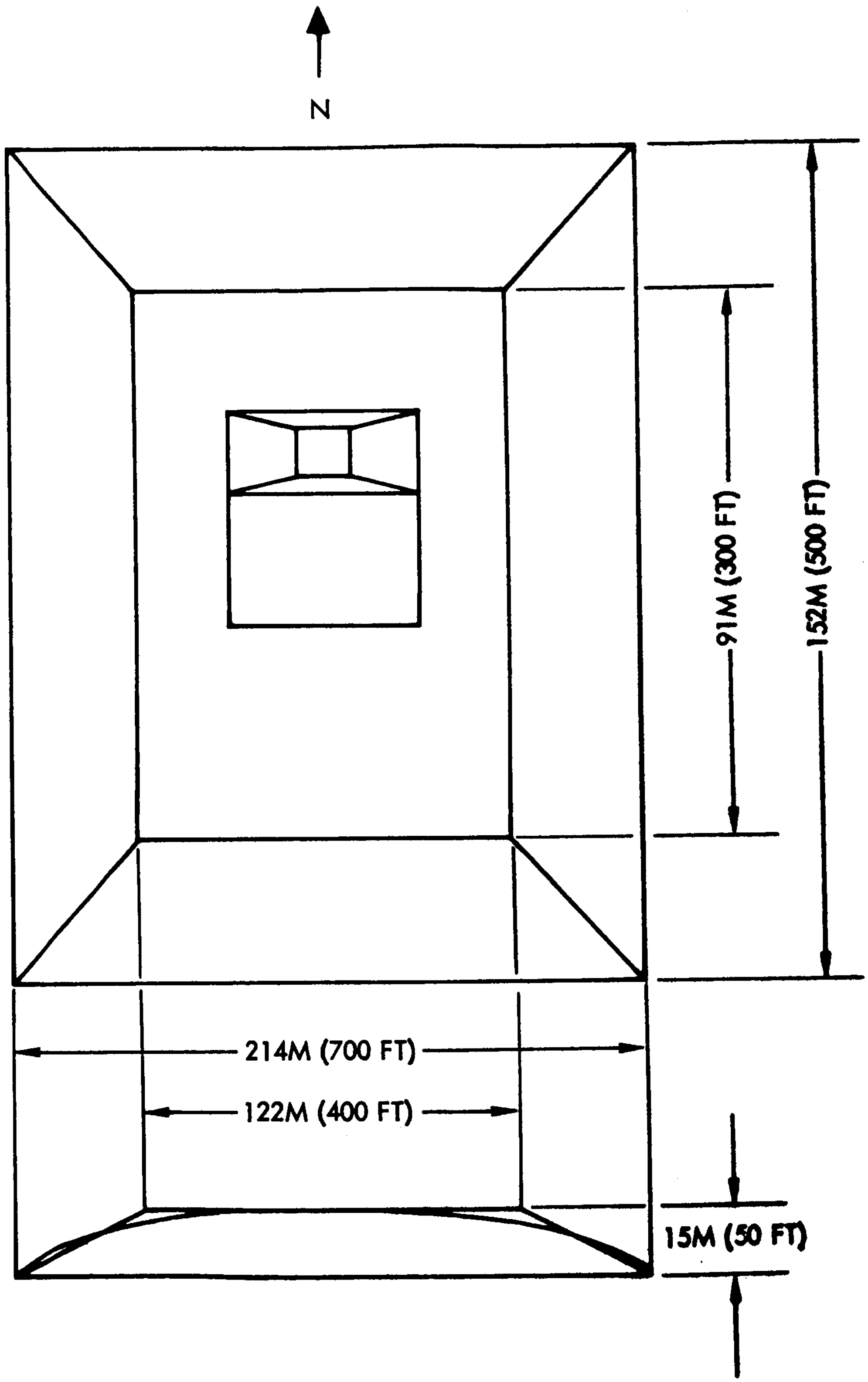


Figure 3. Basic Dimensions of Launch Pad 39A, Vehicle and LUT Shown in Plan View

## INSTRUMENTATION

During the test, four Model C1-14 Climet anemometers (Reference 1) were located on the LUT as shown in Figure 2. The highest (top level) was on a 12-meter (40-ft) mast surmounting the crane and on the centerline of the umbilical tower. This anemometer was 136 meters (445 ft) above deck level and 164 meters (537 ft) above natural grade.

Two anemometers were located on 25-foot booms extending horizontally outward from the tower, at the two corners farthest from the vehicle, and parallel to the side farthest from the vehicle. These anemometers were 59 meters (195 ft) above deck level and 87 meters (287 ft) above natural grade. The fourth anemometer was mounted on a 3.4-meter (11-ft) high mast on the deck of the launcher. This mast was located on the outer periphery of the southwest corner of the pad-positioned launcher attached to two bars of the personnel railing.

Additional wind speed and azimuth data were also obtained from two anemometers, identified as the PLP's, for pad light pole. These were mounted on individual light poles 18 meters (60 ft) above natural grade, and located 300 meters (1000 ft) northwest and southeast of the launch-positioned Saturn V body centerline. The PLP anemometers were also the C1-14 Climet type. Their data were recorded in a manner similar to those for the LUT-mounted anemometer. As shown in Figure 1, comparison of simultaneous PLP and LUT data was not possible.

For all of these anemometers, wind speed (mph), and direction were recorded continuously on a 24-hour basis by 2-channel Esterline-Angus paper strip chart recorders at a chart speed of .076 meters (3 inches) per hour. A sample of this chart data analyzed in this study is shown in Figure 4. Down time for maintenance and calibration adjustment caused some interruption of data. Wind azimuth was measured clockwise from true north to the approaching wind vector.

Perhaps the most serious interruption to the data was that caused by crane movement invalidating wind direction data from the top-level LUT wind vane. Thus, when the crane was not in its normal orientation (i.e., north-south with the boom tip over the vehicle) spurious directions were obtained. This deficiency was especially critical since the top-level wind direction data were the data expected to contain the least contamination from flow interference effects, and would therefore be expected to provide the best set of reference data for comparison with data from the remaining LUT anemometers.

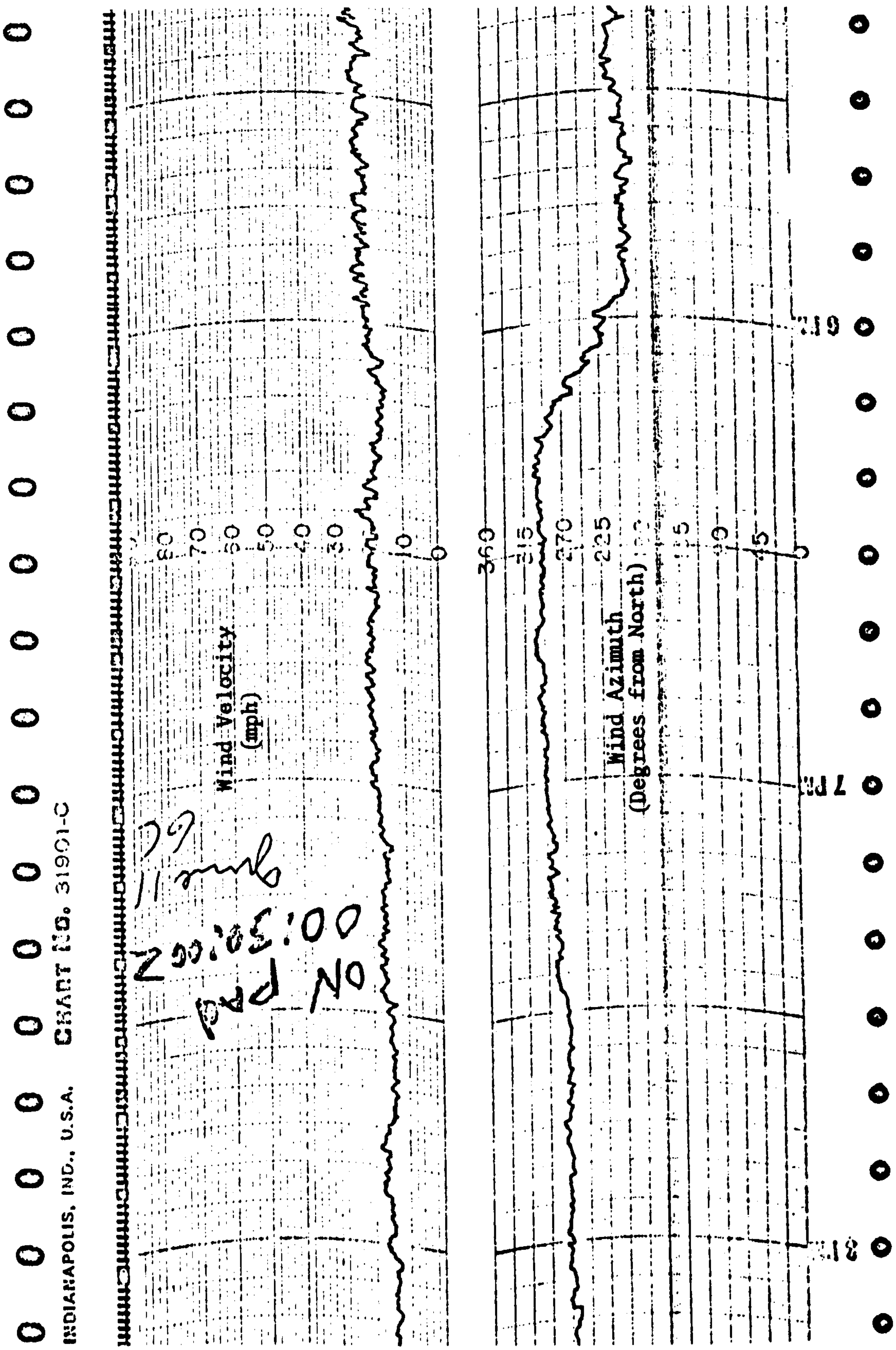


Figure 4. Sample of Paper Strip Chart Data From Wind Load Test Program

For further comparison, computer listings of climatological data from NASA's 150-meter meteorological tower at Cape Kennedy were utilized to obtain concurrent mean values of wind direction and speed at the 150-meter (500 ft) level. These data, also obtained from C1-14 Climet anemometers (Reference 1), consisted of 10-minute mean values around the hour (i.e., from 5 minutes before until 5 minutes after the hour) and maximum values for the same time periods. This meteorological tower is located approximately three and one-half miles west-northwest of Launch Pad 39A. The form of data did not permit analysis of low periodicities near the range of vehicle bending frequencies. Such analyses would require the more detailed data recorded on magnetic tape, which were not considered a part of this study.

In evaluation of these ground wind data, as recorded on dual-channel paper strip charts, emphasis was placed upon the selection of time points characterized by relatively steady wind. Wherever possible high wind conditions were chosen. Winds from the north occurred the least often during the test period, with easterly and westerly winds predominating. The data points were read directly from the strip charts. Errors incurred in both time and ordinate values by reading, roundoff, and slide rule conversion were not evaluated. For wind direction readings, a separate graduated scale was placed at the selected point, first spotted in by pencil, since the given scale was difficult to interpolate.

## EVALUATION AND ANALYSIS OF TEST DATA

The basic question to be answered by analysis of the test data is that of the nature and extent of the wind interference owing to the terrain and structures in the near vicinity of the PLP- and LUT-mounted anemometers.

### Anemometer Above Crane

Of the four anemometer locations employed on the LUT during the ground wind loads test, the one located on the 12-meter mast atop the crane would be expected to provide the most accurate reading of local free stream. Certainly it is the one least obstructed in all azimuths.

The only available comparative data for that approximate height, which data may *a priori* be considered more reliable than the LUT data for exhibiting free-stream characteristics, are those gathered concurrently from NASA's 150-meter meteorological tower. One would not expect the instantaneous readings from the LUT and the meteorological tower to agree, considering their separation (3-1/2 miles). One would expect, however, that the long-duration averages would be in fair agreement, with the agreement improving under stronger and steadier winds. A sample of this long-duration data is presented in Figures 5 through 7. Figure 5 shows ten-minute average directions at the LUT upper-level anemometer versus synchronized ten-minute average directions at the 150-meter level of the meteorological tower. As much as possible in all of this data analysis, the higher wind speeds were favored. Attempts were made to cover all azimuths; however, it is apparent that easterly and westerly winds predominated for the test period in question. Rather clearly this plot does not prove any appreciable average disagreement. The ten-minute average speed comparison between the LUT upper level and meteorological tower 150-meter level anemometers is shown in Figure 6.

The fitted line of Figure 6 was arrived at by sectioning the horizontal axis into one-meter-per-second intervals, for each interval taking a line of unit slope that divides the points in that interval into two equally large groups, marking where that line intersects the mid-abscissa of the interval, and hand-fitting a straight line through these marks. In addition to their ease of application, the main property of these "median methods" is their relative unresponsiveness to spurious extreme points when compared with "arithmetic mean methods" like least squares. Here one sees the improvement of correlation (reduction of scatter) at higher speeds. As it should, the fitted line of Figure 4 does pass through the centroid of data points with an approximate 45-degree slope. However, there is an apparent and distinct deviation of this line from the line of unit slope through the origin (shown dashed). This deviation ranges from about 3 percent at high wind speeds as measured at the meteorological tower to as much as 30 percent at the lower speeds. The actual wind speed difference ranges from about .4 meter/sec to 1 meter/sec respectively.

While the procedure used to determine the fitted line contains some arbitrariness, it is also clear by simple visual inspection that the unit slope line through the origin does not represent the data mean. Several possible explanations exist for some systematic bias in these data, none of which satisfactorily accounts for the type of deviation indicated.

1. The LUT upper level anemometer elevation is 12 meters higher than the 150-meter anemometer on the meteorological tower. Using the wind profile law

$$\frac{U_2}{U_1} = \left(\frac{z_2}{z_1}\right)^{.2} \tag{1}$$

the increase in speed at the LUT upper-level anemometer would be about 1.5 percent.

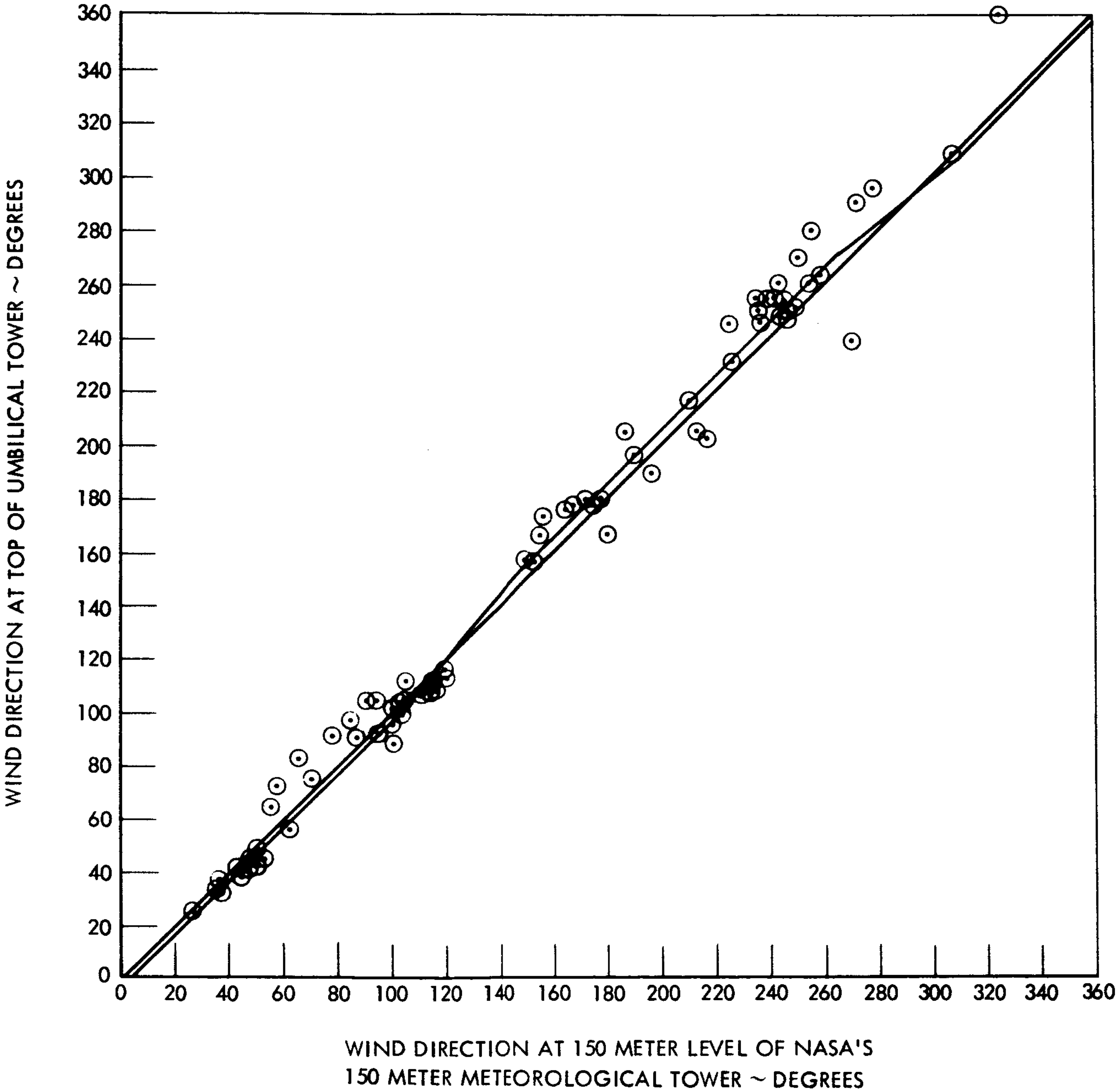


Figure 5. Comparison of Mean Wind Directions for the 150-Meter Level at NASA's 150-Meter Meteorological Tower Versus 445-Foot Level LUT Data, Ten-Minute Averages

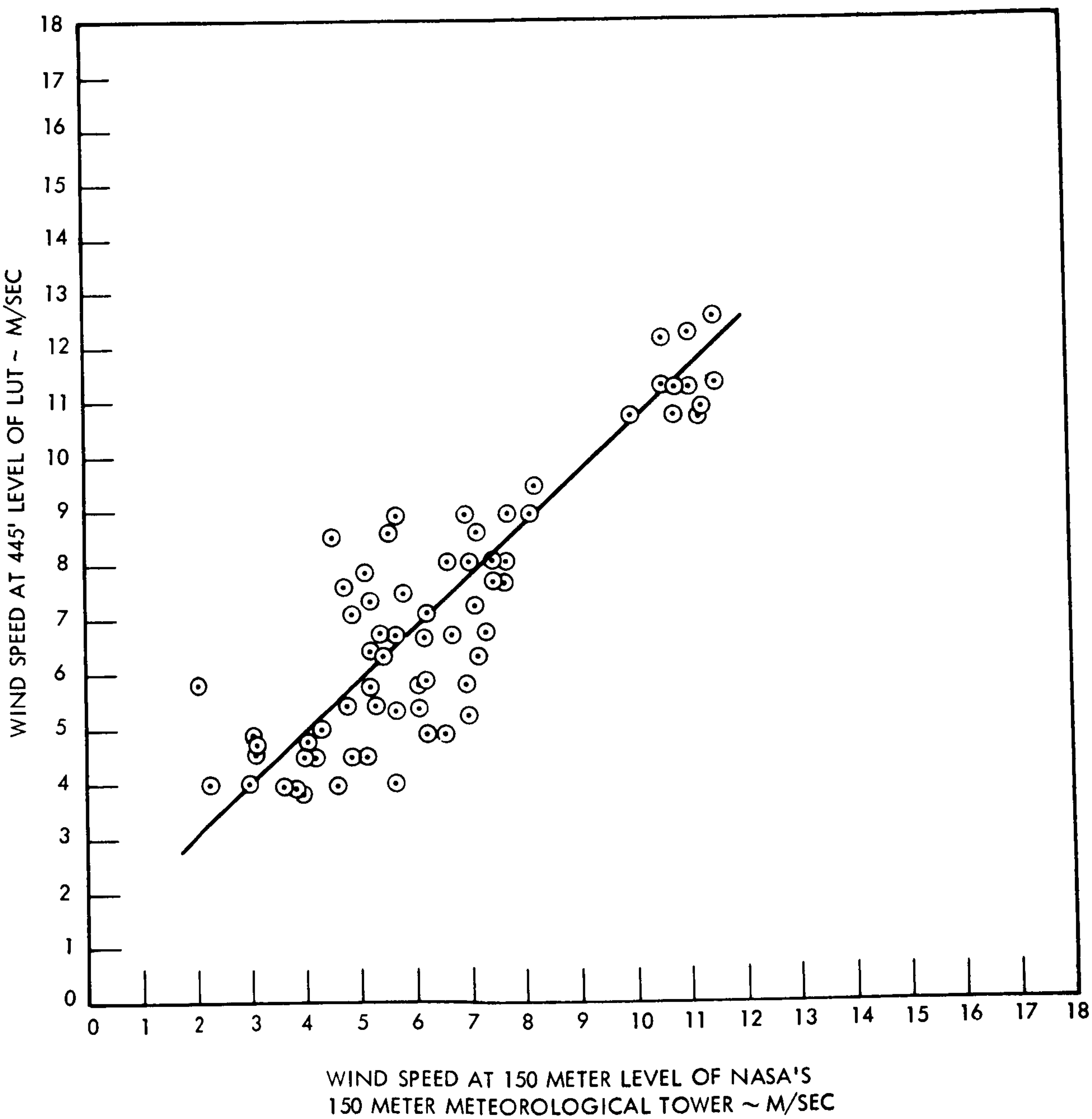


Figure 6. Comparison of Mean Wind Speeds for the 150-Meter Level at NASA's 150-Meter Meteorological Tower Versus 445-Foot Level LUT Data, Ten-Minute Averages

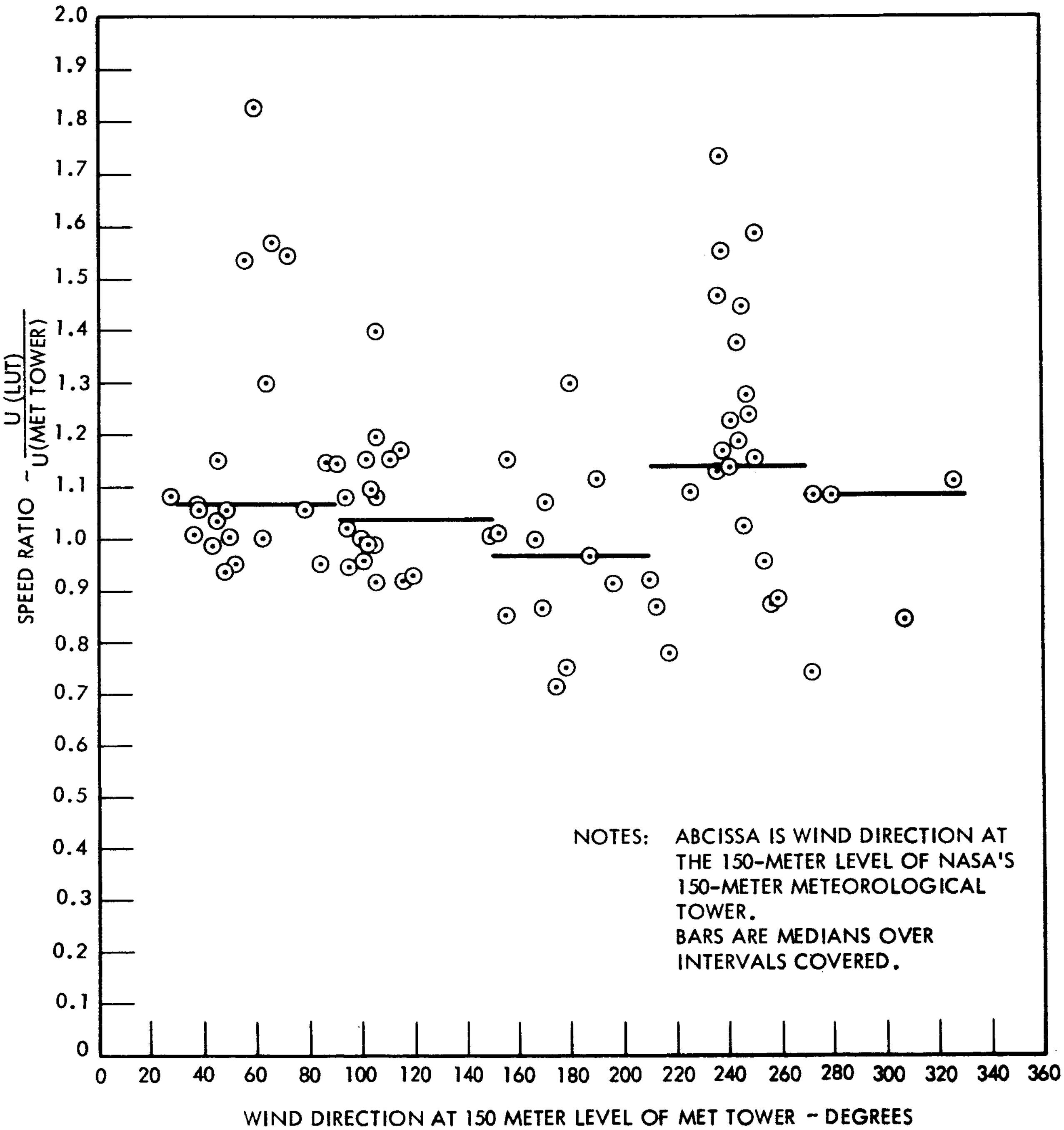


Figure 7. Speed at 445-Foot Level of LUT Divided by Speed at the 150-Meter Level of NASA's 150-Meter Meteorological Tower

2. East-west elevation profile of Launch Pad 39A presents a trapezoidal cross-section of 16 meters (50 ft) height. Using a conservative two-dimensional potential flow assumption, a speed up of about 2 percent as shown in Figure 8 is calculated at the LUT upper level for flow over an equivalent elliptical cross section. This idealized flow is analyzed in greater detail in a subsequent section.

3. A recommendation is made by Gill, et al., (1967) on the basis of observed experimental wind tunnel data for locating an anemometer atop a circular stack without effluent. It is stated herein that ". . . the accuracy of speed and direction measurements can be markedly improved by locating the top set of wind sensors 1/2 D [diameter] or higher above the stack." In the present case, the upper-level anemometer is located about 12 meters above the LUT. Cross section of the LUT is 13 meters square at all heights above the 26-meter level (from Deck Zero). Thus, this recommendation is apparently satisfied.

4. The 25-ton crane atop the LUT (see Figure 2) does represent an additional obstruction of sizeable dimensions. It is approximately 40 meters in length, with maximum cross section 6 meters square. Its maximum effect is estimated by assuming a 6-meter diameter circular cylinder in two-dimensional potential flow. In terms of this cylinder, the anemometer is located at a distance of 5 radii along the vertical centerline. The local velocity at this point is

$$\frac{U}{U_o} = 1 + \frac{1}{(y/R^2)} = 1.04$$

This effect would be felt most strongly for winds within the azimuth range of 90 degrees ±30 degrees, and 270 ± 30 degrees. Approximately half the data points were found to represent wind conditions in this range.

5. Again considering winds primarily from the east or west, the basic breadth dimension may be greater than that of the tower. It is possible that the ratio of tower plus vehicle semi-breadths to their centerline spacing is sufficiently near unity that some blockage may occur, causing significant speed up in the flow up over the extremities. In this case, a pertinent dimension may be the tower-vehicle centerline spacing together with some porosity parameter such as the ratio mentioned above.

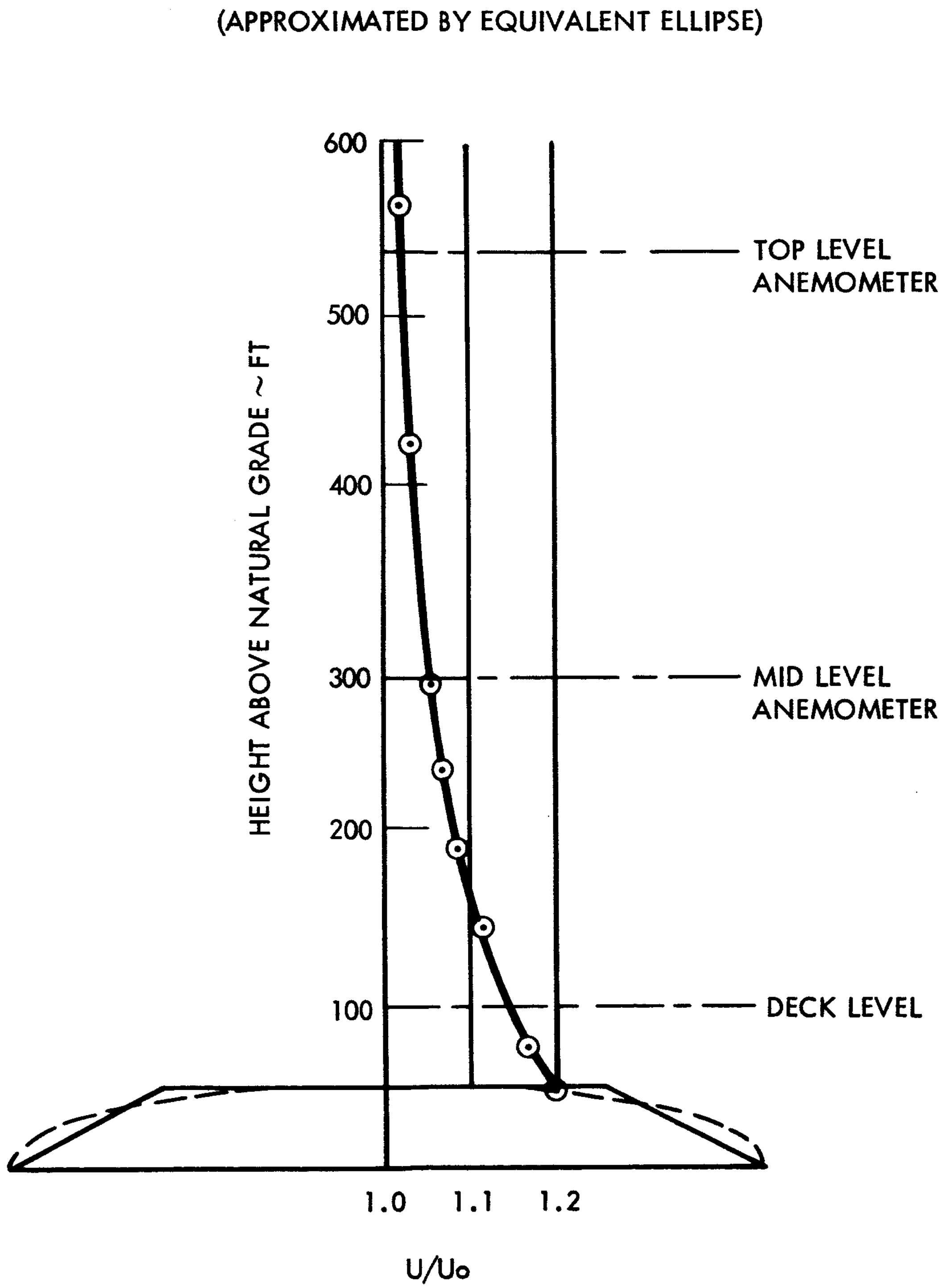


Figure 8. Wind Profile of Steady Two-Dimensional Potential Flow Over Pad Alone, East-West Section (Approximated by Equivalent Ellipse)

All of these possible explanations (1—5) would produce a deviation proportional to free stream velocity. Unfortunately this does not appear to be the type of deviation indicated in Figure 4. It is statistically possible, of course, that the data points selected (about 75 total) coincidentally exhibit the relationship obtained. In this event, it must be concluded that more data points are needed.

In a further attempt to correlate the concurrent data from LUT upper-level anemometers and the 150-meter meteorological tower data, the velocity ratios were plotted against the 150-meter meteorological tower azimuths. These are shown in Figure 7. Extremes in the scatter, as would be expected, occurred at low velocities (less than 6 meters/sec). Median values over 60-degree intervals were determined, and are shown as discontinuous bars over the interval spans. Again, a small but distinct speedup at the LUT upper level is indicated at all azimuth ranges except for the interval centered at 180 degrees azimuth. In view of the several contributing factors indicating some acceleration in the flow, it is concluded that a speedup on the order of 5 to 10 percent should be allowed.

Midlevel Anemometers

Analysis of the data for these locations aims to determine the mean shift in the free stream wind vector at this level. The only available estimate of the free stream vector in question is based on the strip chart data for the anemometer at the top of the LUT. It is felt that the raw readings from the top of the LUT will better estimate the midlevel free stream if they are scaled down to the midlevel of the LUT by means of the wind profile law (Equation 1) previously given.

Two types of plots were prepared: (1) ratio of speed at either of the midlevel anemometers to speed at the top anemometer (scaled or unscaled to midlevel) as a function of azimuth at the top anemometer, and (2) azimuth at either of the midlevel anemometers as a function of azimuth at the top anemometer.

Speed Ratio Plots

Figures 9a, 9b, 10a, and 10b are scattergrams of the speed ratio $U_{MID}/U_{TOP}$ with $U_{TOP}$ uncorrected for height. Least-squared error curves, discussed in Appendix C, were determined for these scattergrams and are shown in Figures 9a and 10a. Each scattergram in Figures 9b and 10b is hand-fitted with a curve passing through the median ratios in 10-degree compass intervals. Figure 9 corresponds to the east midlevel anemometer, Figure 10 the west. Physical symmetry about the north-south centerline of the vehicle LUT assembly leads one to expect mirror behavior of the two midlevel anemometers. Figure 11 compares the west anemometer median curve

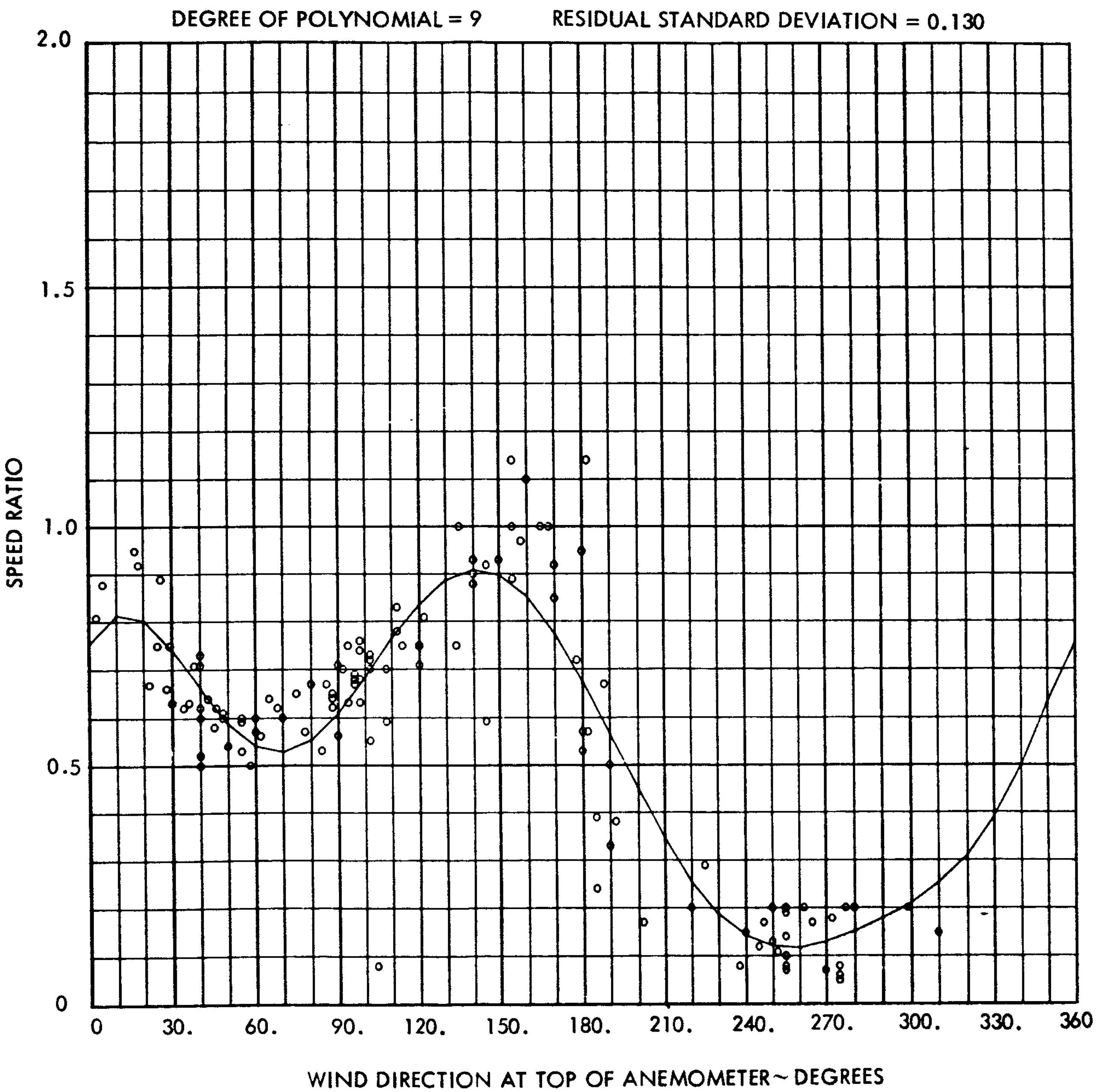


Figure 9a. Speed Ratio $U_{MID}/U_{TOP}$ for East Anemometer

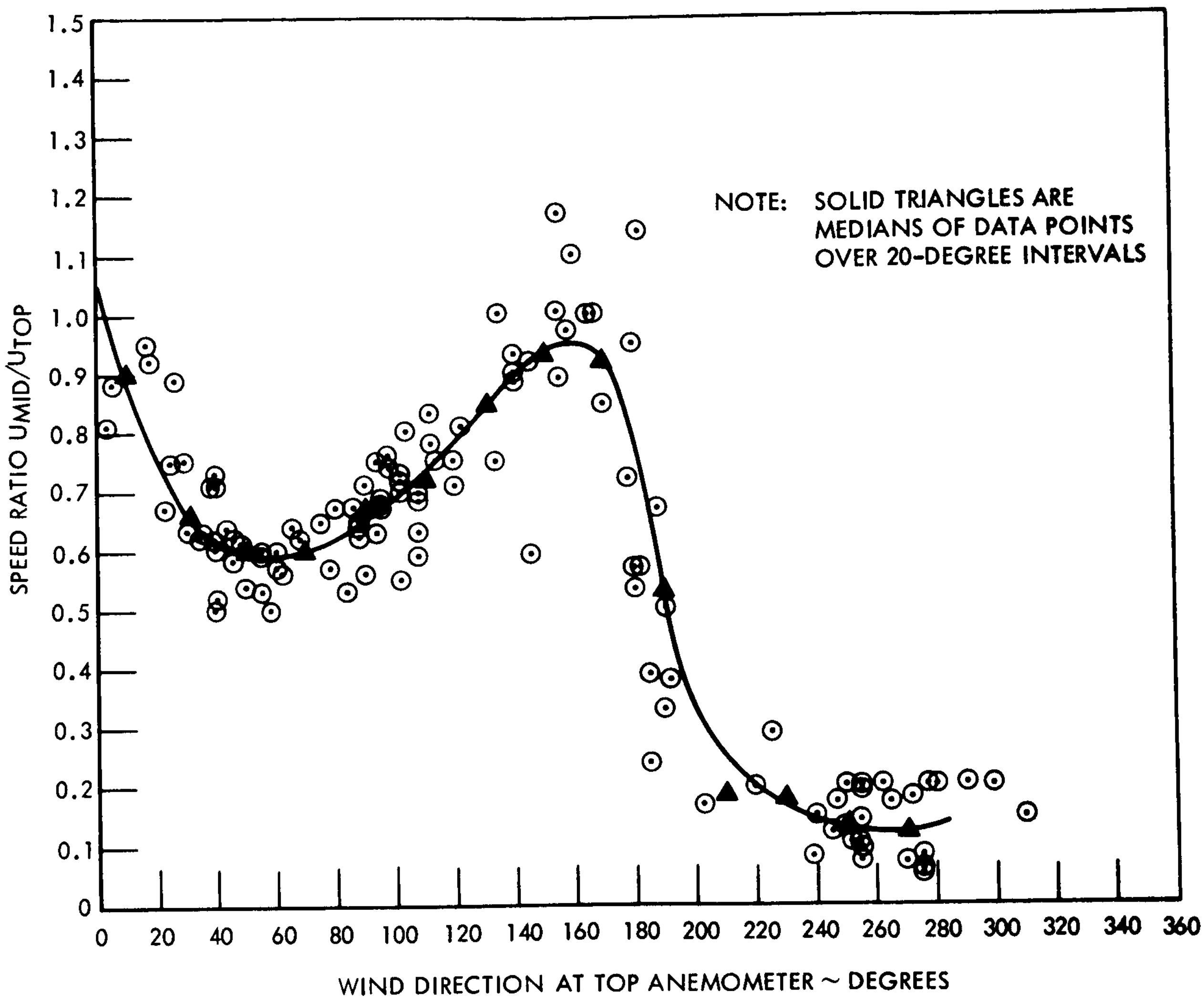


Figure 9b. Speed Ratio $U_{MID}/U_{TOP}$ for East Anemometer

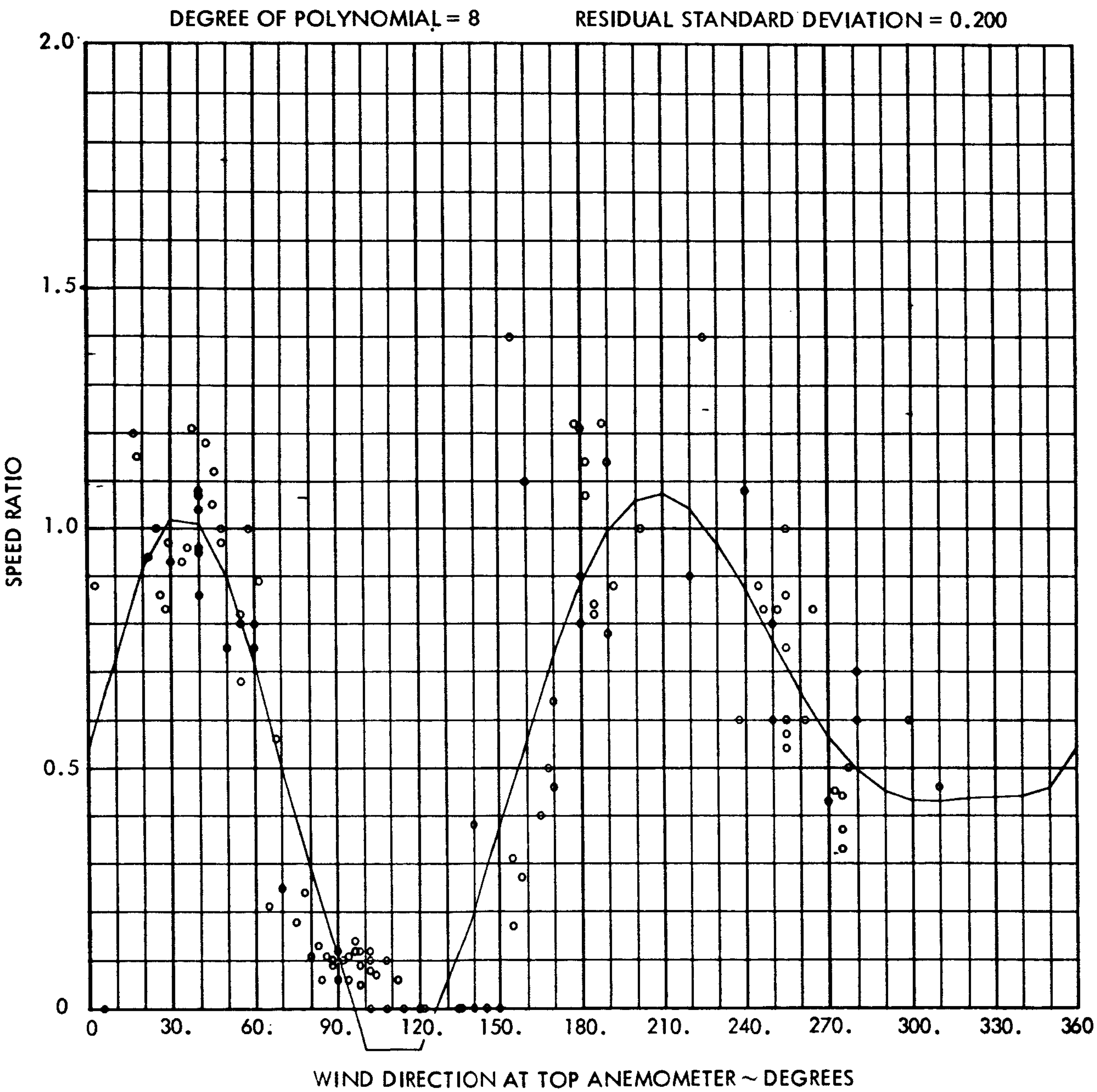


Figure 10a. Speed Ratio $U_{MID}/U_{TOP}$ for West Anemometer

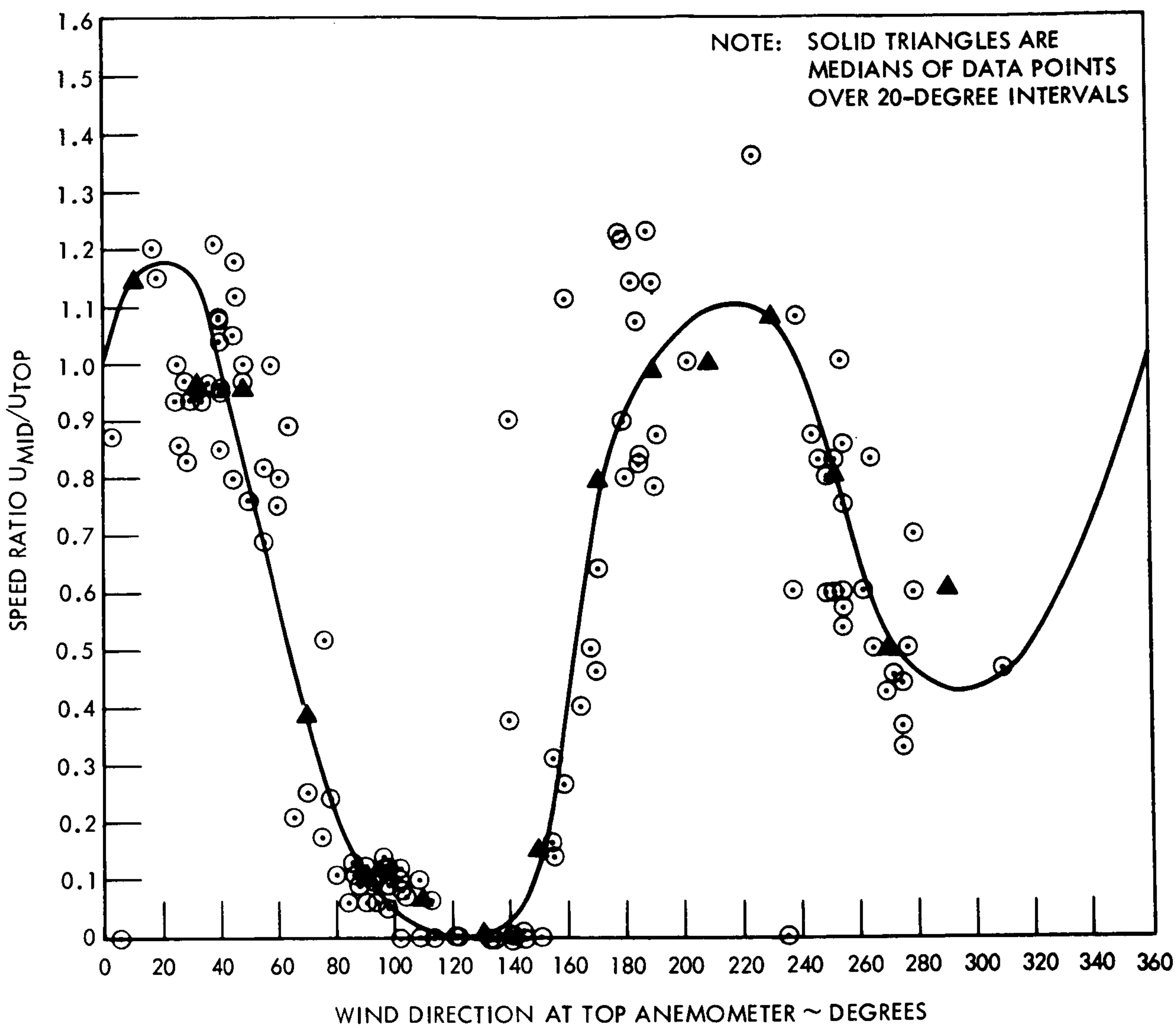


Figure 10b. Speed Ration $U_{MID}/U_{TOP}$ for West Anemometer

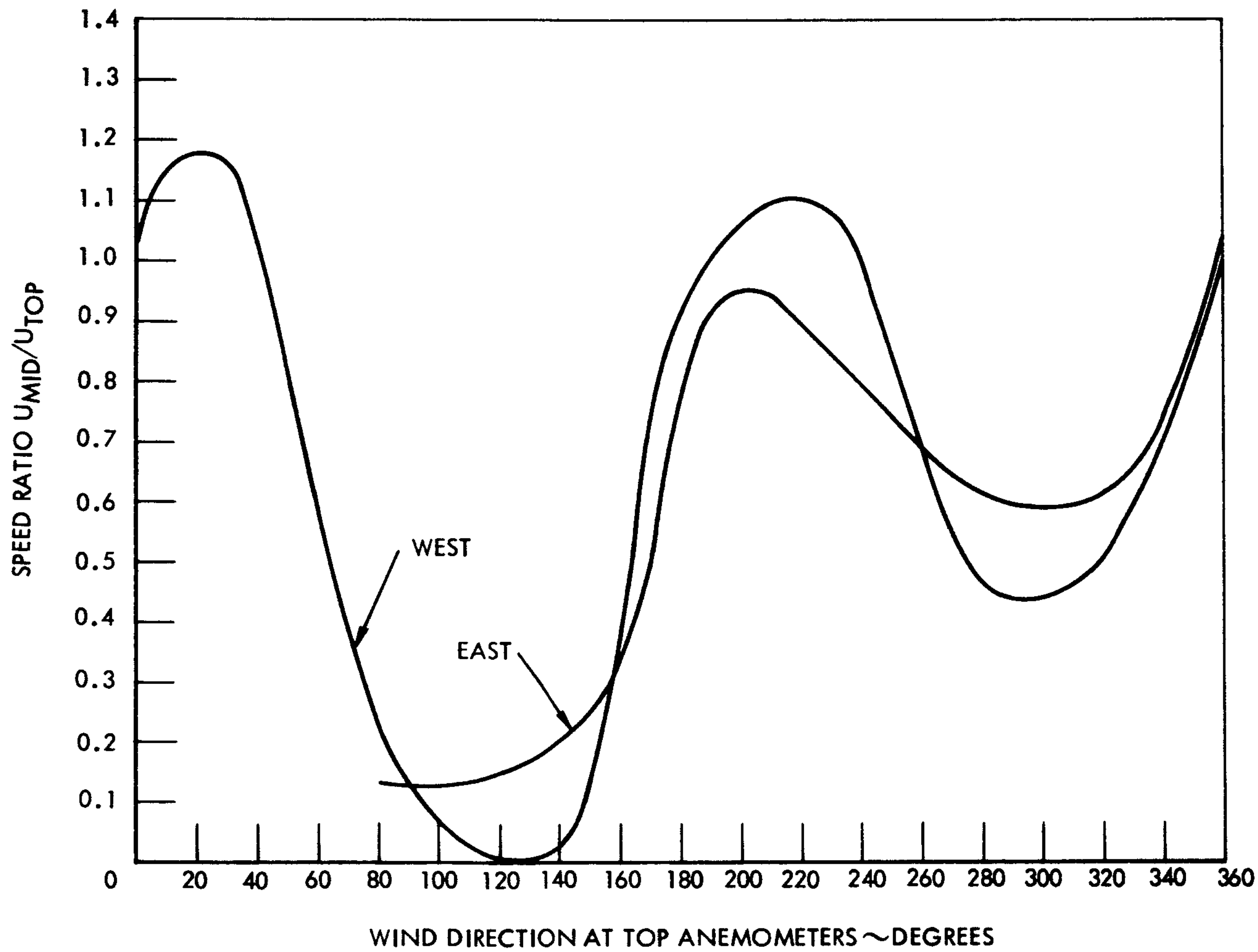


Figure 11. Comparison of Speed Ratio Curves for Midlevel Anemometers, Referred to West Anemometer

with the mirror image of the east anemometer median curve. Apparently the mirror assumption is valid. Hence, in Figures 12a and 12b, data from the two anemometers are pooled with reference to the east anemometer and a curve of the same description as in Figures 10 and 11 is generated.

A polar plot of this curve with the height correction applied to $U_{TOP}$

i.e., $\frac{U_{MID}}{U_{TOP}} = \left(\frac{287}{537}\right)^{.2} = .882$, is shown in Figure 13. It has a nearly

symmetric cardiac shape and plainly shows:

1. Shadowing down to almost zero speed on the leeside of the LUT (azimuth around 250 degrees)

2. Partial stagnation down to .66 of free stream on the windward side of the LUT (azimuth around 60 degrees)

3. Increasing speed as the air flows around the LUT in such a manner that the anemometer boom is athwart the stream (azimuth around 160 degrees or 340 degrees)

Further correlation of this speed ratio plot is obtained from experimental data in the literature. Gill, et al. (1967), report upon wind tunnel tests of triangular and circular cross-sectional tower structures typical of those used for anemometer supports. For the triangular tower, speed ratio plots are presented for shadow densities (ratio of projected frontal area to total enclosed frontal area) of 26 percent and 100 percent. Their test results include those for anemometer arrangement corresponding to that employed for the LUT midlevel. In these tests, an anemometer was mounted on a boom extending outward in the plane of one face a distance of 1/2 tower breadth. In Figure 14 speed ratio plots obtained by Gill, et al., for these particular tests are superimposed upon the plot obtained for the LUT midlevel. In these plots, the curves of Gill, et al., have been rotated so that azimuth relationship to anemometer location are the same as those for the LUT data. As required, both stagnation and speedup are indicated in the same general ranges. The LUT data show a pronounced flatness compared to the triangular tower data.

A point of special interest is the value of speedup at zero azimuth. From separated flow observations, it is known that with the flow directly abutting one face, separation will be triggered at the edges of the face. Roshko (1954) in his application of free streamline theory has shown that flow streamlines are primarily determined by the body shape ahead of separation and the wake width. Hence for winds from zero azimuth, the

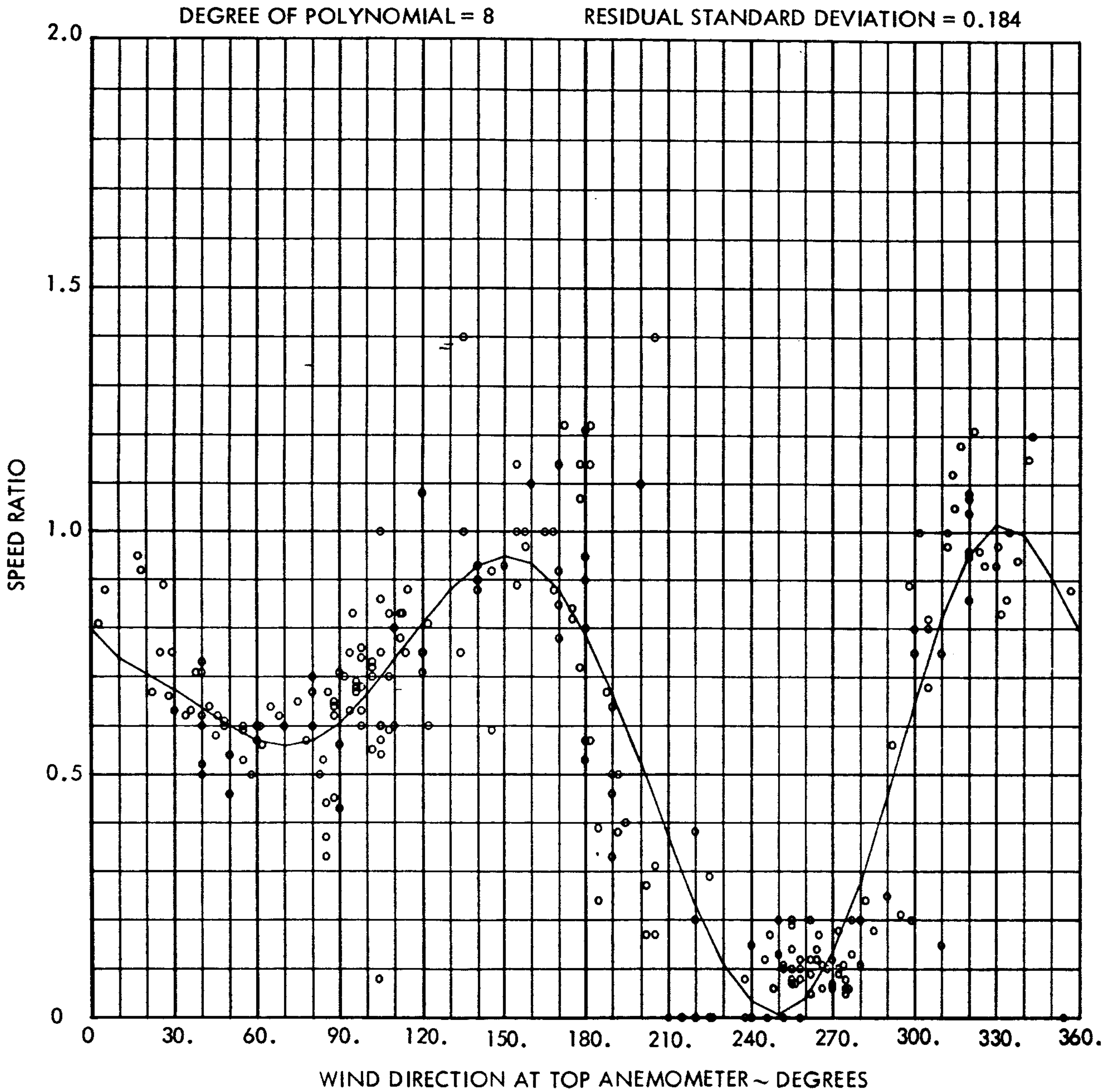


Figure 12a. Wind Speed at 195-Foot East Anemometer Divided by Wind Speed at 445 Feet, Composite of Data From East and West Anemometers, Fitted by Least Squared Error Curve

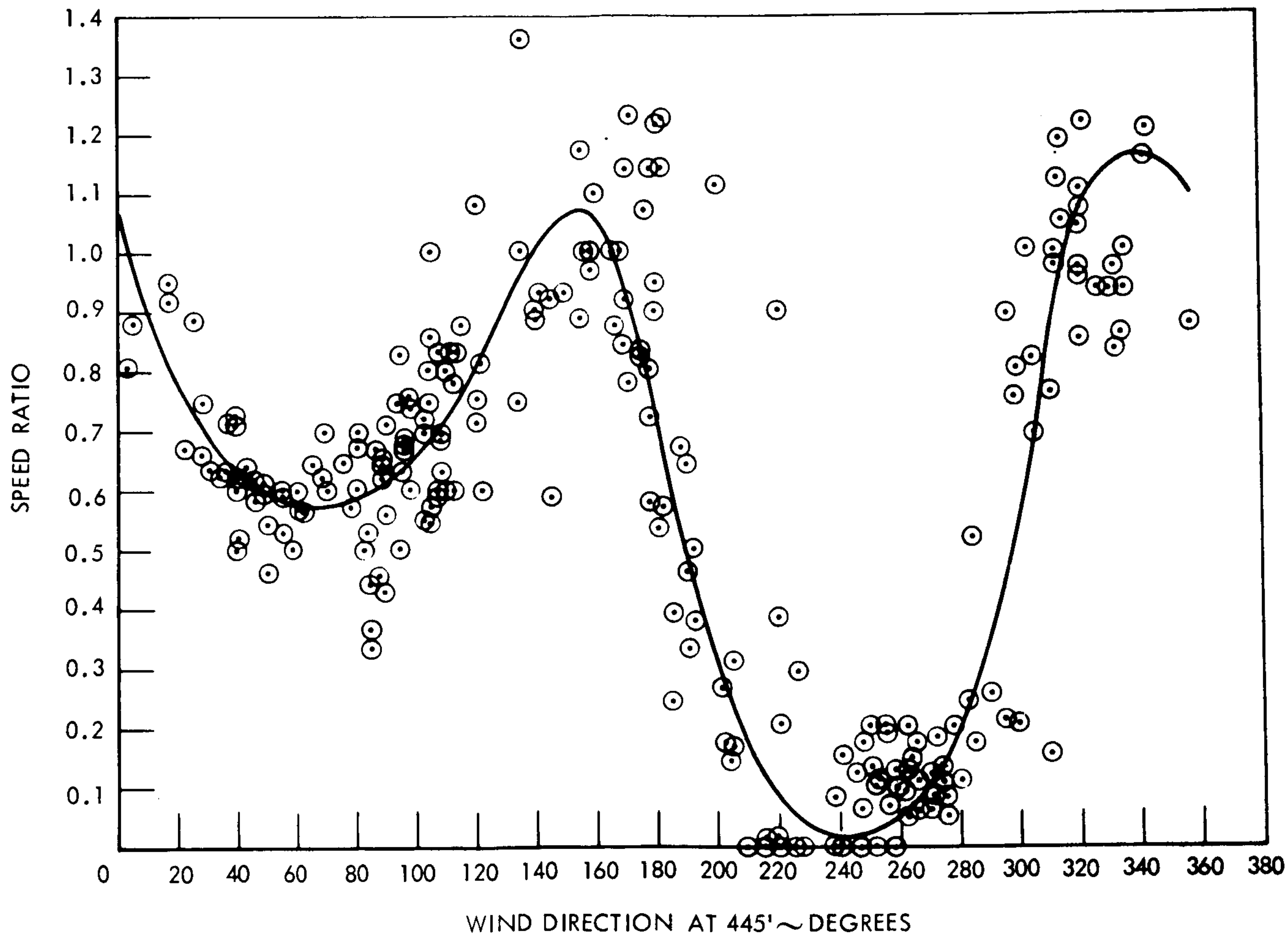


Figure 12b. Wind Speed at 195-Foot East Anemometer Divided by Wind Speed at 445 Feet, Composite of Data From East and West Anemometers, Fitted by Median Curve

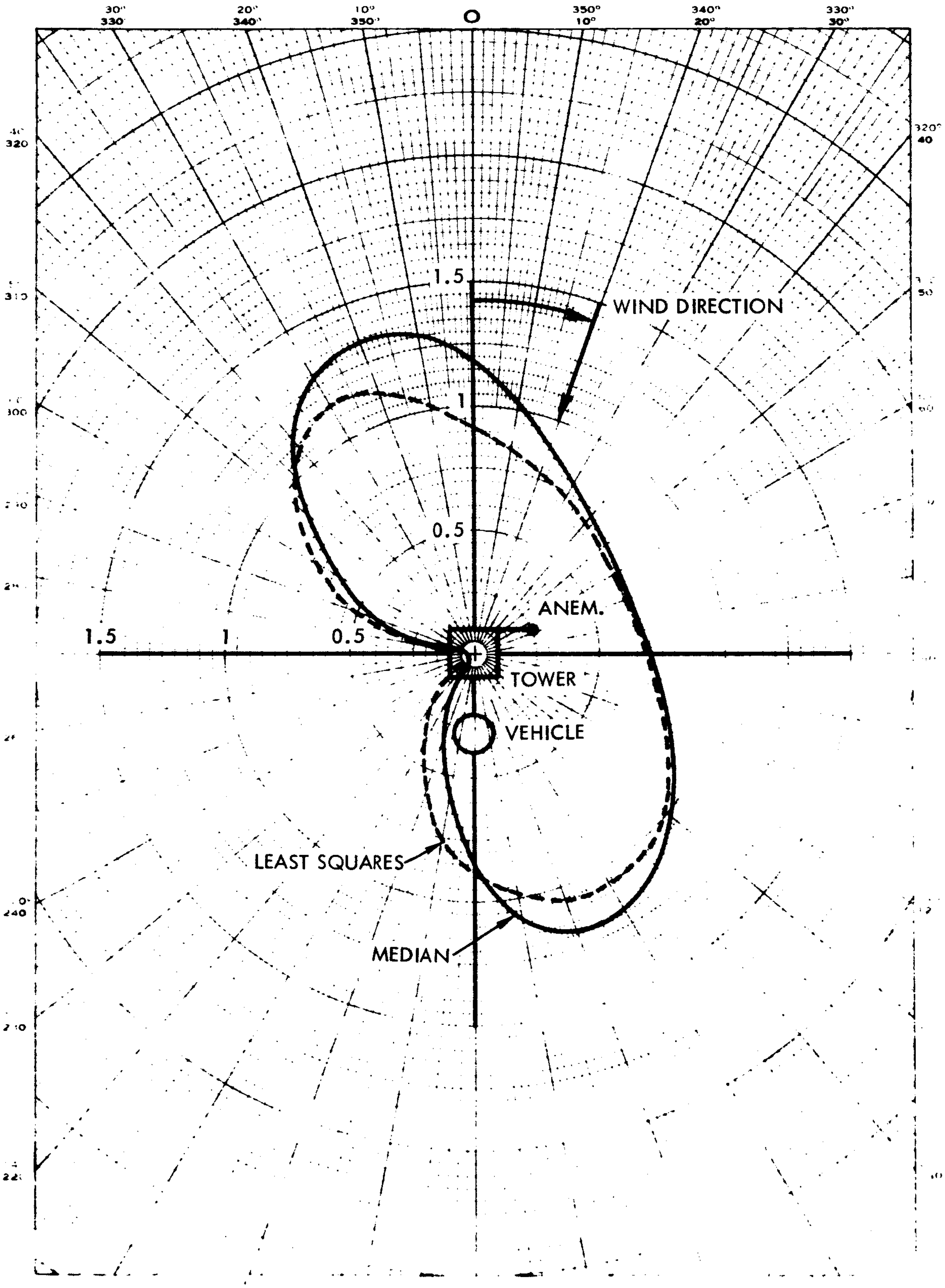


Figure 13. Polar Plot of Corrected Mean Speed Defect at 60-Meter (195-Foot) East Anemometer, Composite of Data From East and West Anemometers

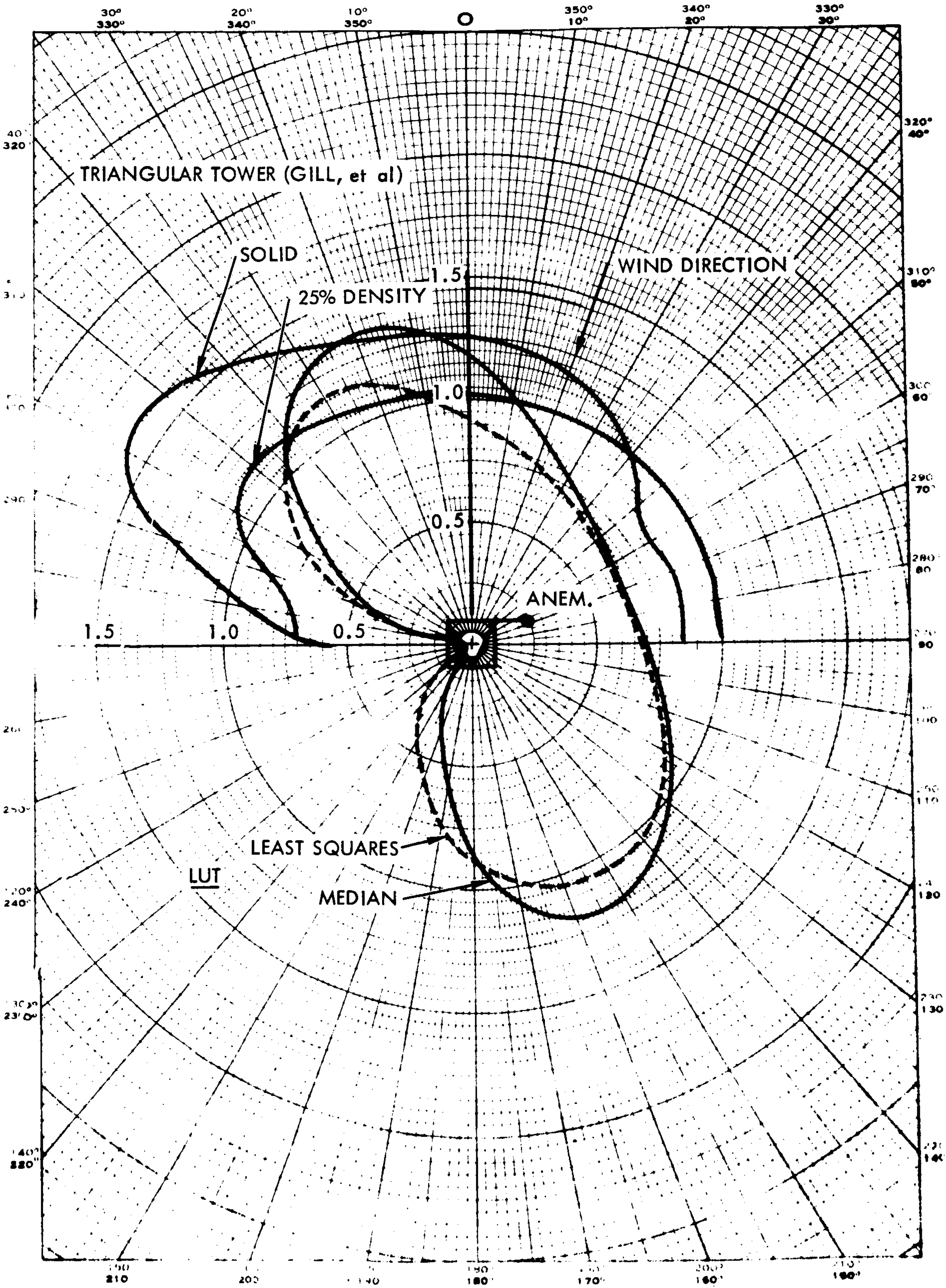


Figure 14. Speed Ratio Plots Superimposed on LUT Midlevel Plot

speedup encountered for the triangular tower should correspond to that encountered for the rectangular tower. Further substantiation of this statement is found in the fact that speedup for the circular stack from Gill, et al., at this same relative position, i. e., at 90-degree azimuth in Figure 15, is also about 1.25, coincident with the triangular tower data. On this premise, then, the LUT data at zero azimuth should fall between the 26 percent and 100 percent density speed ratio plots of Gill, et al. For the median curve, this is indeed the case, and its relative position confirms the estimated LUT shadow density of 60 to 70 percent previously estimated. To a certain extent this unusual agreement must be considered fortuitous, in view of the many ramifications involved. In this respect, the least squares curve does not fit the data nearly so well. The marked flatness of the LUT curves in Figure 14 are caused by at least two factors. One, of course, is the difference in tower cross sections. A second is the mutual interference between tower and vehicle. Considering the rather close similarity of speed ratio curves for solid triangle and circular stack over the azimuth range 0 to 90 degrees in Figure 14 and 90 to 180 degrees in Figure 15, it is tentatively concluded that effect of cross-sectional shape is not of prime importance to speed ratios in this azimuth range. Assuming this to be the case, the major contributor to flatness of the LUT speed ratio curve appears to be mutual interference effects between the umbilical tower and the vehicle.

As in any experimental test, the results and conclusions derived therefrom are never completely irrefutable. In the present case, the extent to which the data have been correlated with the completely independent data of Gill, et al., and the seemingly logical manner in which the LUT midlevel data fits into the overall picture of separated flows, seem to indicate the data and their reduction to be basically correct.

Based upon validity of results obtained, the relative unimportance of Reynolds number effects in establishing the mean characteristics of separated flows with interference has once more been verified. The tests by Gill, et al. (1967), were conducted at a tunnel speed of 12 ft/sec using tower breadths of 1.5 ft, giving a Reynolds number of about 100,000. The LUT data were obtained at speed ranges from 2 to 12 meters per second. Based upon tower breadth of 6.5 meters, the corresponding full scale Reynolds numbers ranged from 750,000 to 5 million.

### Azimuth Versus Azimuth Plots

Figures 16a, 16b, 17a, and 17b are scattergrams of the azimuth at a midlevel anemometer as a function of the azimuth at the top-level anemometer. Least squared error curves as discussed in Appendix C were determined for these scattergrams, and are shown in Figures 16a, and 17a. Each scattergram in Figures 16b and 17b is hand fitted with a curve passing through the median ratios in 20-degree intervals. Figures 16a and 16b are for

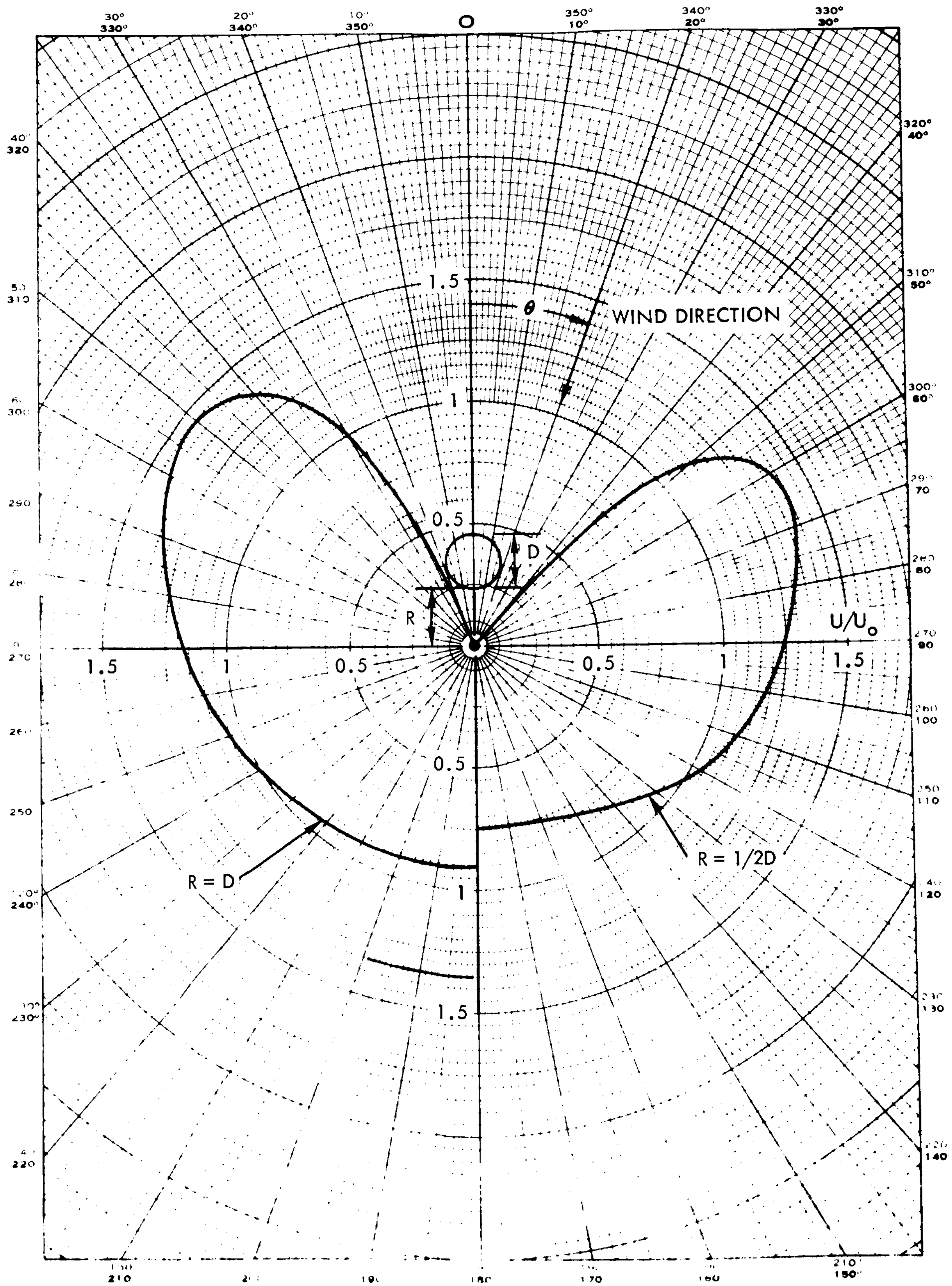


Figure 15. Polar Plot of Speed Ratio for a Circular Stack, Wind Tunnel Data From Gill, et al., September 1967

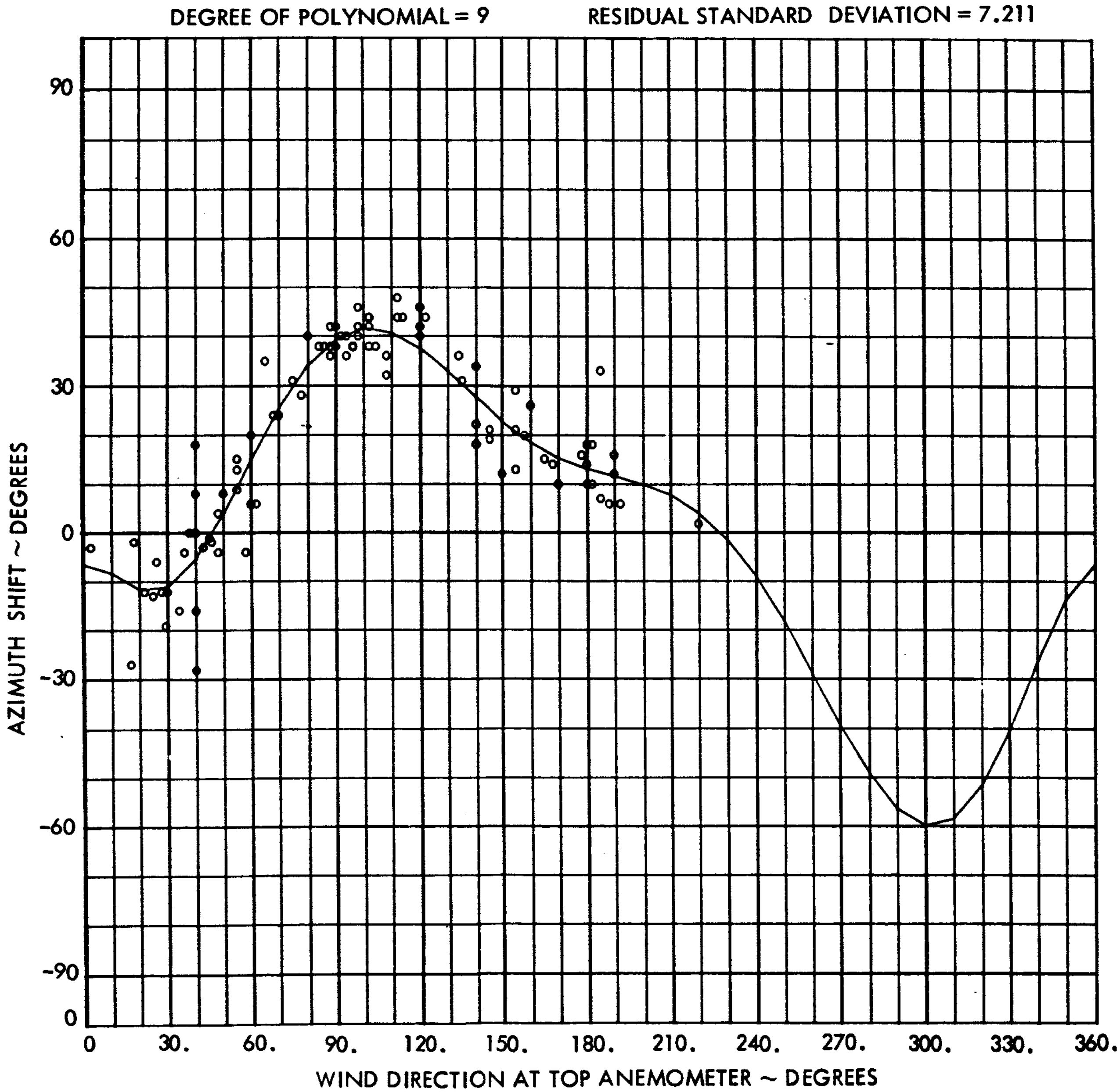


Figure 16a. Wind Direction at East Midlevel Anemometer as a Function of Wind Direction at Top Anemometer

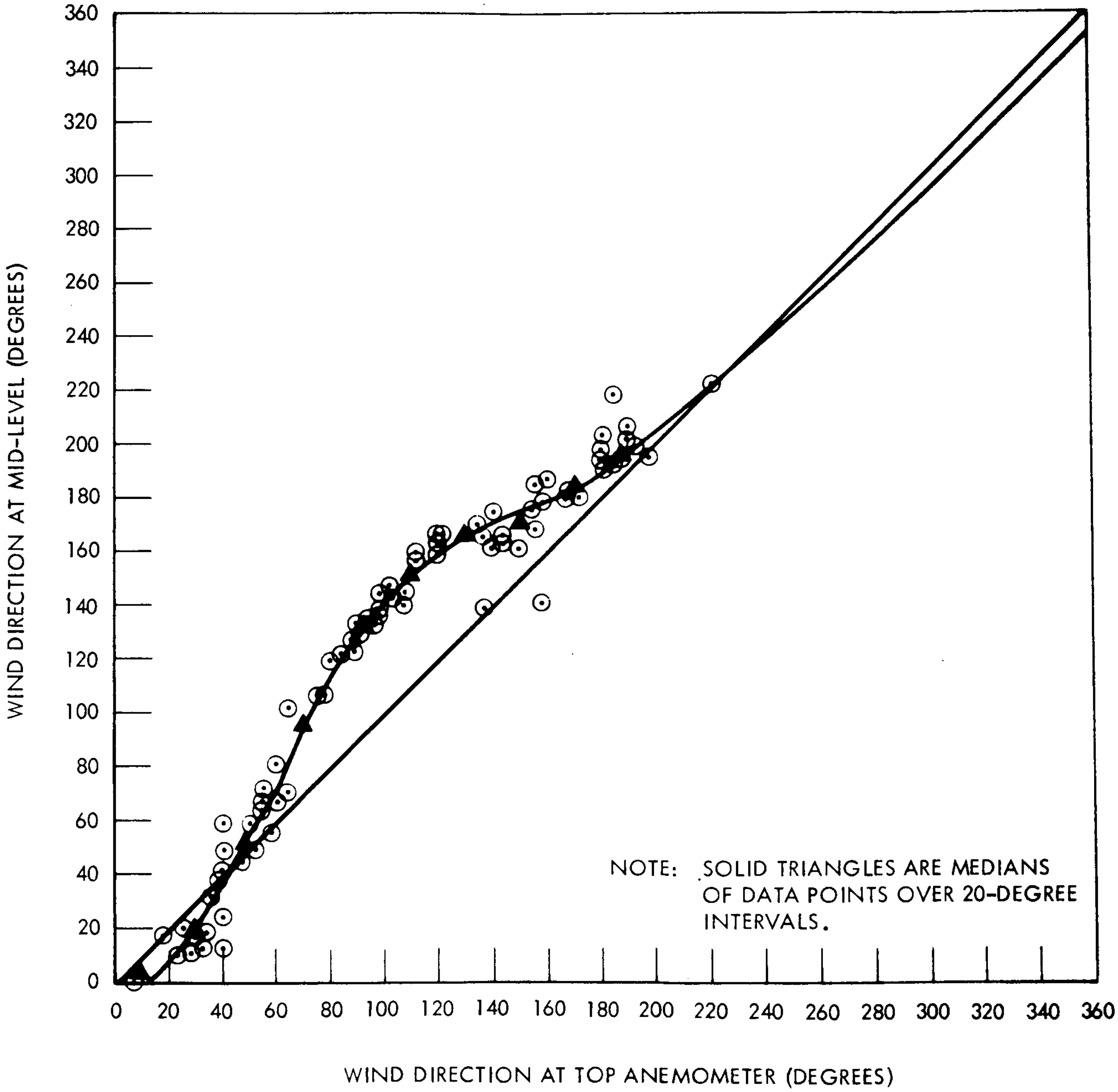


Figure 16b. Wind Direction at East Midlevel Anemometer as a Function of Wind Direction at Top Anemometer

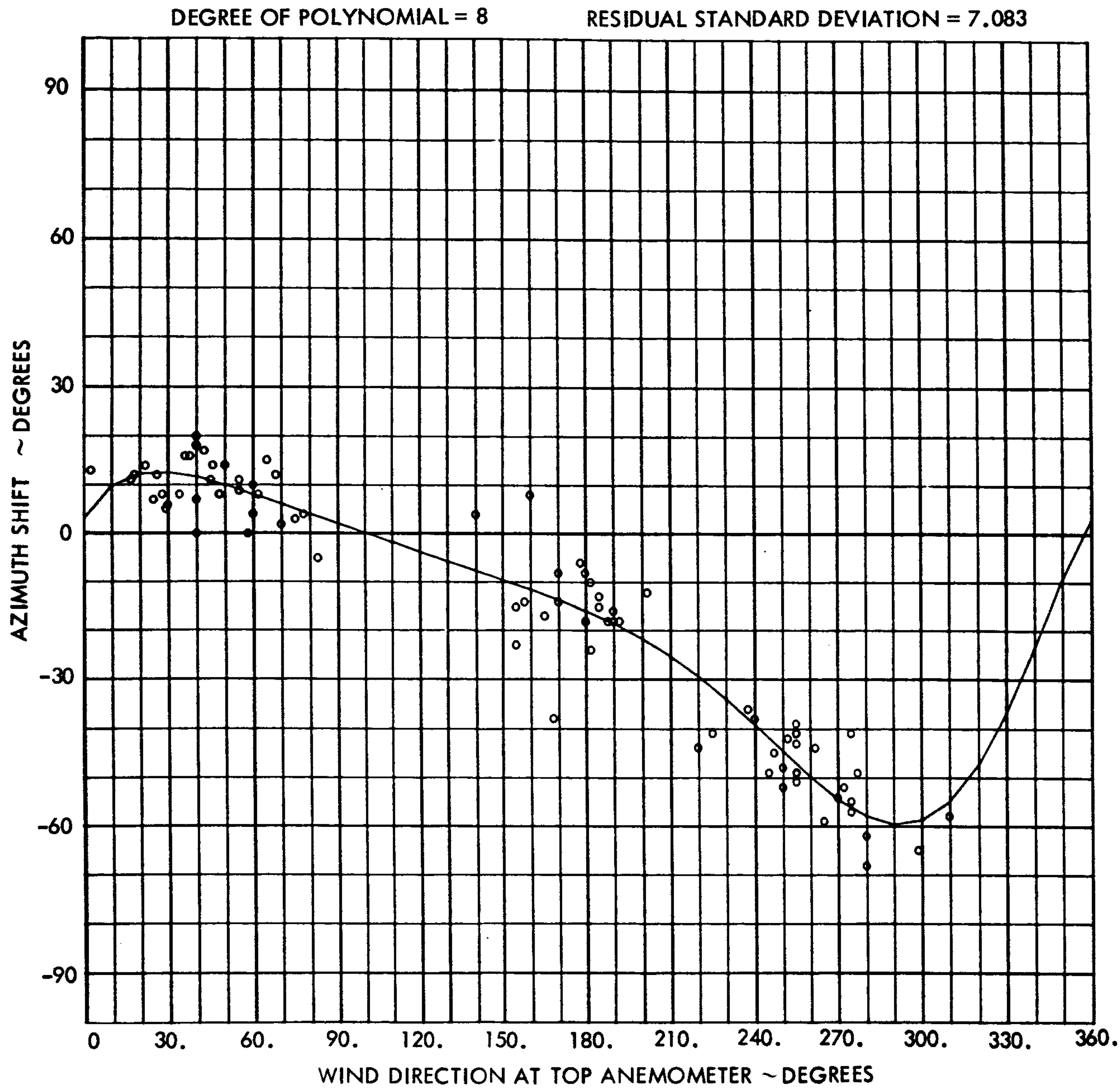


Figure 17a. Wind Direction at West Midlevel Anemometer as a Function of Wind Direction at Top Anemometer

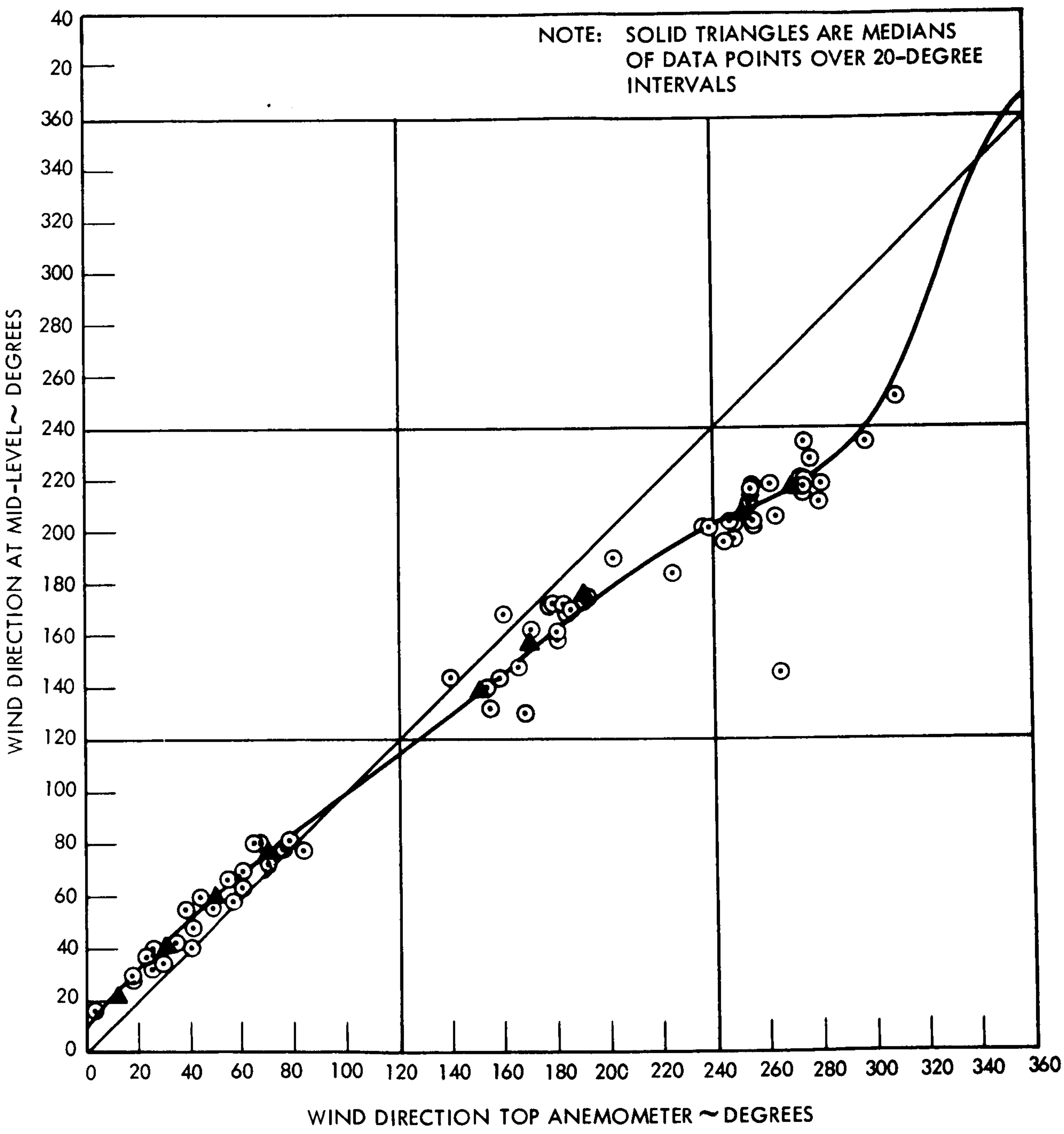


Figure 17b. Wind Direction at West Midlevel Anemometer as a Function of Wind Direction at Top Anemometer

the east midlevel anemometer, and Figures 17a and 17b, for the west. The symmetry assumption is checked in Figure 18, and the pooled data given in Figures 19a and 19b are referred to the east anemometer. Figures 19a and 19b clearly reveal a wind shift to the south on the windward anemometer when the wind is from the east or west. The median shift is as much as 40 degrees, this for winds from 100 to 260 degrees.

Deck Level Anemometer

Strip chart data made available for this study for the deck-level anemometer covered the time period from May 30, 1966, through June 9, 1966. This anemometer was located at a height 3.4 meters (11.0 ft) above the deck-zero level and at an approximate azimuth and distance of 225 degrees southwest and 90 ft, respectively, from the vehicle centerline. Data points obtained were correspondingly sparse. Winds were predominantly from the east or west, and the azimuth range between 130 and 260 degrees could not be covered. Figure 20 shows a plot of speed ratio, normalized to simultaneous top-level speeds, versus the azimuth at the top level. Due to sparsity of data, no attempt was made to calculate median points, and the solid curve was simply faired in visually, taking into account the necessary conditions for continuity of slope and ordinate at the endpoints, and the fact that winds from approximately 150 to 160 degrees would be expected to exhibit maximum values. This curve was then renormalized to the local free stream velocity based upon the 0.2 power law, and is shown in polar form in Figure 21. The near circularity of this plot between 100 and 250 degrees indicates that this location may be of significant value for future wind loads tests in determining wind speeds. The near unity values of wind speed at 270 and 90 degrees is contrary to the notion that appreciable speedup occurs due to pad elevation. It is possible that boundary layer effects from the launcher and pad are decelerating the flow, and, if so, would require that the deck level anemometer be placed somewhat higher than the 11-ft elevation that was employed.

In the azimuth plot shown in Figure 22 a surprising lack of distortion is shown for easterly and westerly winds. For winds in the range from zero to 60 degrees, however, the anemometer is clearly immersed in nonsteady wake flow since the strip chart indicated almost 360 degrees variations, making impossible any estimate of mean values. Such points are indicated by small vertical markings along the abscissa.

Pad Light Pole (PLP) Anemometers

Since the PLP anemometer data were unfortunately not concurrent with the LUT data, no direct comparison could be made. Instead, the velocities of the individual PLP anemometers were compared with each other and are shown in Figure 23. The inference here is that good correlation would indicate negligible contamination from LUT, launch pad, and associated obstructions.

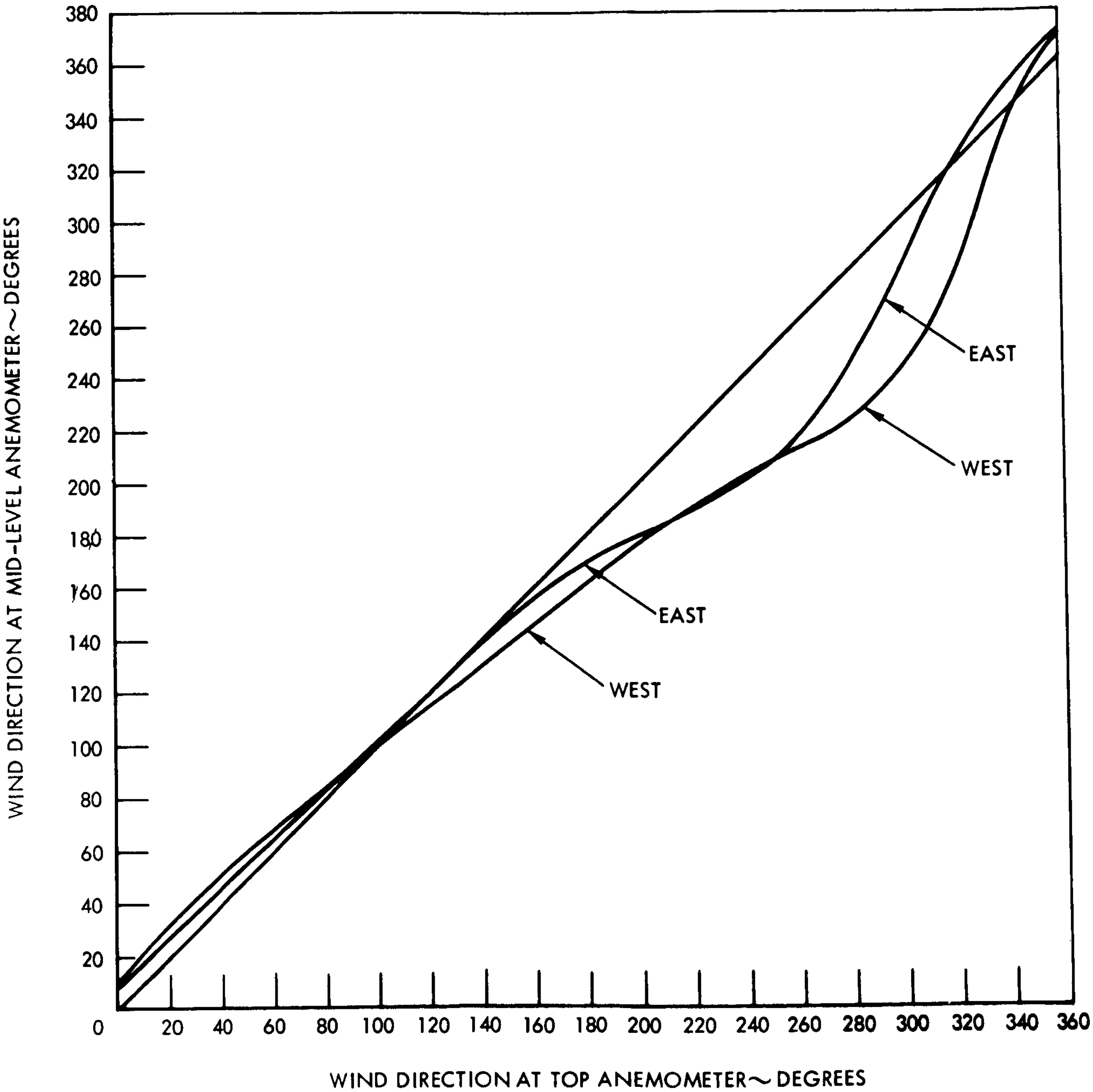


Figure 18. Comparison of Wind Direction Curves at Midlevel Anemometer as a Function of Wind Direction at Top Anemometer, Referred to West Anemometer

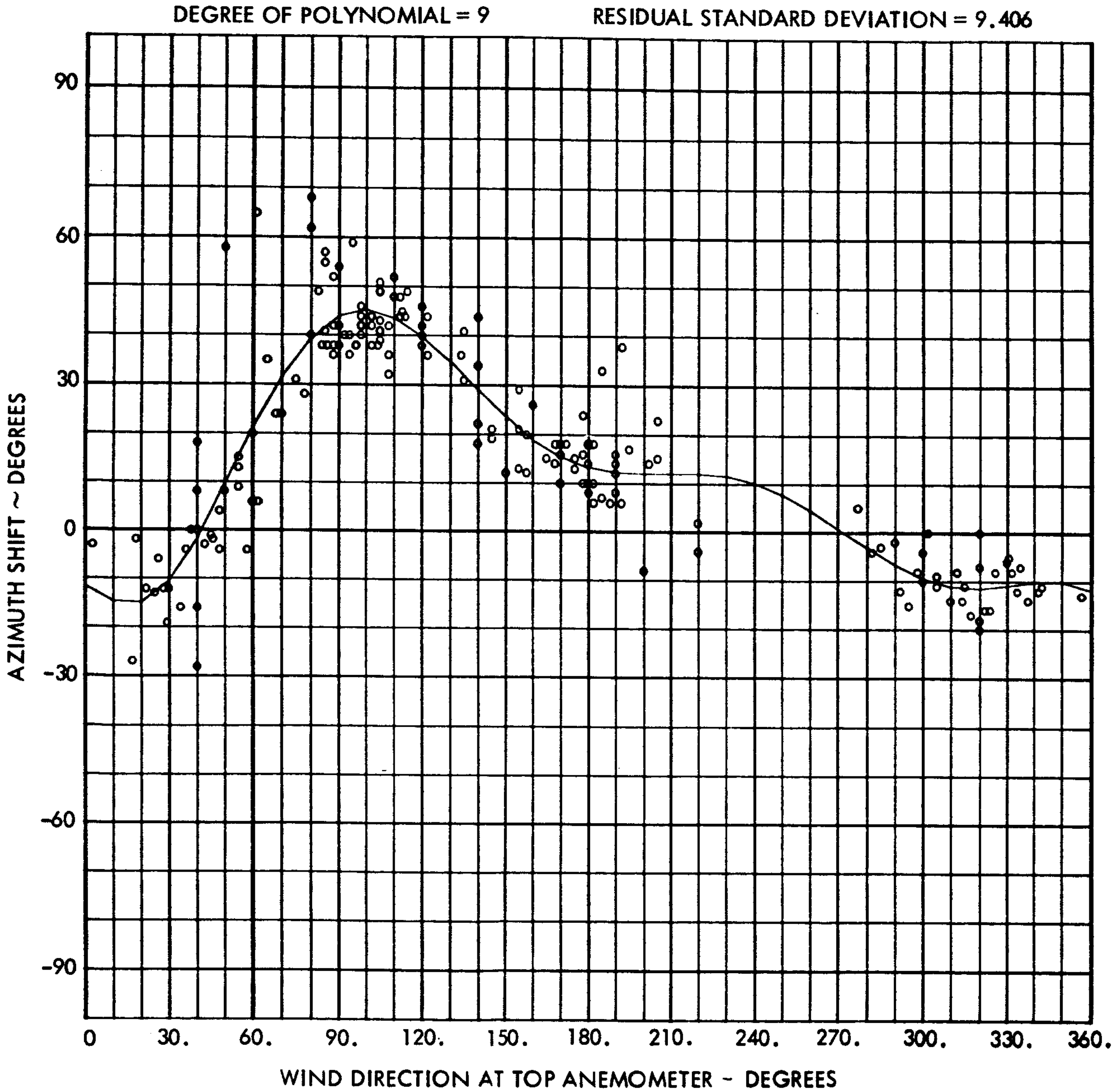


Figure 19a. Azimuth Shift at 195 Feet East Versus Wind Direction at 445 Feet, Composite of Data From East and West Anemometers

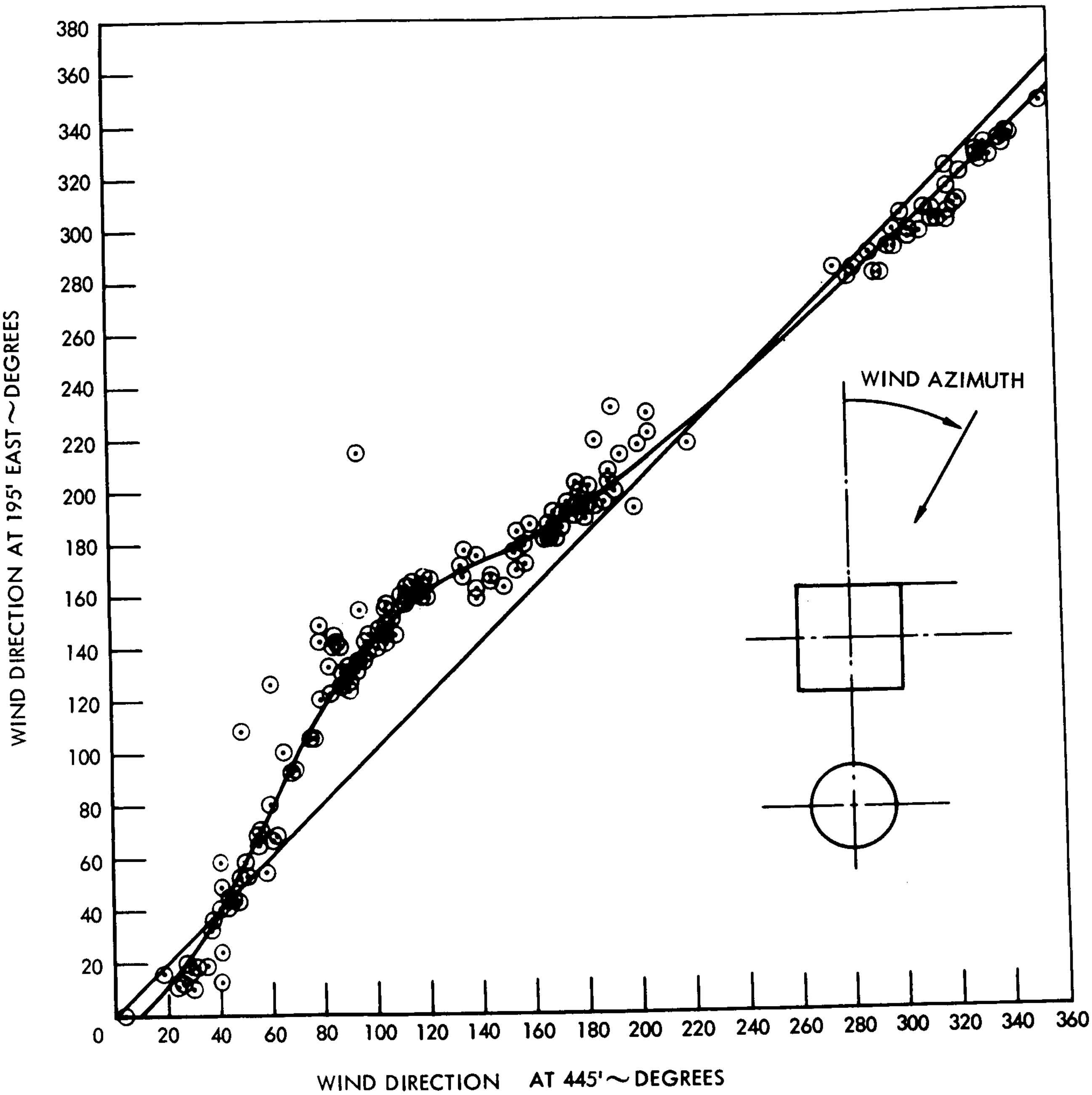


Figure 19b. Wind Direction at 195 Feet East Versus Wind Direction at 445 Feet, Composite of Data from East and West Anemometers

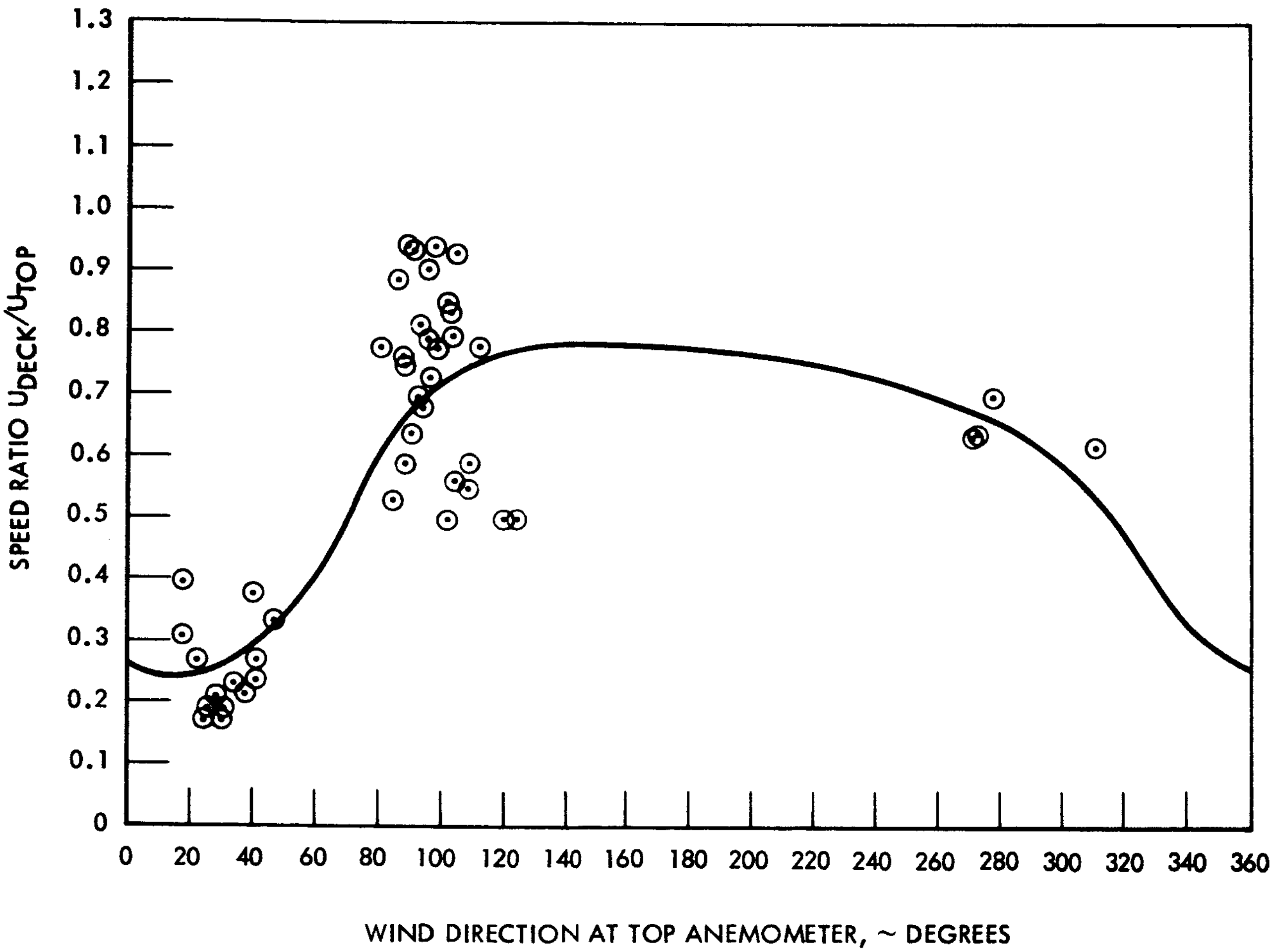


Figure 20. Wind Speed Ratio at Deck Level Versus Wind Direction at Top Anemometers

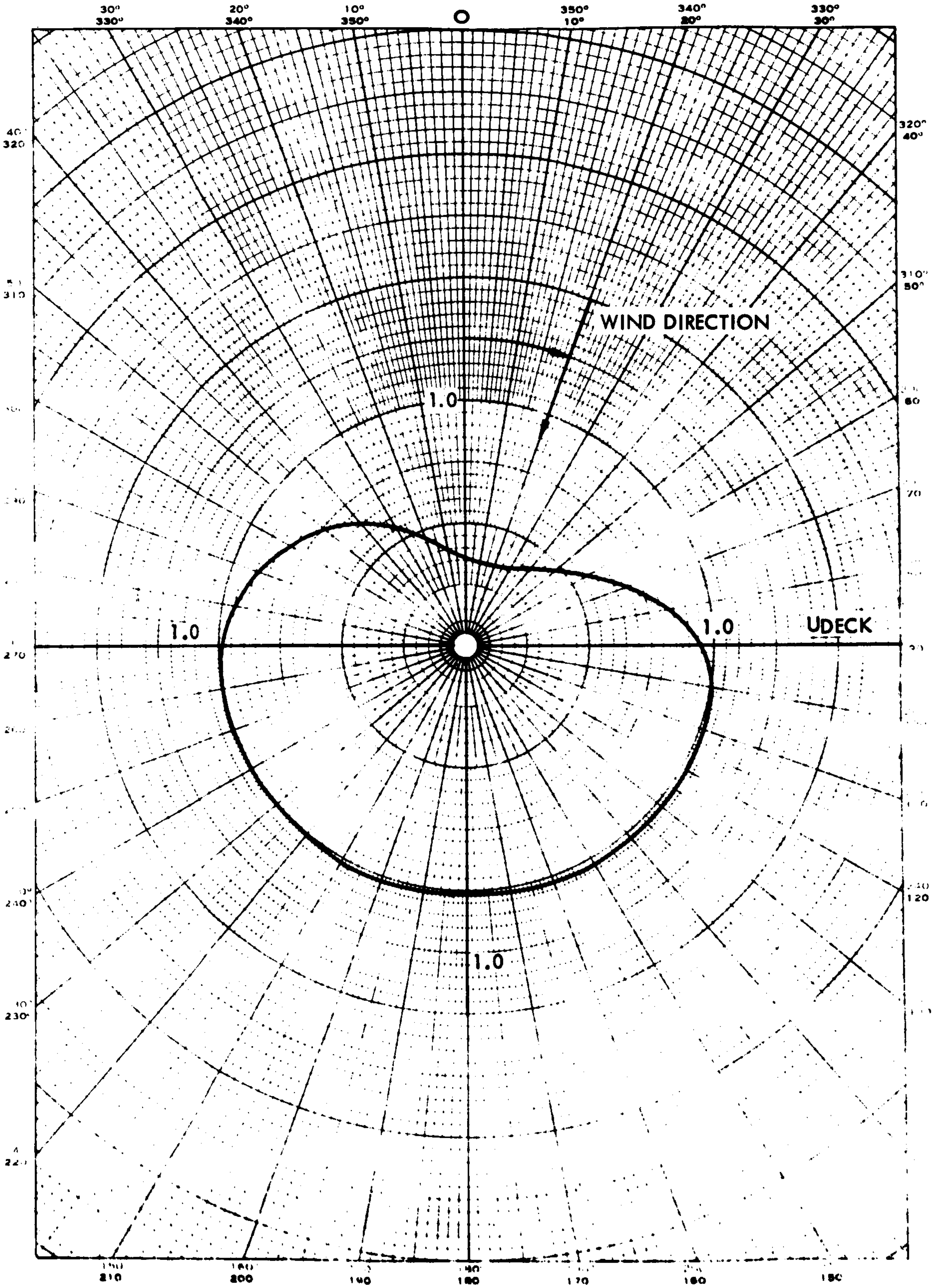


Figure 21. Polar Plot of Corrected Mean Velocity Defect at Deck-Level Anemometer

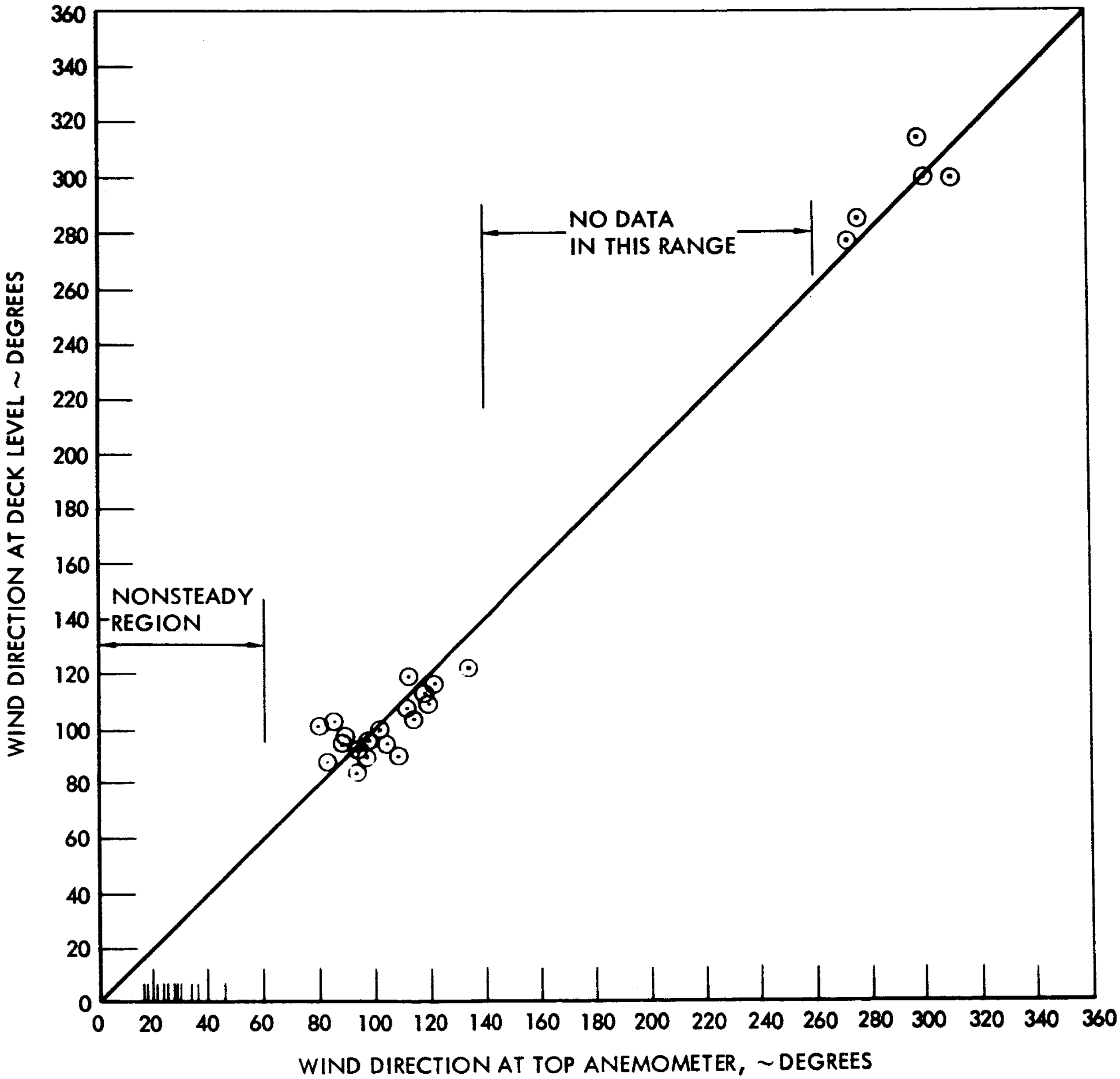


Figure 22. Wind Direction at Deck Level Versus Wind Direction at Top Anemometer

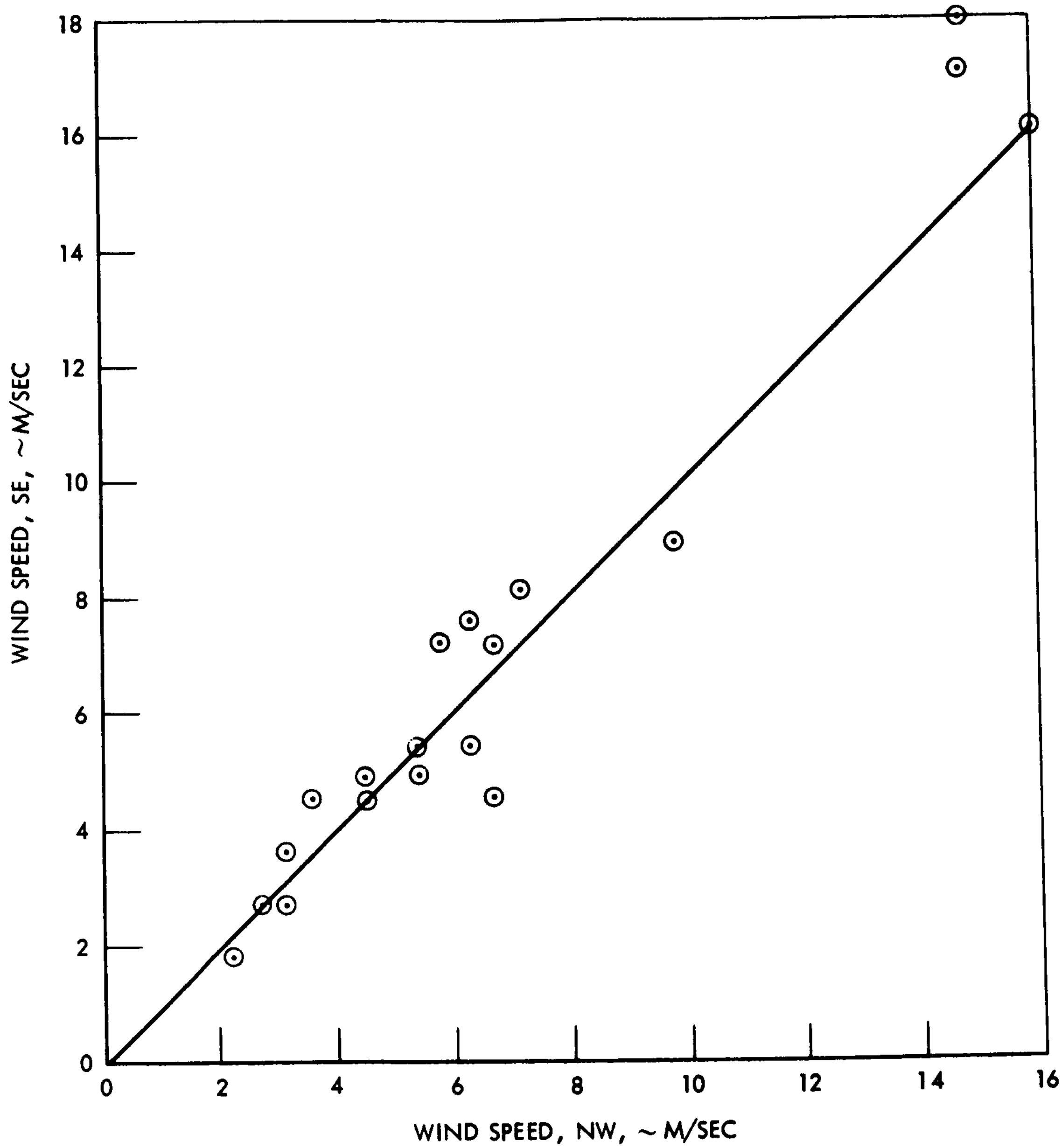


Figure 23. Comparison of Wind Speeds Indicated by PLP Anemometers

The speeds obtained from the two PLP anemometers were analyzed as follows. Assume that at any instant there is a common mean free stream speed for the two locations and that the departures therefrom at a given time are random, statistically independent with the same RMS deviation, and independent from time to time. In that case, the speed difference $U_{NW} - U_{SW}$ has a variance (mean square) equal to twice that of either speed. Using this fact, the data yield, as an estimate of the RMS fluctuation, 0.85 meters/second (1.90 mph).

It was felt that, in order to demonstrate validity of the PLP anemometer readings, it would suffice for the readings from the two to agree to within reasonable limits. Figure 24 is a plot of the azimuth shift ($AZ_{NW}$ minus $AZ_{SE}$) as a function of $AZ_{NW}$. The clear linear trend indicates that there was a scale factor difference on the two strip chart recorders. The NW anemometer showed readings over the entire range of azimuths while the simultaneous readings from the SE anemometer were all under 225 degrees. Had this linear deviation not existed, the two would have differed by approximately the amounts the points scatter around the hand-fitted line. The largest such deviation there is 13 degrees.

## CONCLUSIONS BASED ON TEST DATA

An evaluation of paper strip chart anemometer data obtained during the 1966 Ground Wind Loads Test Program at Launch Complex 39A has resulted in the following assessment regarding the local Launch Pad 39A wind field and placement of anemometers. The anemometer at the 445-foot level is essentially exposed to the local free stream, with no systematic distortion of azimuth. The velocities show increase in local free stream of 5 to 10 percent in magnitude. However, this conclusion must be qualified to the extent that the number of data points does not appear to be quite sufficient. Evidently the 3-1/2 mile separation between Launch Complex 39A and the meteorological tower permits rather wide simultaneous differences in velocity at these points.

Analysis of the midlevel anemometers indicates a considerable interference in the local wind field, and their data would not be useful for establishing the free stream velocity at this level without considerable extensions of their support booms beyond the present 25 ft. Possibly 60- to 80-ft booms would be necessary to permit satisfactory free stream recordings over an appreciable azimuth range, centered about true north, assuming dual anemometers are employed. For complete azimuth coverage, the basic support structure dimension should be considered as the centerline to centerline distance between vehicle and tower. With such a dimension, it becomes evident that the most proficient means for measuring free stream at this level would be the extension of one of the current pad light poles to the necessary height.

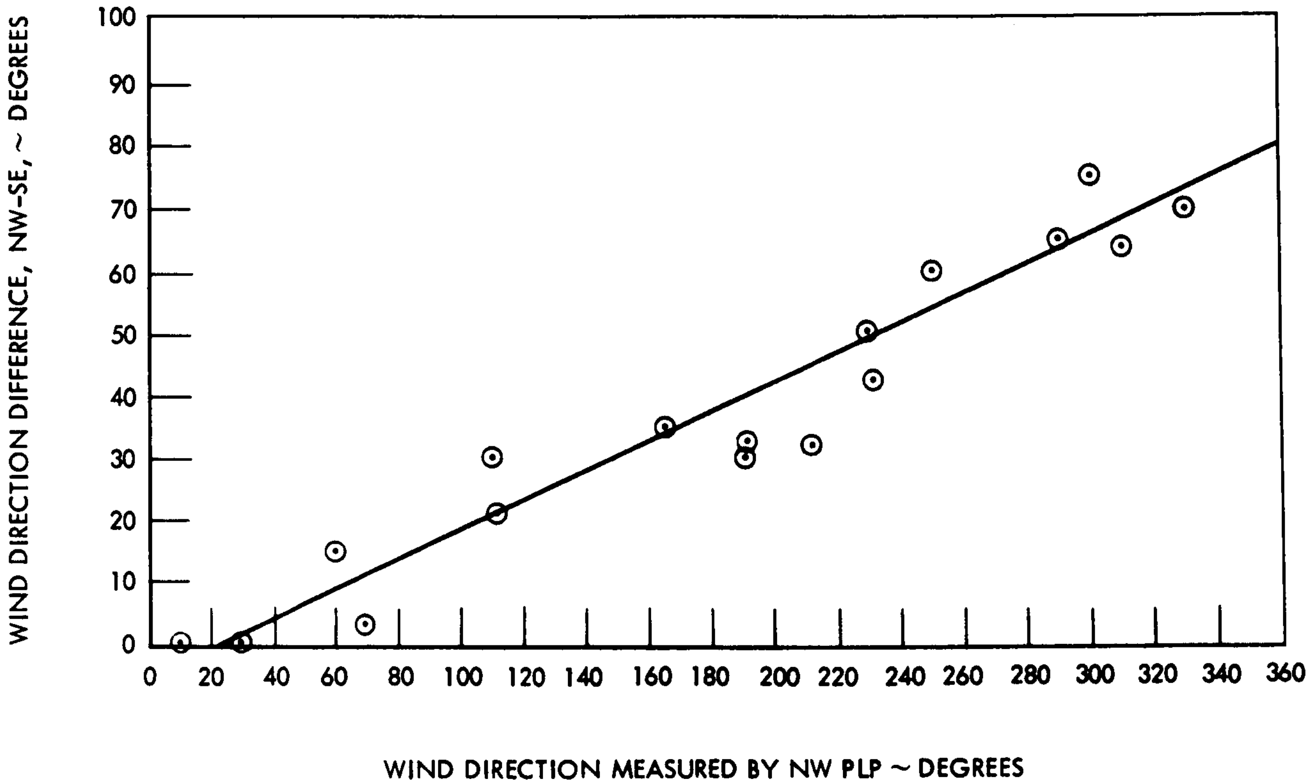


Figure 24. Comparison of Directions Indicated by PLP Anemometers

The deck-level anemometers were represented by the least amount of data and conclusions regarding them are correspondingly qualified. Nevertheless, it does appear that a single deck-level anemometer at the present location, but higher, would provide valid data over the 90- to 270-degree azimuth range. Further tests are indicated in which the deck-level and PLP anemometers are simultaneously employed to ascertain possible wind speedup due to pad elevation. The objective here would be to improve the exponential constant in the speed power law that would account for pad elevation.

The two PLP anemometers, by mutual comparison, are found to exhibit essentially free stream characteristics in both speed and azimuth. The strip chart data themselves indicated a linear distortion of azimuth of the southeast anemometer versus true azimuth which was interpreted as calibration error. Assuming this to be the case, the present locations are considered to be satisfactory for establishing the local free stream.

# III. THEORETICAL ANALYSIS

## APPROACH

The local wind field about the Saturn V - LUT is three-dimensional. The tip and base regions probably exhibit the strongest three-dimensional characteristics. While some methods for their theoretical analysis appear feasible with present state of art in computer technology, such efforts are considered beyond the scope of this study. Nevertheless, meaningful two-dimensional studies can be made to improve knowledge of this complicated flow field. Two such investigations have been made in this study. In the first, the elevation profile of the launch pad (without the LUT) along its narrowest dimension is approximated by an ellipse. Potential and "separated" flow solutions over this ellipse are then obtained. Secondly, the horizontal tower-vehicle cross section at the midlevel (19 meters above elevation zero) are represented by a circular cylinder plus an arrangement of stationary point vortices to represent a rectangular tower cross section. Nonsteady separated flow solutions are then obtained for this configuration oriented at various wind directions.

The following background discussion precedes the detail discussion of these investigations. This background discussion is intended to serve as a descriptive basis for the numerical technique employed herein for the numerical solution of two-dimensional incompressible separated flows. The more rigorous theoretical developments are contained in Appendices.

Consider first the classical potential solution for steady lift on air foils. It is to be recalled that potential theory alone is insufficient to solve this problem. There is required, in addition, one empirically based criterion—that is the Kutta condition which states that the circulation strength at the trailing edge must be zero. This condition essentially accounts for the action of viscosity in the boundary layer in creating the physically observed lift inducing vorticity about the airfoil.

Viewing the separated flow problem in this same context, a necessary assumption is the inviscid nature of flow mechanics in the near wake, separated flow region. Next, a generalization of the Kutta condition is required which will permit the definition of nonsteady (instantaneous) transport of vorticity from the bluff body into the fluid stream. In previous NASA-funded studies (Ujihara, et al., 1965, 1966), such a generalized Kutta condition was developed, with reasonable success, for solution of separated flow about a circular cylinder. This generalized Kutta condition is expressed in the following way.



PRECEDING PAGE BLANK NOT FILMED.

The transport of vorticity past any given point on a flow boundary is

$$\frac{d\gamma}{dt} = \frac{1}{2} U_s^2 \tag{2}$$

where $U_s$ is the potentially calculated slip velocity at that point. The injection of free vorticity into the fluid stream occurs at points of velocity maxima. This free vorticity is expressed in terms of discrete vortices of strength

$$K = \frac{1}{2} \left( \frac{U_s^2 \ \Delta t}{2} \right) \tag{3}$$

where the solution is carried out in finite difference form, and $\Delta t$ is the incremental time period over which the vortex strength is allowed to accumulate.

Successful application of this generalized Kutta condition represents the crux of this method. Basically then the solution of nonsteady separated flow about a bluff body requires the following steps:

1. Determine potential solution of flow about this body in a uniform free stream

2. Find the points of speed maxima on the boundary

3. Introduce free point vortices of proper strength

4. By finite differences compute the new flow field.

5. Return to step 2 and repeat.

This method enables the complete solution of nonsteady separated flows within the realm of potential theory. Flow rotationality in the wake is accounted for by the presence of discrete vortices convected downstream from their injection points. Separated flows about a circular cylinder are known to be strongly influenced by the Reynolds number. It is found upon closer analysis that the Reynolds number is only <u>indirectly</u> responsible for these observed variations. Stated more precisely, it is the attached shear layer thickness which is directly determined by the Reynolds number. The mechanics of vortex formation and shedding are found to be directly related to this shear layer thickness. A train of successive point vortices in potential flow possesses an equivalent shear layer thickness which depends only upon the vortex spacing. This may be related to known variations of attached shear layer thickness with Reynolds number to give a relationship between the finite difference time increment for vortex injection and the flow Reynolds number being simulated. In these previous studies this relationship has been defined as

$$Re = \frac{25}{(\Delta t)^2} \tag{4}$$

where Re is the simulated Reynolds number. Further correlations with experimental data were shown in these previous studies at subcritical Reynolds number in which nonsteady lift, drag, and cylinder pressure distributions are in essential agreement. In particular, a distinct Strouhal frequency of 0.2 was obtained for vortex shedding. A calculated instability of the discrete vortices simulating the shear layer was also shown to correlate well with experimental data by defining (Sato, 1956, Roshko, 1967) the transition of a laminar free shear layer to turbulence.

## TOWER VEHICLE CROSS SECTION AT MIDLEVEL

The midlevel anemometers are located in a region strongly influenced by the presence of tower and vehicle structures. This is clearly indicated from the noncircularity of the experimental wind rosettes of Figure 13. Further clarification of the wind field at this level is desirable; first, to permit more optimal placement of these anemometers with respect to measurement of free stream properties; second, an assessment of the velocity field particularly about the vehicle will hopefully bring insight to the nature of interference dependent flow mechanics which have been found to aggravate vehicle cantilever loads.

A theoretical approach was taken in this study to investigate this interference flow field. It is based upon the two-dimensional numerical method of separated flow analysis employing the previously described generalized Kutta condition. A computer program developed during previous NASA-funded studies was utilized for this study. This program was successfully used in these previous studies to numerically solve the nonsteady vortex shedding flow about a circular cylinder at subcritical Reynolds numbers. A major modification to this computer program consisted of the addition of a second bluff body representing the tower cross section. The method used to accomplish this addition is mathematically developed in Appendix A. A brief description is provided here for continuity of discussion and qualification of the necessary assumptions.

### Discrete Vortex Simulation of Tower Cross Section

The flow field is assumed to be two-dimensional, with the vehicle circular cross section represented by a source sink cylinder in uniform flow. To this is added a configuration of closely arranged stationary vortices representing the second body to be added. This arrangement of vortices may be of an arbitrary configuration, although for the tower representation it was taken to be rectangular. From assessment of the tower cross section, this second body should not entirely block the flow, since structural truss members, the elevator housing, conduits, and personnel railings making up the cross section do not present a completely closed surface. A detailed representation of this cross section would be possible, at the expense of a relatively large number of vortices. However, this represented an original attempt to apply this concept. Therefore, the number of vortices was held to a minimum, both for economy of computer time and in recognition of the exploratory aspects involved. Also a preconceived notion of high aerodynamic solidity was based upon informal remarks of personnel more familiar with wind conditions at the tower midlevel, that the tower seemed to effectively block any significant flow-through. At any rate, a gross representation of the tower cross section was employed in which the stationary vortices were placed in a rectangular arrangement, as shown in Figure 25 with closer spacing near the corners, since the velocity is known to be greater there.

Strengths of these vortices were then calculated instantaneously (in the finite difference scheme of numerical solution) by imposing the boundary condition of zero normal flow at each midpoint between consecutive vortices. Thus, a set of simultaneous equations in the unknown vortex strength is derived, the coefficients of which depend only upon the geometric arrangement of the stationary vortices. One additional equation is necessary to require that the total circulation about the body be equal to the cumulative negative sum of all free vortices generated by that body (condition of constant angular momentum). This residual circulation is satisfied by a stationary vortex at some point within the body, say the center. This complete matrix of coefficients is inverted only once, and instantaneous vortex strengths are subsequently determined by their matrix multiplication with the calculated normal boundary velocities imposed by the free stream, cylinder and free vortices at finite difference time points. The image method is used to satisfy cylinder boundary conditions for all vortices whether stationary or free.

## Generalized Kutta Condition

It was recognized that a realistic solution of interference flow about the tower vehicle cross section would require simulation of vorticity transport from both bodies. Consequently, an empirical scheme was defined for applying the generalized Kutta condition to account for the major portion of vorticity shed from the two bodies.

Depending on the free stream azimuth, the tower wake could impinge upon the circular cylinder and vice versa. The circular cylinder, being

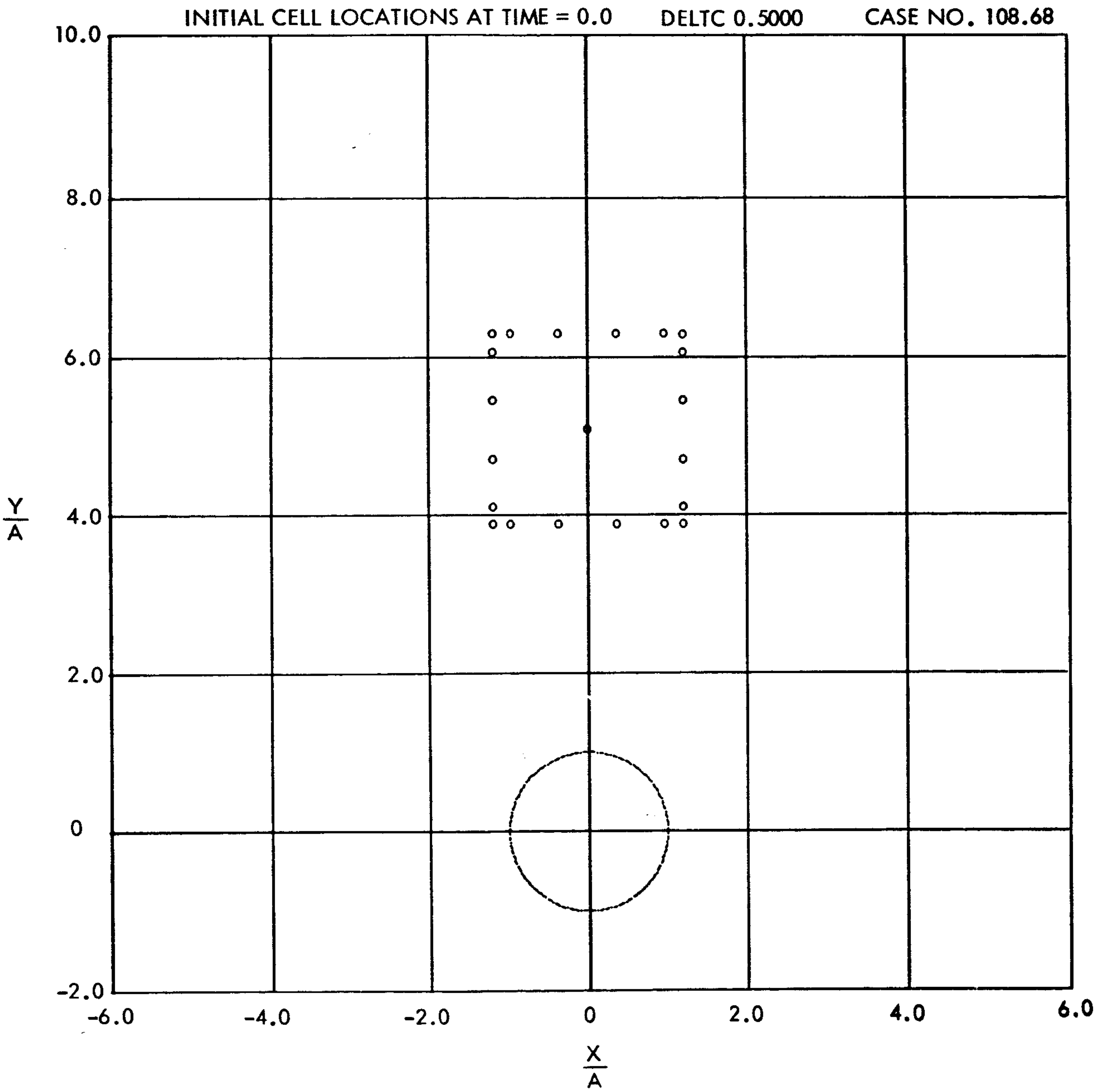


Figure 25. Typical Arrangement of Point Vortices to Represent Tower Cross Section

smoothly curved, is known to exhibit greater sensitivity to flow conditions than sharp-cornered bodies. From previous studies it was also known that significant counter vorticity could sometimes be generated over the wake exposed surfaces. Again considering limitations of the computer program, a total of three possible vortex feeding points was allowed on the circular cylinder. These are internally determined by computing all the instantaneous speed maxima occurring on the cylinder surface, and selecting the three largest of these relative maxima for the incremental vortex feeding points. Thus, as many as three vortices could be introduced from the cylinder at each finite difference feeding time point. The radial distance from the surface at which these vortices are introduced was set equal to $0.28\ u\Delta t$ which is the approximate center of the separating shear layer thickness.

Vorticity from the tower would be expected to shed primarily from the corners. It was also considered physically consistent to require that the primary vorticity be generated at the two corners presenting the broadest dimension to the free stream. It was desirable to keep the number of vortices to a minimum in order to limit the number of computations necessary to achieve a satisfactory solution. In the interest of simplicity in computer logic, the specification of the two corners selected as vortex feeding points was left variable as input data.

Since the characteristics of flow separation from sharp-cornered bodies are ordinarily not sensitive to changes in Reynolds number, the feeding point was located along the extension of the diagonals of the rectangle without regard to requirements for Reynolds number simulation. A distance of 1/10 cylinder radius from the corner vortex was selected for the feeding point location. This value was predicated upon insuring sufficient distance from the corner vortex to preclude any numerical instability. Here again, a non-dimensional feeding period of 0.500 based on cylinder radius was primarily on the basis of computer economy. This corresponds to a cylinder Reynolds number of approximately 100.

## NUMERICAL SOLUTION

In the course of obtaining the numerical solutions shown in this section, a numerical singularity that nearly prevented achievement of satisfactory solutions was encountered. This singularity resulted from placement of a vortex at the center of the square vortex array simulating the tower cross section.

To the investigators of this study the singularity encountered was totally unexpected. Because of its apparently fundamental nature, a discussion of the difficulty is presented with the hope that it may prove useful in possible future applications of this technique.

As previously outlined, the finite element representation of a closed body with discrete vortices requires one vortex within the body to satisfy total circulation requirements. Furthermore, the precise location of this vortex within the body is immaterial, since the circulation about any closed path enclosing the vortex remains constant. For lack of a better choice, the internal vortex was simply placed at the center of the square cross-section. The generated matrix of coefficients was then inverted. A poor inversion was obvious from the product of the matrix multiplied by its inverse. Double precision was incorporated to increase the accuracy, but the inversion check showed no improvement.

Because the matrix of coefficients was suspected of being ill-conditioned, the coding for formation of the coefficients was thoroughly checked and rechecked to no avail. Simple finite element arrangements were then considered in any attempt to discern some physical explanation for the trouble. During this procedure, it was found that a square represented by a single vortex at each corner, with zero normal velocity at the midpoints, is indeed singular if the internal vortex is placed at the center. This system is represented by a matrix of coefficients as shown in the form on the left which may be reduced in two steps to the form on the right.

$$\begin{bmatrix} -a_1 & a_1 & a_2 & -a_2 & 0 \\ -a_2 & -a_1 & a_1 & a_2 & 0 \\ a_2 & -a_2 & -a_1 & a_1 & 0 \\ a_1 & +a_2 & -a_2 & -a_1 & 0 \\ 1 & 1 & 1 & 1 & 1 \end{bmatrix} \quad \begin{bmatrix} -a_1 & 0 & a_2 & 0 & 0 \\ -a_2 & -a_2-a_1 & a_1 & 0 & 0 \\ a_2 & 0 & -a_1 & 0 & 0 \\ a_1 & a_1+a_2 & -a_2 & 0 & 0 \\ 1 & 1 & 1 & 3 & 1 \end{bmatrix}$$

If, however, the internal vortex is placed off-center, the last column will not contain all off-diagonal terms as zeroes, and the singularity disappears. While it is difficult to generalize these results to matrices of higher order, this was considered sufficient reason to re-evaluate the manner in which vortex sheets are successfully employed in aerodynamic theory. It was observed, for example, that vortex sheets are employed invariably for zero-thickness configurations, (i.e., thin airfoils), to determine lift due to camber and angle of attack. In a previous study of this type, a finite-element vortex sheet representation was successfully employed to represent flow about a circular cylinder. In that solution, the "internal" vortex, by necessity, had to be located on the boundary because linearly varying vortex sheet elements were employed. Under this approach, the circular boundary was actually represented by a highly cambered "airfoil" having leading and trailing edges approaching within some arbitrarily small distance to one another.

This concept was pursued for the problem at hand, and the internal vortex was placed to within b/20 of the boundary, where b is the dimension of a side. The resulting matrix premultiplied by its inverse was accurate to six significant figures on the diagonal and was less than $10^{-7}$ on all off-diagonal terms using double precision. The difficulty was considered to have been surmounted.

The scope of numerical investigations of interference flow at midlevel was restricted in view of the effort expended in overcoming this numerical difficulty; consequently, a complete speed ratio plot for comparison with experimental results was not obtained.

Nonseparated, steady potential solutions were obtained for wind directions from 180 degrees and 270 degrees. Computer plots of flow streamlines are shown in Figures 26 and 27 for these two cases.

A single nonsteady separated flow solution was obtained for wind direction from 350 degrees. Steady nonseparated potential flow for this case is shown in Figure 28. A time history of the instantaneous separated flow configuration represented by point vortices is shown in Figures 29a through 29d. The same condition with corresponding streamlines superimposed is shown in Figures 30a through 30d.

For this separated flow solution, eight "anemometer" locations were specified at which wind speed and azimuth shifts were printed out. Six of these locations represent three pairs of symmetrically situated points in the plane of the tower north face. The closest pair (at 5/8 tower breadth from the corner) represents the actual position used in the wind loads test. The remaining two pairs on the tower were situated at one and two tower breadths away from the corner. Finally, locations for one pair of "anemometers" were specified 1. 5 radii directly east and west of the cylinder center.

Speed ratios and azimuth shifts calculated for these points at various nondimensional times are given in Table 1.

The streamline plots of Figures 30a through 30d show one streamline passing through the tower cross section, indicating some leakage. This flow, however, must be small since it appears to be near the stagnation streamline. After a nondimensional time of 6, it is noted that a wake cavity envelops the cylinder, and a large vortex is formed on one side of the cylinder. Shedding of the vortex does not occur within the period covered, but appears to be on the verge of doing so in Figure 29d. Also shown in Figure 29d are two incremental vortices that have passed through the cylinder boundary because of the roughness of numerical integration. This effect indicates that finer integration intervals should be used. The solution represented by Figure 29d was obtained with 10 minutes of computer time during which a total of 154 vortices were introduced.

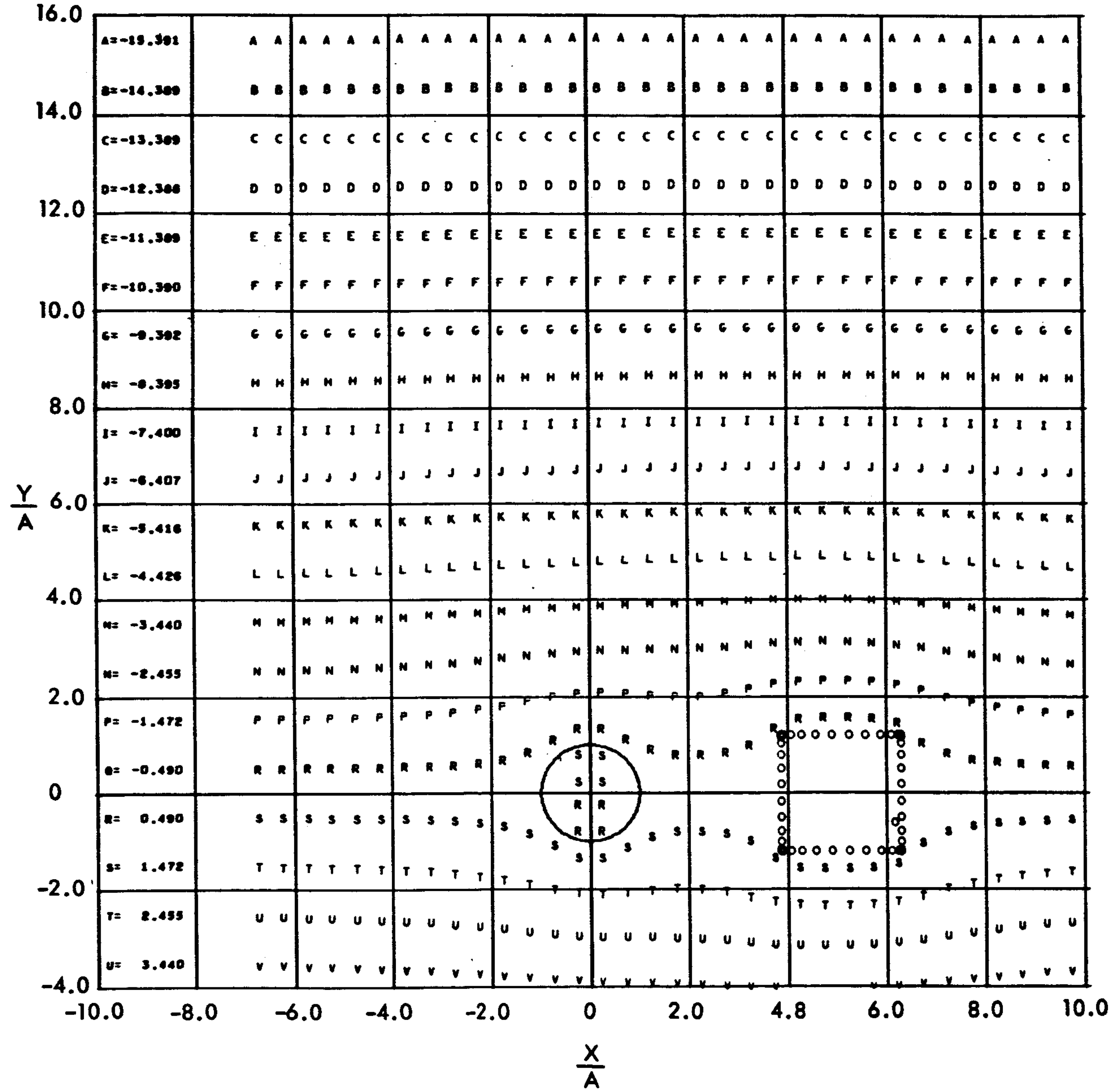


Figure 26. Steady Potential Flow Streamlines for Free Steam at 180 Degrees

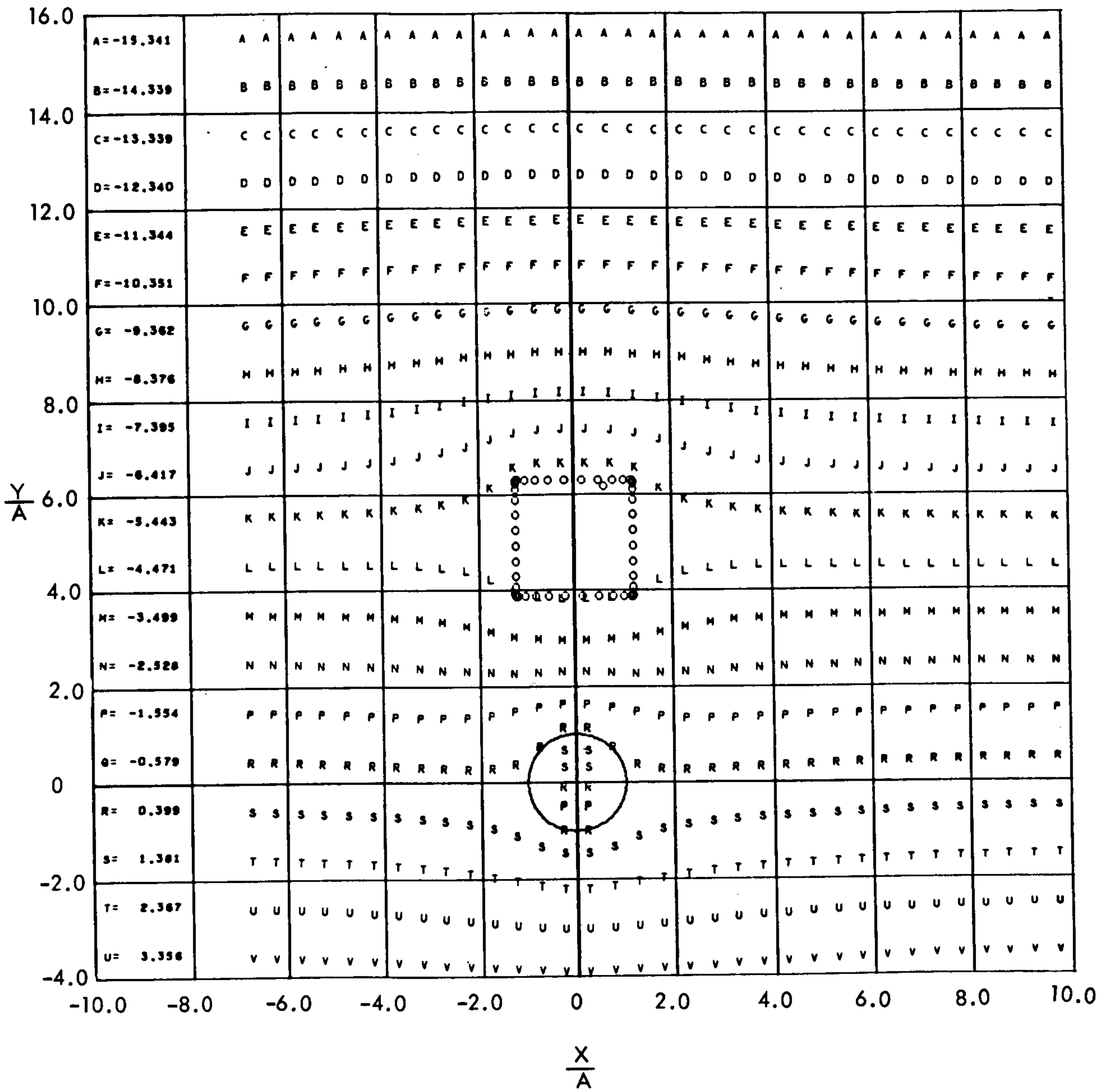


Figure 27. Steady Potential Flow Streamlines for Free Steam at 270 Degrees

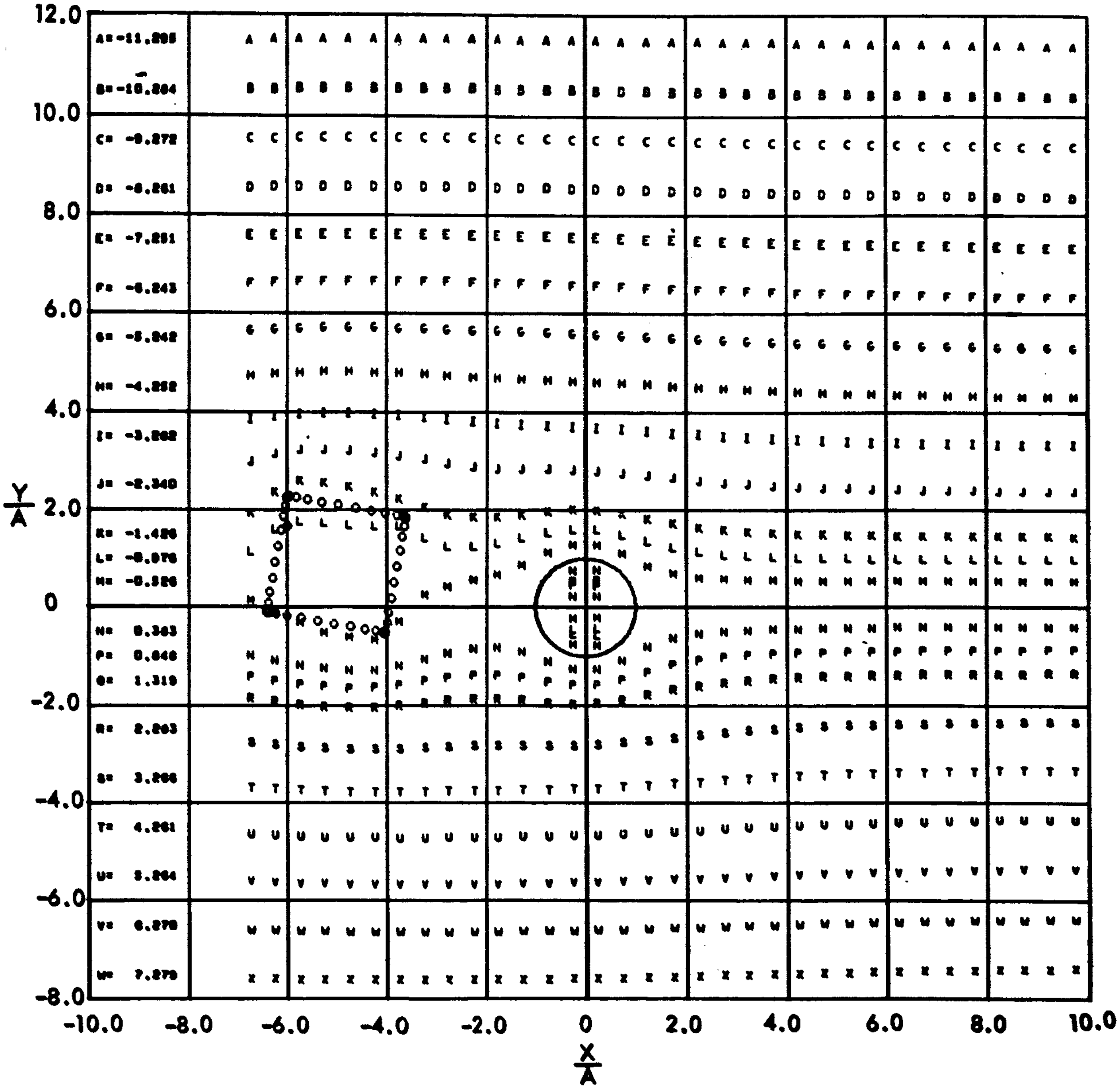


Figure 28. Steady Potential Flow Streamlines for Free Steam at 350 Degrees

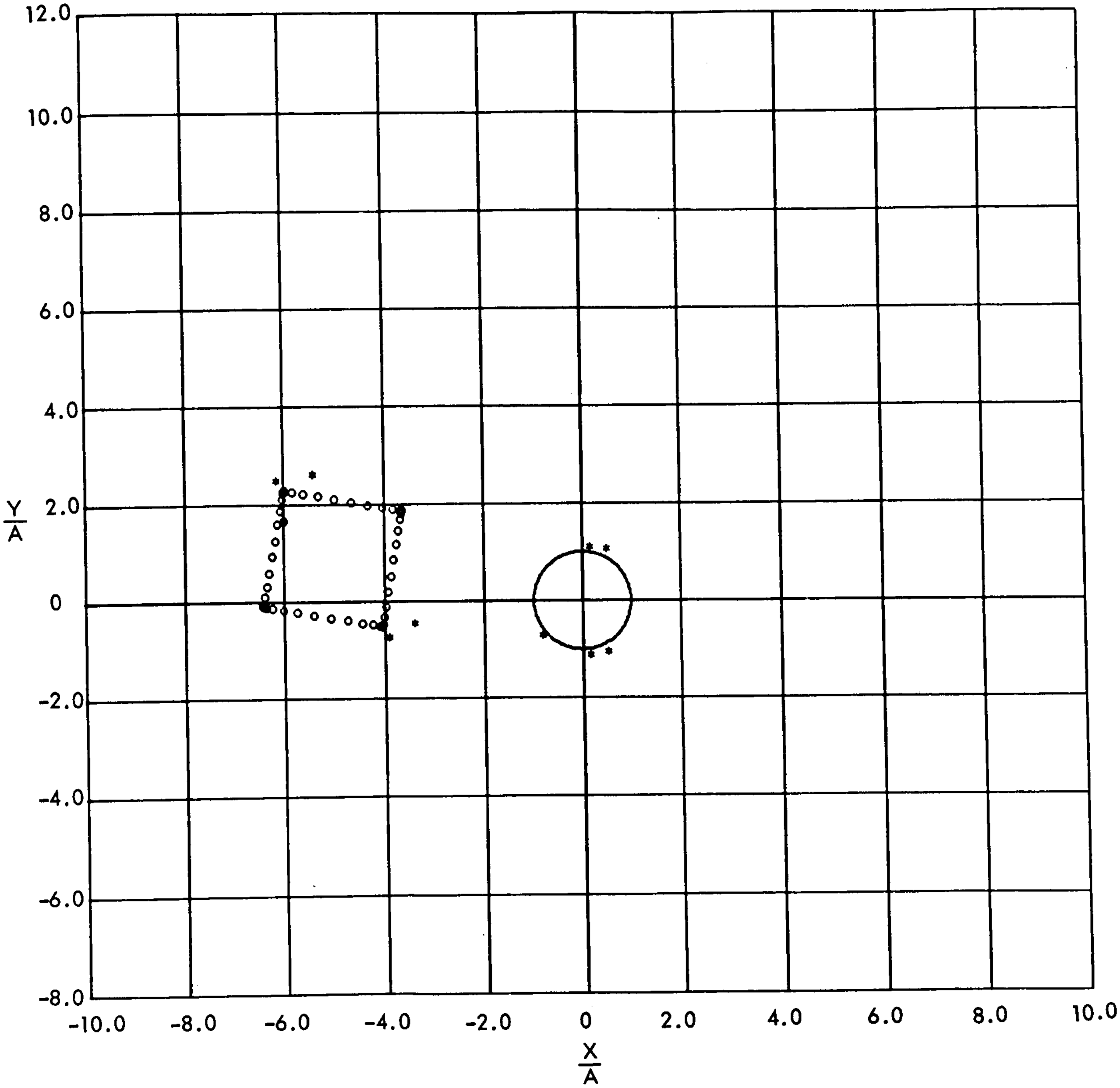


Figure 29a. Instantaneous Vortex Positions for Separated Flow at $T = 1\frac{A}{U}$

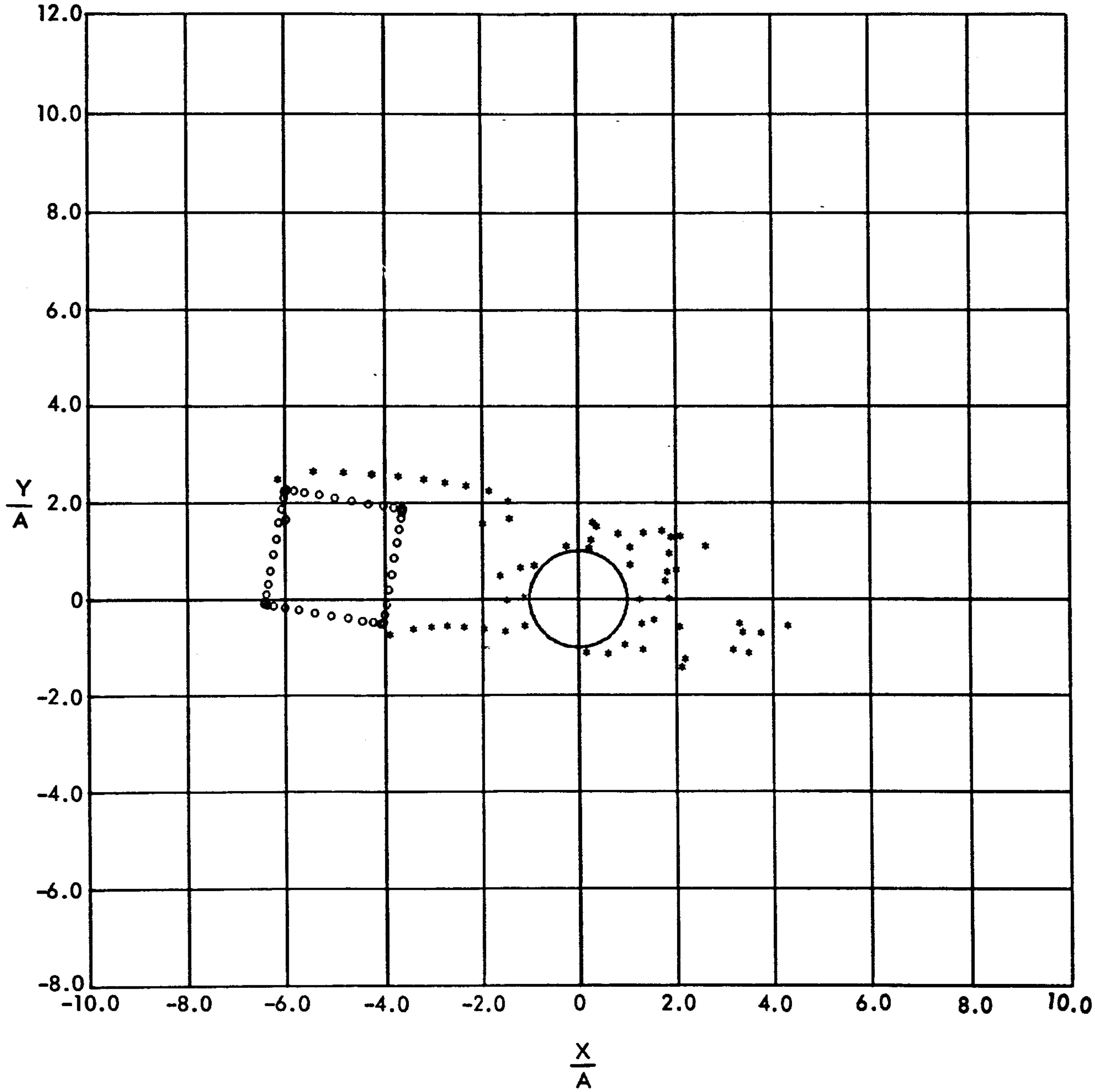


Figure 29b. Instantaneous Vortex Positions for Separated Flow at $T = 6\frac{A}{U}$

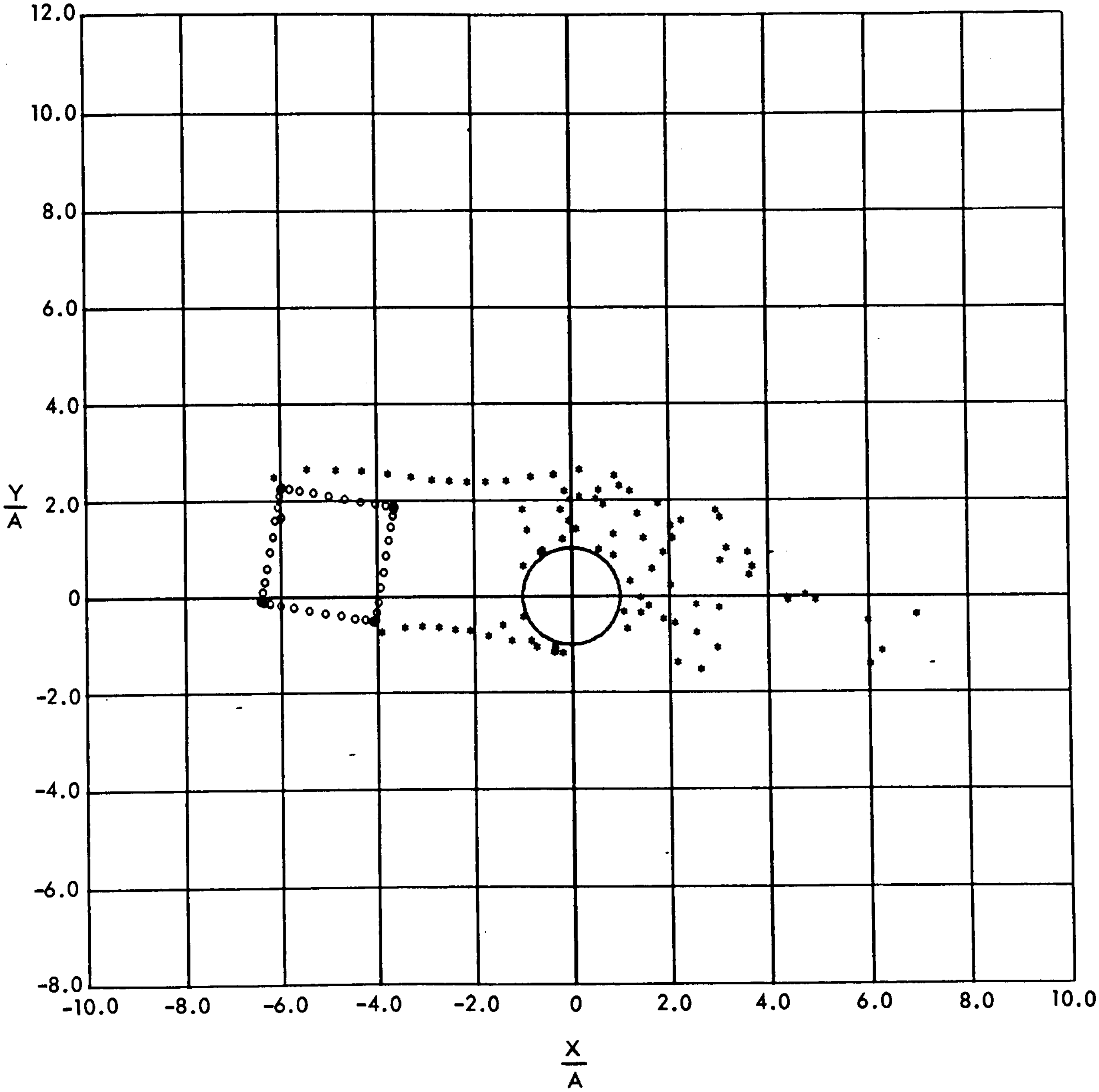


Figure 29c. Instantaneous Vortex Positions for Separated Flow at $T = 9\frac{A}{U}$

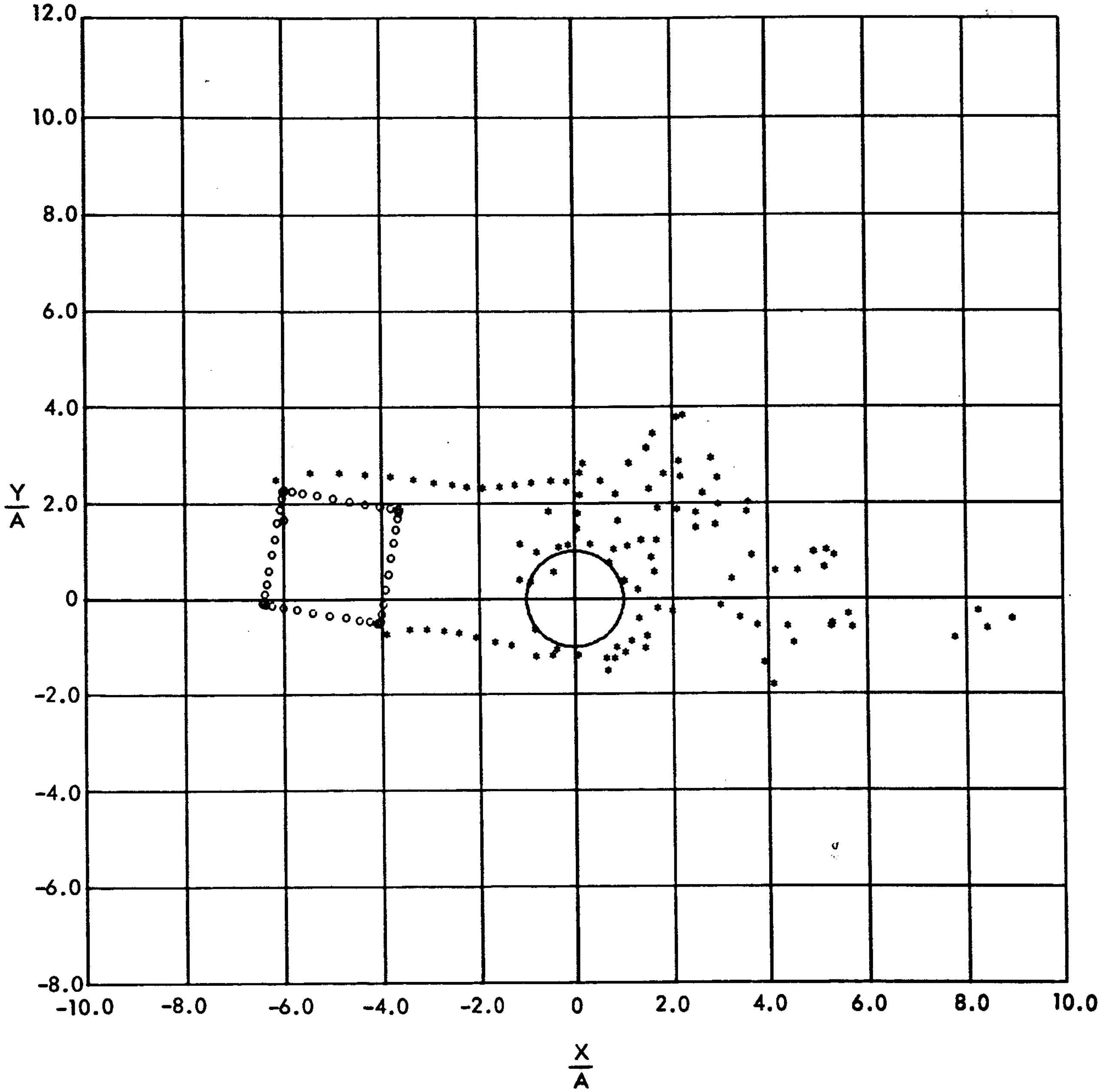


Figure 29d. Instantaneous Vortex Positions for Separated Flow at $T = 11\frac{A}{U}$

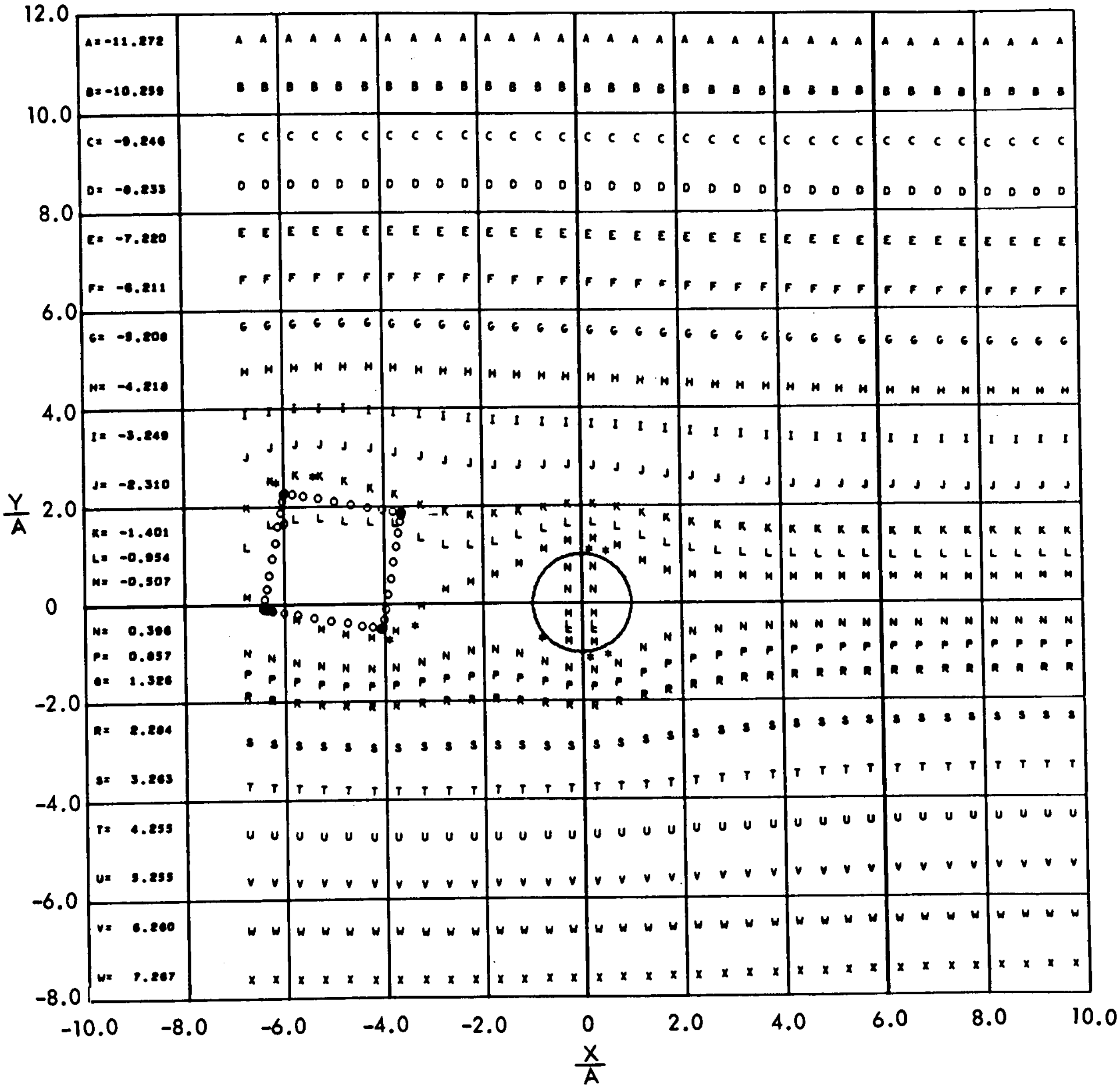


Figure 30a. Instantaneous Flow Streamlines for Vortex Positions of Figure 29a

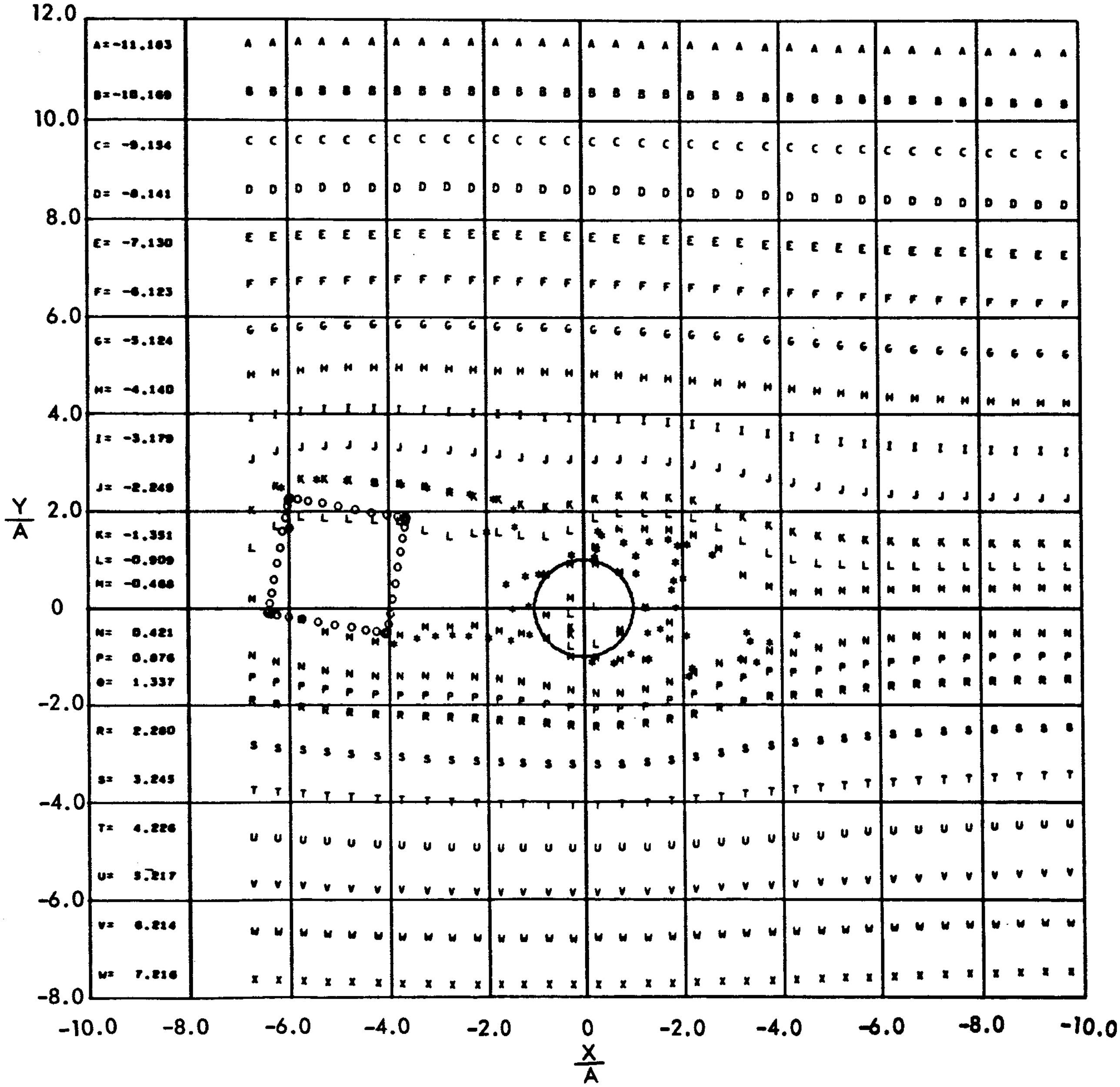


Figure 30b. Instantaneous Flow Streamlines for Vortex Positions of Figure 29b

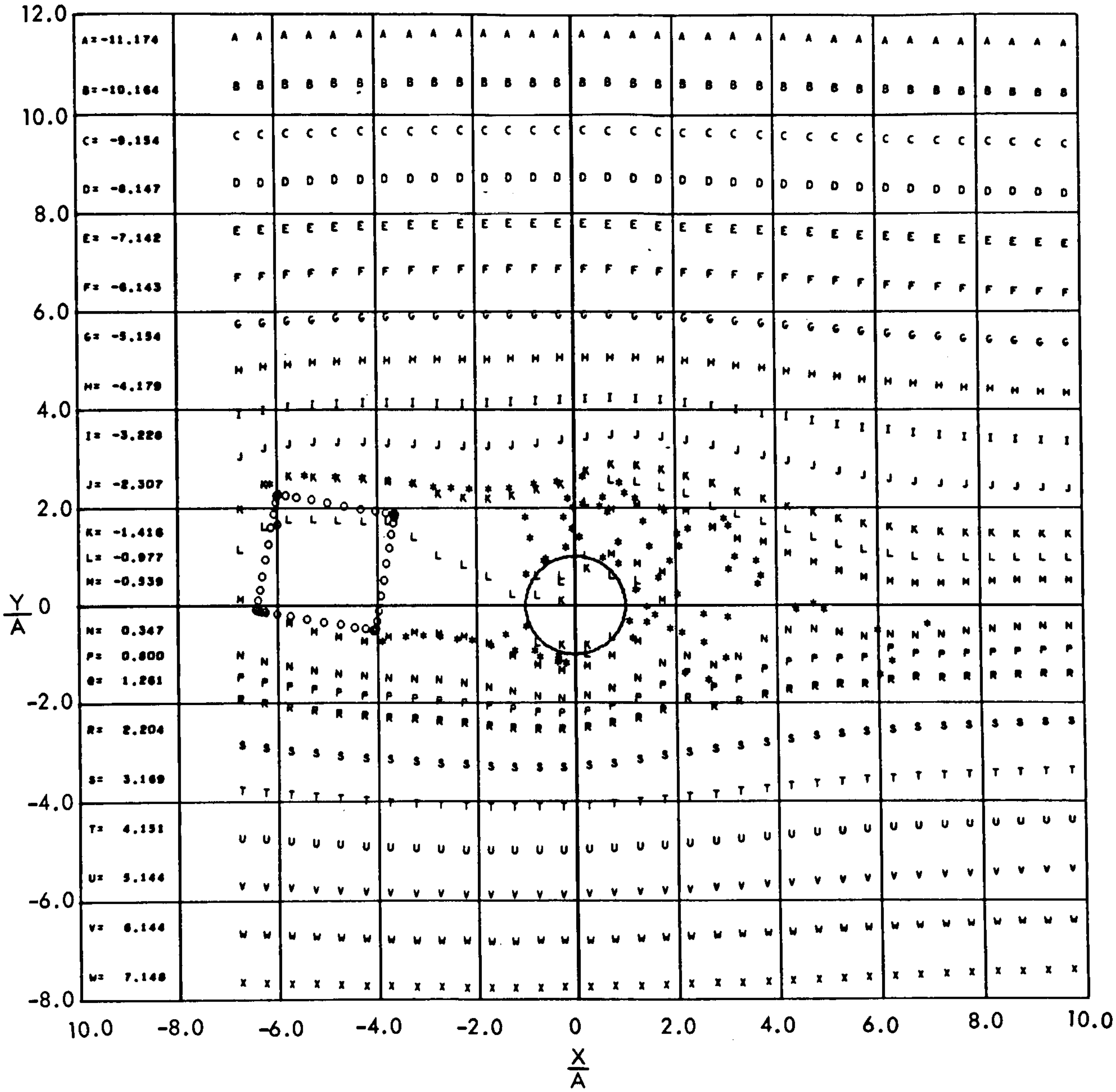


Figure 30c. Instantaneous Flow Streamlines for Vortex Positions of Figure 29c

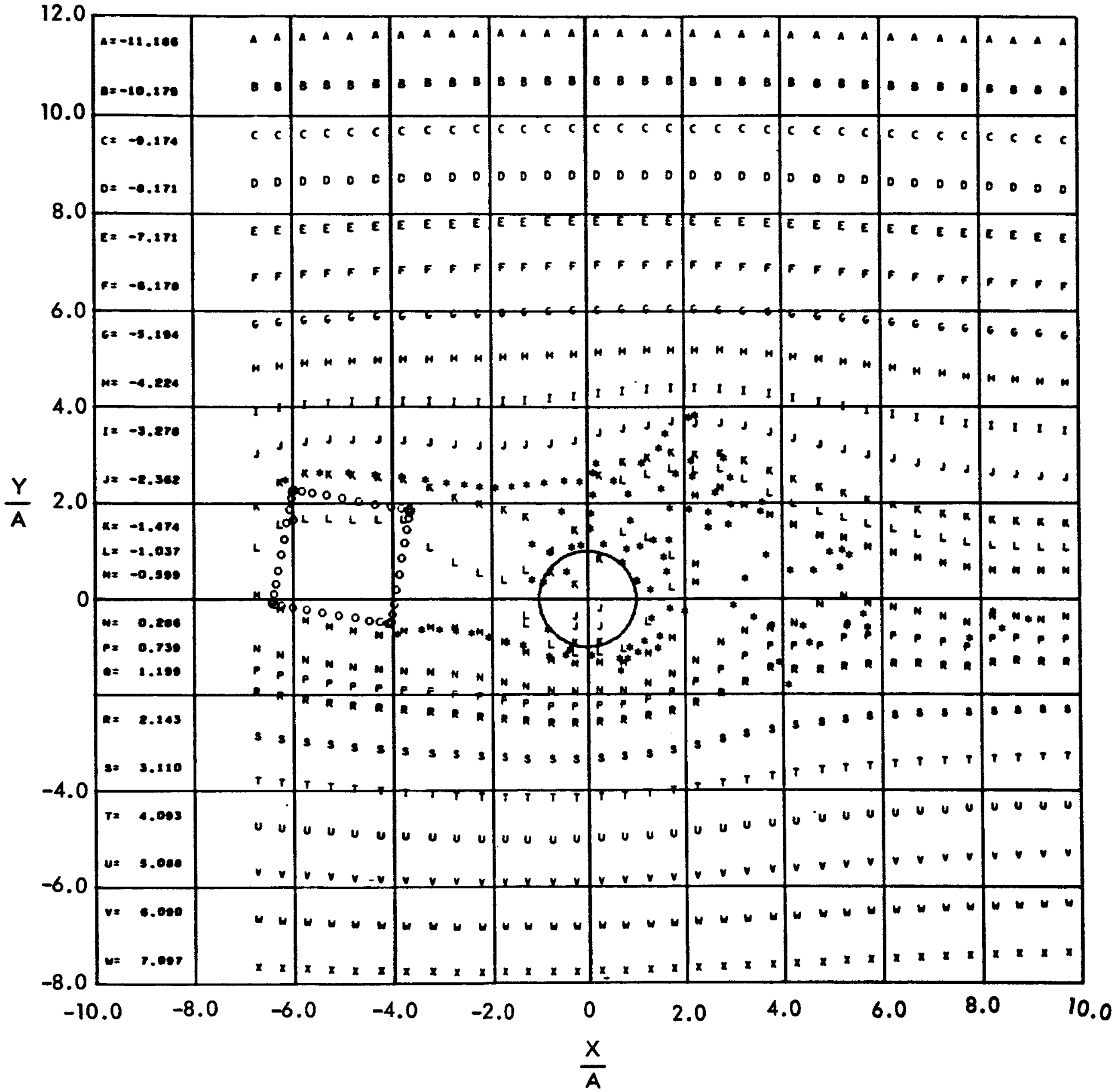


Figure 30d. Instantaneous Flow Streamlines for Vortex Positions of Figure 29d

**Table 1. Anemometer Data for Azimuth of 350 Degrees**

| Anemometer Number | XAN | YAN | Speed | Azimuth | Shift |
|---|---|---|---|---|---|
| | | UT/A = 0 | | | |
| 1 | -5.15 | 7.05 | 1.05 | 350.63 | 0.63 |
| 2 | -5.57 | 4.67 | 1.13 | 352.10 | 2.10 |
| 3 | -5.73 | 3.77 | 1.20 | 353.80 | 3.80 |
| 4 | -6.68 | -1.58 | 1.09 | 340.40 | -9.60 |
| 5 | -6.83 | -2.48 | 1.06 | 343.95 | -6.05 |
| 6 | -7.25 | -4.86 | 1.03 | 347.49 | -2.51 |
| 7 | 0.26 | 1.48 | 1.33 | 343.08 | -6.92 |
| 8 | -0.26 | -1.48 | 1.35 | 345.62 | -4.38 |
| | | UT/A = 3 | | | |
| 1 | -5.15 | 7.05 | 1.07 | 350.84 | 0.84 |
| 2 | -5.57 | 4.67 | 1.15 | 352.98 | 2.98 |
| 3 | -5.73 | 3.77 | 1.23 | 355.44 | 5.44 |
| 4 | -6.68 | -1.58 | 1.06 | 339.59 | -10.41 |
| 5 | -6.83 | -2.48 | 1.04 | 342.98 | -7.02 |
| 6 | -7.25 | -4.86 | 1.03 | 346.70 | -3.30 |
| 7 | 0.26 | 1.48 | 1.35 | 350.75 | 0.75 |
| 8 | -0.26 | -1.48 | 1.45 | 353.43 | 3.43 |
| | | UT/A = 6 | | | |
| 1 | -5.15 | 7.05 | 1.07 | 351.59 | 1.59 |
| 2 | -5.57 | 4.67 | 1.14 | 353.91 | 3.91 |
| 3 | -5.73 | 3.77 | 1.21 | 356.06 | 6.06 |
| 4 | -6.68 | -1.58 | 1.04 | 339.28 | -10.72 |
| 5 | -6.83 | -2.48 | 1.03 | 342.54 | -7.46 |
| 6 | -7.25 | -4.86 | 1.02 | 346.21 | -3.79 |
| 7 | 0.26 | 1.48 | 1.73 | 393.80 | 43.80 |
| 8 | -0.26 | -1.48 | 1.32 | 339.03 | -10.97 |
| | | UT/A = 11 | | | |
| 1 | -5.15 | 7.05 | 1.05 | 352.64 | 2.64 |
| 2 | -5.57 | 4.67 | 1.10 | 354.44 | 4.44 |
| 3 | -5.73 | 3.77 | 1.16 | 356.21 | 6.21 |
| 4 | -6.68 | -1.58 | 1.05 | 338.40 | -11.60 |
| 5 | -6.83 | -2.48 | 1.04 | 341.67 | -8.33 |
| 6 | -7.25 | -4.86 | 1.03 | 345.60 | -4.40 |
| 7 | 0.26 | 1.48 | 1.05 | 407.78 | 57.78 |
| 8 | -0.26 | -1.48 | 1.60 | 356.75 | 6.75 |

Referring to Figures 13, 19a, and 19b, the experimental values of speed ratio and azimuth shift for the east anemometer at a wind direction of 350 degrees are 1.3 and -10 degrees, respectively. These values correspond to 1.22 and 5.4, respectively, listed for anemometer 3 in Table 1. For the west anemometer, this wind direction corresponds to +10 degrees. Again, the experimental values at ten degrees are taken from Figures 13, 19a, and 19b to be 1.04 and 8 degrees, respectively. These values correspond to 1.04 and 10, respectively, listed for anemometer number 4. The general agreement of numerically calculated speed ratios and azimuth shifts with experimental values is fairly close. An interesting indication is that the experimental values based on median curves appear to be significantly better than those based on least-squared error.

## DISCUSSION OF RESULTS

In view of numerical difficulties encountered, perhaps the single most significant result of this section is the demonstration of the fact that flow about arbitrary two-dimensional configurations can be obtained with the method employed. Practicality of the scheme is now substantiated, and the way is opened to further extensions and applications.

Observed differences between test data and numerical results are due in part to the assumed 100-percent solidity for the idealized tower cross-section. Also to be noted is the fact that numerically calculated results in Table 1 are instantaneous values. Average values over sufficiently long periods would be necessary for valid comparison. That instantaneous values are subject to appreciable variations is evident from the values recorded in Table 1 at different time points.

General similarity of numerically calculated speed ratios and azimuth shifts with those of the test data indicate the gross characteristics of the calculated flow to be correct. Further comparative studies could be made by obtaining numerical solutions for the entire range of wind directions, and obtaining the complete speed ratio and azimuth plots. Scope of funding for the present study was unfortunately insufficient for such an analysis. It is noted at this point that, in future studies of this type, lift and drag forces on the cylinder would also be obtainable within the framework of numerical solution obtained.

## LAUNCH PAD

The launch pad dimensions are considerably larger in horizontal planform than those of the LUT. Thus, flow interference induced by the pad may significantly affect its local wind field. For a first estimate the east-west pad elevation was approximated by an equivalent ellipse of the same base-height ratio. Velocity profile was determined along the vertical centerline of this ellipse in symmetric, steady potential flow. This velocity profile is shown in Figure 8. While conservative, it does indicate that an appreciable acceleration of the flow may be expected due to pad elevation.

Based on this result, it was considered of sufficient further interest to determine the influence of a separated wake on the surrounding flow field. A computer program developed during a previous NASA-funded study was modified for this purpose. This computer program employs a Joukowski transformation to determine the two-dimensional symmetric separated flow about an elliptical configuration based upon the generalized Kutta conditions. Modification to this program consisted of fixing the vortex feeding point at a location on the ellipse corresponding to the forward top edge of the trapezoidal pad elevation. This point, 45 meters (150 ft) forward of the pad vertical centerline was calculated as 0.967 transformed circle radii forward of ellipse center. Slope discontinuity and orientation of this edge was considered sufficient to induce flow separation.

Due to numerical difficulties, a point vortex cannot be introduced exactly on the ellipse boundary. The nature of these difficulties stems primarily from the excessive velocity induced by image vortices. Furthermore, in the simulation of shear layer detachment from the boundary, the vortices should be introduced at a point corresponding to the center of the shear layer thickness; this thickness, in turn, is governed by the flow Reynolds number. Based upon a dimension of 100 ft (about twice the pad height), the Reynolds number is expressed by

$$Re = \frac{DV}{\mu} = \frac{100V}{.0016} \cong 6V \times 10^5$$

for a 20 mph wind, Re is $12 \times 10^6$. Reynolds number of this magnitude cannot be simulated by the current computer program without prohibitive computer time and cost. Therefore, a greatly reduced simulated Reynolds number was employed. The vortex feeding period was .125 as nondimensionalized by the transformed circle radius, a, and the free stream velocity, $U_o$.

Substitution into Equation 3 gives an approximate simulated Reynolds number of 1600. Equivalent shear layer thickness represented by a row of equally spaced vortices is 0.56 b, where b is the spacing. Replacing b by $U_s \Delta t$, since $U_s$ is approximately the convective velocity of the vortices at the feeding point, the equivalent nondimensional shear layer thickness is

$$\frac{\delta}{a} = 0.56 \ \frac{U_s}{U_o} \left(\frac{U_o \Delta t}{a}\right) \tag{5}$$

where $\delta$ = shear layer thickness

a = radius of Joukowski cylinder

$U_s$ = vortex convective velocity

$U_o$ = free stream velocity

$\Delta t$ = vortex feeding period

Taking $\dfrac{U_s}{U_o} \cong 1.1$

$$\frac{U_1 \Delta t}{a} = .125$$

$$a = \frac{15.3 + 76.5}{2} = 45.9 \text{ meters (150 ft)}$$

The equivalent shear layer thickness is

$$\frac{\delta}{a} = 0.56\ (1.1)\ (.125)$$

$$\equiv .077$$

$$\delta = 45.9(.077) - 3.53 \text{ meters (11.5 ft)}$$

Using the center of this shear layer, the feeding point height was located at .035 units above the ellipse. Discrete vortices were then introduced at this feeding point according to the generalized Kutta condition already described. While additional velocity maxima occur at the aft edge of the top face, and at possibly additional points due to local influence of convecting vortices, these are considered to be of secondary importance on the overall velocity field.

The simulated Reynolds number is quite low; however, experimental data indicate that for configurations with a stationary separation point, as believed for this case, Reynolds number effects on wake width are not of primary importance. On this basis the gross effects exhibited by the velocity profiles are believed to be valid.

While for an ideal fluid, the assumption of symmetric flow also satisfies the conditions for flow over the half-plane, $y > 0$, this is not true in the case of physical flows. First, the condition of zero slip along the boundary requires that vorticity be generated not only on the ellipse, but also on the half-plane boundary considered. Also since only a finite extent of the half-plane can be considered, some assumption is necessary regarding vertical nonuniformity of the approaching flow.

These two effects could be incorporated by use of initial free vortices to impose a given free stream velocity profile, and calculation of vorticity generation along the plane surface (ground). Such solutions may be warranted in further theoretical ground wind field studies. For the purposes of this study, however, these aspects were not incorporated on the assumption that for initial estimation purposes, the profiles obtained could be directly superimposed with any desired free stream wind profile.

To start the problem, the flow is initially assumed to be steady and without vortices. Horizontal velocity profiles associated with this steady potential flow are shown in nondimensional form in Figure 31. With a 5:1 ellipse representation of the pad, the equivalent Joukowski cylinder has a radius of 46 meters (150 ft), which may be regarded as the reference dimension for converting the vertical scale in Figure 31 to height above natural grade.

As previously discussed, a significant feature appears to be the substantial increase in velocity ratio exhibited by the profile along the vertical centerline.

Figures 32 and 33 are computer plots of vortex positions at nondimensional times of 10 and 12.5. Approximately 7 minutes of computer time was required to reach the solution shown in Figure 33. This solution, containing 100 discrete vortices, shows the wake has fully developed to a nondimensional downstream distance of about 4. Four vortices are shown to have penetrated the boundary due to coarseness of numerical integration. Their effects are considered to be minor, but do cause a peculiarity near the boundary in the velocity profile in Figure 34f for $x/a = 2.0$.

There is an evident periodicity with which vortices are being shed from the ellipse, and appear to be the type reported by Taneda at the IUTAM Symposium, 1964 (edited by Küchemann). For his experiments, periodic oscillation in the streamwise direction caused the formation of symmetrically arranged vortices.

Wake influence on the horizontal velocity profile along the vertical centerline is shown by comparing Figure 34d with the one shown in Figure 31. Except for obvious effects caused by the induced shear layer, the wake influence is seen to be negligible. This appears to be generally true for all the velocity profiles calculated. In other words, the profiles calculated on the basis of steady potential flow should be satisfactory in all regions except those directly in the wake. Within the wake region itself, appreciable velocity decrements are seen to occur; however, its applicability to the pad problem is uncertain, since three-dimensional effects should become more pronounced with downstream distance. Although the solution could have been carried out further to reach a more complete equilibrium condition, the solution obtained is considered to have answered the question in mind; namely, the wake influence on the velocity profile.

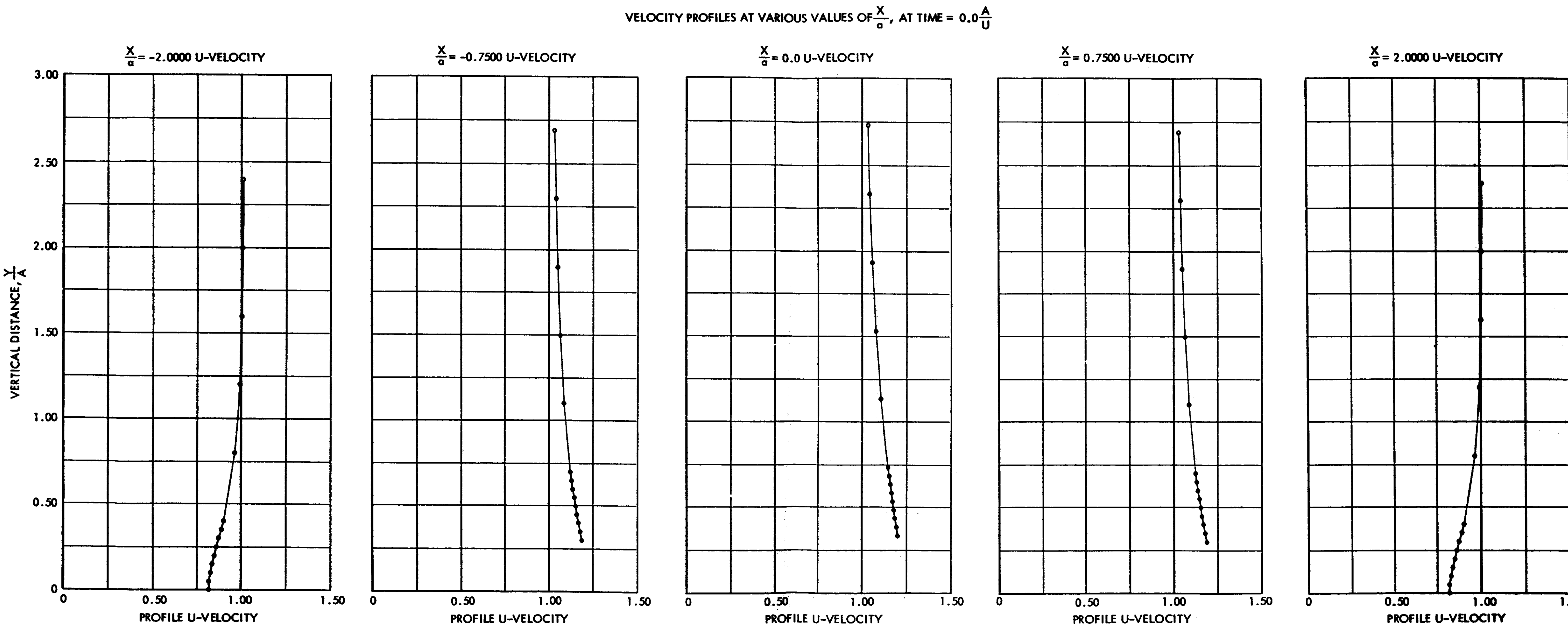


Figure 31. Wind Profile of Steady Potential Flow Over Ellipse



FOLDOUT FRAME

FOLDOUT FRAME

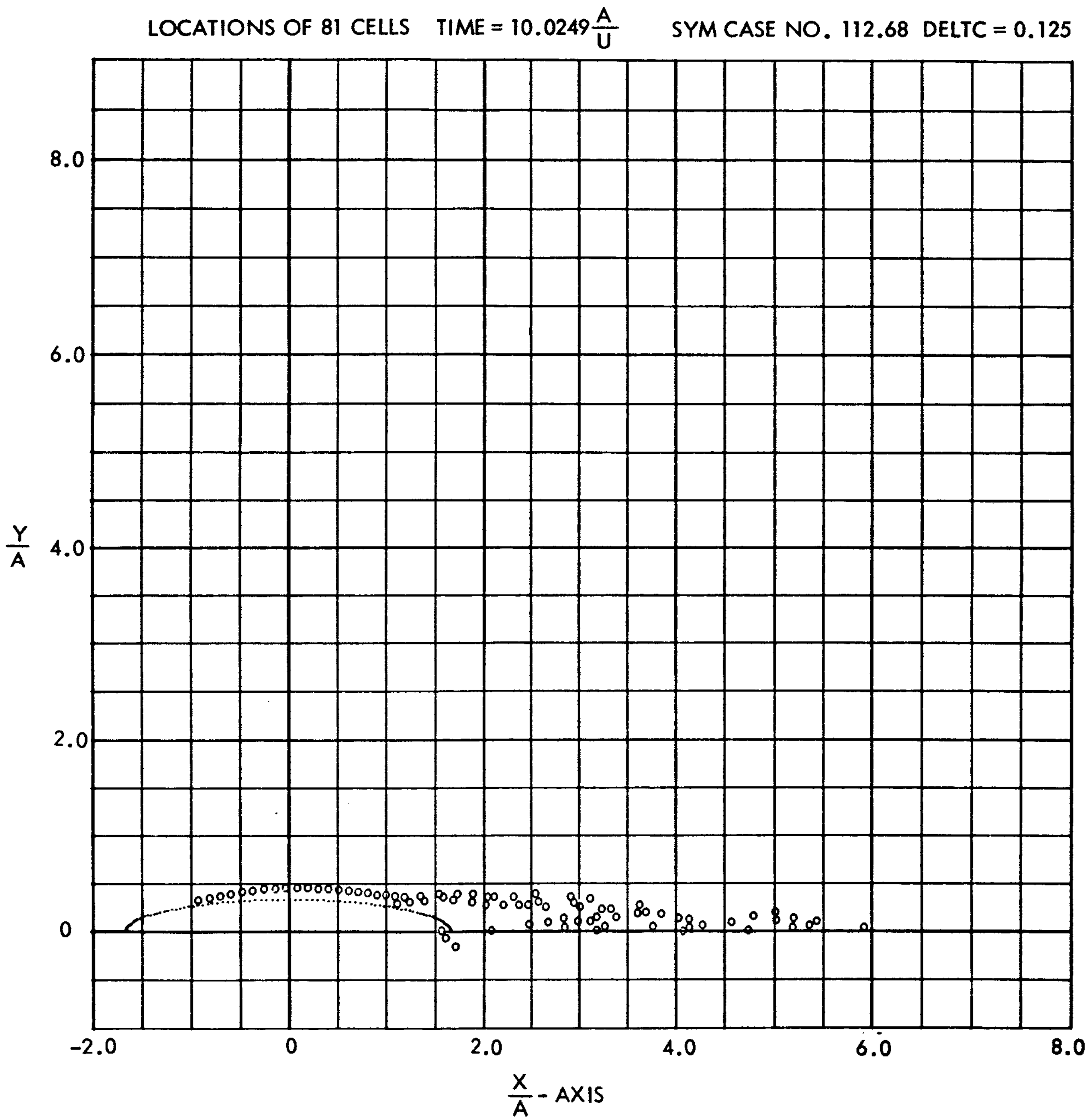


Figure 32. Instantaneous Vortex Positions at t = 10.0249 $\frac{A}{U}$

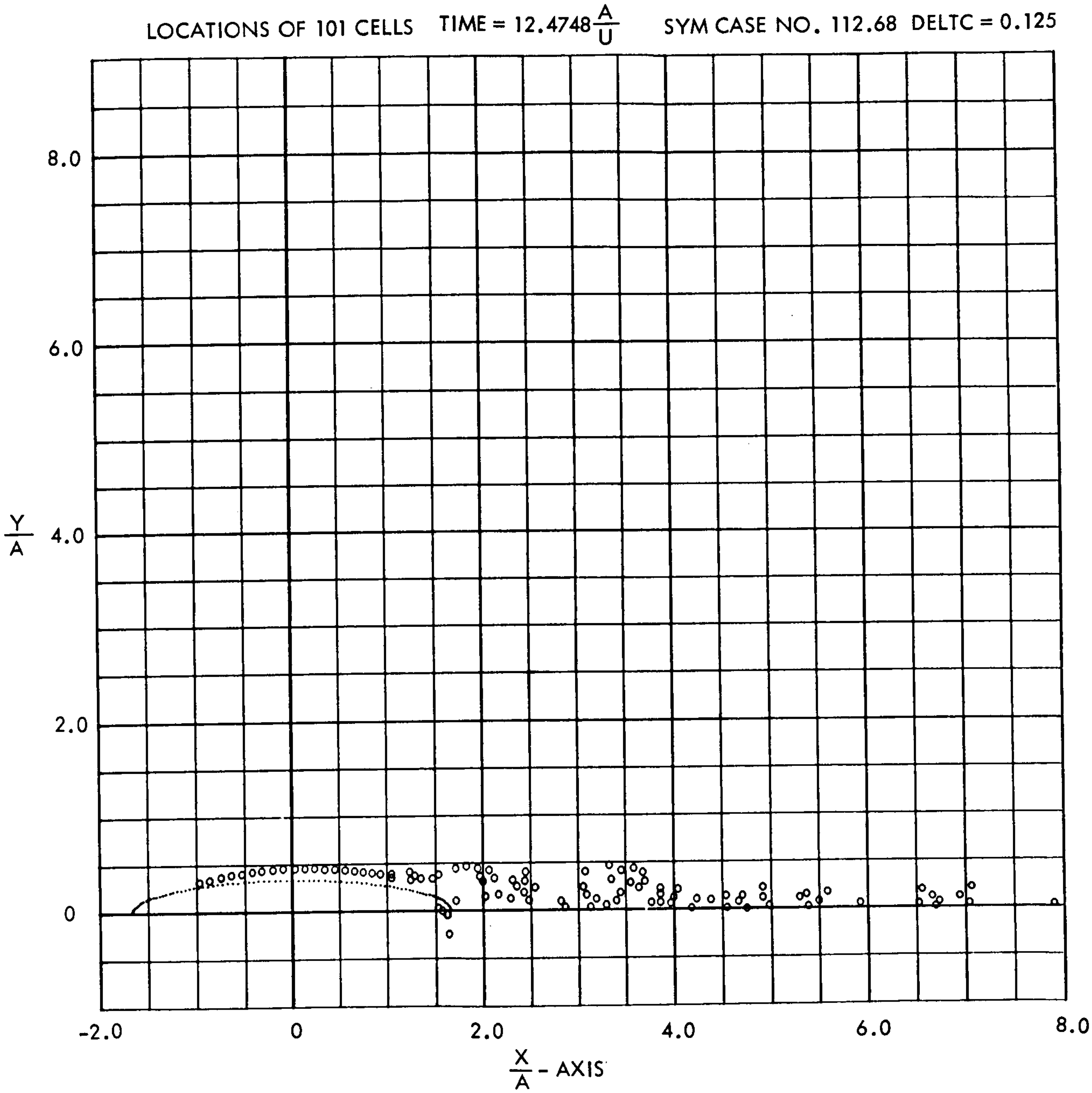


Figure 33. Instantaneous Vortex Positions at $t = 12.4748 \frac{A}{U}$

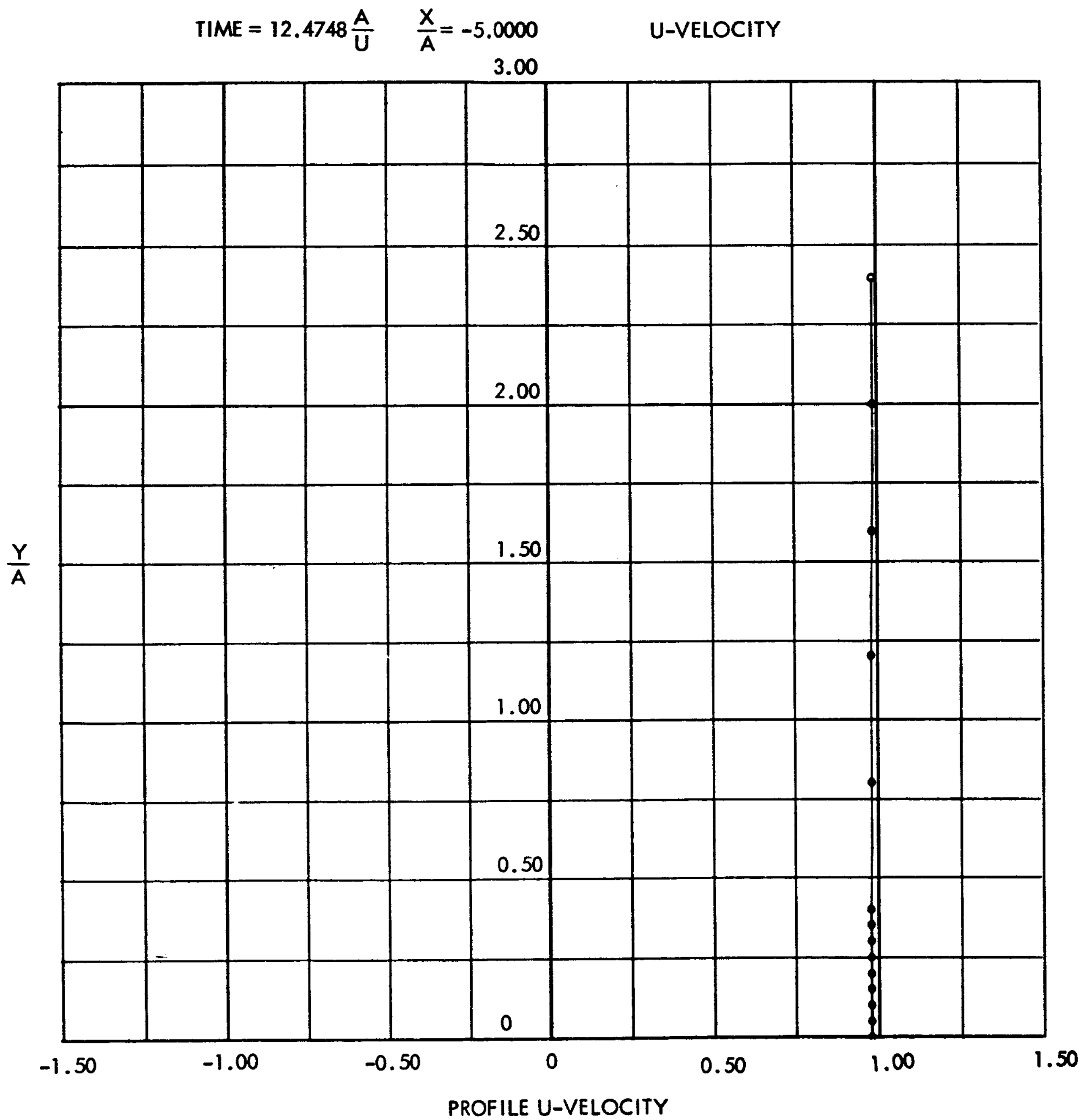


Figure 34a. Horizontal Velocity Profiles at $\frac{X}{A}$ = -5.00

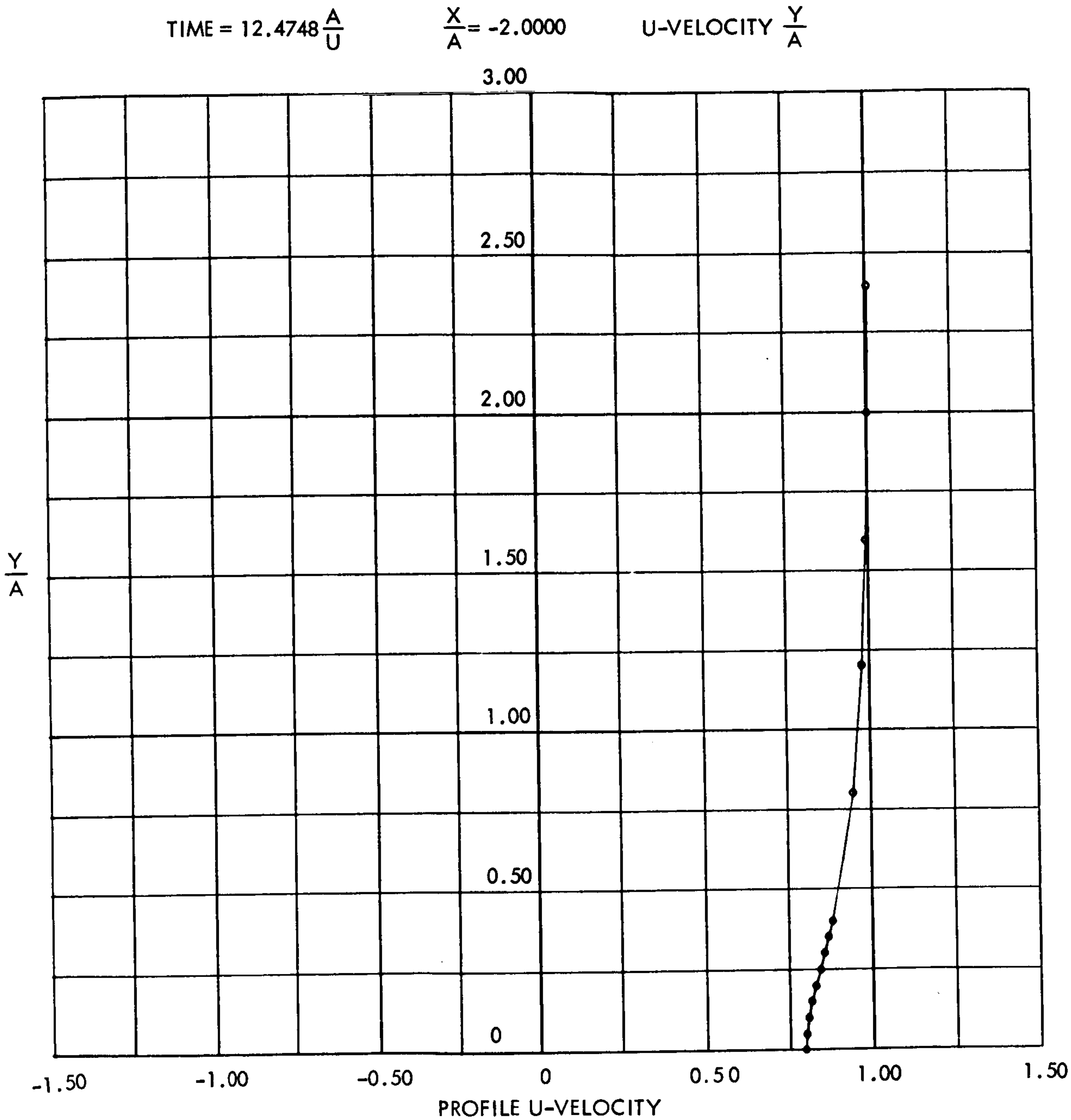


Figure 34b. Horizontal Velocity Profiles at $\frac{X}{A} = -2.00$

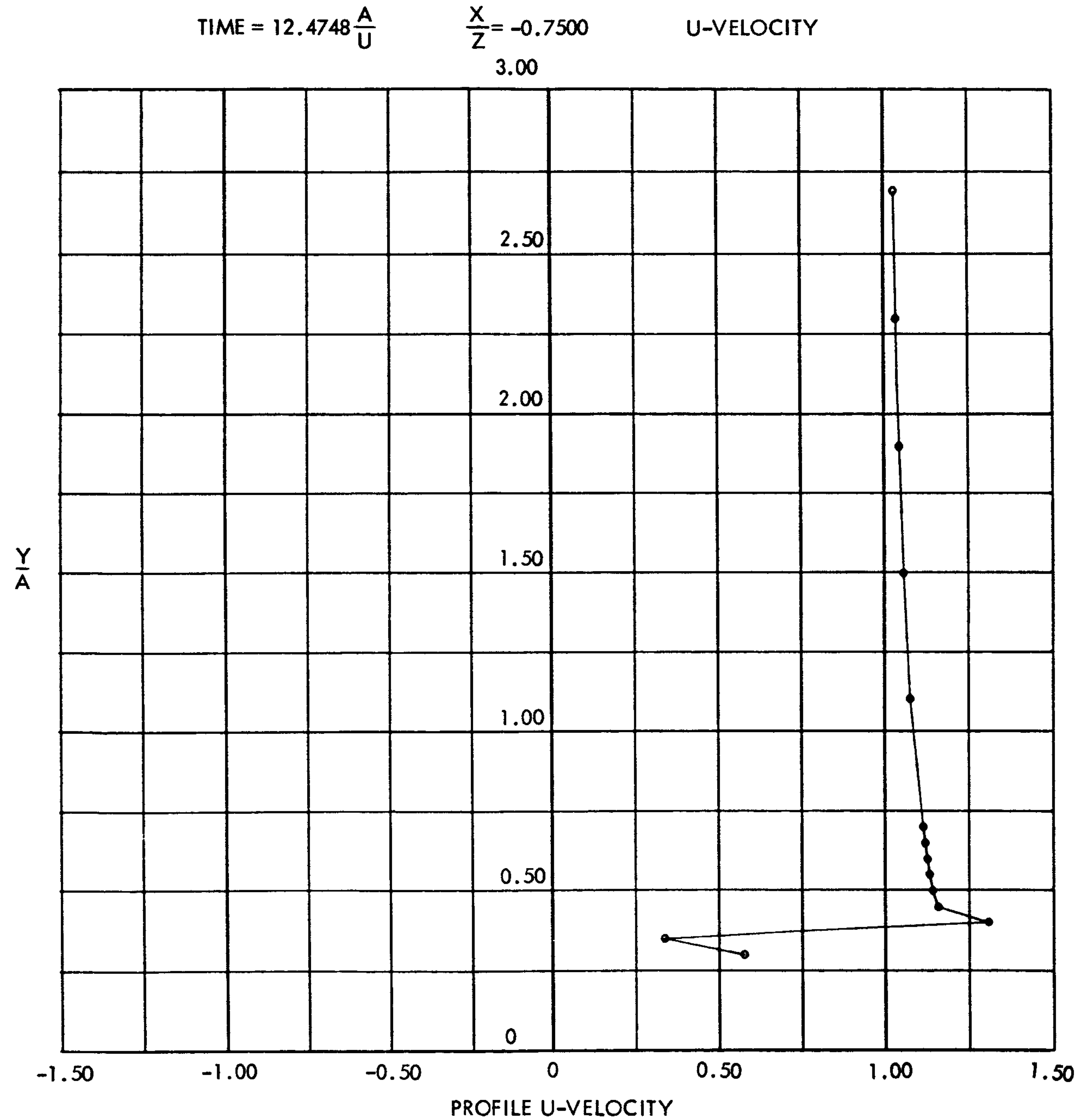


Figure 34c. Horizontal Velocity Profiles at $\frac{X}{A}$ = -0.75

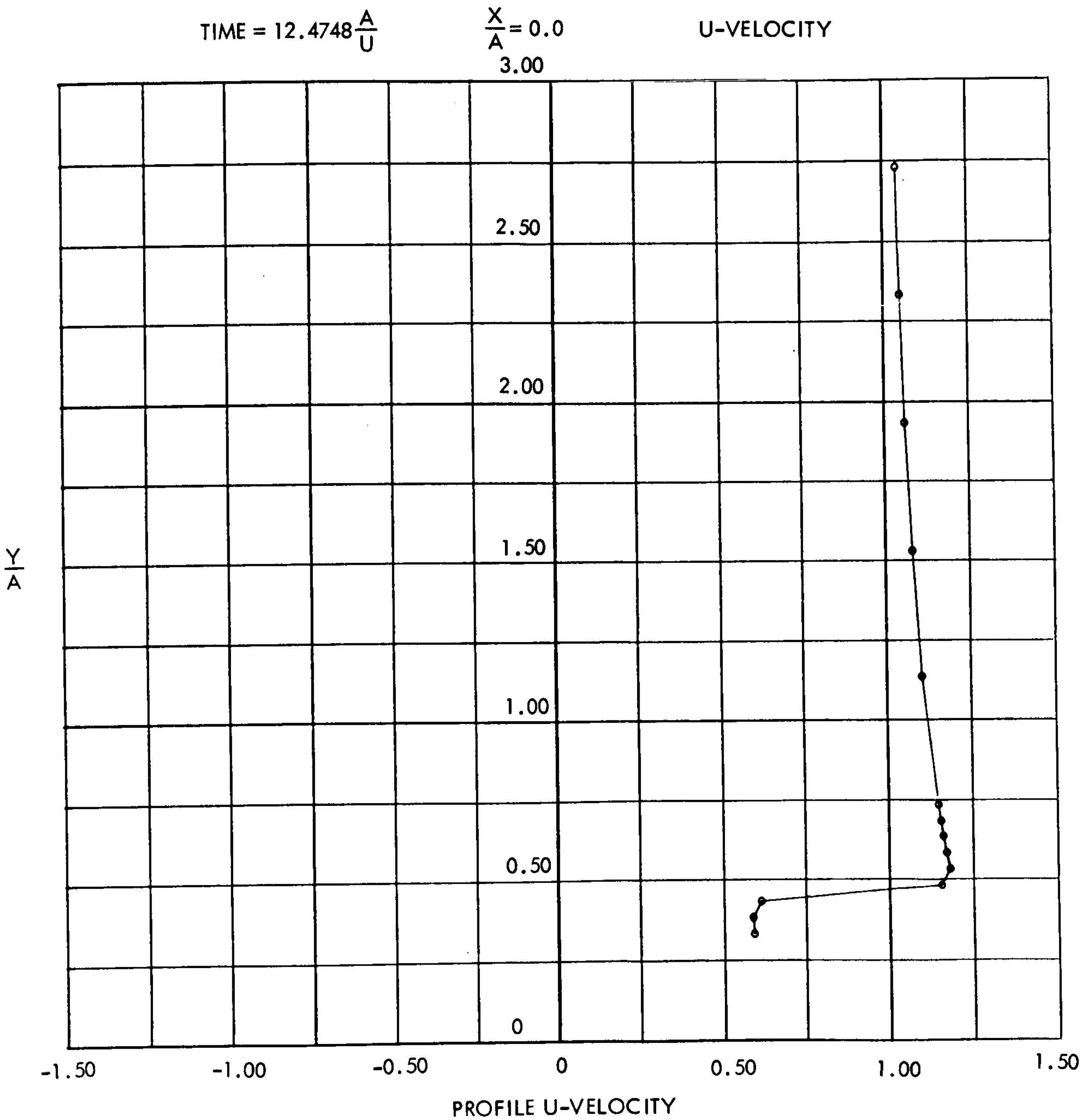


Figure 34d. Horizontal Velocity Profiles at $\frac{X}{A}$ = 0.00

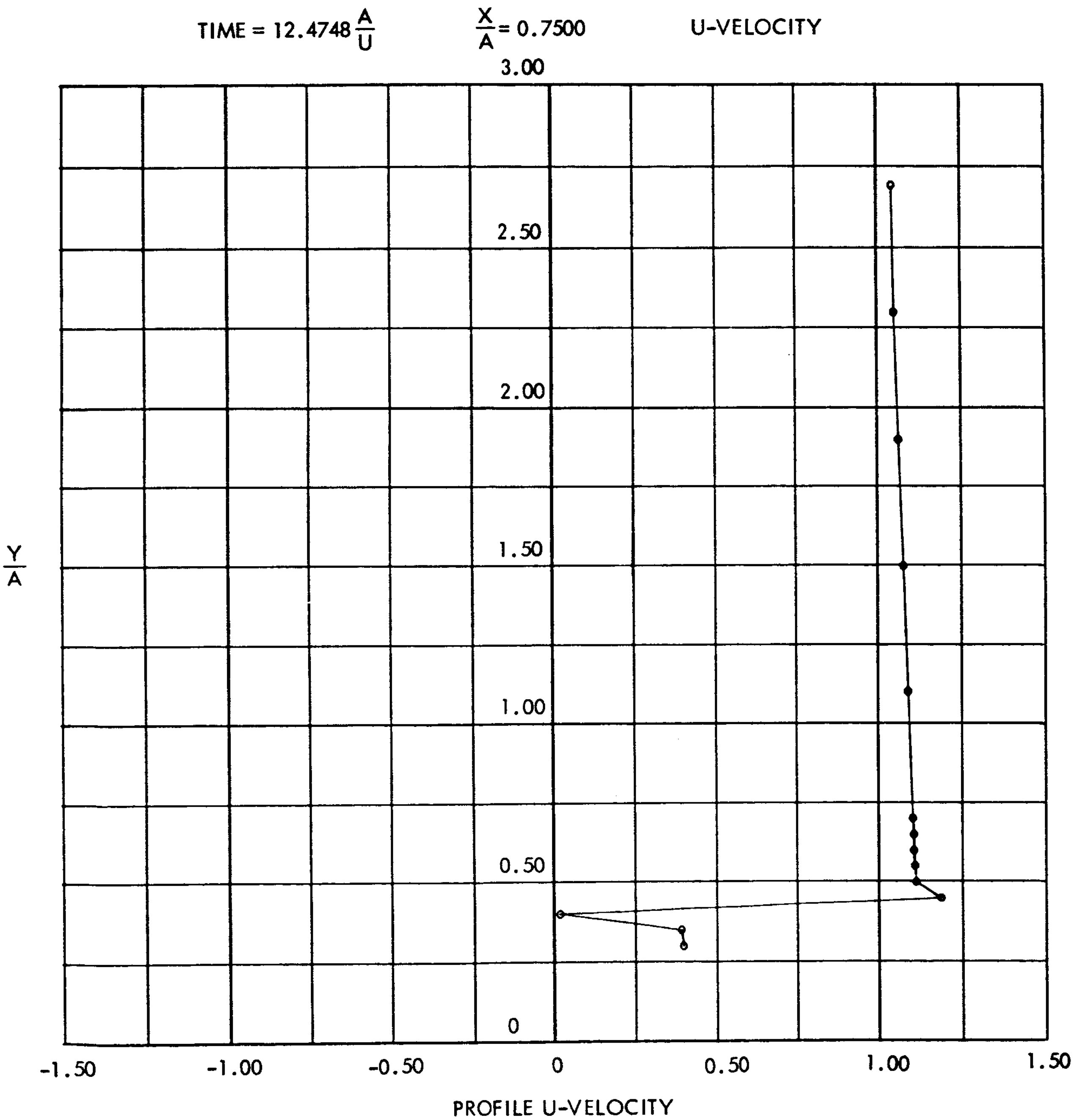


Figure 34e. Horizontal Velocity Profiles at $\frac{X}{A} = 0.75$

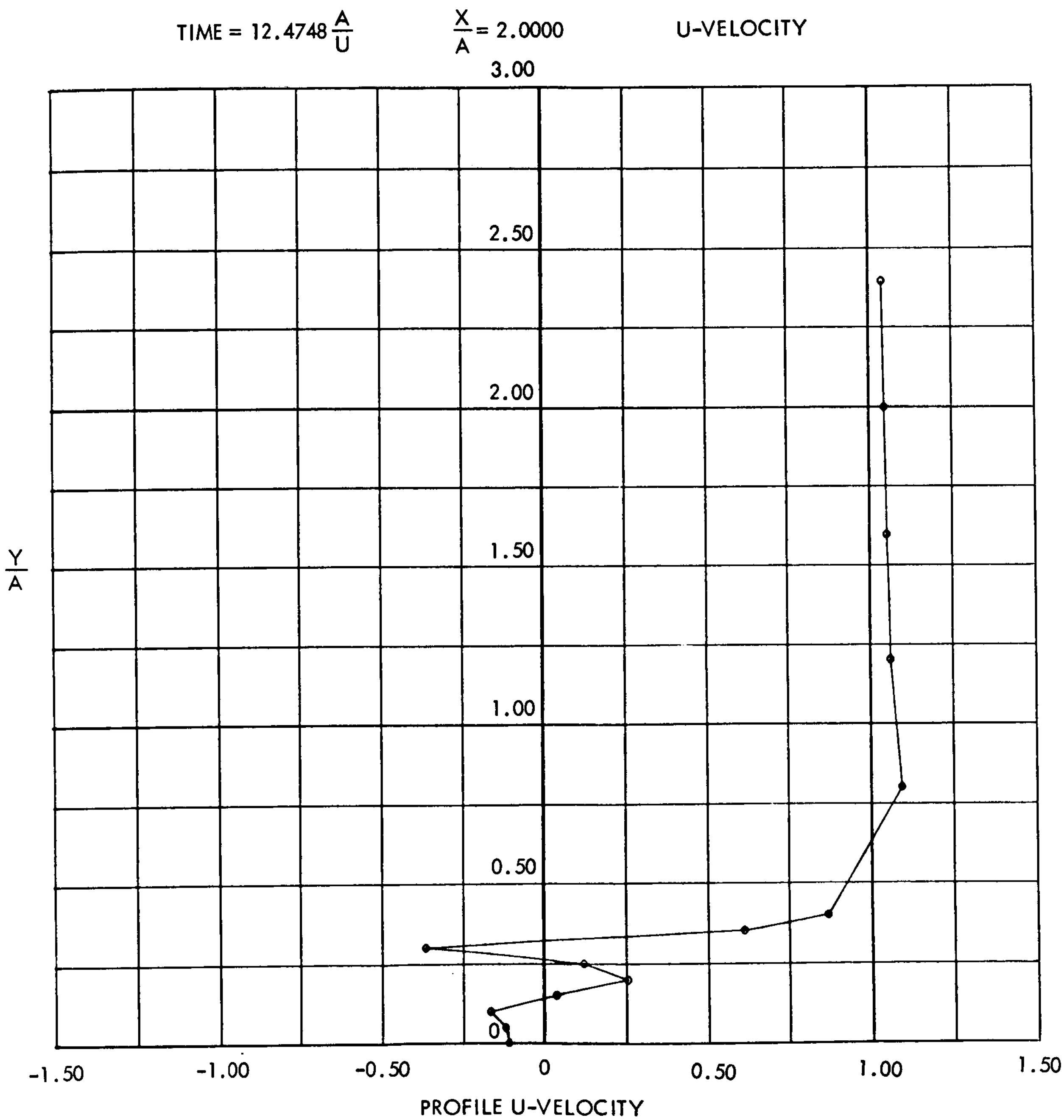


Figure 34f. Horizontal Velocity Profiles at $\frac{X}{A} = 2.00$

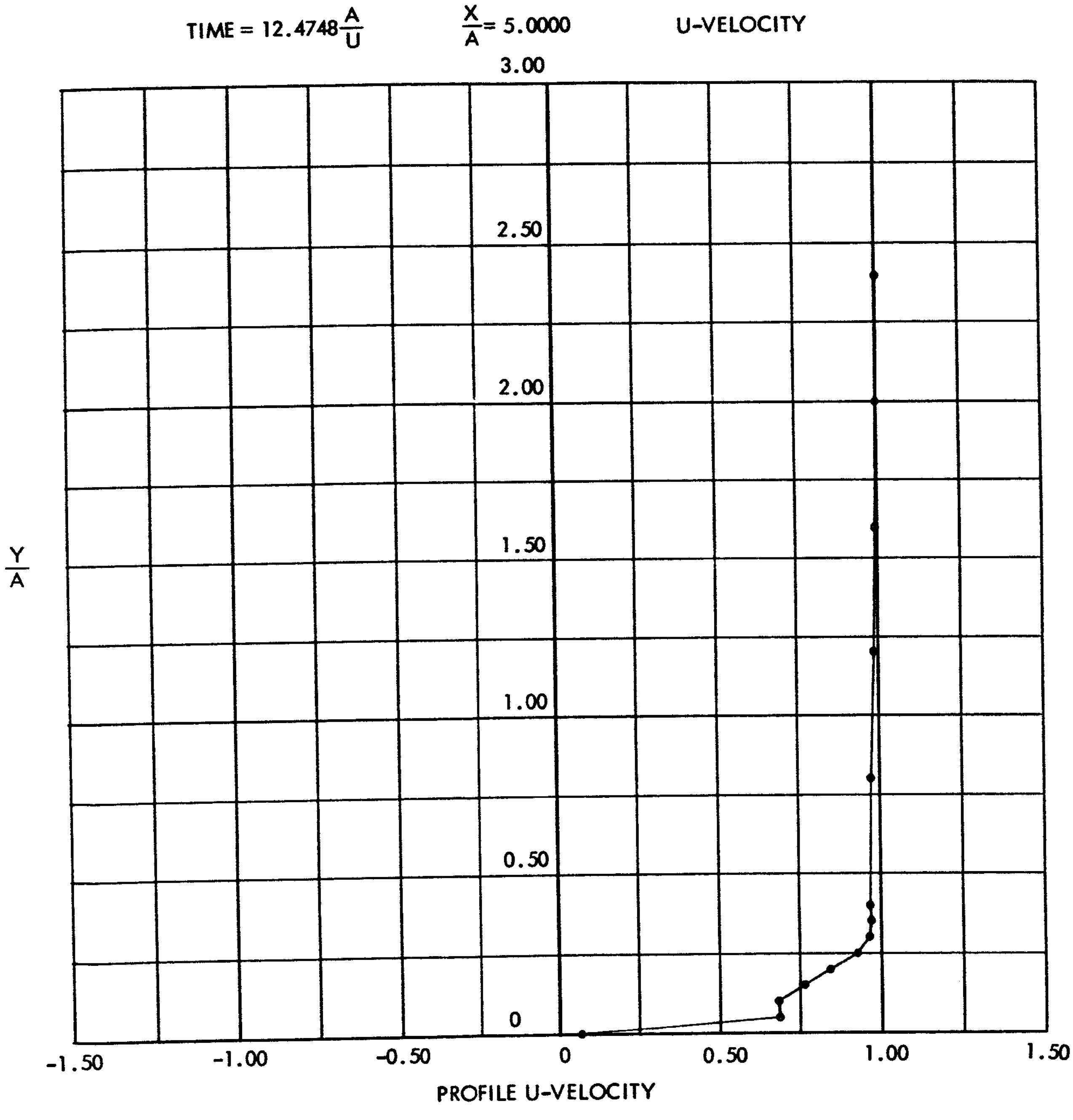


Figure 34g. Horizontal Velocity Profiles at $\frac{X}{A} = 5.00$

## IV. CONCLUSIONS AND RECOMMENDATIONS

It was concluded from an analysis of test data that, for purposes of establishing existing wind conditions, the PLP and 445-ft-level anemometers would be most useful. The deck-zero anemometer should be useful for all wind directions, except those with a significant northerly component. The deck-zero anemometer over its range of usefulness will reflect local speed-up due to pad elevation and deflection by the launcher. For northerly winds, other methods of determining wind velocity are desirable since the anemometer will be exposed to the tower wake. The midlevel anemometers, at least near their present locations, provide data of most doubtful value for purposes of identifying local wind conditions for vehicle cantilever loads.

Previous studies have shown that for a cylinder alone, nonsteady effects of separated flow are of major importance to magnitude of transverse lift and drag loadings. Immersed in an interference flow field, this nonsteady effect would be expected to have even more significance. It is believed, therefore, that for purposes of cantilever load determination, the specification of average flow field characteristics will be insufficient. Computation of nonsteady lift and drag loadings versus wind direction would be much more useful. Using the PLP readings and the analytical method presented herein, one can predict the interference flow field about the vehicle and tower on the launch pad.

PRECEDING PAGE BLANK NOT FILMED.

# APPENDIX A

## TOWER-VEHICLE MIDHEIGHT CROSS SECTION (VSTV)

Index

3. PAPTV (Print and Plot) Subroutine
   1. Flow Chart
   2. Listing
4. KIKTV (Kickoff) Subroutine
   1. Flow Chart
   2. Listing

# APPENDIX A. TOWER-VEHICLE MIDHEIGHT CROSS SECTION (VSTV)

## AI. THEORETICAL DEVELOPMENT

In potential theory, the total flow is a superposition of all the individual flows. Boundary conditions for a circular cylinder may therefore be met by satisfying each flow contribution separately. The uniform flow component is met by a source-sink doublet and the normal flow at the surface induced by each vortex is nulled by an image vortex inside the cylinder according to the circle theorem.

The use of point vortices is especially convenient in nonsteady separated flow analyses since, as free vortices they may be utilized to represent rotationality in the flow, and considered as fixed vortices, they may be arranged to represent bodies of arbitrary shape. In either case the method of solving the resulting velocity field remains essentially unchanged within the framework of finite difference numerical solution.

In this appendix, the velocity field about a source-sink circular cylinder in a field of free vortices, some of which are growing, is developed with potential theory. It is part of a more complete theoretical treatment of the vortex shedding problem in a previous NASA-funded study (Ujihara, et al., 1965). A matrix technique is also developed for the use of stationary vortices to represent bodies of arbitrary configuration in two-dimensional potential flow.

### AI. 1 Flow Field for a System of Vortices Outside a Circular Cylinder in Uniform Flow

For incompressible, inviscid, irrotational, two-dimensional flow, the flow field may be described by a potential function of the complex variable ($z = x + iy$). The complex potential, $w(z)$, of a system of vortices outside a circular cylinder of radius "a" in a uniform stream may be written as the sum of two potentials where

$$w(z) = w_1(z) + w_2(z)$$

$w_1(z)$ ~ uniform flow past a circular cylinder ($r = a$) at angle of attack

$w_2(z)$ ~ system of vortices outside a circular cylinder ($r = w$)

The velocity components are found from the relation

$$(u-iv) = -\frac{dw(z)}{dz} \tag{A-1}$$

From Reference 3, $w_1(z)$ and $w_2(z)$ are found to be

$$w_1(z) = -U_o \left[ze^{-i\alpha} + \frac{a^2}{z}e^{-i\alpha}\right] \tag{A-2}$$

and for n vortices

$$w_2(z) = -i\sum_{j=1}^{n} K_j \log(z-z_j) + i\sum_{j=1}^{n} K_j \log\left(z - \frac{a^2}{z_j}\right)$$

$$= i\sum_{j=1}^{n} K_j \log z + i\sum_{j=1} K_j \log \bar{z}_j \tag{A-3}$$

where $K_j$ strength of the $j^{th}$ vortex filament—positive rotation taken clockwise.

For a vortex outside the cylinder at $z = z_j$, the position of the image vortex inside the cylinder $\frac{a^2}{z_j}$, is denoted;

$$z_j^i = \frac{a^2}{z_j} = \frac{a^2(x_j + iy_j)}{x_j^2 + y_j^2} \tag{A-4}$$

Therefore

$$x_j^i = \frac{a^2 x_j}{x_j^2 + y_j^2}, \quad y_j^i = \frac{a^2 y_j}{x_j^2 + y_j^2} \tag{A-5}$$

The velocity of the $m^{th}$ vortex filament outside the circular cylinder is given by

$$(u-iv)_m = -\left\{\frac{d}{dz}\left[w_2(z) - iK_m \log(z-z_m)\right] + \frac{dw_1(z)}{dz}\right\}$$

$$= \sum_{j=1}^{n} \frac{K_j}{z_m - z_j} - i\sum_{j=1}^{n} \frac{K_j}{z_m - z_j^i} + i\sum_{j=1}^{n} \frac{K_j}{z_m}$$

$$+ U_o \cos\alpha \left(1 - \frac{a^2}{z_m^2}\right) - iU_o \sin\alpha \left(1 + \frac{a^2}{a_m^2}\right) \qquad \text{(A-6)}$$

At this point, it is of some importance to clarify physical significance of the last summation term, in Equation A-6.

This term,

$$i \sum_{j=1}^{n} \frac{K_j}{z_m}$$

included in Equation A-6 insures that total circulation within the fluid region, and around the circle in particular, remains unchanged, as long as rotationality within the external flow remains constant. In the present formulation, however, the concept of small discrete vortices is employed to represent a constantly generated vorticity from the separating boundary layer. In this framework, the addition of a discrete vortex to the external flow, regarded as being generated from the cylinder, requires that an opposite circulation be given to the cylinder in order to maintain the condition of zero total circulation about the entire fluid region. This is automatically accomplished by the image vortex required within the cylinder. On this basis, then, a third vortex at the center, represented by the term,

$$i \sum_{j=1}^{n} \frac{K_j}{z_m}$$

is not required. In the case of multiple bodies in the flow, say, for example, two separate cylinders, it would be necessary to identify from which body the particular vortex was generated. The center vortex would then be omitted from that body, but would be included on the other. If the vortex pre-existed, as an initial condition of the flow, then both bodies must contain the center vortex. In all cases, the condition of constant total circulation is preserved.

Separating Equation A-6 into real and imaginary parts gives the velocity components in non-dimensional form.

$$\left(\frac{U}{U_o}\right)_m = \sum_{\substack{j=1 \\ j\neq m}}^{n} \left(\frac{K_j}{U_o a}\right) \frac{y_m - y_j}{(x_m - x_j)^2 + (y_m - y_j)^2}$$

$$- \sum_{j=1}^{n} \frac{K_j}{U_o a} \frac{y_m - y_j^i}{\left(x_m - x_j^i\right)^2 + \left(y_m - y_j^i\right)^2}$$

$$+ 1 - \frac{x_m^2 - y_m^2}{\left(x_m^2 + y_m^2\right)^2} \cos\alpha - \frac{2\, x_m\, y_m}{\left(x_m^2 + y_m^2\right)^2} \sin\alpha \qquad \text{(A-7)}$$

$$\left(\frac{v}{U_o}\right)_m = - \sum_{\substack{j=1 \\ j \neq m}}^{n} \left(\frac{K_j}{U_o a}\right) \frac{x_m - x_j}{(x_m = x_j)^2 + \left(y_m = y_j^i\right)^2}$$

$$+ \sum_{j=1}^{n} \frac{K_j}{U_o a} \frac{x_m - x_j^i}{\left(x_m - x_j^i\right) + \left(y_m - y_j^i\right)^2}$$

$$- \frac{2x_m - y_m}{\left(x_m^2 + y_m^2\right)^2} \cos\alpha + 1 + \frac{x_m^2 + y_m^2}{\left(x_m^2 + y_m^2\right)^2} \sin\alpha \qquad \text{(A-8)}$$

Having an expression for the velocity field, the problem of nonsteady vortex shedding about a circular cylinder may be approximated by a finite difference technique. At a given time (t) the velocity of the $m^{th}$ vortex is given by Equation A-6. The new coordinates of the $m^{th}$ vortex are then found from the solution of the differential equations,

$$\frac{dx_m}{dt} = u_m (x_1, x_2, \ldots x_n, y_1, y_2, \ldots y_n)$$

$$\frac{dy_m}{dt} = v_m (x_1, x_2, \ldots x_n, y_1, y_2, \ldots y_n)$$

or written as difference equations

$$x_m (t + \Delta t) = x_m (t) + u_m (t) \; \Delta t \qquad \text{(A-9)}$$

$$y_m (t + \Delta t) = y_m (t) + v_m (t) \; \Delta t \qquad \text{(A-10)}$$

This procedure applied to all vortex filaments outside the circular cylinder results in a time history of their displacements. Once the velocity is known, the pressure distributions and resultant forces may be found for each time increment.

## AI. 2. Finite Element Matrix Solution

The method of describing incompressible, inviscid fluid boundaries is in terms of a vortex sheet or source distribution. The finite element matrix methods is a numerical machination of this method in which the source or vortex sheet distribution is approximated by a finite element representation of their strengths. Various methods of representation can be used, the simplest being a lumped parameter approach wherein all the strength over an element is lumped at its midpoint. More sophisticated methods could employ linear or higher order strength distributions over the element.

The approach given herein uses lumped parameters.

The Cartesian velocity components induced at a point, m, by a system of vortices in uniform flow about a source-sink cylinder are given by Equations A-7 and A-8. If the system of vortices covered by index, j, are now required to represent a stationary body in this fluid, the Cartesian velocity components at all midpoints, m, induced by the stationary vortices, may be written in matrix form as

$$\left\{U'_m\right\} = \left[a_{mj}\right] \left\{K'_j\right\} \tag{A-11}$$

$$\left\{V'_m\right\} = \left[b_{mj}\right] \left\{K'_j\right\} \tag{A-12}$$

in which the primed quantities are nondimensional, and

$$a_{mj} = \frac{y_m - y_j}{(x_m - x_j)^2 + (y_m = y_j)^2} - \frac{y_m - y_j^i}{(x_m - x_j^i)^2 + (y_m - y_j^i)^2} \tag{A-13}$$

$$b_{mj} = \frac{-(x_m - x_j)}{(x_m - x_j)^2 + (y_m = y_j)^2} + \frac{x_m - x_j^i}{(x_m - x_j^i)^2 + (y_m = y_j^i)^2} \tag{A-14}$$

The normal velocities, VN, induced by the stationary vortices at points, m, according to the convention below are

$$(VN)_m = - U'_m \cos \theta_m + V'_m \sin \theta_m \qquad \text{(A-15)}$$

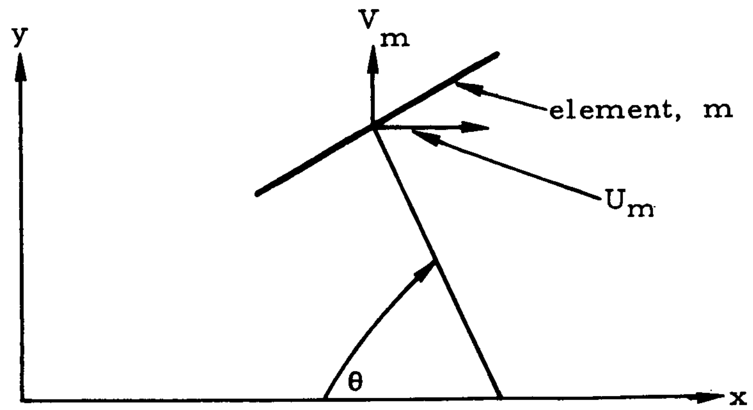


In matrix form this becomes

$$\left\{VN_m\right\} = \left[- a_{mj} \cos \theta_m + b_{mj} \sin \theta_m\right] \left\{K'_j\right\} \qquad \text{(A-16)}$$

Since the total normal velocity must be zero, $(VN)_m$ must be equal to the negative of the normal velocity induced by the free vortices and the source-sink cylinder. Denoting this quantity by VIN (velocity inward normal), Equation A-16 becomes

$$\left\{VIN_m\right\} = \left[a_{mj} \cos \theta_m + b_{mj} \sin \theta_m\right] \left\{K'_j\right\} \qquad \text{(A-17)}$$

One additional equation is required to govern the total circulation represented by the stationary vortices (condition of constant circulation). This is accomplished by having an additional stationary vortex, $K_c$, within the body, say at the center. The magnitude of $K_c$ is such that

$$K_c + K_j = -(KR) \qquad \text{(A-18)}$$

where

the index, j, is summed over the stationary vortices (KR) is the sum of all free vortices generated by the finite element body.

Incorporating this equation into A-17 the last term of $\left\{VIN_m\right\}$ will now contain (-KR), the last term in $\left\{K_j\right\}$ will contain $K_c$ , and the matrix of coefficients in Equation A-17 will be expanded to include an additional row of unit values, including the diagonal term, and an additional column of coefficients for a vortex at center. Defining this final matrix of coefficients by $\left[VON\right]$, velocity outward normal, Equation A-17 becomes

$$\left\{VIN_m\right\} = \left[V\emptyset N_{mj}\right]\left\{K'_j\right\} \quad \text{(A-19)}$$

Strengths of the stationary vortices are determined by the inverse of Equation A-19.

The matrix of coefficients, $A_{mj}$ is seen to depend only upon the geometry of stationary vortices representing the body, hence needs to be determined and inverted only once for a given body. In the finite scheme of solution, the strengths of these stationary vortices are solved by matrix multiplication of $\left[A_{mj}\right]^{-1}$ with the instantaneous values of $\left\{VIN_m\right\}$.

## AII. MAIN PROGRAM (VSTV)

The VSTV program computes the vortex field around the vehicle and tower as assembled on the launch pad. This field is defined by x and y locations, u and v velocities and k, strengths, of the fixed and free vortices as the field grows in time. Within the time loop, the subroutines presented in Section AIII are called. The flow chart of the main program is presented in Section AII. 1.

VSTV is a Fortran G program for the channelled IBM 360-40 and IBM 360-65 computing system. A peripheral system, SC 4020 Optical Plotter, reads magnetic tape output and produces graphic data. The obvious application of this combination is the rapid production of tabulated data and labeled graphs which for this analysis is essential.

The input data allows control of the streamline computation and both printed and graphic output data. Machine run time is dependent upon the frequency of the requested output data relative to the growth of the field. The block data are items which change infrequently and are itemized in Section AII. 2. The input data are defined in Section AII. 3. 1 and a sample case set up in Section AII. 3. 2.

The program is terminated by either of two conditions controlled by input variables DNC, desired number of cells in field, or TFIN, final time. Both tests call subroutine KIKTV which writes terminating case data on

## AII. 1 VSTV Functional Flow Chart

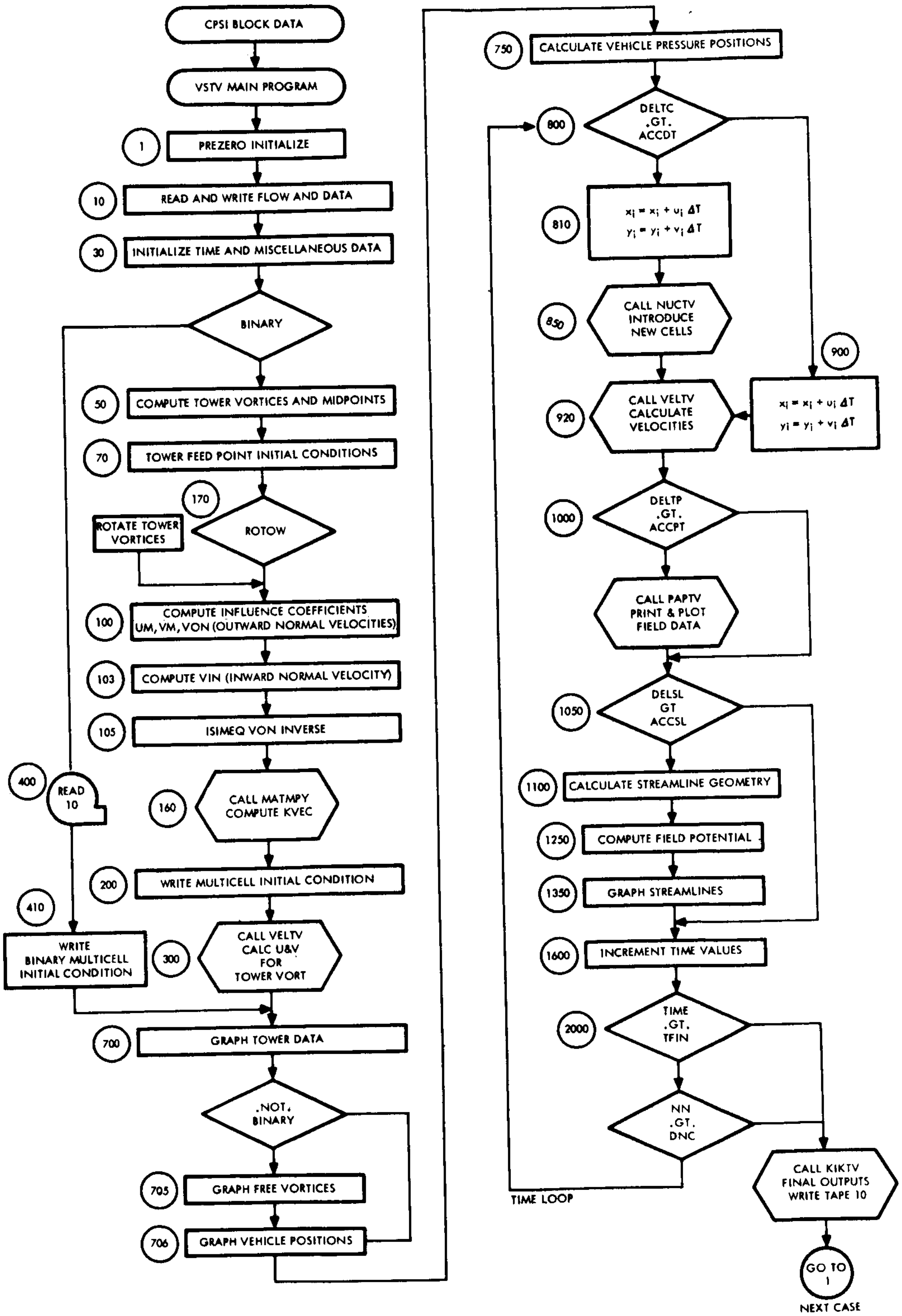

Fortran logical tape 10, calls PAPTV for last computed output. The main program then returns to a read statement for next case input data which is the normal exit.

AII. 2 Block Data

The block data, CPSI, sets up the labels for the streamline graphs in BCD, the distribution of the y values for the field potential calculation as YSIP, and the SC 4020 character symbols for the streamline graphs, KSYM. The YSIP would vary if the graph margins are changed. The program is limited to 24 streamlines, the characters O and X being omitted.

AII. 3 Input Data

AII. 3. 1 Data Definition

The input data consist of two standard Fortran G namelist arrays, FLØW and DATA. The FLØW data control the logical decisions throughout the program and consist of two items:

BINARY = F for the TIME = 0. 0 case

= T for the restart case (Tape 10 data read)

ROTOW = F for the tower positioned upstream from the vehicle

= T for the tower rotated around vehicle center.

The program sets both values to false; hence, only true values need to be included in input data. However, the namelist cards FLØW and END must be in data set when both false.

The DATA namelist array is defined as follows:

TIME = 0. 0 for BINARY = False case
Omit for BINARY = T case (TIME input from Tape 10)

DELTC Incremental time of new vortices

CONKC Constant to compute delta time (DELTA = CONKC * DELTC)

DELTP Time increment to print and graph data

TFIN Time to terminate run

| | |
|---|---|
| DELSL | Time increment to compute streamlines |
| DNC | Total number of vortices to be calculated (run terminates on either DNC or TFIN) |
| RØT | Angle of tower rotation (deg) |
| TFAC | Factor to generate tower feed points |
| TFP1 | First tower feed point equal to position number (see sketch) |
| TFP2 | Second tower feed point equal to position number (see sketch) |

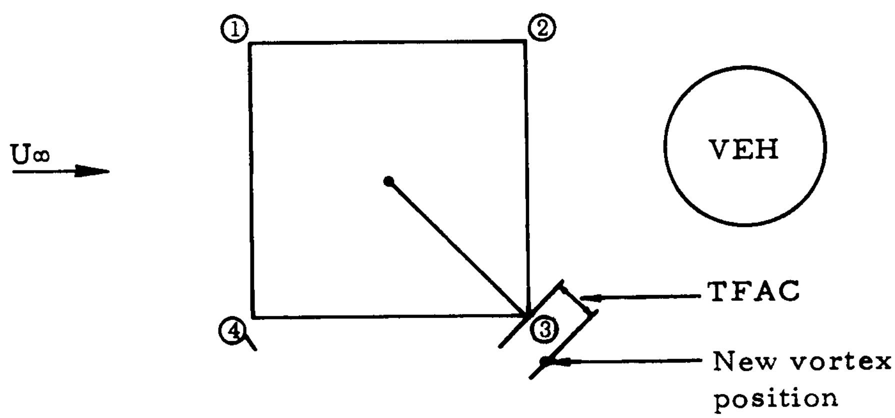


| | |
|---|---|
| XUL | Tower position (x upper left) |
| YUL | Tower position (y upper left) |
| NXR | Number of tower points (x side) |
| NYR | Number of tower points (y side) |
| XREC | Length of tower x side |
| YREC | Length of y side (vehicle radius = unity) |
| NPHAF | Number of points on semi-cylinder |
| UTOP | Maximum velocity to pressure calculation test |
| CONST | Vehicle feed point height |

| | |
|---|---|
| XXL | Graph left margin |
| XR | Graph right margin |
| YB | Graph bottom margin |
| YT | Graph top margin |
| CASENO | Case number in form XXXX. XX (date) |
| XINIT | Streamline initial X location |
| XINC | Streamline delta X |
| NXS | Streamline number of X values |
| NYS | Streamline number of Y values |

AII. 3. 2 Sample Case

The input data and namelist FLOW and DATA arrays for the simple case follow.

## AII. 4 VSTV Listing, Main Program, Memory Map

```
   E-LEVEL LINKAGE EDITOR OPTIONS SPECIFIED MAP,LIST
****MEMBER     DOES NOT EXIST BUT HAS BEEN ADDED TO DATA SET
```

MODULE MAP

| CONTROL SECTION NAME | ORIGIN | LENGTH | ENTRY NAME | LOCATION | NAME | LOCATION | NAME | LOCATION | NAME | LOCATION |
|---|---|---|---|---|---|---|---|---|---|---|
| VSTV# | C0 | 3362 | VSTV | 00 | | | | | | |
| $BLANKCOM | 3368 | 3E5C | | | | | | | | |
| CFLOW | 6BC8 | E | | | | | | | | |
| CINIT | 6BD0 | AC | | | | | | | | |
| CTIMES | 6C80 | 3E | | | | | | | | |
| CGRA | 6C88 | F7C | | | | | | | | |
| CIF | 7C38 | 2C | | | | | | | | |
| CPSI | 7C58 | 2B5E | | | | | | | | |
| CTCW | A7B0 | D33C | | | | | | | | |
| CCYL | 17AE0 | 1C5E | | | | | | | | |
| CRCT | 18B38 | 32C | | | | | | | | |
| NUCTV# | 18E58 | 156E | NUCTV | 18E58 | | | | | | |
| SCOUTV# * | 1A3C0 | 2AE | SCOUTV | 1A430 | SCRTV | 1A54C | | | | |
| KIKTV# | 1A668 | 32C | KIKTV | 1A668 | | | | | | |
| MATMPY# | 1A988 | 324 | MATMPY | 1A988 | | | | | | |
| VELTV# | 1ACB0 | 62E | VELTV | 1ACB0 | | | | | | |
| PAPTV# | 1B2C8 | 58C | PAPTV | 1B2D8 | | | | | | |
| TLOOK1# | 1B858 | 47C | TLOOK1 | 1B858 | | | | | | |
| HOUR# | 1BCC8 | 244 | HOUR | 1BCD8 | | | | | | |
| SMRCRT * | 1BF20 | CE | | | | | | | | |
| SCBUFV | 1BFE8 | E4 | | | | | | | | |
| NHCAWAA * | 1C070 | E4D | FRAMEV | 1C070 | RESETV | 1C088 | CAMRAV | 1C208 | IDFRM# | 1C2A4 |
| CTAPEV * | 1C8C0 | 4 | | | | | | | | |
| IHCFCOMH# | 1C8C8 | FFD | IBCOM# | 1C8C8 | FDIOCS# | 1C984 | | | | |
| IHCTRCH * | 1C8C8 | 27E | | | | | | | | |
| IHCNAMEL* | 1DB40 | EA2 | FRDNL# | 1DB40 | FWRNL# | 1E0C8 | | | | |
| CCSD# * | 1E3E8 | 26A | COSD | 1E428 | SIND | 1E51C | | | | |
| ATANC# * | 1E658 | 17E | ATAND | 1E668 | | | | | | |
| IHCIBERH# | 1E7C8 | CE | IBERH# | 1E7D8 | | | | | | |
| ISIMEQ# * | 1E8A8 | 844 | ISIMEQ | 1E928 | IDETRM | 1EB84 | | | | |
| GRIDIV# * | 1F0F0 | BC2 | GRIDIV | 1F1E0 | | | | | | |
| APRNTV# * | 1F8F8 | 21C | APRNTV | 1FC28 | | | | | | |
| NHCAWAP * | 1FE08 | EE | PRINTV | 1FE08 | | | | | | |
| APLOTV# * | 1FEF0 | 3F4 | APLOTV | 1FF40 | | | | | | |
| NXV# * | 202E8 | 3B4 | NXV | 20328 | IXV | 20438 | NYV | 2040C | IYV | 20558 |
| LABLV# * | 206A0 | 5AA | LABLV | 20760 | | | | | | |
| IHCSSQRT* | 20C50 | AC | | | | | | | | |

| NAME | ORIGIN | LENGTH |
|---|---|---|
| IHCSLOG * | 20D00 | 1CC |
| IHCFMAXR* | 20E10 | C8 |
| NHCAWCE * | 20EE0 | BC |
| NHCAWEO * | 20F90 | 4A8 |
| NHCAWEP * | 21438 | 148 |
| NHCAWEN * | 21580 | 254 |
| NHCAWAC * | 217D8 | 13C |
| IHCFCVTH* | 21908 | FF3 |
| NHCAWER * | 22900 | 358 |
| IHCUATBL* | 22C58 | 2C8 |
| IHCUOPTN* | 22E60 | 8 |
| IHCSSCN * | 22E68 | 1C4 |
| NHCAWCC * | 22F70 | 5C |
| IHCSATN2* | 22FC0 | 16D |
| IHCFOVER* | 23130 | 5C |
| NHCAWAO * | 23180 | C8 |
| LINRV# * | 23248 | 814 |
| XSCALV# * | 23A60 | 36C |
| NHCAWAU * | 23DC0 | 5C |
| NCNLNV# * | 23E50 | 5DC |
| ERRLNV# * | 24420 | 358 |
| ERRNLV# * | 24788 | 32C |
| BRITEV# * | 24AE8 | 162 |
| PLOTV# * | 24C50 | 146 |
| NHCAWBN * | 24D98 | 2E |
| YMODV# * | 24DC8 | FA |
| XMODV# * | 24EC8 | FA |
| NHCAWFC * | 24FC8 | 116 |
| BNBCDV# * | 250E0 | 372 |
| IHCFIOSH* | 25458 | CF2 |
| VXAXV# * | 26150 | 254 |
| IHCFRXPI* | 263E8 | 54 |
| ERMRKV# * | 264B0 | 124 |

ENTRY ADDRESS CO
TOTAL LENGTH 265A4

| NAME | LOCATION | NAME | LOCATION | NAME | LOCATION | NAME |
|---|---|---|---|---|---|---|
| SQRT | 20C50 | | | | | |
| ALOGIC | 20D00 | ALOG | 20D1C | | | |
| MAX1 | 20E10 | MIN1 | 20E26 | AMAX1 | 20E3C | AMIN1 |
| | | | | | | 20E52 |
| CLOCK | 20EE0 | | | | | |
| C4C2CV | 20F90 | T4020V | 20FE8 | P4020V | 2107C | A4020V |
| V4C2CV | 211D4 | | | | | 21130 |
| TRANSV | 21438 | TRANSC | 21480 | | | |
| X4C2CV | 21580 | ENDIOV | 2163A | | | |
| CUTRV | 217D8 | CUTIV | 21844 | | | |
| ADCON# | 21908 | FCVZO | 21A54 | FCVAO | 21AFA | FCVLO |
| FCVIO | 21E90 | FCVEO | 22334 | FCVCO | 2252E | 21B82 |
| FIOCS# | 22900 | | | | | |
| IHCUOPT | 22E60 | | | | | |
| COS | 22E68 | SIN | 22E84 | | | |
| ARGQ | 22F70 | | | | | |
| ATAN2 | 22FC0 | ATAN | 22FDA | | | |
| OVERFL | 23130 | | | | | |
| SCERRV | 23180 | SCERV | 231A6 | SERREV | 231DC | SERSAV |
| | | | | | | 23206 |
| LINRV | 23320 | | | | | |
| XSCALV | 23AA0 | YSCALV | 23BFP | | | |
| STOPTV | 23DC0 | | | | | |
| NONLNV | 23F00 | | | | | |
| ERRLNV | 24490 | | | | | |
| ERRNLV | 24810 | | | | | |
| BRITEV | 24B08 | FAINTV | 24BE4 | | | |
| PLOTV | 24C68 | | | | | |
| HOLLV | 24D98 | | | | | |
| YMODV | 24DD0 | | | | | |
| XMODV | 24ED0 | | | | | |
| INSERT | 24FC8 | | | | | |
| BNBCDV | 25150 | | | | | |
| FIOCS# | 25458 | | | | | |
| VXAXV | 26180 | VYAXV | 262F0 | | | |
| FRXPI# | 263E8 | | | | | |
| ERMRKV | 264A0 | | | | | |

## AII.5 VSTV Listing, Main Program

```
C       MAIN PROGRAM - VORTEX STUDY TOWER AND VEHICLE
C       NORTH AMERICAN ROCKWELL,SPACE DIV. 190-200 J.E.DAVIS X1230
C
C
C       PROGRAM EXITS ON READ FOR NEXT CASE
C
C                 FLOW DEFINITION
C                    BINARY     TRUE FOR CASE TO READ BINARY INPUT
C                               FALSE FOR INITIALIZING NEW CASE
C
C                    ROTOW      TRUE FOR TOWER ROTATION CASE
C                               FALSE FOR TOWER DOWNSTREAM OF VEHICLE
C
C                 DATA DEFINITION
C                    TIME       TIME = 0.0 FOR NEW CASE
C                    DELTC      INCREMENTAL TIME OF NEW VORTEX
C                    CONKC      CONSTANT TO COMPUTE DELTA TIME
C                                 (DELT = CONKC * DELTC)
C                    DELTP      TIME INCREMENT TO GRAPH AND PRINT DATA
C                    TFIN       TIME TO TERMINATE RUN
C                    DELSL      TIME INCREMENT TO COMPUTE STREAMLINES
C                    DNC        TOTAL NUMBER OF VORTICES TO BE CALCULATED
C                                 (RUN TERMINATES ON EITHER DNC OR TFIN)
C                    ROT        ANGLE(DEG) OF TOWER ROTATION
C                    TFAC       FACTOR TO GENERATE TOWER FEED POINTS
C                    TFP1       TOWER FEED POINT (UPPER LEFT)
C                    TFP2       TOWER FEED POINT (UPPER RIGHT)
C                    NPHAF      NUMBER OF POINTS ON SEMI CYLINDER
C                    UTOP       MAXIMUM VELOCITY FOR TEST
C                    CONST      VEHICLE FEED POINT HEIGHT
C                    XXL        GRAPH LEFT MARGIN
C                    XR         GRAPH RIGHT MARGIN
C                    YB         GRAPH BOTTOM MARGIN
C                    YT         GRAPH TOP MARGIN
C                    CASENO     CASE NUMBER IN FORM XXXX.XX (DATE)
C                    XUL        TOWER POSITION - X UPPER LEFT
C                    YUL        TOWER POSITION - Y UPPER LEFT
C                    NXR        NUMBER OF TOWER POINTS (X SIDE)
C                    NYR        NUMBER OF TOWER POINTS (Y SIDE)
C                    XREC       LENGHT OF TOWER X SIDE
C                    YREC       LENGHT OF TOWER Y SIDE
C                                 (VEHICLE RADIUS = UNITY)
C                    XINIT      STREAMLINE INITIAL X LOCATION
C                    XINC       STREAMLINE DELTA X
C                    NXS        STREAMLINE NUMBER OF X VALUES
C                    NYS        STREAMLINE NUMBER OF Y VALUES
C                    NAN        NUMBER OF ANEMOMETER DATA POINTS
C                    XAN        X ANEMOMETER LOCATION
C                    YAN        Y ANEMOMETER LOCATION
C
        INTEGER *4 IA(50)
        INTEGER DNC,TFP1,TFP2
        LOGICAL    BINARY,ROTOW
        REAL  KVEC,KSUM
        DOUBLE PRECISION VOND(50,50),DUNIT(50,50),DFSC(21),DET,SCALE
       *    ,VIND(50)
C
        COMMON     NN, NT,NEX,   B(400,9) ,NEX1,NEX2,NBEG,PI4
        COMMON     /CFLOW/BINARY,ROTOW
        COMMON     /CINIT/XTF(4),YTF(4),     XC(10),YC(10),TFP1,TFP2
       *       ,XHAV,YHAV,GAM    ,PHI(4),SINP(4),COSP(4)
```

```
      COMMON    /CTIMES/TIME,DELT,DELTC,DELTP,ACCDT,ACCPT,TFIN,DNC,CONKC
     *           ,TPO,TCO,TSO,ACCSL,DELSL
      COMMON /CGRA/ DXGRA,DYGRA,NGRA,MGRA,LABX,LABY
     *               ,XXL,XR,YB,YT
     *          ,XL( 200 ), XU( 200 ), YL( 200 ), YU( 200 )
     *           ,CX(45),CYU(45),CYL(45),CXN(45),CASENO
      COMMON/CIP/ NXR,XREC,     NYR,YREC     ,NXS,NYS ,XUL,YUL
      COMMON/CPSI/KSYM(24),BCD(24),XS(100),YS(26,100),YSIP(26)
C
      COMMON/DBL/ VOND,DUNIT,DFSC,VIND
      COMMON/CTOW/
     *           XM( 50),   YM( 50),    PAR(2),     YAR(2),     KOUNT(26)
     *          ,PSI(26,100),            YSII (100),  XSII(100),NNARY(30)
     *                   ,STH(100),  CTH(100),    VIN( 50),VINCK(50)
     *          ,UM( 50, 50),                     VM( 50, 50)
     *          ,VON( 50, 50),                    UNIT( 50, 50)
     *          ,IDUMA(21),TFPX(2),TFPY(2),TFRAD1,TFRAD2
     *          ,KVEC(50),     XV(50), YV(50)    ,THSIDE(50)
C
      COMMON/CCYL/ XCPRES(105),YCPRES(105),NPCIR,UTOP,CONST
     *             ,UCYL(105),VCYL(105),SINCYL(105),TANVEL(105)
     *             ,UABS(105),INDX(105),    INDXFP(3)
     *             ,UFP(50),VFP(50),    UNORM(50),VNORM(50)
      COMMON/CROT/  RXV(50),  RYV(50),  RXM(50),  RYM(50)
      COMMON/ANEM/NAN,ROT,XAN(10),YAN(10),RXAN(10),RYAN(10),
     *   ANRAD(10),AZAN(10),UAN(10),VAN(10),SPEED(10),AZSH(10)
      DIMENSION  ITH(400,1),                      X(400,1),
     *           Y(400,1),                        U(400,1),
     *           V(400,1),                        AUK(400,1),
     *                                            ARAD(400,1)
C
      EQUIVALENCE(B(1,1),ITH(1,1)),               (B(1,2),X(1,1)),
     *           (B(1,3),Y(1,1)),                 (B(1,4),U(1,1)),
     *           (B(1,5),V(1,1)),                 (B(1,6),AUK(1,1)),
     *           (B(1,7),ARAD(1,1))
C
      NAMELIST  /FLOW/BINARY,ROTOW
C
      NAMELIST/DATA/ TIME,DELTC,CONKC,DELTP,TFIN,DELSL,DNC
     *               ,ROT,    TFAC,TFP1,TFP2,     NPHAF,UTOP,CONST
     *                     ,XXL,XR,YB,YT,CASENO
     *               ,NXR,XREC,    NYR,YREC,     XUL,YUL
     *               ,XINIT,XINC,      NXS,NYS
     *               ,NAN,XAN,YAN
C
C
      CALL  SCOUTV
      CALL  CAMRAV(9)
C
      TPO  =  .000001
      TCO  =  .000001
      TSO  =  .000001
      PI4  =  4. * 3.14159
C
      DXGRA = 2.0
      DYGRA = 2.0
      NGRA = -1
      MGRA = -1
      LABX = -1
      LABY = -1
C
    1 DO 2 I= 1,50
      XM(I) = 0.0
      YM(I) = 0.0
```

```
      XV(I) = 0.0
      YV(I) = 0.0
      RXV(I) = 0.0
      RYV(I) = 0.0
      RXM(I) = 0.0
      RYM(I) = 0.0
      KVEC(I) = 0.0
      VIN(I) = 0.0
      VIND(I ) = 0.0 DO
      UFP(I) = 0.0
      VFP(I) = 0.0
      UNORM(I) = 0.0
      VNORM(I) = 0.0
      IA(I) = 0
C
      DO 2 J = 1,50
      UM(I,J)=0.0
      VM(I,J)=0.0
      VON(I,J)=0.0
      VOND(I,J) = 0.0 DO
    2 CONTINUE
C
      DO 3 I = 1,105
      XCPRES(I) = 0.0
      YCPRES(I) = 0.0
      UCYL(I) = 0.0
      VCYL(I) = 0.0
      SINCYL(I) = 0.0
      TANVEL(I) = 0.0
      UABS(I) = 0.0
      INDX(I) = 0.0
    3 CONTINUE
C
      DO 4 I=1,100
      ITH(I,1)=0.0
      XS(I) = 0.0
      YSII(I) = 0.0
      XSII(I) = 0.0
      STH(I) = 0.0
      CTH(I) = 0.0
      DO 4 J=1,26
      PSI(J,I) = 0.0
      YS(J,I) = 0.0
    4 CONTINUE
      DO 6 J=1,9
      DO 6 I=1,400
    6 B(I,J) = 0.0
C
      BINARY = .FALSE.
      ROTOW  = .FALSE.
      ROT = 0.0
C
   10 READ(5,FLOW)
      READ(5,DATA)
      WRITE(6,11)CASENO
   11 FORMAT (1H1,42X    26HVEHICLE - TOWER   ANALYSIS/1H ,43X,
     *          23HVORTEX SHEDDING MODEL 6/1H ,45X5HCASE ,F10.2)
      WRITE (6,12) BINARY,ROTOW
   12 FORMAT (1H0, 24X, 'BINARY' L5,  34X, 'ROTOW' L5 ,/)
      WRITE (6,20) TIME,DELTC,CONKC,DELTP,TFIN,DELSL,DNC,
     *             ROT,TFAC,TFP1,TFP2,XUL,YUL,NXR,XREC,NYR,YREC,
     *             NPHAF,UTOP,CONST,
     *             CASENO,      XXL,XR,YB,YT
      WRITE(6,21)  XINIT,XINC,NXS,NYS
      WRITE (6,22) NAN,(XAN(I),YAN(I), I = 1,NAN)
```

```
C
   20 FORMAT (1H ,     24X,     'TIME DATA' /
     *                 35X,     'TIME '  F10.3, 20X,'DELTC' F10.3 /
     *                 35X,     'CONKC'  F10.3, 20X,'DELTP' F10.3 /
     *                 35X,     'TFIN '  F10.3, 20X,'DELSL' F10.3 /
     *                 35X,     'DNC  '  I10    /
     *                 25X,     'TOWER DATA'/
     *                 35X,     'ROT  '  F10.3, 20X,'TFAC ' F10.3 /
     *                 35X,     'TFP1 '  I10   , 20X,'TFP2 ' I10/
     *                 35X,     'XUL  '  F10.3, 20X,'YUL  ' F10.3 /
     *                 35X,     'NXR  '  I10   , 20X,'XREC ' F10.3 /
     *                 35X,     'NYR  '  I10   , 20X,'YREC ' F10.3 /
     *                 25X,     'VEHICLE DATA'/
     *                 35X,     'NPHAF'  I10   , 20X,'UTOP ' F10.3 /
     *                 35X,     'CONST'  F10.3/
     *                 25X,     'GRAPH DATA'/
     *                 35X,     'CASENO' F 9.3, 20X /
     *                 35X,     'XXL  '  F10.3, 20X,'XR   ' F10.3 /
     *                 35X,     'YB   '  F10.3, 20X,'YT   ' F10.3 )
   21 FORMAT(1H ,      24X,     'STREAMLINE DATA'/
     *                 35X,     'XINIT'  F10.3, 20X,'XINC ' F10.3 /
     *                 35X,     'NXS  '  I10   , 20X,'NYS  ' I10)
   22 FORMAT (1H ,     24X,     'ANEMOMETER DATA'/
     *                 35X,     'NAN  '  I10/
     *                 35X,     'XAN  '  15X,   'YAN'/ (30X,F10.2,10X,F10.2))
      WRITE (6,51)
   51 FORMAT (1H1)
C
C                                INITIALIZE
   30 DELT= CONKC*DELTC
      ACCDT=TCO    + DELT
      ACCPT=TPO          +DELT
      ACCSL = TSO + DELT
      NT= 2*NXR +2*NYR
      NEX = NT+1
      NBEG = NT + 2
      NEX1 = NEX +1
      NEX2 = NEX +2
      NN = NT + 1
C
      DO 40 I = 1,NXR
      THSIDE(I) = 90.
      THSIDE(NXR + I) = 180.
      THSIDE(NXR + NYR + I) = 270.
      THSIDE(2*NXR + NYR + I) = 0.
   40 CONTINUE
C
C                      STREAMLINE GEOMETRY
      XS(1)= XINIT
      DO 42 I = 2,NXS
   42 XS(I)= XS(I-1)+XINC
C
      DO  44 J=1,NXS
      DO  44 I=1,NYS
   44 YS(I,J)= YSIP(I)
C
      IF(BINARY)GO TO 400
C
C                                VORTICES ON TOWER
   50 XV(1)= XUL
      YV(1)= YUL
      NXRP = NXR+1
      DO 52 I= 2,NXRP
```

```
      XV(I) = XV(1) +  XREC * SIND( 90. * (I-1) /NXR) **2
   52 YV(I)= YUL
C
      NYRP = NYR +1
      DO 54 I= 2,NYRP
      N= NXR+I
      XV(N)= XUL + XREC
   54 YV(N) = YUL - YREC * SIND(90. * (I-1) /NYR)   **2
C
      DO 56 I=1,NXR
      M= NXR  +NYR+I
      XV(M) = XV(NXR+2-I)
   56 YV(M) = YUL-YREC
C
      DO 58 I=1,NYR
      J= NXR*2  +NYR+I
      XV(J)= XUL
   58 YV(J)= YV(NXR+2+NYR-I)
C
      XV(NT+1)=XV(1)
      YV(NT+1)=YV(1)
      DO 64 I=1,NT
      XM(I)=(XV(I)+ XV(I+1))/2.
   64 YM(I)=(YV(I)+ YV(I+1))/2.
C
C            VORTICES AT TOWER CENTER
      XV(NEX) = XUL + XREC/20.
      YV(NEX) = YUL - YREC/4.
      IF(YV(NEX) .LT. .0001 .AND. YV(NEX) .GT. -.0001) YV(NEX) = 0.0
C
      IYMID = 1 + NYR/2
      IYM2 = NXR + IYMID
      IYM4 = 2*NXR + NYR +IYMID
      YM(IYM2) = 0.0
      YM(IYM4) = 0.0
C
C                             TOWER FEED POINT INITIAL CELLS
   70 XHAV = XREC/2.
      YHAV = YREC/2.
      TXHAV = TFAC * XHAV
      TYHAV = TFAC * YHAV
      CENX = XUL + XHAV
      CENY = YUL - YHAV
      XTF(1) = CENX    - TXHAV
      YTF(1) = CENY    + TYHAV
      XTF(2) = CENX    + TXHAV
      YTF(2) = CENY    + TYHAV
      XTF(3) = CENX    + TXHAV
      YTF(3) = CENY    - TYHAV
      XTF(4) = CENX    - TXHAV
      YTF(4) = CENY    - TYHAV
C
      XV(NEX1)  =XTF(TFP1)
      YV(NEX1)  =YTF(TFP1)
      XV(NEX2)  =XTF(TFP2)
      YV(NEX2)  =YTF(TFP2)
C
      GAM = ATAND(YHAV,XHAV)
      PHI(1) = ROT + GAM
      PHI(2) = ROT - GAM  + 180.
      PHI(3) = ROT + GAM  + 180.
      PHI(4) = ROT - GAM
```

```
C
      DO  72 I = 1,4
      SINP(I) = SIND(PHI(I))
   72 COSP(I) = COSD(PHI(I))
C
      IF (.NOT. ROTOW) GO TO 80
C
C        ROTATION OF TOWER VORTICES (INCLUDING CENTER AND I.C.)
   74 NN2 = NN + 2
      SI = SIND(ROT)
      CS = COSD(ROT)
      DO  75 I = 1,NN2
      RXV(I) = XV(I) * CS        + YV(I) * SI
      RYV(I) = -XV(I) * SI        + YV(I) * CS
      RXM(I) = XM(I) * CS        + YM(I) * SI
      RYM(I) = -XM(I) * SI        + YM(I) * CS
      XM(I) = RXM(I)
      YM(I) = RYM(I)
      X(I,1) = RXV(I)
      Y(I,1) = RYV(I)
   75 CONTINUE
      DO 78 I = 1,NAN
      RXAN(I) = XAN(I) * CS + YAN(I) * SI
      RYAN(I) = - XAN(I) * SI + YAN(I) * CS
      XAN(I) = RXAN(I)
      YAN(I) = RYAN(I)
   78 CONTINUE
C
      GO TO 86
C
   80 CONTINUE
      DO  82 I= 1,NN
      X(I,1) = XV(I)
   82 Y(I,1) = YV(I)
C
   86 TFPX(1) = X(NEX1,1)
      TFPY(1) = Y(NEX1,1)
      TFPX(2) = X(NEX2,1)
      TFPY(2) = Y(NEX2,1)
      TFRAD1 = TFPX(1)**2 + TFPY(1)**2
      TFRAD2 = TFPX(2)**2 + TFPY(2)**2
C
      NTM = NT - 1
      DO 90  I = 1, NTM
      DENOM = SQRT((X(I+1,1)-X(I ,1))**2 + (Y(I+1,1)-Y(I ,1))**2)
      CTH (I) = (Y(I+1,1) - Y(I,1) ) / DENOM
   90 STH (I) = (X(I+1,1)-X(I,1))/ DENOM
      DENO = SQRT ((X(1,1) - X(NT,1))**2 + (Y(1,1) - Y(NT,1))**2)
      CTH(NT) = (Y(1,1) - Y(NT,1)) / DENO
      STH(NT) = (X(1,1) - X(NT,1))/ DENO
C
      DO 100 I=1,NT
      DO 100 J=1,NEX
      DENOM = (X(J,1) -XM(I))**2 + (Y(J,1) - YM(I))**2
      DEN = X(J,1)**2 + Y(J,1)**2
      XIM = X(J,1) /DEN
      YIM = Y(J,1) /DEN
      DENO = (XIM - XM(I))**2 + (YIM - YM(I))**2
      UM(I,J)=-(Y(J,1) -YM(I)) /DENOM + (YIM - YM(I))/DENO
      VM(I,J)=(X(J,1)  -XM(I)) /DENOM - (XIM - XM(I))/DENO
      VON(I,J)= -UM(I,J)*CTH(I) + VM(I,J)*STH(I)
  100 CONTINUE
      DO 102 J = 1,NEX
  102 VON(NEX,J) = 1.0
```

```
C
      DO 103 I = 1,NT
      ADEN = (XM(I)**2 + YM(I)**2) **2
      UINT = 1. -  (XM(I)**2 -YM(I)**2) / ADEN
      VINT = -2. * XM(I) * YM(I)  /ADEN
      VIN(I) = UINT * COSD(THSIDE(I) +ROT)
     *                    -VINT * SIND(THSIDE(I) + ROT)
  103 CONTINUE
      VIN(NEX) = 0.0
C
      DO 104 J = 1,NEX
      DO 104 I = 1,NEX
  104 VOND(I,J) = VON(I,J)
C
C                          GAUSS-JORDAN REDUCTION
      DO 105 J= 1,NEX
      DO 105 I= 1,NEX
      DUNIT(I,J)= 0.0  D0
      IF( I .EQ. J) DUNIT(I,J) = 1.0 D0
  105 CONTINUE
C
      IMAX = 50
      SCALE = 1.0 D0
      MDET = ISIMDP( IMAX,  NEX,NEX,  VOND, DUNIT,  SCALE,IA)
      IF(MDET .EQ. 1) GO TO 108
      IF (MDET .EQ. 3) GO TO 130
      WRITE (6,106) MDET
  106 FORMAT(1H-, 'MDET IS ' , I4)
C
  108 WRITE(6,110)
  110 FORMAT(1H-,5X,'SUCCESSFUL SOLUTION',//)
      GO TO 160
C
  130 WRITE(6,140)
  140 FORMAT (1H-,10X,'SINGULAR OR ILL-CONDITIONED VON MATRIX' ,// )
C
  160 CONTINUE
C
      DO 161 J = 1,NEX
      DO 161 I = 1,NEX
  161 VON(I,J) = VOND(I,J)
C
      CALL MATMPY(VON, VIN, KVEC, NEX,NEX,1,50,50,1)
C
      DO 163 I = 1,NEX
  163 AUK(I,1) = KVEC(I)
C
C
C
C
      WRITE(6,210)TIME,NN
  210 FORMAT (1H1,  10X, 6HTIME = ,  F10.6,  14X
     *               27HMULTICELL INITIAL CONDITIONI3,2X, 8HVORTICES)
      WRITE(6,5000)
      WRITE (6,5010)  (I      ,X(I,1),Y(I,1),AUK(I,1),  I=1,NN)
  220 FORMAT (I12,3E12.0)
C
C
      GO TO 500
  400  READ(10)NN,NT,NEX,    ((B(I,J), I=1,NN),J=1,7)
     *       ,((VON(I,J), I=1,NEX),  J=1,NEX),  CSNO
     *       ,TIME,TFPX,TFPY,TFRAD1,TFRAD2
      WRITE(6,410)CSNO,NN
```

```
  410 FORMAT (1H1,25X,40HBINARY MULTICELL INITIAL CONDITION (CASE F10.4,VSTV4430
     *    4H)   ,I3,2X,8HVORTICES)                                         VSTV4440
  450 WRITE (6,5020)                                                       VSTV4450
      WRITE (6,5030)((B(I,J),J=1,6), I=1,NN)                               VSTV4460
C                                                                          VSTV4470
  500 CONTINUE                                                             VSTV4480
C     CALCULATE CYLINDER                                                   VSTV4490
      DDEG = 0.                                                            VSTV4500
      DO 510 I = 1,45                                                      VSTV4510
      DDEG = DDEG + 2.                                                     VSTV4520
      CX(I)  =  SIND(DDEG  )                                               VSTV4530
       CXN (I) = -CX(I)                                                    VSTV4540
        CYU(I) =COSD(DDEG)                                                 VSTV4550
  510    CYL (I)  = -CYU(I)                                                VSTV4560
C                                                                          VSTV4570
  700 CONTINUE                                                             VSTV4580
      DO 702 I = 1,NEX                                                     VSTV4590
      XL(I) = X(I,1)                                                       VSTV4600
  702 YL(I) = Y(I,1)                                                       VSTV4610
C                                                                          VSTV4620
      CALL GRIDIV (-3,  XXL,XR,YB,YT,DXGRA,DYGRA,NGRA,MGRA                 VSTV4630
     *                         ,LABX,LABY,6,6)                             VSTV4640
      CALL APRNTV (0,  -13,  3,'Y/A',      4,500)                          VSTV4650
      CALL PRINTV  (3,  'X/A',      450,4)                                 VSTV4660
      CALL APLOTV(  NEX,  XL, YL,     1,1,1,      38,IERR)                 VSTV4670
C                                                                          VSTV4680
      TIME = DELT                                                          VSTV4690
  701 IF( .NOT. BINARY)  GO TO 706                                         VSTV4700
  703 NIC = NN - NEX                                                       VSTV4710
C                                                                          VSTV4720
      DO 705 I=1,NIC                                                       VSTV4730
      NTPI = NT + 1 + I                                                    VSTV4740
      XL(I) = X(NTPI,1)                                                    VSTV4750
  705 YL(I) = Y(NTPI,1)                                                    VSTV4760
      CALL APLOTV(  NIC,  XL,YL,     1,1,1,      44,IERR)                  VSTV4770
C                                                                          VSTV4780
  706 CALL APLOTV(  45,  CX , CYU,    1,1,1,     42, IERR)                 VSTV4790
      CALL APLOTV(  45,  CX , CYL,    1,1,1,     42, IERR)                 VSTV4800
      CALL APLOTV(  45,  CXN, CYU,    1,1,1,     42, IERR)                 VSTV4810
      CALL APLOTV(  45,  CXN, CYL,    1,1,1,     42, IERR)                 VSTV4820
      WRITE (16 ,710    ) TIME , DELTC,CASENO                              VSTV4830
  710 FORMAT (1H+,5X 'INITIAL VORTEX LOCATIONS AT TIME ='1F9.4,6X,15X6HDVSTV4840
     *ELTC=,1F9.4,9X,8HCASE NO.,2XF10.2)                                   VSTV4850
C                                                                          VSTV4860
      CALL STREAM                                                          VSTV4870
C                                                                          VSTV4880
      NPCIR = NPHAF * 2                                                    VSTV4890
      FNPC = NPCIR                                                         VSTV4900
      DEGI = 360./FNPC                                                     VSTV4910
C                                                                          VSTV4920
      DO 750 I= 1,NPCIR                                                    VSTV4930
      DEG= (I-.5)* DEGI                                                    VSTV4940
      XCPRES(I) = -COSD(DEG)                                               VSTV4950
      YCPRES(I) = SIND(DEG)                                                VSTV4960
  750 CONTINUE                                                             VSTV4970
C                                                                          VSTV4980
  800 IF(DELTC.GT.ACCDT)GO TO 900                                          VSTV4990
C                                                                          VSTV5000
      DO 810 I = NBEG,NN                                                   VSTV5010
      X(I,1)= X(I,1) +U(I,1) *DELT                                         VSTV5020
  810 Y(I,1)= Y(I,1) +V(I,1) *DELT                                         VSTV5030
C                                                                          VSTV5040
      NEX1 = NN+1                                                          VSTV5050
```

```
      NEX2 = NN+2
      ACCDT = TCO
C
  850 CALL NUCTV
      GO TO 920
  900 DO 910 I=NBEG,NN
      X(I,1)= X(I,1) +U(I,1) *DELT
  910 Y(I,1)= Y(I,1) +V(I,1) *DELT
  920 CALL VELTV
C
 1000 IF(DELTP.GT.ACCPT)GO TO 1050
C
      CALL PAPTV
      CALL HOUR
      ACCPT =TPO
C
 1050 IF(DELSL .GT. ACCSL)  GO TO 1600
C
      ACCSL = TSO
 1100 CALL STREAM
C
 1600 TIME= TIME + DELT
      ACCDT= ACCDT + DELT
      ACCPT= ACCPT + DELT
      ACCSL = ACCSL + DELT
C
 2000 IF(TIME.GT.TFIN) GO TO 4000
 3000 IF(NN.GT.DNC)GO TO 4000
      GO TO 800
C
 4000 CONTINUE
      CALL KIKTV
      CALL STREAM
C
      GO TO 1
C
 5000 FORMAT (1H-,5X,8HVORTICES,12X,3HX/A,17X,3HY/A,17X,1HK   ,///)
 5010 FORMAT (1H ,8X,I4,1P3E20.7)
 5020 FORMAT (1H-,4X8HVORTICES,3X,3HX/A,15X,3HY/A,15X,7HU/U INF,11X,
     *     7HV/U INF,11X,7HK/U*A    ,///)
 5030 FORMAT (1H ,6X,I4,2X,1P5E18.7)
      END
/*
/*
/*
```

## AIII. SUBROUTINES

All subroutines are Fortran G subroutines called without arguments. The communication between the main program, VSTV, and the subroutines is controlled by blank and several labeled commons. Use of the subroutines is shown in the main program flow chart, Section AII. 1.

### AIII. 1 NUCTV (New Cell) Subroutine

The NUCTV subroutines introduced the new vortices into the field when the ACCDT which is incremented by DELT exceeds the input DELTC, incremental time of new vortices.

Two tower vortices are introduced at the selected input tower feed points, TFP1 and TFP2 as described in data definition, Section AII. 3. 1. TFAC is percentage increment of the line intersecting tower center and corner to calculate the positions of new vortex introduction. The subroutine calculates the tower feed point velocities and positions and the inward normal velocity vector, VIN which, when multiplied by the VON, outward normal velocity influence coefficient matrix, yields the strength, AUK, of the tower vortices.

One to three new vortices are introduced on the vehicle per feed time depending upon the relative extremes of vehicle tangential velocities. The input value UTØP is a limiting value for the tangential velocities to avoid local extreme values. The input value of NPHAF determines the number of points where velocities are calculated.

The flow chart and listing of NUCTV follow.

AIII. 1. 1 Flow Chart of NUCTV

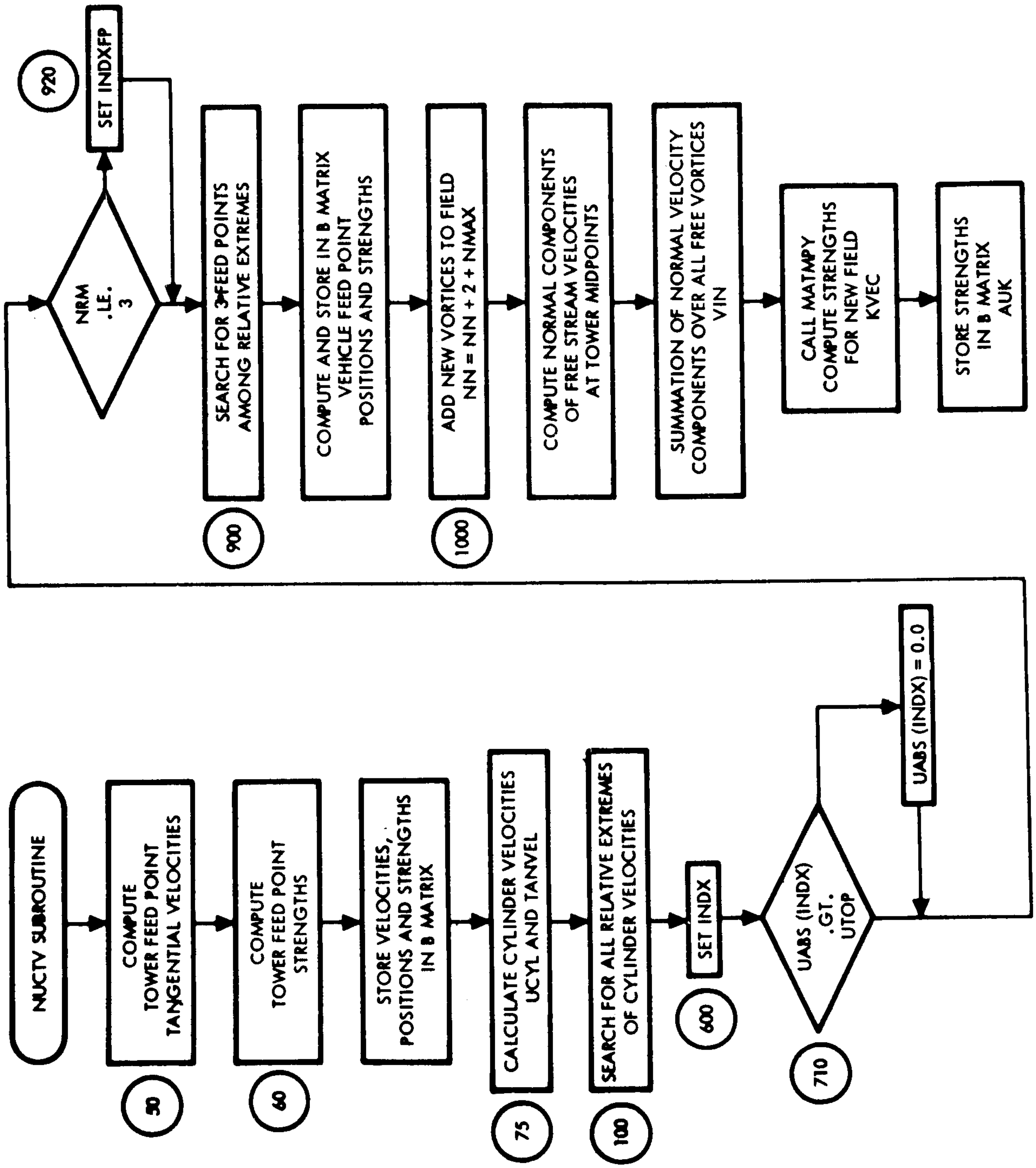

## AIII. 1.2 Listing of NUCTV

```
FORTRAN IV G LEVEL  0, MOD 0                NUCTV              DATE = 68040             00/59/27

                SUBROUTINE NUCTV
                REAL KVEC,KSUM
                INTEGER DNC,TEP1,TEP2
                COMMON       NN, NT,NEX,    B(400,9) ,NEX1,NEX2,NBEG,PI4
                COMMON       /CFLOW/BINARY,ROTOW
                COMMON       /CINIT/XTE(4),YTE(4),     XC(10),YC(10),TEP1,TEP2
               *       ,XHAV,YHAV,GAM    ,PHI(4),SINP(4),COSP(4)
                COMMON       /CTIMES/TIME,DELT,DELTC,DELTP,ACCDT,ACCPT,TFIN,DNC,CONKCKT2M1070
               *             ,TPO,TCO,TSO,ACCSL,DELSL
                COMMON/CTOW/
               *             XM( 50),    YM( 50),    PAR(2),     YAR(2),     KOUNT(26)
               *            ,PSI(26,100),            YSII (100),  XSII(100),NNARY(30)
               *                         ,STH(100),  CTH(100),  VIN( 50),VINCK(50)
               *            ,UM( 50, 50),                       VM( 50, 50)
               *            ,VON( 50, 50),                      UNIT( 50, 50)          00000350
               *           ,IDUMA( 21),TEPX(2),TEPY(2),TERAD1,TERAD2
               *            ,KVEC(50),    XV(50), YV(50)    ,THSIDE(50)
                COMMON/CCYL/ XCPRES(105),YCPRES(105),NPCIR,UTOP,CONST
               *              ,UCYL(105),VCYL(105),SINCYL(105),TANVEL(105)
               *              ,UABS(105),INDX(105),    INDXFP(3)
               *              ,UFP(50),VFP(50),    UNORM(50),VNORM(50)
          C
                DIMENSION  ITH(400,1),                          X(400,1),
               *           Y(400,1),                            U(400,1),
               *           V(400,1),                            AUK(400,1),
               *                                                ARAD(400,1)
          C
                EQUIVALENCE(B(1,1),ITH(1,1)),                   (B(1,2),X(1,1)),
               *           (B(1,3),Y(1,1)),                     (B(1,4),U(1,1)),
               *           (B(1,5),V(1,1)),                     (B(1,6),AUK(1,1)),
               *           (B(1,7),ARAD(1,1))
          C
          C
          C                           TOWER F.P. VELOCITIES
                DO   50 J = NEX1,NEX2
                M = J - NN
          C                FREE STREAM
                XVSQ  =  TEPX( M)**2
                YVSQ  =  TEPY( M)**2
                ADEN  =  (XVSQ + YVSQ) **2

                UFP(M)  =  1. -(XVSQ - YVSQ)/ADEN
                VFP(M)  =-2.*TEPX( M) * TEPY( M)   /ADEN
          C
                DO   50 I  =  1,NN
                DEN  =  X(I,1)**2 + Y(I,1)**2
                XIM  =  X(I,1)/DEN
                YIM  =  Y(I,1)/DEN
                DX  =  X(I,1) - TEPX(M)
                DY  =  Y(I,1) - TEPY(M)
                DXI  =  XIM - TEPX(M)
                DYI  =  YIM - TEPY(M)
                DENOM  =  DX**2 + DY**2
                DENO  =  DXI**2 + DYI**2
                UFP(M)  =UFP(M) +(-DY/DENOM + DYI/DENO) * AUK(I,1)
             50 VFP(M)  =VFP(M) +(DX/DENOM - DXI/DENO) * AUK(I,1)
                UTAN1  =  UFP (M)    *COSP(TEP1) + VFP (M)    *SINP(TEP1)
```

```
FORTRAN IV G LEVEL 0, MOD 0              NUCTV              DATE = 68040            00/59/27
              UTAN2 = UFP (M)    *COSP(TFP2)+ VFP (M)    *SINP(TFP2)
              AUK(NN+1,1) = UTAN1 * ABS(UTAN1) * DELTC/ PI4
              AUK(NN+2,1) = UTAN2 * ABS(UTAN2) * DELTC/ PI4
              VIN(NEX)    = VIN(NEX)    -AUK(NN+1,1) - AUK(NN+2,1)
              X(NN+1,1) = TFPX(1)
              Y(NN+1,1) = TFPY(1)
              ARAD(NN+1,1) = TFRAD1
              X(NN+2,1) = TFPX(2)
              Y(NN+2,1) = TFPY(2)
              ARAD(NN+2,1) = TFRAD2
      C                                   CALCULATE CYLINDER VELOCITIES
              DO 75 J=1,NPCIR
      C                           FREE STREAM
              XCSQ = XCPRES(J)**2
              YCSQ = YCPRES(J)**2
              ADEN =(XCSQ + YCSQ) **2
              UCYL(J) = 1. - (XCSQ - YCSQ)/ADEN
              VCYL(J) = -2. * XCPRES(J) * YCPRES(J) /ADEN
      C
              DO 70 I= 1,NN
      C                        VORTICES
              DEN = X(I,1)**2 + Y(I,1)**2
              XIM = X(I,1)/DEN
              YIM = Y(I,1)/DEN

              DX = X(I,1) -XCPRES(J)
              DY = Y(I,1) - YCPRES(J)
              DXI = XIM - XCPRES(J)
              DYI = YIM - YCPRES(J)
              DENOM = DX**2 + DY**2
              DENO = DXI**2 + DYI**2
           70 UCYL(J) = UCYL(J) + (-DY/DENOM +DYI/DENO) * AUK(I,1)
           75 TANVEL(J) = UCYL(J)/YCPRES(J)
      C
      C        SEARCH FOR ALL RELATIVE EXTREMES OF CYLINDER VELOCITIES
              DO 100 I= 1,NPCIR
          100 UABS (I)   = ABS ( TANVEL(I))
              NPM = 0
              IF(UABS(1) .GT. UABS(2) .AND. UABS(1) .GT. UABS(NPCIR))
             *        GO TO 200
              GO TO 300
          200 NPM = 1
              INDX(NPM) = 1
          300 IF(UABS(NPCIR) .GT. UABS(1) .AND. UABS(NPCIR) .GT. UABS(NPCIR-1))
             *        GO TO 400
              GO TO 500
          400 NPM = NPM + 1
              INDX(NPM) = NPCIR
          500 CONTINUE
              NCM = NPCIR - 1
              DO 700 I= 2,NCM
              IF(UABS(I) .GT. UABS(I-1) .AND. UABS(I) .GT. UABS(I+1))
             *     GO TO 600
              GO TO 700
          600 NPM =  NPM + 1
              INDX(NPM) = I
          700 CONTINUE
      C
      C        SEARCH FOR 3 FEEDING POINTS AMONG THE REL EXTREMES
              IOVER = 0
              DO 710 I = 1,NPM
              IF(UABS(INDX(I)) .GT. UTOP)  GO TO 705
```

```
FORTRAN IV G LEVEL  0, MOD 0              NUCTV                    DATE = 68040              00/59/27
    0082                GO TO 710
    0083            705 UABS(INDX(I)) = 0.0
    0084                IOVER = IOVER + 1

    0085            710 CONTINUE
    0086                NRM = NRM - IOVER
    0087                IF (NRM .EQ. 0) GO TO 760
    0088                GO TO 750
                  C
    0089            760 WRITE (6,761) NRM,(TANVEL(I), I=1,NPCIR)
    0090            761 FORMAT (1H1, 4X 'NRM IS '  I4,//
                       *      5X   'TANGENTIAL VELOCITIES  ' //  (5X, 5F20.4) )
    0091                STOP
                  C
                  C
    0092            750 NMAX = NRM
    0093                NRMM = NRM - 1
    0094                IF(NRM .LE. 3)  GO TO 920
    0095                DO 900 I = 1,3
                  C
                  C          UTOP IS MAX VELOCITY LIMIT
    0096                MAX = INDX (1)
    0097                UABSJ = UABS (MAX)
                  C
    0098                DO  805  J = 1, NRMM
    0099                IF ( UABS ( INDX (J+1)) .GT. UABSJ )  GO TO 800
    0100                GO TO 805
    0101            800 MAX  = INDX (J+1)
    0102                UABSJ  = UABS (MAX)
    0103            805 CONTINUE
                  C
    0104                INDXEP(I)  = MAX
    0105                UABS(MAX)  = 0.
    0106            900 CONTINUE
    0107                NMAX = 3
    0108                GO TO 950
                  C
    0109            920 KNT = 0
    0110                NRMPI = NRM + IOVER
    0111                DO 930 I = 1,NRMPI
    0112                IF( UABS(INDX(I)) .EQ. 0.0) GO TO 930
    0113                KNT = KNT + 1
    0114                INDXEP(KNT) = INDX(I)
    0115            930 CONTINUE
                  C
    0116            950 CONTINUE
    0117                U1 = TANVEL(INDXEP(1))
    0118                DELR = CONST * ABS(U1) * DELTC
    0119                NARG = INDXEP(1)
    0120                X(NN+3,1) = -(1. + DELR) * XCPRES(NARG)
    0121                Y(NN+3,1) = (1.+DELR) * YCPRES(NARG)
    0122                AUK(NN+3,1) = U1 * ABS(U1) * DELTC/ PI4
    0123                ARAD(NN+3,1) = X(NN+3,1)**2 + Y(NN+3,1)**2
    0124                IF(NMAX .LT. 2) GO TO 1000
                  C
    0125                U2 = TANVEL(INDXEP(2))
    0126                DELR = CONST * ABS(U2) * DELTC
    0127                NARG = INDXEP(2)
    0128                X(NN+4,1) =-(1. + DELR) * XCPRES(NARG)
    0129                Y(NN+4,1) =  (1. + DELR) * YCPRES(NARG)
    0130                AUK (NN+4,1) = U2 * ABS(U2) * DELTC / PI4
    0131                ARAD(NN+4,1) = X(NN+4,1)**2 + Y(NN+4,1)**2
    0132                IF(NMAX .LT. 3) GO TO 1000
```

```
FORTRAN IV G LEVEL  0, MOD  0              NUCTV              DATE = 68040              00/59/27

                 C
 0133                   U3 = TANVEL(INDXFP(3))
 0134                   DELR = CONST * ABS(U3) * DELTC
 0135                   NARG = INDXFP(3)
 0136                   X(NN +5,1)=-(1. + DELR) * XCPRES(NARG)
 0137                   Y(NN+5,1) =  (1. + DELR) * YCPRES(NARG)
 0138                   AUK(NN+5,1) = U3 * ABS(U3) * DELTC / PI4
 0139                   ARAD(NN+5,1) = X(NN+5,1)**2 + Y(NN+5,1)**2
 0140              1000 NN = NN + 2 + NMAX
                 C
                 C        COMPUTE NORMAL COMPONENT OF VELOCITY AT EACH MIDPOINT
 0141                   DO 1030 J = 1,NT
                 C        INITIALIZE WITH FREE STREAMVALUES
 0142                   RESULT = XM(J) **2 + YM(J)**2
 0143                   ADEN = RESULT**2
 0144                   UNORM(J) = 1.  - (XM(J)**2 - YM(J)**2) / ADEN
 0145                   VNORM(J) = -2.    * XM(J) * YM(J) / ADEN
                 C        SUMMATION OVER ALL FREE VORTICES
 0146                   DO 1025 I = NBEG,NN
 0147                   DEN = X(I,1)**2 + Y(I,1)**2
 0148                   XIM = X(I,1)/DEN
 0149                   YIM = Y(I,1)/DEN
 0150                   DX = X(I,1) - XM(J)
 0151                   DY = Y(I,1) - YM(J)
 0152                   DXI = XIM - XM(J)
 0153                   DYI = YIM - YM(J)
 0154                   DENOM = DX**2 + DY**2
 0155                   DENO = DXI**2 + DYI**2
 0156                   UNORM(J) =UNORM(J)+(-DY/DENOM + DYI/DENO) * AUK(I,1)
 0157              1025 VNORM(J) =VNORM(J) +(DX/DENOM - DXI/DENO) * AUK(I,1)
 0158              1030 VIN(J) = UNORM(J)*CTH(J)   - VNORM(J) * STH(J)
                 C
 0159                   CALL MATMPY(VON,VIN,KVEC,NEX,NEX,1,50,50,1)
 0160                   KSUM = 0.0
 0161                   DO 1032 I = 1,NEX
 0162              1032 KSUM = KSUM + KVEC(I)
                 C
                 C          PUT KVEC INTO B
 0163                   DO 1035 I = 1,NEX
 0164              1035 AUK(I,1) = KVEC(I)
 0165                   RETURN
 0166                   END
```

AIII. 2 VELTV (Velocities) Subroutine

The VELTV subroutine is called by the main program, VSTV, in the time-loop to compute free stream velocity components for all free vortices in the field and the velocities induced by the free vortices. The tower velocities are unnecessarily computed to take advantage of the symmetrical calculation.

AIII. 2. 1 Flow Chart of VELTV

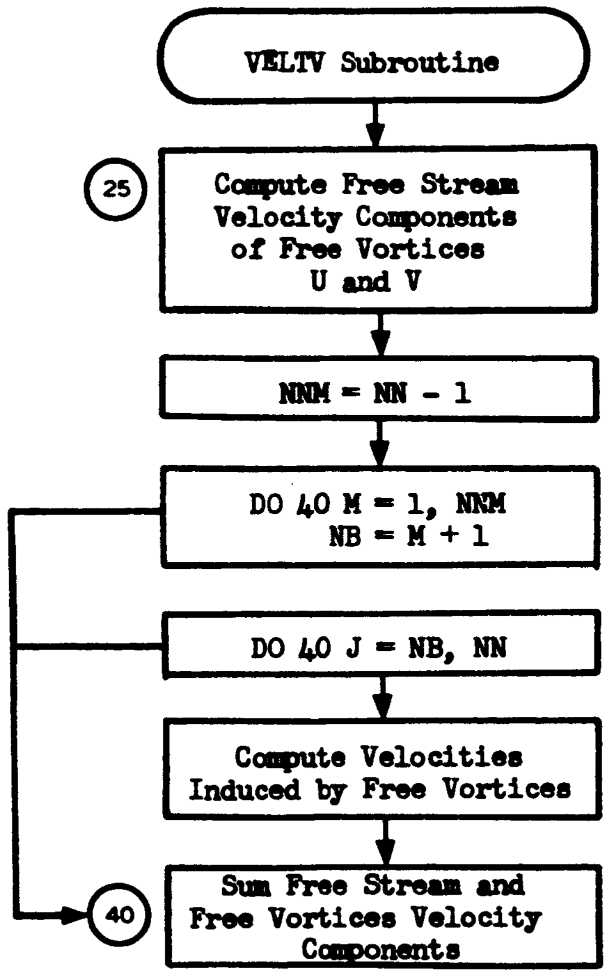

## AIII. 2. 2 Listing of VELTV

```
 FORTRAN IV G LEVEL 0, MOD 0             VELTV               DATE = 68040          00/59/27

 0001                  SUBROUTINE VELTV
             C                 VELOCITY COMPUTATION IN TIME CYCLE       VSTV PROGRAM
             C
 0002                  COMMON      NN, NT,NEX,    B(400,9)  ,NEX1,NEX2,NBEG,PI4
 0003                  REAL        NUJU,NUJV,NUMU,NUMV
             C
 0004                  DIMENSION  X(400,1),Y(400,1),U(400,1),V(400,1),AUK(400,1)
                      *       ,ARAD(400,1)
             C
 0005                  EQUIVALENCE(B(1,2),X(1,1)),                    (B(1,3),Y(1,1)),
                      *           (B(1,4),U(1,1)),                    (B(1,5),V(1,1)),
                      *           (B(1,6),AUK(1,1)),                  (B(1,7),ARAD(1,1))
             C
             C
             C          VELOCITY COMPUTATION FOR FREE VORTICES
 0006                  DO 25 I= NBEG,NN
 0007                  ARAD(I,1) = X(I,1)**2 + Y(I,1)**2
 0008                  ADEN = ARAD (I,1)**2
 0009                  BDEN = 1. - ARAD(I,1)
 0010                  U(I,1)= 1.-((X(I,1)**2 -Y(I,1)**2)/ ADEN) +AUK(I,1)*Y(I,1) /BDEN
 0011               25 V(I,1)= -(2.* X(I,1)* Y(I,1)/ ADEN) -AUK(I,1) *X(I,1) /BDEN
             C
             C                 VELOCITIES CALCULATED FOR TOWER VORTICES TO TAKE
             C                                 ADVANTAGE OF SYM. CALC.
 0012                  NNM = NN - 1
 0013                  DO 40 M = 1, NNM
 0014                  NB  = M+1
 0015                  DO 40 J= NB  , NN
 0016                  ARAD(M,1) = X(M,1)**2 + Y(M,1)**2
 0017                  DENOM = 1. - 2.* (X(J,1)*X(M,1)+Y(J,1)*Y(M,1))
                      *        + ARAD(J,1)*ARAD(M,1)
 0018                  ANY = Y(J,1) - Y(M,1)
 0019                  ANX = X(J,1) - X(M,1)
 0020                  FDN = ANX **2  + ANY ** 2
 0021                  NUJU = Y(M,1) - Y(J,1)* ARAD(M,1)
 0022                  NUJV = X(M,1) - X(J,1) * ARAD(M,1)
 0023                  NUMU = Y(J,1) - Y(M,1)* ARAD(J,1)
 0024                  NUMV = X(J,1) - X(M,1)* ARAD(J,1)
 0025                  U(J,1) =U(J,1) +AUK(M,1)*(NUJU / DENOM + ANY / FDN )
 0026                  V(J,1) =V(J,1) -AUK(M,1)*(NUJV / DENOM + ANX / FDN )
 0027                  U(M,1) =U(M,1) +AUK(J,1)*(NUMU / DENOM - ANY / FDN )
 0028               40 V(M,1) =V(M,1) -AUK(J,1)*(NUMV / DENOM - ANX / FDN )
             C
 0029                  RETURN
 0030                  END
 FORTRAN IV G LEVEL 0, MOD 0             VELTV               DATE = 68040          00/59/27          PAGE 000
```

COMMON BLOCK /        / MAP SIZE    385C

| SYMBOL | LOCATION | SYMBOL | LOCATION | SYMBOL | LOCATION | SYMBOL | LOCATION | SYMBOL | LO |
|---|---|---|---|---|---|---|---|---|---|
| NN | 0 | NT | 4 | NEX | 8 | B | C | X | |
| Y | C8C | U | 12CC | V | 190C | AUK | 1F4C | ARAD | |
| NEX1 | 384C | NEX2 | 3850 | NBEG | 3854 | PI4 | 3858 | | |

SCALAR MAP

| SYMBOL | LOCATION | SYMBOL | LOCATION | SYMBOL | LOCATION | SYMBOL | LOCATION | SYMBOL | LO |
|---|---|---|---|---|---|---|---|---|---|
| I | AC | ADEN | B0 | BDEN | B4 | NNM | B8 | M | |
| NB | C0 | J | C4 | DENOM | C8 | ANY | CC | ANX | |
| FDN | D4 | NUJU | D8 | NUJV | DC | NUMU | F0 | NUMV | |

TOTAL MEMORY REQUIREMENTS 000452 BYTES

AIII. 3 PAPTV (Print and Plot) Subroutine

The PAPTV subroutine produces the vehicle and tower interference printed and graphic output when the ACCPT, which is incremented by DELT, exceeds the input DELTP.

The HOUR subroutine is called in PAPTV and extracts the IBM machine time and prints both IBM and problem times. The CRT output shows the positions of vehicle, tower which may be in rotated position, and the free vortices. A good graph reproduces this data with the streamlines which are calculated in the main program. The input DELSL, incremental time to calculate streamlines, must be equal to or a multiple of DELTP.

The subroutines CRIDIV, APRNTV, PRINTV, and APLOTV are Fortran G, SC 4020 standard routines.

AIII. 3. 1 Flow Chart

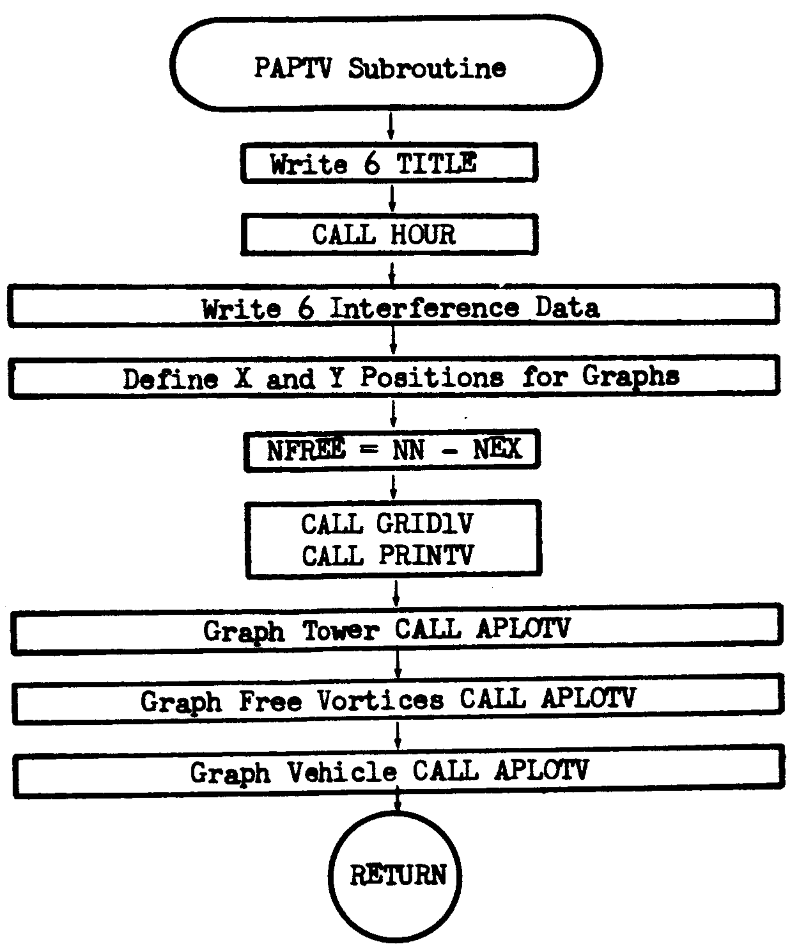

## AIII. 3. 2 Listing of PAPTV

```
FORTRAN IV G LEVEL 0, MOD 0              PAPTV              DATE = 68014          01/52/33

 0001               SUBROUTINE PAPTV
            C              PRINT AND PLOT FOR VSTV VORTEX SHEDDING PROGRAM
            C                                                                       KT2M2070
 0002                INTEGER DNC,HR,SEC                                             KT2M2075
            C                                                                       KT2M2085
 0003               COMMON     NN, NT,NEX,    B(400,9) ,NEX1,NEX2,NBEG,PI4
 0004               COMMON     /CFLOW/BINARY,ROTOW
 0005               COMMON     /CTIMES/TIME,DELT,DELTC,DELTP,ACCDT,ACCPT,TFIN,DNC,CONKCKT2M2100
                  *            ,TPC,TCO,TSO,ACCSL,DELSL
 0006               COMMON /CGRA/ DXGRA,DYGRA,NGRA,MGRA,LABX,LABY
                  *            ,XXL,XR,YB,YT
                  *          ,XL( 200 ), XU( 200 ), YL( 200 ), YU( 200 )
                  *          ,CX(45),CYU(45),CYL(45),CXN(45),CASENO
            C                                                                       KT2M2125
 0007               DIMENSION  X(400,1),  Y(400,1)
            C                                                                       KT2M2140
 0008               EQUIVALENCE(B(1,2),X(1,1)),                    (B(1,3),Y(1,1))  KT2M2145
            C                                                                       KT2M2150
            C                                                                       KT2M2155
 0009               WRITE (6,10)
 0010            10 FORMAT (1H1, 25X,'VEHICLE AND TOWER INTERFERENCE DATA'////)
            C                                                                       KT2M2160
            C                                                                       KT2M2165
 0011               ACCPT =TPO                                                      KT2M2170
            C                                                                       KT2M2175
 0012            20 CALL HOUR
            C                                                                       KT2M2210
 0013               WRITE (6,40)                                                    KT2M2215
 0014            40 FORMAT (1H0,8HVORTEX   ,3X,          9X,3HX/A,15X,3HY/A,15X,
                  *        7HU/U INF,11X, 7HV/U INF,11X,8HK / U*A ,//)              KT2M2225
            C                                                                       KT2M2230
 0015               WRITE(6,50)(I,(B(I,J),J=2,6),I=1,NN)
 0016            50 FORMAT (1H ,  I4,7X,    1X,1P5F18.7)                            KT2M2240
            C                                                                       KT2M2245
 0017               DO 400 I = 1,NEX
 0018               XL(I) = X(I,1)
 0019           400 YL(I) = Y(I,1)
            C
 0020               DO  500  I = NBEG,NN
 0021               XU(I)   =   X(I,1)                                              KT2M2275
 0022           500 YU(I)   =   Y(I,1)                                              KT2M2285
            C                                                                       KT2M2290
 0023               NFREE = NN - NEX
 0024           520 CALL GRIDIV (-3,   XXL,XR,YB,YT,DXGRA,DYGRA,NGRA,MGRA
                  *                         ,LABX,LABY,6,6)
 0025               CALL APRNTV (0,  -13,  3,'Y/A',       4,500)
 0026               CALL PRINTV  (3,   'X/A',       450,4)
 0027               CALL APLOTV(NEX,   XL,YL,      1,1,1,     38   ,IERR)
 0028               CALL APLOTV(NFREE,   XU, YU,     1,1,1,       44, IER)
 0029               CALL APLOTV(  45,   CX  , CYU,      1,1,1,       42, IERR)
 0030               CALL APLOTV(  45,   CX  , CYL,      1,1,1,       42, IERR)
 0031               CALL APLOTV(  45,   CXN, CYU,      1,1,1,       42, IERR)
 0032               CALL APLOTV(  45,   CXN, CYL,      1,1,1,       42, IERR)
 0033               WRITE ( 16 , 60     )NN,TIME,DELTC,CASENO
 0034            60 FORMAT (1H+,14X,I4, 2X,
                  *           'VORTEX LOCATIONS AT TIME =',1F8.4,2X,5HA/U   ,15X,6H
                  *DELTC=,1F9.4,5X,9HCASE NO.      ,F10.2)
            C                                                                       KT2M2355
 0035          7050 RETURN                                                          KT2M2465
 0036               END                                                             KT2M2470
```

COMMON BLOCK /          / MAP SIZE     385C

| SYMBOL | LOCATION | SYMBOL | LOCATION | SYMBOL | LOCATION | SYMBOL | LOCATION | SYMBOL | LOCATION |
|---|---|---|---|---|---|---|---|---|---|
| NN | 0 | NT | 4 | NEX | 8 | B | C | X | 64C |
| Y | C8C | NEX1 | 384C | NEX2 | 3850 | NBEG | 3854 | PI4 | 3858 |

COMMON BLOCK /CFLOW    / MAP SIZE     8

| SYMBOL | LOCATION | SYMBOL | LOCATION | SYMBOL | LOCATION | SYMBOL | LOCATION | SYMBOL |
|---|---|---|---|---|---|---|---|---|
| BINARY | 0 | ROTOW | 4 | | | | | |

```
FORTRAN IV G LEVEL 0, MOD 0              PARTV              DATE = 68014          01/52/33

                                  COMMON BLOCK /CTIMES  / MAP SIZE      38
  SYMBOL    LOCATION      SYMBOL    LOCATION      SYMBOL    LOCATION      SYMBOL    LOCATION      SYMBOL
  TIME           0        DELT          4         DELTC          8        DELTP          C        ACCDT     10
  ACCPT         14        TFIN         18         DNC           1C        CONKC         20        TPO       24
  TCO           28        TSC          2C         ACCSL         30        DELSI         34

                                  COMMON BLOCK /CGRA    / MAP SIZE     F7C
  SYMBOL    LOCATION      SYMBOL    LOCATION      SYMBOL    LOCATION      SYMBOL    LOCATION      SYMBOL
  DXGRA          0        DYGRA         4         NGRA           8        MGRA           C        LABX      10
  LABY          14        XXI          18         XR            1C        YR            20        YT        24
  XL            28        XU          348         YL           668        YU           988        CX       CA8
  CYU          D5C        CYL         E10         CXN          EC4        CASENO       F78

                                  SCALAR MAP
  SYMBOL    LOCATION      SYMBOL    LOCATION      SYMBOL    LOCATION      SYMBOL    LOCATION      SYMBOL
  I             84        J            88         NERFE         BC        IERR          C0        IER       C4

                                  SUBPROGRAMS CALLED
  SYMBOL    LOCATION      SYMBOL    LOCATION      SYMBOL    LOCATION      SYMBOL    LOCATION      SYMBOL
  IBCOM#        C8        HOUR         CC         GRIDIV        D0        APRNTV        D4        PRINTV    D8
  APLOTV        DC

                                  FORMAT STATEMENT MAP
  SYMBOL    LOCATION      SYMBOL    LOCATION      SYMBOL    LOCATION      SYMBOL    LOCATION      SYMBOL
      10       202            40      231             50     274            60       286

    TOTAL MEMORY REQUIREMENTS 000590 BYTES
```

# APPENDIX B

## LAUNCH PAD WIND PROFILE ANALYSIS

### Index

# APPENDIX B. LAUNCH PAD WIND PROFILE ANALYSIS

## BI. THEORETICAL DEVELOPMENT

### BI. 1 Flow Field for a System of Vortices Outside an Elliptical Cylinder in Uniform Flow

The following development was originally presented in Reference 3 as part of a more complete theoretical treatment of a nonsteady potential flow field containing a stationary cylinder and free vortices in uniform flow.

The analysis for the circular cylinder (Appendix A) may be extended to the case of an elliptical cylinder by a conformal transformation. The circular cylinder is mapped into an elliptical cylinder by the well-known Joukowski transformation.

In the plane of the circular cylinder, say the $z_1$-plane, the circle of radius $r_o = (a+b)/2$ is mapped by the transformation

$$z = z_1 + \frac{C^2}{4z_1} \text{ where } C^2 = a^2 - b^2 \qquad \text{(B-1)}$$

into an ellipse in the z-plane with major axis, 2a, and minor axis, 2b.

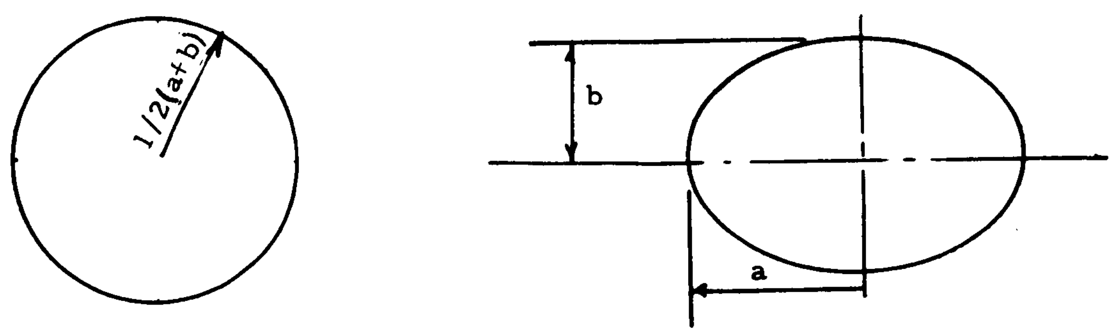


When $b \to 0$ we have the degenerate case of a flat plate of length 2a in the z-plane.

The velocity field in the z-plane is completely determined from the $z_1$-plane and the mapping transformation. For a general system of vortices in the z-plane (plane of ellipse), the velocity of the $m^{th}$ vortex is

$$(u - iv)_m = \frac{dF(z)}{dz} \tag{B-2}$$

where

$$F(z) = -w(z_1) + iK_m \log (z - z_m) \tag{B-3}$$

and from Equations A-2 and A-3;

$$w(z_1) = i \sum_{j=1}^{n} K_j \left[\log (z_1 - z_{1j}) - \log\left(z_1 - \frac{1}{\bar{z}_{1j}}\right) + \log z_1 - \log \bar{z}_{1j}\right]$$

$$- U_o \left[z_1 e^{-i\alpha} + \frac{1}{z_1} e^{i\alpha}\right] \tag{B-4}$$

where the circle in the $z_1$-plane is chosen to have unit radius.

Therefore

$$z = \left(\frac{a+b}{2}\right) z_1 + \left(\frac{a-b}{2}\right) \frac{1}{z_1}$$

The derivative, $\frac{dF(z)}{dz}$, may be written

$$\frac{dF(z)}{dz} = \frac{dF(z)}{dz_1} \frac{dz_1}{dz} \tag{B-5}$$

where the mapping function is

$$z = f(z_1)$$

and

$$\frac{dz}{dz_1} = \frac{df(z_1)}{dz_1} = f'(z_1) \tag{B-6}$$

From Equations B-3 and B-4

$$\frac{dF(z)}{dz_1} = i \sum_{j=1}^{n} K_j \left[\frac{1}{z_1 - z_{1j}} - \frac{z_{1j}}{z_1 z_{1j} - 1} + \frac{1}{z_1}\right] + U_o \cos\alpha\left(1 - \frac{1}{z_1^2}\right)$$

$$- i U_o \sin\alpha \left(1 + \frac{1}{z_1^2}\right) - \frac{i K_m f'(z_1)}{f(z_1) - f\left(z_{1_m}\right)} \qquad \text{(B-7)}$$

Thus,

$$\frac{dF(z)}{dz} = \Bigg|_{z=z_m} = \left[ i \sum_{j=1}^{n} K_j \left( \frac{1}{z_1 - z_{1j}} - \frac{z_{1j}}{z_1 z_{1j} - 1} + \frac{1}{z_1} \right) \right.$$

$$+ U_o \cos\alpha \left(1 - \frac{1}{z_1^2}\right) - U_o \sin\alpha \left(1 + \frac{1}{z_1^2}\right)$$

$$\left. - \frac{iK_m f'(z_1)}{f(z_1) - f(z_{1m})} \right]_{z_1 = z_{1m}} \times \left( \frac{1}{f'(z_1)} \right)_{z_1 = z_{1m}} \qquad \text{(B-8)}$$

The first and last terms in the brackets have singularities when $z_1 = z_{1m}$, but the other terms are regular if $|z_1| > 1$. Rewriting Equation B-8

$$\frac{dF(z)}{dz}\Bigg|_{z=z_m} = F'(z_m)$$

$$= \frac{1}{f'(z_{1m})} \; i \left\{ \sum_{\substack{j=1 \\ j \neq m}}^{n} \frac{K_j}{z_{1m} - z_{1j}} - i \sum_{j=1}^{n} \frac{K_j}{z_{1j}\,(z_{1m} z_{1j} - 1)} \right.$$

$$+ U_o \cos\alpha \left(1 \; \frac{1}{z_1^2}\right) - i\, U_o \sin\alpha \left(1 - \frac{1}{z_1^2}\right)$$

$$\left. + iK_m \left[ \frac{1}{z_1 - z_{1m}} - \frac{f'(z_1)}{f(z_1) - f(z_{1m})} \right]_{z_1 = z_{1m}} \right\} \qquad \text{(B-9)}$$

Expanding $f(z_1)$ in a Taylor's series about the point $z_1 = z_{1m}$ results in

$$\left[ \frac{1}{z_1 - z_{1m}} - \frac{f'(z_1)}{f(z_1) - f(z_{1m})} \right]_{z_1 = z_{1m}} = \frac{1}{2} \frac{f''(z_{1m})}{f'(z_{1m})} \qquad \text{(B-10)}$$

Finally

$$(u-iv)_m = f'(z_m)$$

$$= \frac{1}{f'(z_m)} \; i \left[ \sum_{\substack{j \neq m \\ j \neq 1}}^{n} \frac{K_j}{z_{lm} - z_{lj}} - i \sum_{j=1}^{n} z_{lj} \frac{K_j}{(z_{lm} z_{lj} - 1)} \right.$$

$$+ U_o \cos\alpha \left(1 - \frac{1}{z_1^2}\right) - i\, U_o \sin\alpha \left(1 + \frac{1}{z_1^2}\right)$$

$$\left. + \frac{iK_m}{2} \; \frac{f''(z_{lm})}{f'(z_{lm})} \right] \tag{B-11}$$

As discussed in Appendix A, the last term of Equation B-11 represents the contribution of a center vortex, which within the framework of this study is to be omitted as long as the vortices are generated by the ellipse, and no other body is present in the flow.

This being the case, the expression within brackets is identical to the flow field equation for a circular cylinder, and must be multiplied by the transformation expression, $\frac{1}{f'(z_m)}$. For symmetrical flow further obvious simplification can be made.

## BII. MAIN PROGRAM (PADPRØ)

### BII. 1 Functional Flow Chart

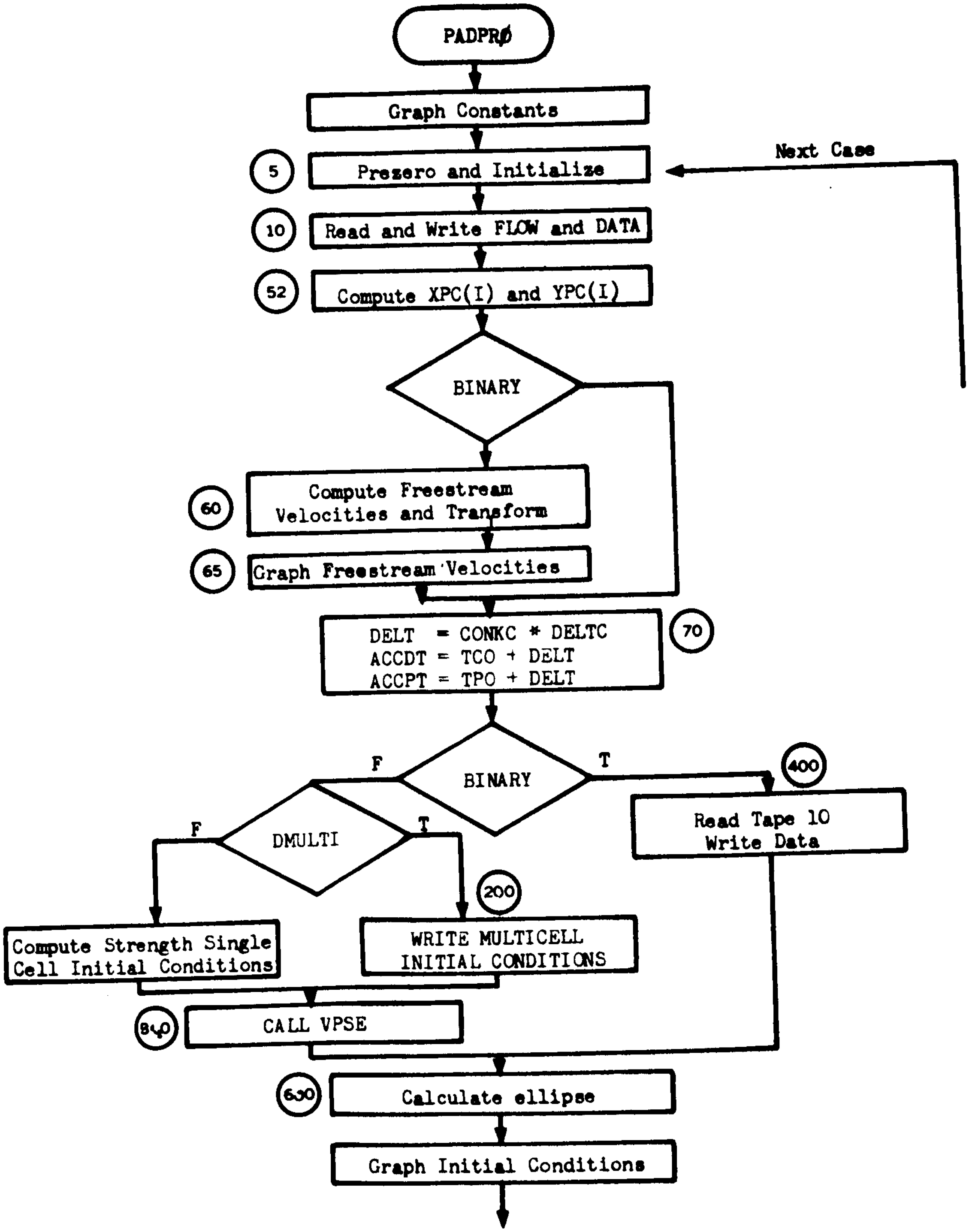

BII. 1 Functional Flow Chart (Cont)

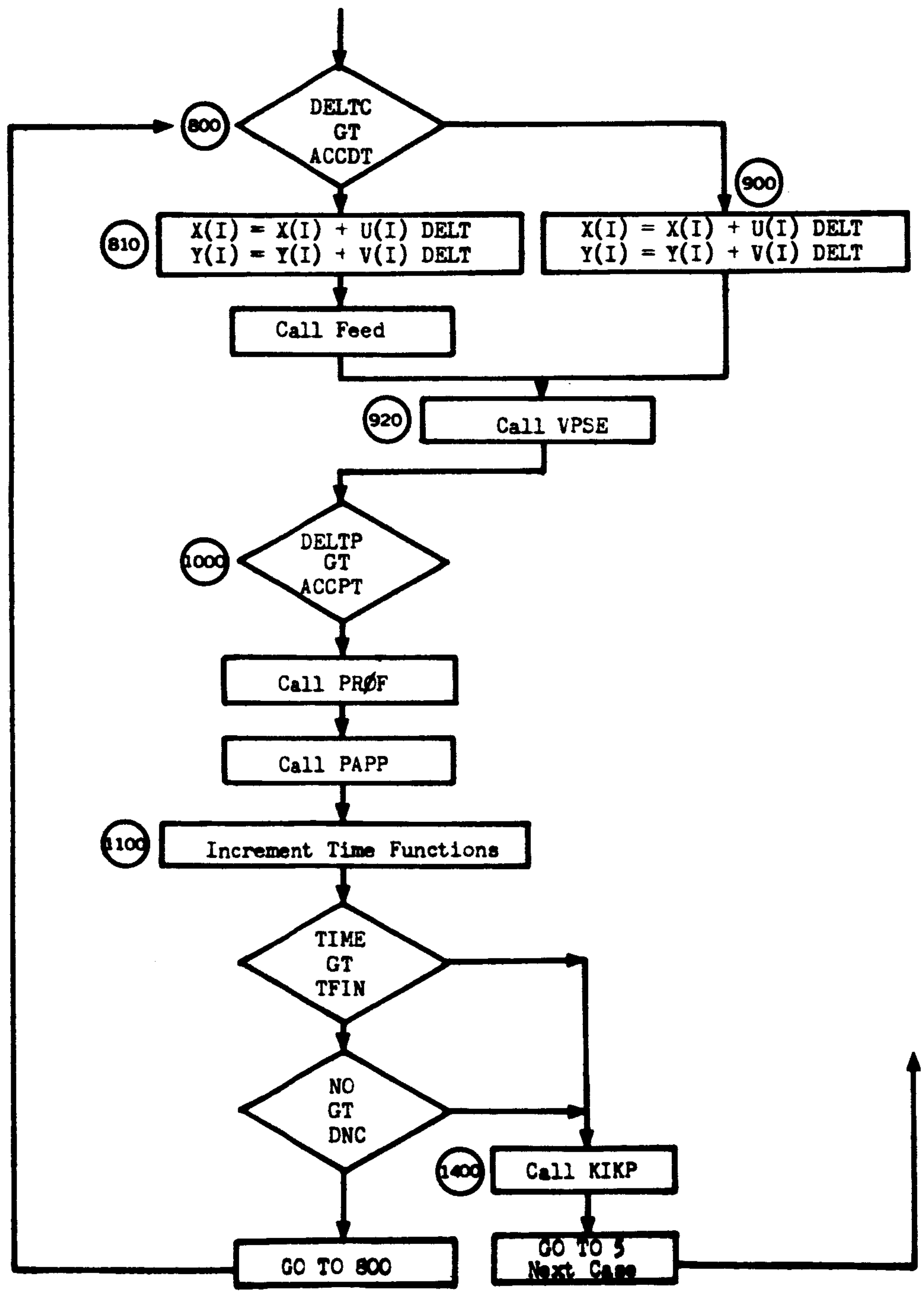

## BII. 2. Input Data

### BII. 2. 1. Data Definition

The input data read are in two namelist arrays, FLOW and DATA.

FLOW has two logical items:

| | | |
|---|---|---|
| BINARY | = | F for initial case |
| | = | T for restart case |
| DMULTI | = | F for single cell case |
| | = | T for multicell case |

The DATA array is defined:

| | |
|---|---|
| TIME | Start time ( = 0 for initial) |
| TFIN | Final time |
| DNC | Number of cells to terminate |
| CONKC | Factor to compute integration increment |
| DELTC | Time increment to introduce new vortex |
| DELTP | Time increment to output data |
| NØ | Initial number of vortices |
| XØU | X-Location of feeding point |
| YØU | Y-Location of feeding point |
| BETA | Ellipse defined by — <br> A = 1 + BETA <br> B = 1 - BETA |
| NP | Number of YIP points |
| YIP | Y-location of profiles (Max NP) |
| NPRO | Number of profiles |
| XIP | X-locations of profiles (Max NPRØ) |
| CASENØ | Case number (Mo Da Yr) |

## BII. 3 Program Listing

```
C      MAIN PROGRAM - LAUNCH PAD INTERFERENCE STUDY -
C                     VORTEX SHEDDING MODEL 6
C                         SYMMETRICAL FLOW
C
C      PROGRAM EXITS ON READ FOR NEXT CASE
C
C
       LOGICAL     BINARY,DMULTI
       INTEGER     DNC
C
       COMMON NO,B(400,7),XOU,YOU,BETA,ALFAS
       COMMON    /CFLOW/BINARY,DMULTI
       COMMON    /CTIMES/TIME,DELT,DELTC,DELTP,ACCDT,ACCPT,TFIN,DNC,CONKC
      *           ,TPO,TCO
       COMMON    /CGRAF/XXL,XR,YB,YT,DXGRA,DYGRA,NGRA,MGRA,LABX,LABY
      *           ,CX(45),CYU(45),CYL(45),CXN(45),CASENO
       COMMON /CPAD/XP(20,50),YP(20,50),NP, XPC(20,50),YPC(20,50)
      * ,UCYL,VCYL,XFP,YFP,CC,DD,UP(20,50),VP(20,50),NPRO
C
       DIMENSION  ITH(400,1),                          X(400,1),
      *           Y(400,1),                            U(400,1),
      *           V(400,1),                            AUK(400,1),
      *                                                ARAD(400,1 ),
      *           XU(200),                             XL(200),
      *           YU(200),                             YL(200),
      *           XE(400,20),                          YE(400,20),
      *           H(50),               XIP(50),        YIP(20)
C
C
       EQUIVALENCE(B(1,1),ITH(1,1)),                   (B(1,2),X(1,1)),
      *           (B(1,3),Y(1,1)),                     (B(1,4),U(1,1)),
      *           (B(1,5),V(1,1)),                     (B(1,6),AUK(1,1)),
      *           (B(1,7),ARAD(1,1))
C
C
       NAMELIST /FLOW/ BINARY,DMULTI
       NAMELIST /DATA/ TIME,TFIN,DNC,CONKC,DELTC,DELTP,NO,XOU,YOU,BETA
      *                ,NP,YIP,NPRO,XIP,CASENO
C
C
       REWIND 10
       CALL SCOUTV
       CALL CAMRAV(9)
       XXL = -2.0
       XR = 8.0
       YB = -1.0
       YT = 9.0
       DXGRA = .5
       DYGRA = .5
       NGRA = -4
       MGRA = -4
       LABX = -4
       LABY = -4
C
       TPO = .00001
       TCO = .00001
```

```
C
    5 DO 6 J=1,7
      DO 6 I=1,400
    6 B(I,J) = 0.0
      DO 7 J = 1,50
      H(J) = 0.0
      DO 7 I = 1,20
      XP(I,J)  = 0.0
      YP(I,J)  = 0.0
      UP(I,J)  = 0.0
      VP(I,J)  = 0.0
      XPC(I,J) = 0.0
      YPC(I,J) = 0.0
    7 CONTINUE
C
      DMULTI = .FALSE.
      BINARY = .FALSE.
C
      READ(5,FLOW)
      READ(5,DATA)
C
      WRITE (6,10) CASENO
   10 FORMAT (1H1,  39X,  'LAUNCH PAD INTERFERENCE STUDY'  /
     *               43X,    'VORTEX SHEDDING MODEL 6'     /
     *               43X,  'NORTH AMERICAN ROCKWELL'       /
     *               45X,  'DEPARTMENT 190/200'            //////
     *               40X,  'INPUT DATA FOR CASE NO.'  ,F8.2 ,////)
      WRITE (6,FLOW)
C
      WRITE (6,12)  TIME,TFIN,DNC,CONKC,DELTC,DELTP,NO,XOU,YOU,BETA
     *             ,XAUK,YAUK
     *             ,CASENO
     *             ,NP, (YIP(I), I=1,NP)
      WRITE (6,13)                          NPRO,(XIP(I),I=1,NPRO)
C
   12 FORMAT (1H-, 9X, 'TIME 'F10.3,20X'TFIN 'F10.3,20X'DNC   'I10  ///
     *            10X    'CONKC'F10.3,20X'DELTC'F10.3,20X'DELTP'F10.3///
     *            10X    'NO   'I10  ,20X'XOU  'F10.3,20X'YOU  'F10.3///
     *            10X    'BETA 'F10.3,20X'XAUK 'F10.3,20X'YAUK 'F10.3///
     *            10X    'CASENO' F9.2  ///
     *            10X    'NP   'I10  ,20X'YIP '/  (51X,5F10.3  ))
C
   13 FORMAT(1H0,9X    'NPRO 'I10  ,20X'XIP '/  (51X,5F10.3  ))
C
C
      OPB = 1. + BETA
      OPBSQ = OPB * OPB
      OMB = 1. - BETA
      DIF = OMB/OPB
      DO 30 J=1,NPRO
      DO 30 I=1,NP
      XP(I,J) = XIP(J)
      YP(I,J) = YIP(I)
      IF(XIP(J) .GE. -OPB .AND. XIP(J) .LE. OPB)  GO TO 20
      GO TO 30
C
   20 H(J) = DIF * SQRT (OPBSQ - XIP(J)**2)
      YP(I,J) = H(J) + YIP(I)
   30 CONTINUE
C
```

```
C                            INITIALIZE
      NPP = NP+ 1
      XP(NPP,1)=XOU
      YP(NPP,1)=YOU
C
      DO 59  J=1,NPRO
      DO 59 I= 1,NPP
      XE(I,J) = XP(I,J)
      YE(I,J) = YP(I,J)
      ARG1=2.*XE(I,J)*YE(I,J)
      ARG2 =(XE(I,J)**2) - (YE(I,J)**2) -4.*BETA
      ROT = (ARG1**2) + (ARG2**2)
      RO=SQRT(ROT)
      RO=SQRT(RO)
      TH=ATAN2(ARG1,ARG2)
      IF(TH) 50,51,51
   50 TH=2.*3.1415926+ TH
   51 TH= TH/2.
      A=RO*COS(TH)
      C=RO*SIN(TH)
      XPC(I,J)=(XE(I,J) + A) /2.
      YPC(I,J)=(YE(I,J) +C) /2.
      ARAT = XPC(I,J)**2+YPC(I,J)**2
      IF(ARAT - .99999) 52,52,59
   52 XPC(I,J)=(XE(I,J) -A) /2.
      YPC(I,J) = (YE(I,J) -C) /2.
   59 CONTINUE
C
      XFP = XPC(NPP,1)
      YFP = YPC(NPP,1)
C
      IF(BINARY) GO TO 70
C
      DO  60 JJ= 1,NPRO
      DO  60 J=1,NP
      DENO = (XPC(J,JJ)**2 + YPC(J,JJ)**2)**2
      UPRO = 1. - (XPC(J,JJ)**2 - YPC(J,JJ)**2)/DENO
      VPRO = -2. * XPC(J,JJ) * YPC(J,JJ) /DENO
C
C
C             TRANSFORMATION OF VELOCITY
      AA = XPC(J,JJ)**2 - YPC(J,JJ)**2
      BB = 2. * XPC(J,JJ)  * YPC(J,JJ)
       DENOM = (AA - BETA)**2 + BB**2
      CM = 1. + BETA * (AA - BETA) /DENOM
      DM = BB * BETA/DENOM
      UP(J,JJ)=CM*UPRO- DM * VPRO
      VP(J,JJ)=CM*VPRO+ DM * UPRO
   60 CONTINUE
C
      WRITE (6,65)
   65 FORMAT (1H1,  42X, 'FREESTREAM PROFILES')
      CALL PLOTPR
C
   70 DELT= CONKC*DELTC
      ACCDT=TCO    + DELT
      ACCPT=TPU          +DELT
C
      DO  80 I=1,45
      CX(I) = 0.0
      CXN(I) = 0.0
      CYU(I) = 0.0
   80 CYL(I) = 0.0
```

```
C
      IF(BINARY)GO TO 400
      IF(DMULTI)GO TO 200
      WRITE(6,100)
  100 FORMAT(1H1,40X,38HSINGLE CELL ******** INITIAL CONDITION )
C
      CALL HOUR
C
      X(1,1)=XOU
      Y(1,1)=YOU
      ITH(1,1) = 1
C
      SQFUN = SQRT(XFP**2 + YFP**2)
      XCYL = XFP/SQFUN
      YCYL = YFP/SQFUN
      UCYL = 2. * YCYL**2
      VCYL = -2. * XCYL * YCYL
      AA = XCYL**2 - YCYL**2
      BB = -VCYL
      DENOM = (AA-BETA)**2 + BB**2
      CC = 1. +  BETA *(AA-BETA)/DENOM
      DD = BB*BETA/DENOM
      UFP = CC *UCYL - DD *VCYL
      VFP = CC *VCYL + DD *UCYL
      ALFAS = (UFP**2 + VFP**2)
C
      AUK(1,1)=DELTC * ALFAS / (4.0 * 3.14159)
      WRITE (6,5000)
      WRITE(6,5010)(ITH(I,1),X(I,1),Y(I,1),AUK(I,1),I=1,NO)
      GO TO 300
C
  200 WRITE(6,210)TIME,NO
  210 FORMAT (1H1,  10X, 6HTIME = ,  F10.6,  14X
     *               27HMULTICELL INITIAL CONDITIONI3,2X, 5HPAIRS)
      DO 215 I=1,NO
  215 READ (5,220)      ITH(I,1),X(I,1),Y(I,1),AUK(I,1)
      WRITE(6,5000)
      WRITE (6,5010)  (ITH(I,1),X(I,1),Y(I,1),AUK(I,1),  I=1,NO)
  220 FORMAT (I12,3E12.0)
C
  300 CALL VPSE
      GO TO 600
C
  400 READ (10,ERR=9999) NO,((B(I,J),I=1,NO),J=1,7),CSNO,TIME
      WRITE(6,410)CSNO,NO
  410 FORMAT (1H1,25X,40HBINARY MULTICELL INITIAL CONDITION (CASE F10.4,
     *     4H)    ,I3,2X5HPAIRS)
  450 WRITE (6,5020)
      WRITE(6,5030)((B(I,J),J=1,6),I=1,NO)
C
C
  600 CONTINUE
C     CALCULATE ELLIPSE
      DDEG=0.0
      DO 610  I=1,45
      DDEG=DDEG+2.0
      CX(I)=(1.+BETA)*COSD(DDEG)
      CXN(I)=-CX(I)
  610 CYU(I)=(1.-BETA)*SIND(DDEG)
C
```

```
  700 CONTINUE
      CALL GRIDIV( -3, XXL, XR, YB, YT, DXGRA,DYGRA,  NGRA,MGRA,
     *            LABX,LABY,   3,3)
      CALL PRINTV(11,  'X/A - AXIS ',      472,4)
C
      IF(DMULTI) GO TO 705
      CALL APLOTV( NO,  XOU,YOU,   1,1,1,38,IERR)
      GO TO 725
C
  705 DO 720 I=1,NO
      XU(I) = X(I,1)
  720 YU(I) = Y(I,1)
C
      CALL APLOTV( NO,  XU,YU,   1,1,1,38,IERR)
C
  725 CALL APLOTV( 45, CX, CYU, 1,1,1,  42,IERR)
      CALL APLOTV( 45, CXN,CYU, 1,1,1,  42,IERR)
      WRITE (16,750)  TIME,CASENO,DELTC
  750 FORMAT (1H+,5X34H INITIAL CELL LOCATIONS AT TIME = 1F9.4,2X,3HA/U,
     *           20X,8HCASE NO.,2X,F8.2,     8X, 'DELTC = ' F5.3)
C
  800 IF(DELTC.GT.ACCDT)GO TO 900
C
      DO  810 I=1,NO
      X(I,1)= X(I,1) +U(I,1) *DELT
  810 Y(I,1)= Y(I,1) +V(I,1) *DELT
C
C     INTRODUCE NEW CELLS
C
      CALL FEED
C
      NO=NO+1
      X(NO,1)= XOU
      Y(NO,1)= YOU
      AUK(NO,1)= DELTC*ALFAS /(4.*3.14159)
      ITH(NO,1)= NO
      ACCDT=TCO
C     END OF INTRODUCTION OF NEW CELL
C
      GO TO 920
  900 DO 910 I=1,NO
      X(I,1)= X(I,1) +U(I,1) *DELT
  910 Y(I,1)= Y(I,1) +V(I,1) *DELT
  920 CALL VPSE
C
 1000 IF(DELTP.GT.ACCPT)GO TO 1100
C
      CALL PROF
C
      CALL PAPP
C
 1100 TIME= TIME + DELT
      ACCDT= ACCDT + DELT
      ACCPT= ACCPT + DELT
C
 1200 IF(TIME.GT.TFIN) GO TO 1400
 1300 IF(NO.GT.DNC) GO TO 1400
      GO TO 800
C
 1400 CALL KIKP
```

```
C
      GO TO 5
 9999 I=16000000
      HHHHHH=H(I)
      STOP
C
C
 5000 FORMAT (1H-,5X,8HITH CELL,12X,3HX/A,17X,3HY/A,17X,1HK   ,//)
 5010 FORMAT (1H ,8X,I4,1P3E20.7)
 5020 FORMAT (1H-,4X8HCELL NO.,3X,3HX/A,15X,3HY/A,15X,7HU/U INF,11X,
     *     7HV/U INF,11X,7HK/U*A    ,//)
 5030 FORMAT (1H ,6X,I4,2X,1P5E18.7)
      END
/*
```

## BIII. SUBROUTINES

Subroutines for the PADPRØ Program have functions that are similar to those of the subroutines for the VSTV Program (Appendix A, AIII). No flow charts will be presented; listings are in Section BIII. 1. The VPSE (velocity) subroutine parallels the VELTV (AIII. 2.); the FEED (feeding-point) subroutine parallels NUCTV (AIII. 1.), the PAPP (print-and-plot) subroutine parallels PAPTV, the KIKP subroutine parallels the KIKTV (AIII. 4.). The new subroutine PROF (profile) computes (NPRO, input) velocity profiles at the XIP (input), X locations over the NP (number of points) on the YIP (input), and Y locations. The HOUR subroutine calculates the IBM machine time and prints on header of profile output data. All subroutine listings are in Section BIII. 1.

BIII. 1 Listings

```
      SUBROUTINE VPSE
C     ELLIPTICAL  VELOCITY COMPUTATION ,SYMMETRICAL
C                      PAD PROFILE
C
C
      COMMON NO,B(400,7),XOU,YOU,BETA,ALFAS
C
C
      DIMENSION  X(400,1),Y(400,1),U(400,1),V(400,1),AUK(400,1),ARAD(400
     *    ,1)
      DIMENSION  XE(400,1),YE(400,1),
     *XSQ(400,1),YSQ(400,1)
C
      EQUIVALENCE(B(1,2),X(1,1)),                      (B(1,3),Y(1,1)),
     *            (B(1,4),U(1,1)),                     (B(1,5),V(1,1)),
     *            (B(1,6),AUK(1,1)),                   (B(1,7),ARAD(1,1))
C
      DO  10 I=1,NO
      XE(I,1)= X(I,1)
   10 YE(I,1)= Y(I,1)
C
      DO 300 I=1,NO
      ARG1=2.*XE(I,1)*YE(I,1)
      ARG2 =(XE(I,1)**2) - (YE(I,1)**2) -4.*BETA
      ROT = (ARG1**2) + (ARG2**2)
      RO=SQRT(ROT)
      RO=SQRT(RO)
      TH=ATAN2(ARG1,ARG2)
C
      IF(TH) 50,51,51
   50 TH=2.*3.1415926+ TH
   51 TH= TH/2.
      A=RO*COS(TH)
      C=RO*SIN(TH)
      X(I,1)=(XE(I,1)+A)/2.
      Y(I,1)=(YE(I,1)+C)/2.
      XSQ(I,1) = X(I,1)**2
      YSQ(I,1)=Y(I,1) **2
      ARAD(I,1) = XSQ(I,1)+ YSQ(I,1)
C
      IF(ARAD(I,1)-.99999)   11,11,12
   11 X(I,1)=(XE(I,1)-A)/2.
      Y(I,1)=(YE(I,1)-C)/2.
   12 XSQ(I,1)=X(I,1)**2
      YSQ(I,1)=Y(I,1) **2
      ARAD(I,1) = XSQ(I,1)+ YSQ(I,1)
      RSQ=ARAD(I,1)**2
      DEN2=(1.-2.*ARAD(I,1)+RSQ)*(1.-2.*(X(I,1)**2-Y(I,1)**2)+RSQ)
      AB=4.*(Y(I,1)**2)/DEN2
      D=2.*(1.-2.*X(I,1)**2+RSQ)/DEN2
      ALPHA=0.0
      SAL=SIN(ALPHA)
      CAL=COS(ALPHA)
      XX=1.-(X(I,1)**2-Y(I,1)**2)/RSQ
      YY= 2.*X(I,1)*Y(I,1)/RSQ
      U(I,1)=-AUK(I,1)*Y(I,1)*(ARAD(I,1)*AB-D)+XX*CAL-YY*SAL
     * -AUK(I,1)/(2.*Y(I,1))
  300 V(I,1)=AUK(I,1)*X(I,1)*AB*(ARAD(I,1)-1.)-YY*CAL-XX*SAL
C
```

```
      NNM=NO-1
      IF(NNM)  101,105,101
  101 CONTINUE
      DO 301 M=1,NNM
      MP= M+1
C
      DO 301 J=MP,NO
      DX=(X(M,1)-X(J,1))**2+(Y(M,1)-Y(J,1))**2
      DY=1.-2.*(X(J,1)*X(M,1)+Y(J,1)*Y(M,1))+ARAD(J,1)*ARAD(M,1)
      YYY=Y(J,1)*Y(M,1)
      DEN1=DX*(DX+4.*YYY)
      DEN2=DY*(DY+4.*YYY)
      A=4.*YYY/DEN1
      AB=4.*YYY/DEN2
      C= 2.*(DX+2.*YYY)/DEN1
      D =2.*(DY+2.*YYY)/DEN2
      E=A-AB
      F=C-D
      G=A-ARAD(J,1)*AB
      H=A-ARAD(M,1)*AB
      USUMM=Y(M,1)*G-Y(J,1)*F
      USUMJ=Y(J,1)*H-Y(M,1)*F
      VSUMM=X(M,1)*G-X(J,1)*E
      VSUMJ=X(J,1)*H-X(M,1)*E
      U(M,1)=U(M,1)+AUK(J,1)*USUMM
      U(J,1)=U(J,1)+AUK(M,1)*USUMJ
      V(M,1)=V(M,1)-AUK(J,1)*VSUMM
  301 V(J,1)=V(J,1)-AUK(M,1)*VSUMJ
C
  105 DO 110 I=1,NO
      A=XSQ(I,1)-YSQ(I,1)
      P=A-BETA
      C=2.*X(I,1)*Y(I,1)
      DEN1=P**2+C**2
      D=3.*XSQ(I,1)-YSQ(I,1)-BETA
      E=XSQ(I,1)-3.*YSQ(I,1)-BETA
      DEN2=XSQ(I,1)*(E**2)+YSQ(I,1)*(D**2)
      F=A*P+C**2
      G=C*BETA
      U(I,1)=(U(I,1)*F-V(I,1)*G)/DEN1+(Y(I,1)*BETA*AUK(I,1)*D)/DEN2
  110 V(I,1)=(V(I,1)*F+U(I,1)*G)/DEN1-(X(I,1)*BETA*AUK(I,1)*E)/DEN2
C
      DO 22 I=1,NO
      X(I,1)= XE(I,1)
   22 Y(I,1)= YE(I,1)
      RETURN
      END
/*
      SUBROUTINE FEED
C             FEED POINT VELOCITY COMPUTATION
C
C
C
      COMMON NO,B(400,7),XOU,YOU,BETA,ALFAS
      COMMON /CPAD/XP(20,50),YP(20,50),NP, XPC(20,50),YPC(20,50)
     * ,UCYL,VCYL,XFP,YFP,CC,DD,UP(20,50),VP(20,50),NPRO
C
C
      DIMENSION  X(400,1),Y(400,1),U(400,1),V(400,1),AUK(400,1),ARAD(400
     *   ,1)
      DIMENSION  XE(400 ,20), YE(400,20),
     *XSQ(400,1),YSQ(400,1)
C
```

```
      X(I,1)= XE(I,1)
   22 Y(I,1)= YE(I,1)
      RETURN
      END
/*
      SUBROUTINE PROF
C
C     CALCULATE THE UPSTREAM VELOCITY PROFILES
C
C
      COMMON NO,B(400,7),XOU,YOU,BETA,ALFAS
      COMMON /CPAD/XP(20,50),YP(20,50),NP, XPC(20,50),YPC(20,50)
     * ,UCYL,VCYL,XFP,YFP,CC,DD,UP(20,50),VP(20,50),NPRO
C
C
      DIMENSION  X(400,1),Y(400,1),U(400,1),V(400,1),AUK(400,1),ARAD(400
     *    ,1)
      DIMENSION  XE(400,1),YE(400,1),
     *XSQ(400,1),YSQ(400,1)
C
      EQUIVALENCE(B(1,2),X(1,1)),                   (B(1,3),Y(1,1)),
     *           (B(1,4),U(1,1)),                   (B(1,5),V(1,1)),
     *           (B(1,6),AUK(1,1)),                 (B(1,7),ARAD(1,1))
C
C
C           TRANSFORMATION OF POINTS TO CIRCULAR PLANE
      DO  10 I=1,NO
      XE(I,1)= X(I,1)
   10 YE(I,1)= Y(I,1)
C
      DO 300 I=1,NO
      ARG1=2.*XE(I,1)*YE(I,1)
      ARG2 =(XE(I,1)**2) - (YE(I,1)**2) -4.*BETA
      ROT = (ARG1**2) + (ARG2**2)
      RO=SQRT(ROT)
      RO=SQRT(RO)
      TH=ATAN2(ARG1,ARG2)
C
      IF(TH) 50,51,51
   50 TH=2.*3.1415926+ TH
   51 TH= TH/2.
      A=RO*COS(TH)
      C=RO*SIN(TH)
      X(I,1)=(XE(I,1)+A)/2.
      Y(I,1)=(YE(I,1)+C)/2.
      XSQ(I,1) = X(I,1)**2
      YSQ(I,1)=Y(I,1) **2
      ARAD(I,1) = XSQ(I,1)+ YSQ(I,1)
C
      IF(ARAD(I,1)-.99999)   11,11,300
   11 X(I,1)=(XE(I,1)-A)/2.
      Y(I,1)=(YE(I,1)-C)/2.
      ARAD(I,1) = X(I,1)**2 + Y(I,1)**2
  300 CONTINUE
C
C           COMPUTATION OF VELOCITY IN CIRCULAR PLANE
C
      DO 500 JJ= 1,NPRO
      DO 500 J=1,NP
      DENO = (XPC(J,JJ)**2 + YPC(J,JJ)**2)**2
      UPRO = 1. - (XPC(J,JJ)**2 - YPC(J,JJ)**2)/DENO
      VPRO = -2. * XPC(J,JJ) * YPC(J,JJ) /DENO
```

```
      EQUIVALENCE(B(1,2),X(1,1)),                         (B(1,3),Y(1,1)),
     *            (B(1,4),U(1,1)),                        (B(1,5),V(1,1)),
     *            (B(1,6),AUK(1,1)),                      (B(1,7),ARAD(1,1))
C
C
C             TRANSFORMATION OF POINTS TO CIRCULAR PLANE
C
      DO  10 I=1,NO
      XE(I,1)= X(I,1)
   10 YE(I,1)= Y(I,1)
C
      DO 300 I=1,NO
      ARG1=2.*XE(I,1)*YE(I,1)
      ARG2 =(XE(I,1)**2) - (YE(I,1)**2) -4.*BETA
      ROT = (ARG1**2) + (ARG2**2)
      RO=SQRT(ROT)
      RO=SQRT(RO)
      TH=ATAN2(ARG1,ARG2)
      IF(TH) 50,51,51
   50 TH=2.*3.1415926+ TH
   51 TH= TH/2.
      A=RO*COS(TH)
      C=RO*SIN(TH)
      X(I,1)=(XE(I,1)+A)/2.
      Y(I,1)=(YE(I,1)+C)/2.
      XSQ(I,1) = X(I,1)**2
      YSQ(I,1)=Y(I,1) **2
      ARAD(I,1) = XSQ(I,1)+ YSQ(I,1)
      IF(ARAD(I,1)-.99999)   11,11,300
   11 X(I,1)=(XE(I,1)-A)/2.
      Y(I,1)=(YE(I,1)-C)/2.
      ARAD(I,1) = X(I,1)**2 + Y(I,1)**2
  300 CONTINUE
C
C             COMPUTATION OF VELOCITY ON CYLINDER IN CIRCULAR PLANE
C                                  FOR FEEDING POINT
      UCFP = UCYL
      VCFP = VCYL
C
      DO 400 I = 1,NO
      XI = X(I,1) /ARAD(I,1)
      YI = Y(I,1) /ARAD(I,1)
      DX = XFP - X(I,1)
      DY = YFP - Y(I,1)
      DYL = YFP + Y(I,1)
      DXI = XFP - XI
      DYUI = YFP - YI
      DYLI =    YFP + YI
      DSU = DX**2 + DY**2
      DSL = DX**2 + DYL**2
      DSUI = DXI**2 + DYUI**2
      DSLI = DXI**2 + DYLI**2
      UCFP = UCFP + AUK(I,1) * (DY/DSU -DYUI/DSUI -DYL/DSL +DYLI/DSLI)
      VCFP = VCFP - AUK(I,1) * (DX/DSU -DXI/DSUI -DX/DSL + DXI/DSLI)
  400 CONTINUE
C
C             TRANSFORMATION OF VELOCITY FOR FEED POINT
      UFP = CC * UCFP - DD * VCFP
      VFP = CC * VCFP + DD * UCFP
      ALFAS = (UFP**2 + VFP**2)
C
      DO 22 I=1,NO
```

```
      DO 400 I = 1,NO
      XI = X(I,1) /ARAD(I,1)
      YI = Y(I,1) /ARAD(I,1)
      XLI = XI
      YLI = -YI
      DX = XPC(J,JJ) - X(I,1)
      DY = YPC(J,JJ) - Y(I,1)
      DYL = YPC(J,JJ) + Y(I,1)
      DXI = XPC(J,JJ) - XI
      DYUI = YPC(J,JJ) -YI
      DYLI  = YPC (J, JJ ) + YI
      DSU = DX**2 + DY**2
      DSL = DX**2 + DYL**2
      DSUI = DXI**2 + DYUI**2
      DSLI = DXI**2 + DYLI**2
      UPRO = UPRO + AUK(I,1) * (DY/DSU -DYUI/DSUI -DYL/DSL +DYLI/DSLI)
      VPRO = VPRO - AUK(I,1) * (DX/DSU -DXI/DSUI -DX/DSL + DXI/DSLI)
  400 CONTINUE
C
C
C            TRANSFORMATION OF VELOCITY
      AA = XPC(J,JJ)**2 - YPC(J,JJ)**2
      BB = 2. * XPC(J,JJ)  * YPC(J,JJ)
      DENOM = (AA - BETA)**2 + BB**2
      CM = 1. + BETA * (AA - BETA) /DENOM
      DM = BB * BETA/DENOM
      UP(J,JJ)=CM*UPRO- DM * VPRO
      VP(J,JJ)=CM*VPRO+ DM * UPRO
  500 CONTINUE
C
      DO 22 I=1,NO
      X(I,1)= XE(I,1)
   22 Y(I,1)= YE(I,1)
      RETURN
      END
/*
      SUBROUTINE PAPP
C           PRINT AND PLOT FOR LAUNCH PAD INTERFERENCE PROGRAM
C
       INTEGER DNC,HR,SEC
C
      COMMON NO,B(400,7),XOU,YOU,BETA,ALFAS
C
       COMMON    /CTIMES/TIME,DELT,DELTC,DELTP,ACCDT,ACCPT,TFIN,DNC,CONKC
     *           ,TPO,TCO
       COMMON    /CGRAF/XXL,XR,YB,YT,DXGRA,DYGRA,NGRA,MGRA,LABX,LABY
     *           ,CX(45),CYU(45),CYL(45),CXN(45),CASENO
       COMMON /CPAD/XP(20,50),YP(20,50),NP, XPC(20,50),YPC(20,50)
     * ,UCYL,VCYL,XFP,YFP,CC,DD,UP(20,50),VP(20,50),NPRO
C
       DIMENSION X(400,1),Y(400,1),YL(200)
     *     , YGRA(400),  UGRA(400), VGRA(400)
C
       EQUIVALENCE(B(1,2),X(1,1)),                     (B(1,3),Y(1,1))
C
       ACCPT =TPO
C
       DO 5 I= 1,400
       YGRA(I) = 0.0
       UGRA(I) = 0.0
       VGRA(I) = 0.0
```

```
    5 CONTINUE
C
      WRITE (6,10)
   10 FORMAT (1H1, 40X, 'VORTEX DATA'/)
      CALL HOUR
C
      WRITE (6,20)
   20 FORMAT (1H-,8HCELL NO.,3X,        9X,3HX/A,15X,3HY/A,15X,
     *        7HU/U INF,11X, 7HV/U INF,11X,8HK / U*A ,//)
C
      WRITE(6,25)  ((B(I,J),J=1,6),I=1,NO)
   25 FORMAT (1H ,  I4,7X,   1X,1P5E18.7)
C
      CALL PLOTPR
C
C
      CALL GRID1V( -3, XXL, XR, YB, YT, DXGRA,DYGRA,  NGRA,MGRA,
     *                LABX,LABY,   3,3)
      CALL PRINTV(11,  'X/A - AXIS ',      472,4)
      CALL APLOTV( NO,  X ,Y,    1,1,1,38,IERR)
      CALL APLOTV( 45, CX, CYU, 1,1,1,  42,IERR)
      CALL APLOTV( 45, CXN,CYU, 1,1,1,  42,IERR)
      WRITE(16,60)  NO,TIME,CASENO,DELTC
   60 FORMAT (1H+ 6X, 'LOCATIONS OF' I4 ' CELLS    TIME = 'F8.4,2X,3HA/U
     *  ,20X,  'SYM. CASE NO. ' F8.2 ,5X, 'DELTC = ',F5.3)
C
C
      DO 6000 I=1,NO
      IF (X(I,1)   .GT. XR) GO TO 6005
 6000 CONTINUE
      GO TO 7000
C
 6005 XRR = XR-XXL+XR
      CALL GRID1V( -3, XR,  XRR,YB, YT, DXGRA,DYGRA,  NGRA,MGRA,
     *                LABX,LABY,   3,3)
      CALL PRINTV(11,  'X/A - AXIS ',      472,4)
      CALL APLOTV( NO,  X,Y,     1,1,1,38,IERR)
      WRITE(16,60)  NO,TIME,CASENO,DELTC
      DO 6010 I=1,NO
      IF (X(I,1)  .GT. XRR) GO TO 6015
 6010 CONTINUE
      GO TO 7000
C
 6015 XRRR = XRR +XR-XXL
      CALL GRID1V( -3, XRR, XRRR,YB,YT, DXGRA,DYGRA,  NGRA,MGRA,
     *                LABX,LABY,   3,3)
      CALL PRINTV(11,  'X/A - AXIS ',      472,4)
      CALL APLOTV( NO,  X,Y,     1,1,1,38,IERR)
      WRITE(16,60)  NO,TIME,CASENO,DELTC
C
 7000 CONTINUE
C
      RETURN
      END
/*
      SUBROUTINE KIKP
C        KICK ROUTINE FOR PAD INTERFERENCE PROBLEM
C
      COMMON NO,B(400,7),XOU,YOU,BETA,ALFAS
      COMMON    /CTIMES/TIME,DELT,DELTC,DELTP,ACCDT,ACCPT,TFIN,DNC,CONKC
      COMMON    /CGRAF/XXL,XR,YB,YT,DXGRA,DYGRA,NGRA,MGRA,LABX,LABY
     *           ,CX(45),CYU(45),CYL(45),CXN(45),CASENO
```

```
C
      TIME = TIME - DELT
C
      CALL PROF
      CALL PAPP
C
      WRITE(10) NO,((B(I,J), I=1,NO), J=1,7),CASENO,TIME
      WRITE (6,10) CASENO
   10 FORMAT(1H1,5X, '  DATA FOR CASE NO.' F10.4,' ON LOGICAL TAPE 10'//
     * 6X, 'RESERVE TAPE NO.(                          ) '    ,//)
      REWIND 10
      WRITE (6,20)
   20 FORMAT (1H1)
      RETURN
      END
/*
```

## APPENDIX C. LEAST SQUARE CURVE FIT (CONLSQ)

In this section is presented the theory leading to a least squares polynomial intended to fit periodic data. It is assumed that one has in hand a random process whose mean or expected values depend on a parameter x which takes on values around the circle, i.e., 0-360 degrees. It is further assumed that a polar plot of the (unknown) locus of means is a smooth curve, i.e., has no jumps or kinks, in fact, that the locus of mean values is a polynomial of degree n in x that is constrained to have the same value, slope, and curvature at zero and 360 degrees. If the unknown polynomial is denoted by $P_n(x)$, and if m observations are taken at $x = x_1, x_2, \ldots, x_m$, then the observations $y_i$, $i = 1, 2, \ldots, m$, are given by $y_i = P_n(x_i) + e_i$, where the deviations $e_i$ are independent with zero mean and common standard deviation $\sigma$.

If the deviations $e_i$ are normally distributed, then the expectation of $y_i$ is $P_n(x_i)$ and the joint probability density of $y_1, ;;;, y_m$ is

$$f(y_1, \ldots, y_m; x_1, \ldots, x_m) = \frac{1}{(\sigma\sqrt{2\pi})^m} e^{-1/2 \sum_{i=1}^{m} \left(\frac{y_i - P_n(x_i)}{\sigma}\right)^2}$$

This density is maximized when the quantity $\sum_{i=1}^{m}\left(\frac{y_i - P_n(x_i)}{\sigma}\right)^2$ is minimized. Hence the polynomial $\hat{P}_n(x)$ that minimizes the sum of squared deviations of $y_1, \ldots, y_m$ therefrom is the maximum likelihood estimate of the unknown locus of means $P_n(x)$.

The polynomial $\hat{P}_n(x)$ that minimizes the sum of squared deviations and is constrained to repeat value, slope and curvature is found with the aid of Lagrange multipliers.

For an arbitrary polynomial $P_n(x)$, the deviation of $y_i$ therefrom is given by

$$e_i = P_n(x_i) - y_i$$

and the sum of squared deviations is

$$\sum_{i=1}^{m} e_i^2 = \sum_{i=1}^{m} \left(P_n(x_i) - y_1\right)^2 = \sum_{i=1}^{m} \left(\sum_{j=0}^{n} a_j x_i^j - y_i\right)^2 .$$

The constraints

$$y(0) = y(360)$$

$$y'(0) = y'(360)$$

$$y''(0) = y''(360)$$

reduce to

$$a_1 + a_2(360) + \ldots + a_n(360)^{n-1} = 0$$

$$2a_2 + 3a_3(360) + \ldots + na_n(360)^{n-2} = 0$$

$$2.3a_3 + 3.4a_4(360) + \ldots + n(n-1)a_n(360)^{n-3} = 0$$

respectively. Denote these linear combinations of $a_1, \ldots, a_n$ by

$$L_1(a_1, \ldots, a_n)$$

$$L_2(a_2, \ldots, a_n)$$

$$L_3(a_3, \ldots, a_n)$$

respectively.

To find the desired polynomial, we form the function

$$F(a_0, \ldots, a_n) = \sum_{i=1}^{n} \left( \sum_{j=0}^{m} a_j x_i^j - y_i \right) + \lambda_1 L_1 (a_1, \ldots, a_n)$$

$$+ \lambda_2 L_2 (a_2, \ldots, a_n) + \lambda_3 L_3 (a_3, \ldots, a_n),$$

set each of its partial derivatives equal to zero, append the constraints

$$L_1 = 0$$

$$L_2 = 0$$

$$L_3 = 0$$

and solve this system of equations for $a_0, \ldots, a_n$. The equations to be solved are then

$$\frac{\partial F}{\partial a_0} = 2 \sum_{i=1}^{m} \left( \sum_{j=0}^{n} a_j x_i^j - y_i \right) = 0$$

$$\frac{\partial F}{\partial a_1} = 2 \sum_{i=1}^{m} \left( \sum_{j=0}^{n} a_j x_i^j - y_i \right) x_i + \lambda_1 = 0$$

$$\frac{\partial F}{\partial a_2} = 2 \sum_{i=1}^{m} \left( \sum_{j=0}^{n} a_j x_i^j - y_i \right) x_i^2 + 360 \lambda_1 + 2 \lambda_2 = 0$$

$$\frac{\partial F}{\partial a_3} = 2 \sum_{i=1}^{m} \left( \sum_{j=0}^{n} a_j x_i^j - y_i \right) x_i^3 + (360)^2 \lambda_1 + 3\,(360)\,\lambda_2 + 2.\,3\lambda_3 = 0$$

$$\frac{\partial F}{\partial a_k} = 2 \sum_{i=1}^{m} \left( \sum_{j=0}^{n} a_j x_i^j - y_i \right) x_i^k + (360)^{k-1} \lambda_1$$

$$+ k\,(360)^{k-2} \lambda_2 + k(k-1)\,(360)^{k-3} \lambda_3 = 0$$

$$k = 4, \ldots, n$$

$$L_1 (a_1, \ldots, a_n) = 0$$

$$L_2 (a_2, \ldots, a_n) = 0$$

$$L_3 (a_3, \ldots, a_n) = 0$$

Expanding sums, dividing the first n+1 equations by 2, and redefining $\lambda_1$, $\lambda_2$ and $\lambda_3$, the system of equations becomes, in matrix form, as shown in Figure C-1.

In practice, one usually does not know a priori what degree polynomial to use. However, the sum of squared deviations for various degrees may furnish a clue. Suppose the degree of the unknown polynomial is n. Then whether or not the deviations are normally distributed, the sum of squared deviations about the fitted curve divided by m - n - 1 is an unbiased estimate of the unknown variance $\sigma^2$. In fact, unbiasedness obtains whenever the degree of the fitted polynomial is at least the degree of the unknown locus of means. Then as one proceeds upward from degrees too low, the estimate of $\sigma^2$ can be expected to steadily drop until the correct degree is reached and then level off and fluctuate irregularly around the value $\sigma^2$ as the degree of the fitted curve exceeds by more and more the degree of the unknown curve of expected values.

$$
\begin{bmatrix}
m & \Sigma x_i & \Sigma x_i^{2} & \Sigma x_i^{3} & \cdots & \Sigma x_i^{n} & 0 & 0 & 0 \\
\Sigma x_i & \Sigma x_i^{2} & \Sigma x_i^{3} & \Sigma x_i^{n} & \cdots & \Sigma x_i^{n+1} & 1 & 0 & 0 \\
\Sigma x_i^{2} & \Sigma x_i^{3} & \Sigma x_i^{4} & \Sigma x_i^{5} & \cdots & \Sigma x_i^{n+2} & 360 & 2 & 0 \\
\Sigma x_i^{3} & \Sigma x_i^{4} & \Sigma x_i^{5} & \Sigma x_i^{6} & \cdots & \Sigma x_i^{n+3} & (360)^{2} & (360)^{2} & 3(360) \\
\cdot & & & & & & & & \\
\cdot & & & & & & & & \\
\cdot & & & & & & & & \\
\Sigma x_i^{n} & \Sigma x_i^{n+1} & \Sigma x_i^{n+2} & \Sigma x_i^{n+3} & \cdots & \Sigma x_i^{2n} & (360)^{n-1} & n(360)^{n-2} & n(n-1)\,(360)^{n-3} \\
0 & 1 & 360 & (360)^{2} & \cdots & (360)^{n-1} & 0 & 0 & 0 \\
0 & 0 & 2 & 3(360) & \cdots & n(360)^{n-2} & 0 & 0 & 0 \\
0 & 0 & 0 & 3\cdot 2 & \cdots & n(n-1)\,(360)^{n-3} & 0 & 0 & 0
\end{bmatrix}
\begin{bmatrix}
a_0 \\ a_1 \\ a_2 \\ a_3 \\ \\ \\ \\ a_n \\ \lambda_1 \\ \lambda_2 \\ \lambda_3
\end{bmatrix}
=
\begin{bmatrix}
\Sigma y_i \\ \Sigma x_i y_i \\ \Sigma x_i^{2} y_i \\ \Sigma x_i^{3} y_i \\ \\ \\ \\ \Sigma x_i^{n} y_i \\ 0 \\ 0 \\ 0
\end{bmatrix}
$$

Figure C-1. Matrix of Normal Equation

The degree of the fitted curve must be at least four or the curve will degenerate into a horizontal line through the means of all points. For, if the selected degree is three, then the second derivative is linear, hence constant in order to match at zero and 360. Hence, the curve will be a quadratic and the slope will be linear. Then the slope must be a constant in order to match. But then the curve is a straight line and must be constant for the values to match.

## DESCRIPTION AND USE

The main program, CONLSQ, reads the wind azimuth and speed information for the various anemometer locations, the degree, or degrees, of the desired polynomials, and the number of evenly spaced points at which the fitted curve is to be computed, and prepares the data for subroutine SUMPOW. Each time SUMPOW is called, it solves the system of equations previously given for $a_0, \ldots, a_n$, computes the fitted curve at the number of points requested, and plots the input data and fitted curve as an azimuth shift or a velocity ratio, depending on the value of a logical variable set in CONLSQ.

The inputs to CONLSQ are read in the NAMELIST format and include NTOP (the number of data points for the top anemometer), AZMTH (500, 4) (azimuths for the various anemometers), VELOC (500, 4) (speeds), DEGLOW (the lowest degree polynomial desired), DEGHI (the highest degree polynomial desired), DEGINC (the step size desired going from DEGLOW to DEGHI), and NGRAPH (the number of points desired on the fitted curve).

The first column in each of AZMTH and VELOC is for the top anemometer data, the second for the east anemometer, the third for the west anemometer, and the fourth for the deck level. The last was not used because of the paucity of data from the deck-level anemometer. If an azimuth for any of columns 2 through 4 is unavailable, a value greater than 370 should be entered and ignored; if a velocity is unavailable, a value of 500 should be entered and ignored.

The order of computation, first for the east anemometer and then the west:

1. Compute azimuth shift for the azimuths available (at the east or west anemometer), counting the number of "good" points NOGP and calling SUMPOW once for each degree polynomial from DEGLOW to DEGHI in steps of size DEGINC;

2. Compute speed ratio for the number of speeds available (at the east or west anemometer) and proceed as in Step 1.

After these computations, the data for the east and west anemometers are pooled (referred to the east anemometer) and SUMPOW is called twice, once for azimuth shifts and once for velocity ratios.

The only output is in the form of CRT plots prepared in the subroutine SUMPOW. Typical graphs are Figures C-2 and C-3. There are no options concerning the scales, labeling, etc., of the CRT output.

The solution of the simultaneous equations is obtained by calling the double precision subroutine DMSEQ in SUMPOW.

Listings for the main program CONLSQ and subroutine SUMPOW are given at the end of this section.

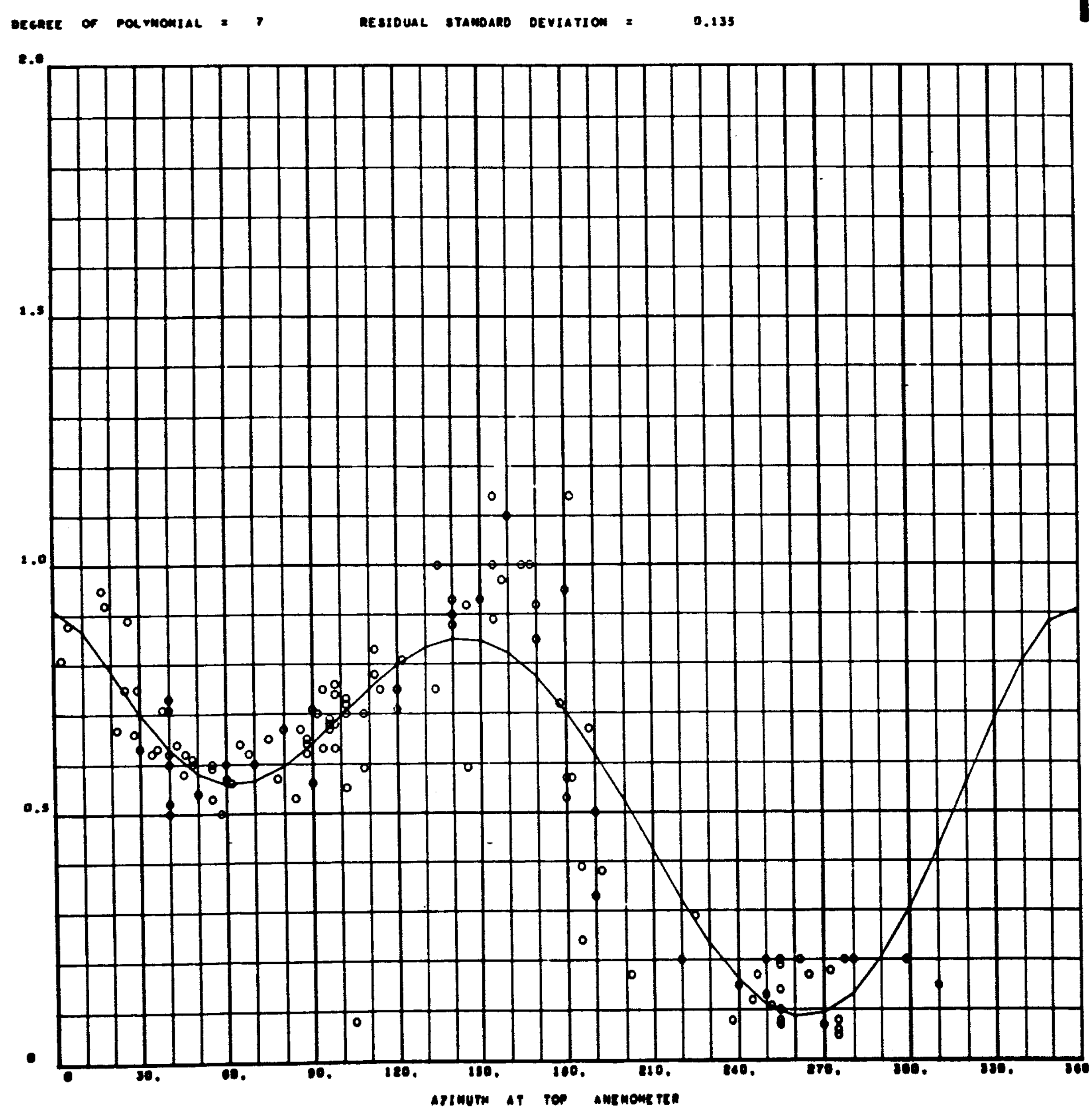


Figure C-2. Typical Least-Error Polynomial Output by CONLSQ Program

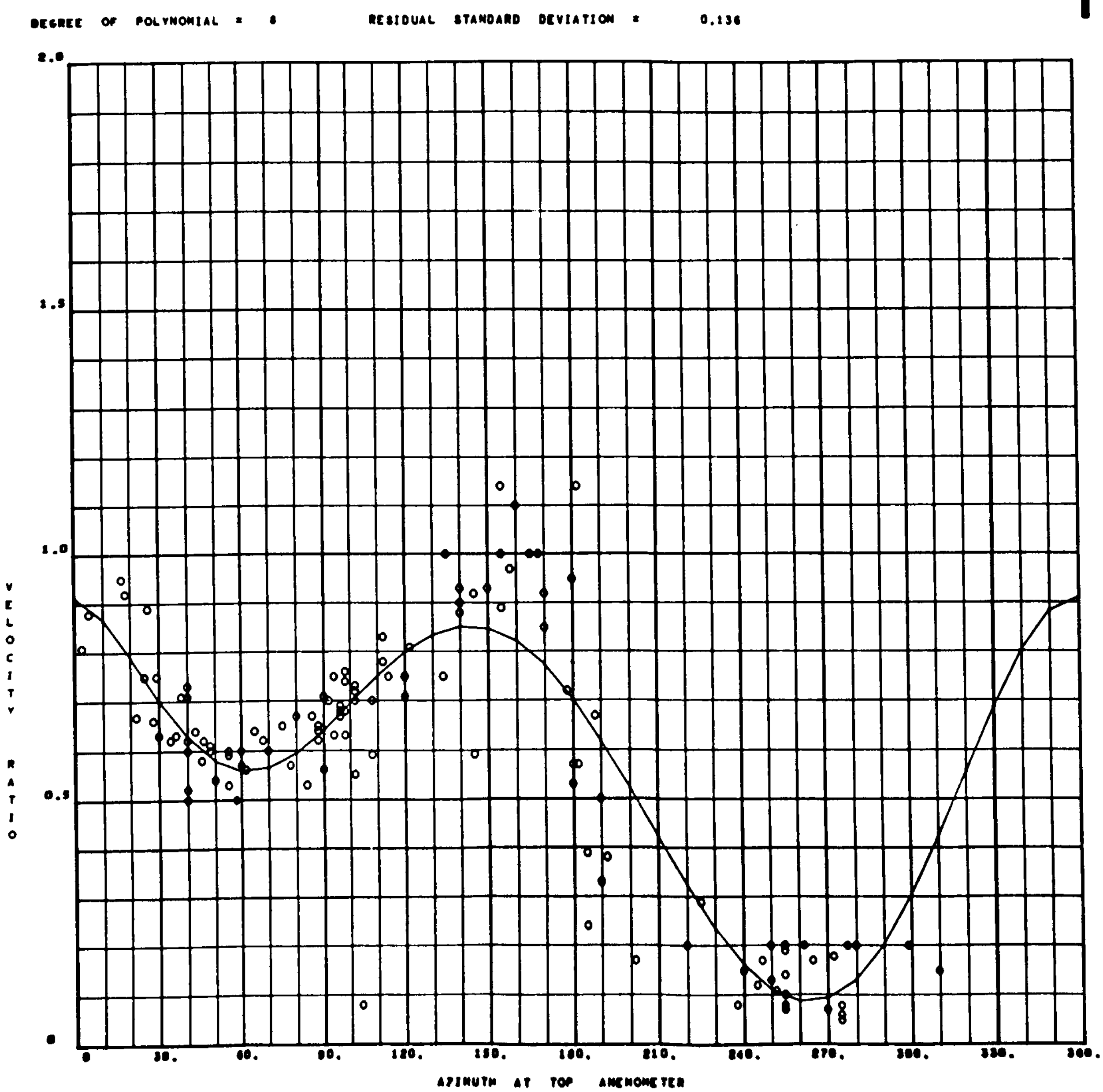


Figure C-3. Typical Least-Error Polynomial Output by CONLSQ Program

Listing of CONLSQ Program

```
                                                                        ==01
C      CONLSQ PROGRAM                    J.E.DAVIS   190-220
C        CONSTRAINED LEAST FIT OF PERIODIC WIND DATA
C
      REAL*8 X,Y,PDXC,PDXG
      INTEGER DEGLOW, DEGHI, DEGINC
      LOGICAL AZTST
      COMMON /SUB/ X(1000),Y(1000),NDEG,NOGP,RMS,NGP
     *              ,XGRAPH(500),YGRAPH(500),NGRAPH,IBLK,JBLK
      COMMON /CIP/ DEGLOW,DEGHI,DEGINC,AZMTH,VELOC,NTOP,CASEND
      COMMON / TEST / AZTST
C
      DIMENSION IAZ(4), AZS(500,4),XAZ(500,4), AZT(500),
     *   VELR(500,4), XVEL(500,4), IVEL(10),AZMTH(500,4),VELOC(500,4)
C
      EQUIVALENCE (AZMTH(1,1),AZT(1))
C
      CALL SCOUTV
      CALL CAMRAV( 9 )
C
    5 READ (5,DATA)
C
      NGP = NGRAPH + 1
      DO  8  I = 1, NGP
    8 XGRAPH(I) = (I-1) * 360. /(NGRAPH)
C
      DO 30 J=2,3
      IAZ(J) = 0
      DO 10 I=1,NTOP
      IF(AZMTH(I,J) .GT. 370.) GO TO 10
      IF(AZMTH(I,J) .GT. 360. .AND. AZMTH(I,J) .LE. 370.)
     *                     AZMTH(I,J) = AZMTH(I,J) - 360.
      IAZ(J) = IAZ(J) +1
      AZS(IAZ(J),J) = AZMTH(I,J)   - AZT(I)
      Y(IAZ(J))    = AZS(IAZ(J),J)
      XAZ(IAZ(J),J) = AZT(I)
      X(IAZ(J))= XAZ(IAZ(J),J)
      AYIAZJ =DABS(Y( IAZ(J) ))
      IF ( AYIAZJ .GT. 90.)  IAZ(J) = IAZ(J) -1
   10 CONTINUE
C
      NOGP = IAZ(J)
      DO 15 JJ = DEGLOW,DEGHI,DEGINC
      NDEG = JJ
      AZTST = .TRUE.
      CALL SUMPOW
   15 CONTINUE
C
      IVEL(J) = 0
      DO 20 N=1,NTOP
      IF(VELOC(N,J) .EQ. 500.) GO TO 20
      IVEL(J) = IVEL(J) +1
      X(IVEL(J)) = AZT(N)
      Y(IVEL(J)) = VELOC(N,J)/VELOC(N,1)
      XVEL ( IVEL (J), J)  = X ( IVEL (J))
      VELR (IVEL (J), J)  = Y (IVEL (J))
   20 CONTINUE
C         X IS XVEL, Y IS VELR
C
      NOGP = IVEL(J)
      DO 25 JJ= DEGLOW,DEGHI,DEGINC
```

**02

```
      NDEG   = JJ
      AZTST = .FALSE.
      CALL SUMPOW
   25 CONTINUE
   30 CONTINUE
C
C     POOL DATA FROM EAST AND WEST
      NN = IVEL(2)
      DO 40 I=1,NN
      Y(I) = VELR(I,2)
      X(I) = XVEL(I,2)
   40 CONTINUE
C
      NN = IVEL(3)
      DO 50 I= 1,NN
      Y(I+IVEL(2)) = VELR(I,3)
      X(I+IVEL(2)) =  360. - XVEL(I,3)
   50 CONTINUE
      DO 55 JJ= DEGLOW,DEGHI,DEGINC
      NDEG = JJ
      NOGP   =  IVEL (2) +  IVEL (3)
      AZTST = .FALSE.
      CALL SUMPOW
   55 CONTINUE
C
      NN = IAZ(2)
      DO 60 I=1,NN
      Y(I) = AZS(I,2)
      X(I) = XAZ(I,2)
   60 CONTINUE
      NN = IAZ(3)
      DO 70 I= 1,NN
      Y(I+IAZ(2)) = -AZS(I,3)
      X(I+IAZ(2)) = 360. - XAZ(I,3)
   70 CONTINUE
C
C
      DO 75 JJ= DEGLOW,DEGHI,DEGINC
      NDEG = JJ
      NOGP   = IAZ (2) + IAZ (3)
      AZTST = .TRUE.
      CALL SUMPOW
   75 CONTINUE
C
C
      GO TO 5
      END
/*
/*
/*
```

Listing of Subroutine SUMPOW

```
                                                                             **01
      SUBROUTINE SUMPOW                                                  SUMP1000
      INTEGER*4 E(50)
      REAL*8 X,Y,POXC,POXG,POX,POXY,XGRA,YGRA,YCURVE,RESD,DERMS
      REAL*8    A(18,18),  SX(50),  XP(50), SXY(50),B(18),DET,SCALE(50)
      DIMENSION XS(1000),YS(1000)
      COMMON /SUB/ X(1000),Y(1000),NDEG,NOGP,RMS,NGP
     *             ,XGRAPH(500),YGRAPH(500),NGRAPH,IBLK,JBLK
      COMMON / TEST / AZTST
      LOGICAL SING , AZTST
C
C     COMPUTE SUMS OF POWERS OF X AND YTIMES POWERS OF X                 00000040
C
      DET = 1.0D0
      SCALE(1) = 1.0 D0
      NPX = 2*NDEG + 1
      NVR = NDEG + 1
      NEQ = NVR+3
C
      DO 100 J = 1 , 50
      SX( J ) = 0.0 D0
  100 SXY( J ) = 0.0D0
C
      DO 300 I = 1 , NOGP                                                SUMP1110
      POX = 1.0 D0
      DO 200 J = 1 , NPX                                                 00000030
      SX( J ) = SX(J) + POX                                              00000040
  200 POX = POX*X( I )                                                   00000050
  300 CONTINUE                                                           00000060
C
      DO 500 I = 1 , NOGP                                                00000070
      POXY = Y( I )                                                      00000080
      DO 400 J = 1 , NVR                                                 00000090
      SXY(J) = SXY(J) + POXY
  400 POXY = POXY*X( I )                                                 00000010
  500 CONTINUE                                                           00000020
C
C                           INITIALIZE MATRICES
      DO 520 I=1,18
      B(I)    = 0.0 D0
      DO 510 J = 1 ,18
  510 A(I,J) = 0.0 D0
  520 CONTINUE
C     COMPUTE MATRIX OF COEFFICIENTS                                     SUMP1230
      DO 700 I = 1 , NVR                                                 00000040
      B( I )      = SXY( I )
      DO 600 J = 1 , NVR
  600 A( I , J ) = SX( I + J - 1 )                                       00000070
  700 CONTINUE                                                           00000080
C
      XP( 1 ) = 1.0 D0
      DO 800 I = 2 , NVR
  800 XP( I ) = XP( I - 1 ) * 360.                                       00000010
C
      DO 900 J = 2 , NVR
  900 A( NEQ - 2 , J ) = XP( J - 1 )                                     00000040
C
      DO 1000 J = 3 , NVR
 1000 A( NEQ - 1 , J ) = ( J - 1 )*XP( J - 2 )                           00000080
C
      DO 1100 J = 4 , NVR
```

```
                                                                      **02
 1100 A( NEQ , J ) = ( J - 1 )*( J - 2 )*XP( J - 3 )                 00000030
C
      NVRP= NVR +1
      DO 1200 I = NVRP,NEQ
      DO 1300 J = 1 , NVR
 1300 A(J,I) = A(I,J)
 1200 CONTINUE
C
      RET = DMSEQ(18,NEQ,1,A,B,E,DET,SCALE)
      IF(RET.EQ.0.0) WRITE(6,1350)
 1350 FORMAT (1H- , 'A MATRIX IS SINGULAR' ,//)
C
C
C          COMPUTE FITTED CURVE
      DO 1500 I=1,NGP
      YGRA  =  0.0D0
      XGRA = XGRAPH(I)
      POXG = 1.0 D0
      DO 1400 J= 1,NVR
      YGRA       = YGRA       + A(J,1) * POXG
 1400 POXG = XGRA          * POXG
      YGRAPH(I) = YGRA
 1500 CONTINUE
C
C          COMPUTE RESIDUAL STANDARD DEVIATION
      RESD = 0.0 D0
      DO 1700 I= 1,NOGP
      YCURVE = 0.0 D0
      POXC = 1.0 D0
      DO 1600 J = 1,NVR
      YCURVE = YCURVE + POXC * A(J,1)
 1600 POXC = POXC * X(I)
      RESD = RESD + (Y(I) - YCURVE) **2
 1700 CONTINUE
      DERMS = NOGP - NVR
      ARG = RESD/DERMS
      RMS = SQRT( ARG )
C
      NNGR = NOGP
C
      DO 1750 I = 1,NOGP
      XS(I) = X(I)
 1750 YS(I) = Y(I)
      IF( AZTST ) GO TO 1800
      XL = 0.0
      XR = 360.0
      YB = 0.0
      YT = 2.0
      DXGRA = 10.0
      DYGRA = 0.1
      NGRA = 3
      MGRA = 5
      LABX = -3
      LABY = -5
      CALL GRIDIV( -3 , XL , XR , YB , YT , DXGRA , DYGRA , NGRA ,
     *           MGRA , LABX , LABY , 4 , 3 )
      CALL PRINTV( 31 , ' AZIMUTH  AT  TOP   ANEMOMETER ' , 400 , 4 )
      CALL APRNTV( 0 , -17 , 17 , ' VELOCITY  RATIO ' , 4 , 500 )
      CALL APLOTV( NNGR , XS, YS, 1 , 1 , 1 , 38 , IERR )
      WRITE( 16 , 1900 ) NDEG , RMS
 1900 FORMAT(1H+ , ' DEGREE  OF  POLYNOMIAL  =  ' , I2 , 10X , ' RESIDUA
     *L  STANDARD  DEVIATION  =  ' , F10.3 )
      GO TO 2010
```

```
                                                                            ==03
1800 XL = 0.0
     XR = 360.0
     YB = -100.0
     YT = 100.0
     DXGRA = 10.0
     DYGRA = 10.0
     NGRA = 3
     MGRA = 3
     LABX = -3
     LABY = -3
     CALL GRIDIV( -3 , XL , XR , YB , YT , DXGRA , DYGRA , NGRA ,
    *            MGRA , LABX , LABY , 4 , 3 )
     CALL PRINTV( 31 , ' AZIMUTH  AT   TOP  ANEMOMETER ' , 400 , 4)
     CALL APRNTV( 0 , -16 , 16 , ' AZIMUTH  SHIFT ' , 4 , 500 )
     CALL APLOTV( NNGR , XS, YS, 1 , 1 , 1 , 38 , IERR )
     WRITE( 16 , 2000) NDEG , RMS
2000 FORMAT(1H+ , ' DEGREE  OF  POLYNOMIAL  =  ' , I2 , 10X , ' RESIDUA
    *L  STANDARD  DEVIATION  =  ' , F10.3 )
2010 CONTINUE
     DO 3000 I=2,NGRAPH
     IX1 = NXV(XGRAPH(I-1))
     IY1 = NYV(YGRAPH(I-1))
     IX2 = NXV(XGRAPH(I))
     IY2 = NYV(YGRAPH(I))
     CALL LINEV(IX1,IY1,IX2,IY2)
3000 CONTINUE
     IX3 = NXV(360.)
     IY3 = NYV(YGRAPH(1))
     CALL LINEV (IX2,IY2,IX3,IY3)
C
     RETURN                                                          00000050
     END                                                             00000060
/*
/*
/*
```

## REFERENCES

1. Camp, Dennis W., Analysis of Wind Tunnel Data for Several Beckman & Whitley Series 50 and Climet Model C1-14 Anemometers, NASA TMX-53271 (May 26, 1965).

2. Ujihara, B.H., J.W. Cottrell, J.E. Davis, and P.W. Welch. Analytical Study of Two Dimensional Vortex Shedding, NR SD, SID 66-1805 (1966).

3. Ujihara, B.H., J. E. Davis, and T. Sugimura. Analytical Study of Separated Flow About a Circular Cylinder, NR SD, SID 65-1730 (1966).

4. Farmer, M. G. and George W. Jones. Summary of Langley Wind Tunnel Studies of Ground-Wind Loads on Launch Vehicles, Compilation of papers presented at the NASA Langley Research Center (7-8 June 1966).

5. Gill, Gerald C., Lars E. Olsson, Josef Sela, and Motozo Suda. "Accuracy of Wind Measurements on Towers and Stacks," Bulletin, American Meteorological Society, Vol. 48, No. 9 (September 1967).

6. Hsi, G., and J. E. Cermak. Meteorological Tower Induced Wind Field Perturbations, AD 623 946 (October 1965).

7. Kucheman, Report on the IUTAM Symposium on Concentrated Vortex Motions in Fluids," J. of Fluid Mechanics, Vol. 21, Part 1, pp. 1-20 (1965).

8. Meyer, R. A., H. B. Reese and J. R. Ziler. Results of a Wind Tunnel Program to Investigate the Interference or Shadowing Effects of a Meteorological Tower, Chrysler Corporation Space Division Report TN AE 65-98 (1965).

9. Roshko, Anatol. A New Hodograph for Free Streamline Theory, NACA TN 3168 (July, 1954).

10. Roshko and Lau. Some Observations on Transition and Reattachment of a Free Stream Layer in Incompressible Flow, Proceedings of the 1965 Heat Transfer and Fluid Mechanics Institute, Edited by A. F. Charwat.

11. Sato, H. "Experimental Investigation on the Transition of Laminar Separated Shear Layer," J. Phys. Soc. Japan, Vol. II(6), pp. 702, 709 (1956).

DISTRIBUTION

DIR

R-AERO-DIR
Dr. Geissler
Mr. Jean

R-AERO-A
Mr. Dahm
Mr. Reed
Mr. R. Walker

R-AERO-D
Mr. Horn
Mr. Rheinfurth
Mr. Ryan

R-AERO-F
Mr. Lindberg
Mr. Hagood

R-AERO-G
Mr. Baker

R-AERO-T
Dr. Heybey

R-AERO-Y
Mr. Vaughan (2)
Mr. Kaufman (10)
Mr. Fichtl
Mr. Susko
Mr. Hill (10)
Mr. Camp
Mrs. Alexander
Mr. R. Smith
Mr. O. Smith
Mr. C. Brown
Mr. Daniel
Mr. R. Turner

R-P&VE
Dr. Lucas
Mr. Hunt
Mr. Showers
Mr. Stevens
Mr. Moore
Mr. Green
Mr. Kroll

R-ASTR
Mr. Blackstone

R-SE
Mr. Richards

R-EO
Dr. Johnson

R-SSL
Dr. Stuhlinger

I-MO
Dr. Speer

I-DIR
Gen O'Connor

MS-IP

MS-IL (6)

Dr. Isaac Van der Hoven, ARL
Environ. Meteorology Res. Br.
U. S. Dept of Commerce
Weather Bureau
Washington, D. C. 20235

Lt. Col. Harold R. Montague
U. S. Air Force Staff Meteorologist
Eastern Test Range
Patrick Air Force Base, Fla. 32925

Dept. of Meteorology
College of Mineral Industries
Pa. State Univ.
University Park, Pa. 16802
Attn: Dr. Hans A. Panofsky

Mr. N. Sissenwine, CREW
Air Force Cambridge Res. Labs.
L. G. Hanscom Field
Bedford, Mass. 01731

Mr. Roy Endlich
Stanford Res. Inst.
Menlo Park, Calif. 94026

EXTERNAL DISTRIBUTION (Continued)

Martin-Marietta Corp.
Aerospace Div.
P. O. Box 179
Denver 1, Col.

Mr. Marvin White
TRW
One Space Park
Redondo Beach, Calif.

Dr. J. Scoggins
Texas A&M
College Station, Texas

Chief, Structural Dynamics Lab.
AF System Command
Wright-Patterson AFB, Ohio

Mr. Roland Pilie
Cornell Aeronautical Labs.
Buffalo, N. Y.

North American Rockwell Corp.
Space Div.
12214 Lakewood Blvd.
Downey, Calif. 90241
Attn: Mr. R. F. Stevenson
Mr. H. S. Oder
Mr. H. D. McLaughlin
Mr. B. H. Ujihara
Mrs. J. E. Davis

NASA-Kennedy Space Center
Mr. R. Jones
Dr. Bruns
Mr. Keene
Mr. A. Taiani
Mr. Jelen
Mr. R. P. Dodd
Mr. D. D. Buchanan
Dr. H. Knothe
Mr. E. Ammon
Mr. R. Wilkinson
Mr. J. P. Claybourne
Mr. E. O. Raley
Library

NASA Headquarters
Office of Space Sci. & Appl.
Director
Dr. M. Tepper

Office of Manned Space Flt.
Mr. A. Kinny

OART
Mr. D. Michael
Mr. T. Cooney
Mr. M. Ames

NASA-Langley Res. Center
Langley Sta.
Hampton, Va. 23365
Attn: Director
Library
Mr. H. B. Tolefson
Mr. W. Reed, III

NASA-Manned Spacecraft Center
Houston, Texas 77058
Attn: Director
Library
Mr. D. Wade (2)

NASA-Wallops Sta.
Wallops Island, Va. 23337
Attn: Director
Mr. J. Spurling

NASA-Lewis Research Center
Cleveland, Ohio
Attn: Director
Library

Aerospace Corp.
El Segundo, Calif.

The Boeing Co.
Space Div.
Huntsville Industrial Center
Huntsville, Ala.
Attn: Mr. J. Hathorn
Mr. E. Lamb

Environmental Science Services Administration
National Severe Storms Lab.
1616 Halley Ave.
Norman, Okla. 73069

Dr. H. Crutcher
ESSA
National Weather Records Center
Asheville, North Carolina 28801

Scientific and Technical Inf. Facility(25)
S-AK/RKT
P.O. Box 33
College Park, Md. 20740